

Customer	: ESRIN	Document Ref	: SST_CCI-CAR-UKMO-201
Contract No	: 4000109848/13/I-NB	Issue Date	: 16 June 2019
WP No	: 50	Issue	: 1

Project : **SST-CCI-Phase-II**

Title : **SST CCI Climate Assessment Report**

Abstract : This document presents a climate assessment of the European Space Agency Sea Surface Temperature Climate Change Initiative (ESA SST CCI) Phase 2 products, Release version CDR2.0. It includes comparison of the products to other climate data sets of SST and Release version 1.0.




Author : Nick Rayner, Yoko Tsushima, Chris Atkinson, Simon Good, Malcolm Roberts, Gill Martin, Duncan Ackerley, Holly Titchner, Chongyuan Mao, Prince Xavier, Ruth Comer, Yuwei Hu, Helen Beggs, Xiao Hua Wang, Georgios Margaritis, Richard Renshaw, Luísa Lamas, Rita Esteves, Sara Almeida, Eduardo de Azevedo, Cecília Correia, Francisco Reis and Ulrika Willén

Checked : Chris Merchant
Science Leader

Accepted by : Craig Donlon
ESA : ESA

Distribution : SST_cci team members
Craig Donlon (ESA)

**EUROPEAN SPACE AGENCY
CONTRACT REPORT**

The work described in this report was done under ESA contract. Responsibility for the contents resides in the author or organisation that prepared it.

AMENDMENT RECORD

This document shall be amended by releasing a new edition of the document in its entirety. The Amendment Record Sheet below records the history and issue status of this document.

AMENDMENT RECORD SHEET

ISSUE	DATE	REASON FOR CHANGE
0.1	10/02/2019	First incomplete draft
0.2	10/02/2019	Added reports from trailblazer users, GMPE comparison and write up of modelling experiments
0.3	24/02/2019	Added two further trailblazer user reports and made the figure captions consistent throughout
0.4	01/03/2019	Implemented comments from Chris Merchant and included Exec Summary
0.5	31/03/2019	Accepted all changes
0.6	29/04/2019	Version for review
1	16/06/2019	Revision after ESA review

TABLE OF CONTENTS

1. INTRODUCTION.....	6
1.1 Purpose and Scope.....	6
1.2 Structure of the Document.....	6
1.3 Referenced Documents.....	7
1.4 Definitions of Terms.....	9
2. EXECUTIVE SUMMARY.....	10
3. ASSESSMENT OF TRENDS AND VARIABILITY IN SST CCI PRODUCTS AND COMPARISON TO OTHER PRODUCTS.....	15
3.1 Introduction.....	15
3.2 Data sets.....	15
3.2.1 Gridded reference data.....	15
3.2.2 HadSST3.....	16
3.2.3 AVHRR Pathfinder.....	16
3.2.4 HadISST.....	17
3.2.5 ERSSTv3b.....	17
3.2.6 COBE SST.....	17
3.2.7 NOCS Surface Flux data set v2.0.....	17
3.2.8 OI.v2.....	17
3.2.9 MyOcean OSTIA reanalysis.....	18
3.2.10 Daily OI.....	18
3.3 Methods.....	18
3.3.1 Linear trends.....	18
3.3.2 Indices.....	21
3.3.3 Multi-annual and decadal averages.....	21
3.3.4 Autocorrelations.....	21
3.4 Results.....	21
3.4.1 Time series, linear trends and indices.....	21
3.4.1.1 Global average SST anomaly.....	21
3.4.1.2 Hemispheric time series.....	24
3.4.1.3 Linear trends.....	27
3.4.1.4 Modes of variability.....	32
3.4.1.5 Other points to note.....	35
3.4.2 Multi-year averages.....	39
3.4.3 Auto-correlations.....	42
4. SST CCI V2.0 PRODUCTS IN GHR SST MULTI-PRODUCT ENSEMBLE.....	45
4.1 Introduction.....	45
4.2 Argo validation statistics.....	46
4.3 Differences between the analyses and the GMPE median.....	50
4.4 SST features and gradients.....	50
4.5 Conclusions.....	53
4.6 Acknowledgments.....	57
4.7 References.....	57
5. ANALYSIS OF DEDICATED MODELLING EXPERIMENTS.....	59
5.1 Key messages.....	59
5.2 Scientific analysis.....	59
5.2.1 Aims of the study.....	59
5.2.2 Method.....	60
5.2.3 Results.....	60
5.2.3.1 SST.....	60
5.2.3.1.1 SST Annual Mean Climatology.....	60
5.2.3.1.2 SST Climatological Seasonal Variation.....	61

5.2.3.1.3	SST Variability	63
5.2.3.2	Sea Ice	65
5.2.3.2.1	Sea Ice Annual Mean Climatology	65
5.2.3.2.2	Sea Ice Climatological Seasonal Mean	65
5.2.3.2.3	Other comments relating to sea ice differences	66
5.2.3.3	Cloud Regimes	67
5.2.3.3.1	Method and Data for Cloud regime projections	67
5.2.3.3.2	Global Mean Climatology	67
5.2.3.3.3	Global Distributions	68
5.2.3.3.4	Stratocumulus	70
5.2.3.3.5	Organized Deep Convective System regime	71
5.2.3.3.6	Summary	73
5.2.3.4	Tropical Cyclones	73
5.2.3.4.1	Tropical cyclone tracking	73
5.2.3.4.2	Mean tropical cyclone activity per ocean basin	74
5.2.3.4.3	Tropical cyclone interannual variability	75
5.2.3.4.4	Tropical cyclone track density	76
5.2.3.4.5	Conclusions	76
5.2.3.5	Effects on South Asian summer monsoon	78
5.2.3.5.1	Climatology	78
5.2.3.5.2	Interannual variability	83
5.2.3.5.3	Intraseasonal variability	84
5.2.3.5.4	Summary	86
5.2.3.6	Madden-Julian Oscillation	87
5.2.3.7	El Niño Southern Oscillation	88
5.2.3.8	Mid-latitude Weather Systems	91
5.2.3.8.1	Storm Tracks	91
5.2.3.8.2	Blocking	95
5.2.3.8.3	North Atlantic Oscillation	97
5.2.4	Conclusions	98
5.2.5	Future potential areas of study	98
5.2.6	Recommendations for future developments of the SST CCI products	99
5.2.7	Acknowledgments	100
5.2.8	References	100
6.	VOLUNTARY REPORTS BY TRAILBLAZER USERS	104
6.1	Inter-comparison of High-Resolution SST Climatology data sets over the Australian region 104	
6.1.1	Key messages	104
6.1.2	Scientific analysis	104
6.1.2.1	Aims of the study	104
6.1.2.2	Method	105
6.1.2.2.1	Climatology Datasets	105
6.1.2.2.2	Density Distribution of the Differences	107
6.1.2.2.3	Climatology validation using tropical mooring data	107
6.1.2.3	Results	109
6.1.2.3.1	Mean Difference and STD of Residual Difference	109
6.1.2.3.2	Density Distribution of the Differences	111
6.1.2.3.3	In-situ Measurement Validation	115
6.1.2.4	Conclusions	116
6.1.2.5	References	117
6.1.3	Feedback on scientific utility of the SST CCI products	117
6.2	Using gridded sea surface temperature products to estimate the temperature experienced by tropical corals: Implications for coral reef monitoring	118
6.2.1	Key messages	118
6.2.2	Scientific analysis	118
6.2.2.1	Aims of the study	118
6.2.2.2	Method	118
6.2.2.2.1	In situ data	118

6.2.2.2	Gridded SST products	120
6.2.2.2.3	Statistical analysis methodology	121
6.2.2.3	Results	121
6.2.2.4	Conclusions	127
6.2.3	Feedback on scientific utility of the SST CCI products.....	127
6.2.4	References	128
6.3	Regional ocean reanalysis for the North-West European Shelf Seas	129
6.3.1	Key messages	129
6.3.2	Scientific analysis	129
6.3.2.1	Aims of the study	129
6.3.2.2	Method	129
6.3.2.3	Results	129
6.3.2.4	Conclusions	130
6.3.3	Feedback on scientific utility of the SST CCI products.....	130
6.4	Feedback from the ESA SST CCI v2.0 product over the Eastern Atlantic	131
6.4.1	Key messages	131
6.4.2	Scientific analysis	131
6.4.2.1	Aims of the study	131
6.4.2.2	Methods	132
6.4.2.3	Results	134
6.4.2.4	Conclusions	141
6.4.3	Feedback on scientific utility of the SST CCI products.....	141
6.5	Evaluating coupled climate model EC-Earth3-Veg	142
6.5.1	Key messages	142
6.5.2	Scientific analysis	142
6.5.2.1	Aims of the study	142
6.5.2.2	Method	143
6.5.2.3	Results	143
6.5.2.4	Conclusions	144
6.5.3	Feedback on scientific utility of the SST CCI products.....	144
7. FURTHER ISSUES AND RECOMMENDATIONS REPORTED BY REGISTERED USERS		
151		
7.1	Feedback on ease of use of the products and documentation	151
7.2	Recommendations	151

1. INTRODUCTION

1.1 Purpose and Scope

This document presents a climate assessment of the European Space Agency Sea Surface Temperature Climate Change Initiative (ESA SST CCI) Phase 2 products, Release version CDR2.0. It includes comparison of the products to other climate data sets of SST and Release version 1.0 to provide a link to previous Climate Assessment Reports.

We assess the following CDR2.0 products:

- ATSR. SSTs from Along Track Scanning Radiometer (ATSR) instruments in L3U format at 0.05° latitude by 0.05° longitude resolution covering 1991 – April 2012. (Shortened to SST CCI ATSR.)
- AVHRR. SSTs from AVHRR instruments in L2P format at Global Area Coverage (GAC) resolution covering 24th August 1981 – 2016. (Shortened to SST CCI AVHRR.)
- Analysis. Satellite-only SST-depth L4 daily analysis created by the Operational Sea Surface Temperature and sea Ice Analysis (OSTIA) system from the SST CCI ATSR and SST CCI AVHRR products at 0.05° latitude by 0.05° longitude resolution covering September 1981 – 2016. (Shortened to SST CCI analysis.)

1.2 Structure of the Document

After this introduction, the document is divided into a number of major sections that are briefly described below:

Section 2 gives an Executive Summary of the key scientific results.

Section 3 presents an assessment of trends and variability in the CDR2.0 products and comparison to other SST products. In order to assess the multi-annual and decadal behaviour of the long-term products, comparisons are made to existing SST data sets used in high profile monitoring reports. Differences between the SST CCI products and the comparison datasets are highlighted. The SST CCI products are also assessed against their Release version 1.0 counterparts from Phase 1 of the SST CCI project to determine what progress has been achieved.

Section 4 details voluntary reports received from registered users of the SST CCI products, describing their application and what they have discovered from using the products.

Section 5 lists any further reported issues identified by registered users and any other recommendations they have made for future SST CCI products.

1.3 Referenced Documents

The following is a list of documents with a direct bearing on the content of this report. Where referenced in the text, these are identified as RD.n, where 'n' is the number in the list below:

RD.72	Rayner, N.A., P.Brohan, D.E.Parker, C.K.Folland, J.J.Kennedy, M.Vanicek, T.Ansell and S.F.B.Tett 2006: Improved analyses of changes and uncertainties in sea surface temperature measured in situ since the mid-nineteenth century: the HadSST2 data set. <i>Journal of Climate</i> , 19(3) pp. 446-469
RD.74	Rayner, N. A.; Parker, D. E.; Horton, E. B.; Folland, C. K.; Alexander, L. V.; Rowell, D. P.; Kent, E. C.; Kaplan, A. (2003) Global analyses of sea surface temperature, sea ice, and night marine air temperature since the late nineteenth century <i>J. Geophys. Res.</i> Vol. 108, No. D14, 4407 10.1029/2002JD002670
RD.76	Reynolds, Richard W., Thomas M. Smith, Chunying Liu, Dudley B. Chelton, Kenneth S. Casey, Michael G. Schlax, 2007: Daily High-Resolution-Blended Analyses for Sea Surface Temperature. <i>J. Climate</i> , 20, 5473–5496. doi: http://dx.doi.org/10.1175/2007JCLI1824.1
RD.79	Smith, T.M., R.W. Reynolds, Thomas C. Peterson, and Jay Lawrimore, 2008: Improvements to NOAA's Historical Merged Land-Ocean Surface Temperature Analysis (1880-2006). <i>Journal of Climate</i> , 21, 2283-2296.
RD.85	Ishii, M., Shouji, A., Sugimoto, S. and Matsumoto, T. (2005), Objective analyses of sea-surface temperature and marine meteorological variables for the 20th century using ICOADS and the Kobe Collection. <i>Int. J. Climatol.</i> , 25: 865–879. doi: 10.1002/joc.1169
RD.103	Berry, David I.; Kent, Elizabeth C. 2011 Air–Sea fluxes from ICOADS: the construction of a new gridded dataset with uncertainty estimates. <i>International Journal of Climatology</i> , 31 (7). 987-1001. 10.1002/joc.2059
RD.210	Kennedy J.J., Rayner, N.A., Smith, R.O., Saunby, M. and Parker, D.E. (2011b). Reassessing biases and other uncertainties in sea-surface temperature observations since 1850 part 1: measurement and sampling errors. <i>J. Geophys. Res.</i> , 116, D14103, doi:10.1029/2010JD015218
RD.211	Kennedy J.J., Rayner, N.A., Smith, R.O., Saunby, M. and Parker, D.E. (2011c). Reassessing biases and other uncertainties in sea-surface temperature observations since 1850 part 2: biases and homogenisation. <i>J. Geophys. Res.</i> , 116, D14104, doi:10.1029/2010JD015220
RD.212	Reynolds, R.W., N.A. Rayner, T.M. Smith, D.C. Stokes, and W. Wang, 2002: An improved in situ and satellite SST analysis for climate. <i>J. Climate</i> , 15, 1609-1625
RD.216	Casey, K.S., T.B. Brandon, P. Cornillon, and R. Evans (2010). "The Past, Present and Future of the AVHRR Pathfinder SST Program", in <i>Oceanography from Space: Revisited</i> , eds. V. Barale, J.F.R. Gower, and L. Alberotanza, Springer. DOI: 10.1007/978-90-481-8681-5_16.
RD.239	Roberts-Jones, Jonah, Emma Kathleen Fiedler, Matthew James Martin, 2012: Daily, Global, High-Resolution SST and Sea Ice Reanalysis for 1985–2007 Using the OSTIA System. <i>J. Climate</i> , 25, 6215–6232. doi: http://dx.doi.org/10.1175/JCLI-D-11-00648.1

RD.299	Merchant C J, Harris A R, Murray M J and Zavody A M (1999), Toward the elimination of bias in satellite retrievals of skin sea surface temperature 1. Theory, modeling and inter-algorithm comparison, <i>J Geophys Res</i> , 104, C10, 23565-23578.
RD.326	Atkinson, C.P., N.A. Rayner, J. Roberts-Jones, R.O. Smith (2013), Assessing the quality of sea surface temperature observations from drifting buoys and ships on a platform-by-platform basis. <i>Journal of Geophysical Research - Oceans</i> , 118, 3507–3529, doi:10.1002/jgrc.20257.
RD.330	ESA SST CCI Product Validation and Intercomparison Report
RD.332	Woodruff, S.D., S.J. Worley, S.J. Lubker, Z. Ji, J.E. Freeman, D.I. Berry, P. Brohan, E.C. Kent, R.W. Reynolds, S.R. Smith, and C. Wilkinson, 2011: ICOADS Release 2.5: Extensions and enhancements to the surface marine meteorological archive. <i>Int. J. Climatol. (CLIMAR-III Special Issue)</i> , 31, 951-967 (doi:10.1002/joc.2103).
RD.334	Rayner, N. A., J. J. Kennedy, R. O. Smith and H. A. Titchner (2013) The Met Office Hadley Centre Sea Ice and Sea Surface Temperature data set, version 2, part 3: the combined analysis. In prep. for <i>JGR Atmospheres</i>
RD.341	Good, S.A., M.J. Martin and N.A. Rayner (2013) EN4: Quality controlled ocean temperature and salinity profiles and monthly objective analyses with uncertainty estimates, <i>Journal of Geophysical Research: Oceans</i> , doi: 10.1002/2013JC009067.
RD.342	Kaplan, A., Y. Kushnir, M. Cane, and M. Blumenthal (1997) Reduced space optimal analysis for historical data sets: 136 years of Atlantic sea surface temperatures, <i>J. Geophys. Res.</i> , 102, 27,835– 27,860
RD.343	Lanzante, J.R. (1996), Resistant, Robust and Non-Parametric Techniques for the Analysis of Climate Data: Theory and Examples, Including Applications to Historical Radiosonde Station Data. <i>Int. J. Climatol.</i> , 16: 1197–1226. doi: 10.1002/(SICI)1097-0088(199611)16:11<1197::AID-JOC89>3.0.CO;2-L
RD.371	SST CCI Climate Assessment Report (CAR), SST_CCI-CAR-UKMO-001, Issue 1, 24 January 2014 http://www.esa-sst-cci.org/sites/default/files/Documents/public/SST_CCI-CAR-UKMO-001-Issue_1-signed-accepted.pdf
RD.389	Yeo, S.-R., and K.-Y. Kim (2015), Decadal changes in the Southern Hemisphere sea surface temperature in association with El Niño-Southern Oscillation and Southern Annular Mode, <i>Clim. Dyn.</i> , doi: 10.1007/s00382-015-2535-z.

1.4 Definitions of Terms

The following terms have been used in this report with the meanings shown.

Term	Definition
AATSR	Advanced Along-Track Scanning Radiometer
AMSR	Advanced Microwave Scanning Radiometer
ATSR	Along-Track Scanning Radiometer
ATSR-1	First ATSR instrument
ATSR-2	Second ATSR instrument
AVHRR	Advanced Very High Resolution Radiometer
CAR	Climate Assessment Report
CCI	Climate Change Initiative
COBE	Centennial in situ Observation-Based Estimates of variability of SSTs
DMI	Dipole Mode Index
EN4	Met Office Hadley Centre dataset
ENSO	El Niño Southern Oscillation
ERA-CLIM	ECWMF Reanalysis Archive for Climate
ERSSTv3	Extended Reconstruction SST V3
ESA	European Space Agency
GAC	Global Area Coverage
HadISST	Hadley Centre Global sea-Ice coverage and SST
HadSST	Hadley Centre Sea Surface Temperature
ICOADS	International Comprehensive Ocean-Atmosphere Data Set
K	Kelvin
L2P	Level 2 (Pre-processed)
L3U	Level 3 uncollated
L4	Level 4
LT	Long term products
NOAA	National Oceanic and Atmospheric Administration (USA)
NOCS	National Oceanographic Centre Southampton
OI	Optimum interpolation
OI.v2	Reynolds et al (2002) Optimal Interpolation analysis
OSTIA	Ocean Surface Temperature and Ice Analysis
PVIR	Product Validation and Inter-comparison Report
RD	Reference Document
SST	Sea Surface Temperature
TAMG	Tropical Atlantic Meridional SST Gradient

2. EXECUTIVE SUMMARY

Here we provide a bullet point summary of the key points from this Climate Assessment Report (CAR). The ESA SST CCI version 2.0 products assessed are:

- ATSR. SSTs from ATSR instruments in L3U format at 0.05° latitude by 0.05° longitude resolution covering 1991 – April 2012. (Hereafter, SST CCI v2.0 ATSR.)
- AVHRR. SSTs from AVHRR instruments in L2P format at Global Area Coverage (GAC) resolution covering 24th August 1981 – 2016. (Hereafter, SST CCI v2.0 AVHRR.)
- Analysis. Satellite-only SST-depth L4 daily analysis created by the Operational Sea Surface Temperature and sea Ice Analysis (OSTIA) system from the SST CCI v2.0 ATSR and SST CCI v2.0 AVHRR products at 0.05° latitude by 0.05° longitude resolution covering (September 1981 – 2016). (Hereafter, SST CCI v2.0 analysis.)

These are utilised over the full period, September 1981-2016.

Comparison of SST CCI products to other climate SST data sets and SST CCI v1.0 products (Section 3 and 4):

- SST CCI v2.0 products now extend back to September 1981, providing over 36 years of satellite-derived SST information
- The SST CCI v2.0 AVHRR retrievals are much improved over the SST CCI v1.0 retrievals.
- The SST CCI v2.0 ATSR retrievals are also much improved during the period following the eruption of Mt Pinatubo in 1991 and the failure of ATSR-1.
- Some potentially undesirable features remain to be improved, these include: apparently erroneous SSTs in 1982/3 (very localised in time, but a large enough effect to be reflected in the decadal average anomaly map for 1982-1991) and dust contamination in northern Indian Ocean and eastern tropical Atlantic. Users should use the data for the period 01/10/1982-30/09/1983 with caution.
- Over the period, 1982-2016, the SST CCI v2.0 products show linear trends which are consistent with those of the comparison data sets in all regions except the North Pacific and the eastern tropical Atlantic. The North Pacific is an area of extensive stratus cloud and is also an area where SST data sets often disagree.
- SST anomaly time series in the Nino regions in the Pacific demonstrate that SST CCI v2.0 products are consistent with the comparison data sets here.
- In the sub-period with the best observational coverage, 1991-2010, the autocorrelation in the different SST CCI v2.0 products is highly consistent and likely provides a good measure of the real persistence in the SST field.
- The GHRSSST Multi-Product Ensemble (GMPE) has been used to compare and assess different long-term analyses. The SST CCI analysis v2.0 was found to perform relatively well compared to other analyses (except CMC) when compared to independent Argo data. The SST CCI analysis v2.0 data were found to be cooler than the Argo data. There are larger differences between the SST CCI

analysis v2.0 and the GMPE median prior to 1991. Gradients in SST CCI analysis v2.0 are sharper and larger than the other analyses in the Gulf Stream region

Use of SST CCI products in dedicated modelling experiments undertaken by the Climate Research Group (Section 5):

- We have analysed the influence of using the SST CCI analysis v2.0 as lower boundary forcing in atmosphere-only simulations at two horizontal resolutions, compared with the influence of using the HadISST.2.2.0.0 dataset.
- Overall, the impact of using SST CCI analysis v2.0 is relatively small, particularly in comparison with the influence of increasing the model's horizontal resolution.
- Where changes are seen, they are sometimes beneficial and sometimes detrimental.
- The warmer SST around the Maritime Continent and cooler SST at the equatorial Atlantic and the Eastern Boundary Upwelling regions seem to reduce the bias in cloud regimes and radiation there. However, it is not clear whether this is because these SST values are closer to reality, or these SST values are artefacts of aerosols and clouds which overcast the surface and such temperature is preferred by parameterizations for representing organized convection or boundary-layer clouds more realistically.
- The smaller sea ice cover in the SST CCI analysis v2.0 reduces the overestimate of the frequency of clear-sky over the regions when compared to International Satellite Cloud Climatology Project (ISCCP) information, which suggests that the sea ice fraction in the CCI dataset is more consistent with the sea ice product used in ISCCP.
- No significant impact of the smaller sea ice fraction on atmospheric phenomena was found.
- Comparison of the atmospheric run with two different SST datasets was a good opportunity to investigate the influence of the range of uncertainty in observational SST data and estimate the local and remote impacts.

Key points arising from use of the SST CCI products by trail blazer users (Section 6):

- The SST CCI analysis v2.0 data provided a relatively flexible and accurate reference for climatology comparison studies.
- The long reference period of SST CCI analysis v2.0 data provides a convincing SST climatology.
- SST climatology datasets derived from SST CCI analysis v2.0 data are highly consistent with tropical mooring measurements in the western Pacific.
- SST CCI analysis v2.0 provided a longer time span of data than SST CCI analysis v1.0 enabling comparison to more coral monitoring sites and *in situ* data
- SST CCI analysis v2.0 and the NOAA CoralTemp gridded SST products both provide a good representation of daily subsurface temperatures, by comparison to near-coral logger temperature data at depths 3 – 6 m.

- Differences in trends exist between the SST CCI analysis v2.0 and NOAA CoralTemp products that will lead to different estimates of coral stress due to changing temperatures.
- SST CCI analysis v2.0 compares well with the *in situ* observations at the locations considered off Belize and Florida.
- Reprocessed SSTs are a key data source for regional ocean reanalysis. The requirement is for SST observations with small bias, good coverage, and with consistent processing (no jumps) over a long period. The SST CCI v2.0 product is the major source of observation data in this reanalysis. It ensures that the reanalysis sea surface temperature is realistic and coherent geographically and through time. Well-constrained temperatures at the surface influence the full 3D ocean dynamics and so also contribute to the accuracy of the reanalysis at depth.
- SST CCI analysis v2.0 provides a spatial and temporal coverage of the sea surface temperature field that is essential for climate studies over the Eastern Atlantic where *in situ* data are sparse and insufficient.
- SST CCI analysis v2.0 agreed within 0.3 to 0.4°C with oceanic (offshore) buoys and within 0.3 to 0.8°C for coastal buoys in Portuguese marine waters.
- SST CCI analysis v2.0 captured the overall seasonal and inter-annual variability and magnitude of the surface temperature measured by the moored buoys in Portuguese marine waters.
- A first evaluation of ENSO in the coupled climate model EC-Earth3-Veg using SST CCI analysis v2.0 showed that the model has a substantially reduced cold tongue bias and the seasonal variability has improved compared to EC-Earth2. However, the eastern tropical Pacific Ocean warm bias remains and the variability for this region is underestimated.
- SST CCI analysis v2.0 data is found to be very useful for investigating ENSO variability for the last 30+ years and for evaluation of climate models. For the longer perspective of ENSO and other climate variability the SST CCI data can be used in combination with HadISST1.1.
- It is beneficial to have high temporal and spatial resolution consistent SST data with uncertainties, for process studies, evaluation of climate models and for initialisation of seasonal and decadal climate predictions.

Feedback on ease of use of the products (Section 7):

- The SST CCI analysis v2.0 data files are well organised and contain essential information, thus very easy to use.
- It would help users if short information is supplied in the data access folder, e.g. a README file describing the data sets.
- It would have been useful to have a climatology (or sets of climatologies with different base periods) provided
- The use of NetCDF format makes the data technically straightforward to use.

- Daily global datasets are readily accessible and easy to work with. The processing and analysis of the data during this work was performed using SNAP and Python 2.7 and no relevant problems were encountered.
- The documentation (SST_CCI-PUG-UKMO-001) was clear and sufficient to understand the data and use it.
- The ESA CCI SST website contains valuable information on how to process the data (making monthly means) and on using a “simulator”. A link to that web page could also be included in the README file.

Further recommendations for the future (Section 7):

- Provision of monthly mean SST CCI analysis v2.0 files are suggested alongside the daily files.
- Producing a night-only SST CCI analysis v2.0 would enable it to be used for applications that require a consistent night-time SST, such as coral bleaching studies.
- The temporal and spatial resolution of the SST CCI analysis v2.0 product are sufficient for open ocean studies, but with finer spatial resolution the data could be extended to coastal and shelf areas. A spatial resolution of 1 km could considerably improve the results in shallower areas (less than 100m depth).
- It would be good to make the data available through Obs4MIP, including a link to the “simulator” so modellers compare the “same thing”.
- Variance of SST in SST CCI v2.0 is implied to be smaller than in HadISST.2.2.0.0 over the tropical ocean, except the Eastern Pacific at various timescales (daily, intra-seasonal, inter-annual). Construction of the dataset with a longer time period would be useful to verify the results on the interannual timescale.
- Studies such as Klein and Hartmann (1993), Qu et al (2014), Brient and Schneider (2016) produced metrics to evaluate the seasonal variation/interannual variation of the stratocumulus regime with the local SST variation. Accurate observations of the SST over the region, as well as the Maritime Continent and the surrounding region, is critical for such metrics.
- It would be useful to examine the regions in which the SST CCI product has cooler SST than other datasets (in the tropical-subtropical Atlantic, Indian Ocean); hypothesised to be due to dust contamination. The tropical cyclone analysis suggests that this can impact on simulation performance, and hence it would be useful to know which dataset should be trusted more.
- While we have compared the influence of two daily SST and sea-ice datasets in our dedicated modelling experiments, the usage of daily SST is not necessarily common in the climate model community. For example, standard Coupled Model Intercomparison Project atmosphere-only experiments (including those for the current CMIP6) are forced with interpolated monthly SSTs. Klingaman et al (2008) conducted atmosphere-only (AGCM) experiments with daily SST, analysed the active/break cycles of the monsoon and showed that “high-frequency SST anomalies not only increased variance in intra-seasonal rainfall but helped to organize and maintain coherent convective events, such as northward-propagating intra-seasonal oscillation (NPISO). Further, the results indicate that an AGCM can respond to realistic and frequent SST forcing to generate an NPISO that closely resembles observations. These results have

important implications for simulating the NPISO in AGCMs and coupled climate models, as well as for predicting tropical intra-seasonal variability in short- and medium-range weather forecasts.” Their results suggest that daily SSTs do make a difference to shorter-timescale variability, and may affect longer timescales. This could be investigated in future work to further investigate the value of using daily data, like the SST CCI dataset.

- The stratocumulus regime is the biggest source of cloud feedback uncertainty. Many metrics/diagnostics have been developed to investigate this. The stratocumulus regime in climate models is less frequent than observed but too bright. SST in the stratocumulus region given to the model could partly contribute to the biases in models. The SST dataset used in CMIP Model Intercomparison projects has a different spatial pattern from the SST CCI analysis v2.0. Examination of the impact of these differences will be useful for the community.

3. ASSESSMENT OF TRENDS AND VARIABILITY IN SST CCI PRODUCTS AND COMPARISON TO OTHER PRODUCTS

This section assesses the trends and variability in the ESA SST CCI v2.0 products and compares them to other SST products to determine to what extent the new SST CCI products are credible Climate Data Records. The SST CCI v2.0 products are also assessed against SST CCI v1.0 products to determine what progress has been achieved.

3.1 Introduction

In order to assess the multi-annual and decadal behaviour of the SST CCI v2.0 products, comparisons are made to existing lower resolution SST data sets. These data sets include those used in high profile monitoring reports. Differences between the SST CCI products and the comparison datasets are highlighted.

3.2 Data sets

SST CCI v2.0 products assessed are:

- ATSR. SSTs from ATSR instruments in L3U format at 0.05° latitude by 0.05° longitude resolution covering 1991 – April 2012. (Hereafter, SST CCI v2.0 ATSR.)
- AVHRR. SSTs from AVHRR instruments in L2P format at Global Area Coverage (GAC) resolution covering 24th August 1981 – 2016. (Hereafter, SST CCI v2.0 AVHRR.)
- Analysis. Satellite-only SST-depth L4 daily analysis created by the Operational Sea Surface Temperature and sea Ice Analysis (OSTIA) system from the SST CCI v2.0 ATSR and SST CCI v2.0 AVHRR products at 0.05° latitude by 0.05° longitude resolution covering (September 1981 – 2016). (Hereafter, SST CCI v2.0 analysis.)

These are compared to the following data sets over the period 1982-2016.

3.2.1 GRIDDED REFERENCE DATA

This data set comprises quality-improved in situ observations from ships and buoys from Atkinson et al. (2013, RD.326) with near-surface observations from Argo profiling floats from EN4 [Good et al (2013), RD.341]. The ship and buoy data are a subset of those used to create HadSST3 (Section 3.2.2). Data from these two sources were averaged onto a regular 5-degree latitude by 5-degree longitude grid at monthly resolution using the method of Rayner et al. (2006, RD.72). The data were not bias adjusted.

This data set will be referred to as the “gridded reference data set” since it comprises information from the reference data set utilised in the PVIR [RD.330, their Section 4.2.4, information reproduced below] together with measurements from ships that have undergone additional quality checking.

The ship and buoy data are a blend of observations taken from ICOADS 2.5 (Woodruff et al., 2011; RD.332) and Met Office Hadley Centre QC flags. The QC flags provided have been produced by the HadISST2 QC system. The general QC procedures are described in Rayner et al. (2006; RD.72) and the high-resolution background climatology and land-sea mask used by this system is described in Rayner et al. (2013; RD.334). This system carries out the following suite of checks: (i) observations are checked for a meaningful location, date and time and that they are not surrounded on all sides by land, (ii) each

platform with an individual callsign is tracked to verify its reported position, speed and direction (those without a callsign or with a generic callsign, e.g. SHIP, are passed unchecked), (iii) each SST observation is checked that it is above the freezing point of seawater and within $\pm 8^{\circ}\text{C}$ of the 1961-1990 background climatology interpolated to that day, (iv) each SST observations has a “buddy check” applied which compares the value of an individual SST anomaly to the mean anomaly from neighbouring observations; individual observations differing too much from their neighbours are flagged as bad. The HadSST2 QC flags have been supplemented as follows:

1. Drifting buoy SST observations from ICOADS deck 715 have been blacklisted as investigation suggests they are of variable quality. An ICOADS deck identifies the source of the data and refers to the decks of punched cards on which earlier versions of the data set were based. Deck 715 identifies ‘German Deep Drifter Data’ (originally collected by the Institut für Meereskunde, at the University of Kiel) and provides < 2% of the drifting buoy observations in ICOADS 2.5.
2. Drifting buoy and ship SST observations have an additional QC flag set which follows the procedures described in Atkinson et al. (2013; RD.326). This flag is generated by tracking the quality of observations made by individual drifting buoys and ships over time using the Met Office Operational Sea surface Temperature and sea Ice Analysis (OSTIA) as a reference (a globally complete satellite based analysis). It differs from the SST checks described above in that observation quality is tracked over time to detect biases/instrument failures etc., rather than assessing observations individually. Drifting buoys observations are flagged where they are deemed to be too biased or too noisy, or a buoy is deemed to be out of water having run aground or been picked up. Ship observations are flagged when observations from a particular ship (identified by its callsign) are deemed unreliable (i.e. if a ship callsign is blacklisted all observations from this ship are flagged). In general, ship observations are of variable quality and this flag is intended to reduce ship observations to a higher quality subset; the extra QC excludes between 50 and 60% of ship observations. The development of this extra QC step was funded by the FP7 ERA-CLIM project.

3.2.2 HADSST3

HadSST3 [Kennedy et al. 2011b, RD.210; Kennedy et al. 2011c, RD.211] is an in situ-only data set. Individual observations from International Comprehensive Ocean-Atmosphere (ICOADS) Release 2.5 [Woodruff et al. 2011, RD.332] are averaged onto a 5-degree latitude by 5-degree longitude grid at monthly resolution using the method of Rayner et al. (2006, RD.72). The ship and buoy data used in the gridded reference data set (see above Section 3.2.1) are a subset of the ship and buoy data in HadSST3. Adjustments are applied to the gridded data to account for the effect of systematic errors associated with changes in measurement methods over time. In the period examined here, the principal change is the switch from mostly ship-based observations in the 1980s to a mixture of ship and buoy observations in the late 2000s. Because the exact size of the systematic errors is not known, the data set is presented as an ensemble of 100 different versions (realisations), which are indicative of the uncertainty in the adjustments applied. Parameters used in the statistical modelling of the biases are varied within their likely ranges to produce an ensemble of bias adjustments. These are then used to create the ensemble of adjusted SST anomaly fields. In addition to the uncertainty associated with the adjustments, there are uncertainties arising from measurement and sampling errors and these are also used.

3.2.3 AVHRR PATHFINDER

The Advanced Very High Resolution Radiometer instruments measure top of atmosphere radiances in the infrared part of the spectrum. AVHRRs have flown on US National

Oceanographic and Atmospheric Administration (NOAA) polar orbiting satellites since the early 1980s. The measured radiances can be used to estimate SSTs. This is usually done using coefficients estimated from a regression against drifting buoy or ship data that also vicariously adjusts the AVHRR instrument calibration. Pathfinder v5.2 [Casey et al. 2010, RD.216] is a consistent reprocessing of the AVHRR data from 1981 to 2007. The version used in this analysis was presented on a 1/24-degree equidistant cylindrical grid.

3.2.4 HADISST

Met Office Hadley Centre sea Ice and SST (HadISST) is a globally complete analysis of sea-surface temperature and sea-ice concentrations. It is based on in situ and satellite (AVHRR) measurements of SST. Gaps in the data coverage are filled using a statistical technique known as Reduced Space Optimal Interpolation (Kaplan et al. 1997, RD.342). In areas of the ocean where there is an estimated non-zero sea ice concentration, the SST is inferred from the sea ice concentration. HadISST1.1 [Rayner et al. 2003, RD.74] is presented on a 1-degree latitude by 1-degree longitude monthly grid, although the anomaly analysis is performed on a 2-degree latitude by 2-degree longitude grid (and then added to a 1-degree latitude by longitude climatology) in the modern period (1949 onwards) including the whole period covered in this report.

3.2.5 ERSSTV3B

Extended Reconstruction SST (ERSSTv3b, Smith et al. 2008, RD.79) is another globally complete SST data set. It is based on in situ measurements of SST and uses a combination of Empirical Orthogonal Teleconnections and a low-frequency smoothing to reconstruct SSTs globally. ERSSTv3b is presented on a 2-degree latitude by 2-degree longitude grid. The grid is offset by one degree latitudinally, such that the equator passes through the centre of one of the grid boxes rather than forming the boundary of one of the grid boxes.

3.2.6 COBE SST

The Centennial in situ Observation-Based Estimates of the variability of SSTs (COBE SST, [Ishii et al. 2005, RD.85]) is a globally complete SST data set based on in situ data. The data are reconstructed using optimal interpolation. In the absence of data the reconstruction relaxes to the climatological average. In marginal ice zones, SSTs are inferred from sea ice concentrations. The data are presented on a 1-degree latitude by 1-degree longitude monthly grid.

3.2.7 NOCS SURFACE FLUX DATA SET V2.0

The National Oceanography Centre, Southampton Surface Flux data set [Berry et al. 2011, RD.103] is based on ship data from ICOADS Release 2.1. The daily data are reconstructed using optimal interpolation. In the absence of data the reconstruction relaxes to the climatological average. The data are presented on a 1-degree latitude by 1-degree longitude daily or monthly grid. The monthly grids were used herein.

3.2.8 OI.V2

The Reynolds et al. [2002, RD.212] weekly and monthly OI.v2 is based on in situ and satellite data. The satellite SST retrievals come from the AVHRR series of instruments and biases in the data are adjusted to more closely match the in situ data. The resulting fields are interpolated using optimal interpolation and the data are presented on a 1-degree latitude by 1-degree longitude weekly and monthly grid. The monthly grids are used herein.

3.2.9 MYOCEAN OSTIA REANALYSIS

The Operational Sea Surface Temperature and Sea Ice Analysis (OSTIA) reanalysis v1.0 [Roberts-Jones et al. 2012, RD.239] from 1985 to 2007 is based on reprocessed satellite and in situ measurements. AVHRR Pathfinder SSTs and retrievals from the ATSR instruments are combined with data from ICOADS Release 2.1 using a multiscale optimal-interpolation scheme. The data are presented on a 0.05-degree latitude by 0.05-degree longitude daily grid.

3.2.10 DAILY OI

Two varieties of the Daily optimum interpolation (OI) version 2 [Reynolds et al. 2007, RD.76] data set were used. One incorporates AVHRR and in situ SSTs and runs from 1981 to present. The other incorporates AVHRR, Advanced Microwave Scanning Radiometer (AMSR-E) and in situ SSTs and runs from 2002 to 2011 covering the period of operation of the AMSR-E instrument. Both varieties use an optimal interpolation scheme to reconstruct missing values and are presented on a 0.25-degree latitude by 0.25-degree longitude daily grid.

3.3 Methods

The SST CCI products and the comparison data sets are presented on a range of different grids and also, in those cases where the data are presented as anomalies, relative to different climatological averages. In order to make a direct comparison, the data were first converted into anomalies relative to the MyOcean OSTIA reanalysis climatology for the period 1985-2007. The climatology was regridded from 0.05-degree latitude by 0.05-degree longitude daily to have the same resolution as the data set being processed. Secondly, a common mask was applied to the data. Again this was based on the MyOcean OSTIA reanalysis climatology.

3.3.1 LINEAR TRENDS

Time series of area-averaged temperatures were calculated from each of the data sets for the regions shown in Figure 3-1. Area averages were calculated as a weighted average of all non-missing grid box values within the area. The weights were proportional to the area of ocean within the grid box. In coastal grid boxes which were not entirely covered by ocean, the area of ocean was estimated using the OSTIA reanalysis climatology. Grid boxes in the climatology, which had an assigned SST, were assumed to be 100% ocean.

Area averages were calculated for each data set with its native coverage and also after the coverage had been reduced to that of HadSST3. To reduce the coverage to that of HadSST3, each data set first had to be regridded to 5-degree resolution.

Linear trends in the area averages were calculated from all non-missing monthly values using the ordinary least squares method. A resistant method for estimating the trends – median of pairwise slopes [Lanzante 1996, RD.343] - was also used (not shown) to check that outliers did not have a strong effect on the results. Little difference was seen in any region, apart from the Nino 1+2 and Nino 3 regions, where the resistant method increased the trends relative to those calculated using the ordinary last squares method over both 1982-2016 and 1992-2010. Trends were calculated over two periods, 1982-2016 and 1992-2010 (the latter period to enable comparison between SST CCI v1.0 and v2.0 products).

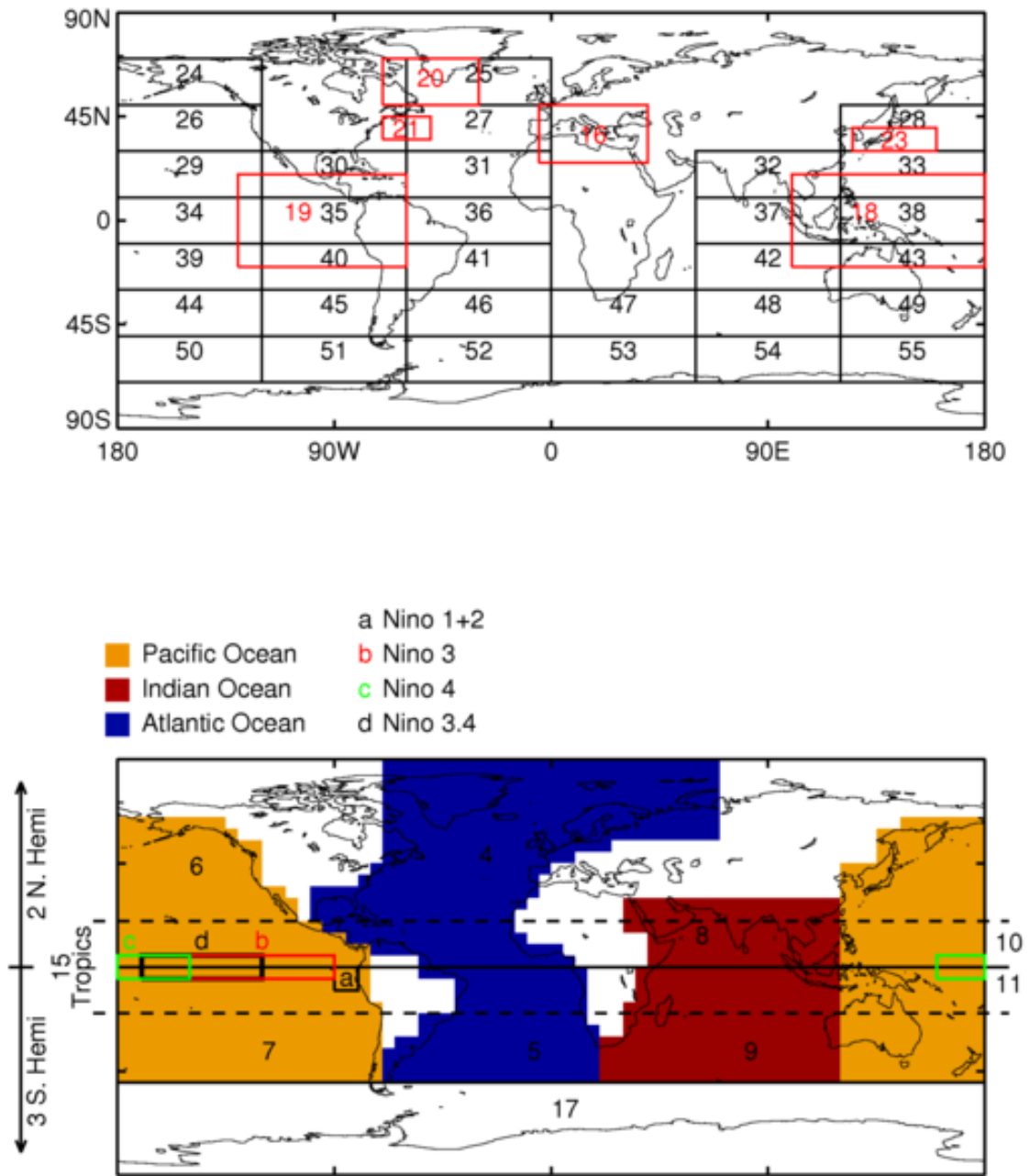


Figure 3-1. Maps showing regions used in the analysis of trends and indices. The regions are also regions are also described in

Table 3-1.

Table 3-1. List of regions used for the analysis of trends. The regions are shown in Figure 3-1.

Region Name	Region Number	Region Name	Region Number
Globe	1	Area 30°-50°N, 120°-180°E	28
Northern Hemisphere	2	Area 10°-30°N, 180°-120°W	29
Southern Hemisphere	3	Area 10°-30°N, 120°-60°W	30
North Atlantic Ocean	4	Area 10°-30°N, 60°-0°W	31
South Atlantic to 50°S	5	Area 10°-30°N, 60°-120°E	32
North Pacific Ocean	6	Area 10°-30°N, 120°-180°E	33
South Pacific to 50°S	7	Area 10°N-10°S, 180°-120°W	34
North Indian Ocean	8	Area 10°N-10°S, 120°-60°W	35
South Indian Ocean to 50°S	9	Area 10°N-10°S, 60°-0°W	36
Northern Tropics	10	Area 10°N-10°S, 60°-120°E	37
Southern Tropics	11	Area 10°N-10°S, 120°-180°E	38
Atlantic Ocean to 50°S	12	Area 10°-30°S, 180°-120°W	39
Pacific Ocean to 50°S	13	Area 10°-30°S, 120°-60°W	40
Indian Ocean to 50°S	14	Area 10°-30°S, 60°-0°W	41
Tropics (20°N-20°S)	15	Area 10°-30°S, 60°-120°E	42
Mediterranean	16	Area 10°-30°S, 120°-180°E	43
Southern Ocean, 50°S Southwards	17	Area 30°-50°S, 180°-120°W	44
Western Tropical Pacific	18	Area 30°-50°S, 120°-60°W	45
Eastern Tropical Pacific	19	Area 30°-50°S, 60°-0°W	46
Greenland 50°-70°N, 30°-70°W	20	Area 30°-50°S, 0°-60°E	47
Gulfstream 35°-45°N 50°-70°W	21	Area 30°-50°S, 60°-120°E	48
Southern Hemisphere and Northern Indian Ocean minus rest of NH	22	Area 30°-50°S, 120°-180°E	49
Kuroshio 30°-40°N, 125°-160°E	23	Area 50°-70°S, 180°-120°W	50
Area 50°-70°N, 180-120W	24	Area 50°-70°S, 120°-60°W	51
Area 50°-70°N, 60°-0°W	25	Area 50°-70°S, 60°-0°W	52
Area 30°-50°N, 180°-120°W	26	Area 50°-70°S, 0°-60°E	53
Area 30°-50°N, 60°-0°W	27	Area 50°-70°S, 60°-120°E	54
		Area 50°-70°S, 120°-180°E	55

3.3.2 INDICES

In addition to the time series for the regions described in Figure 3-1 and

Table 3-1, indices for certain standard modes of variability were also calculated. These were:

1. Niño 1+2 [0°-10°S, 90°-80°W]
2. Niño 3 [5°N-5°S, 150°W-90°W]
3. Niño 4 [5°N-5°S, 160°E-150°W]
4. Niño 3.4 [5°N-5°S, 170°W-120°W]
5. Dipole Mode Index (DMI) calculated as the difference between the area-average SST anomalies for the regions [50°-70°E, 10°S-10°N] and [90°-110°E, 10°S-10°N]
6. Tropical Atlantic Meridional SST gradient (TAMG) calculated as the difference between the area-average SST anomalies for the regions [60°W-African Coast, 5°-28°N] and [60°W-20°E, 20°S-5°N]

These six indices are all based on area-averages which were calculated in the same way as for the area averages in Section 3.3.1.

3.3.3 MULTI-ANNUAL AND DECADEAL AVERAGES

Decadal averages were calculated for the periods 1982-1991, 1991-2000 and 2001-2010. An average was calculated when at least 30% of monthly values were non-missing.

3.3.4 AUTOCORRELATIONS

Lagged correlations were calculated for each data set. In order to make a direct comparison, all data sets were re-gridded to 5-degree monthly resolution. Lag correlations at lags of 1, 2, 3 and 4 months were calculated in all grid boxes for which at least 30% of monthly values were non-missing.

3.4 Results

3.4.1 TIME SERIES, LINEAR TRENDS AND INDICES

3.4.1.1 GLOBAL AVERAGE SST ANOMALY

The SST anomaly time series calculated for this analysis (of which a subset is presented in this section) provide a useful means for assessing the relative biases and evolution of variability in the different data sets considered.

In terms of climate variability over the 1981-2016 period of interest, several well-known phenomena are observed in the global-average SST anomalies (Figure 3-2). In particular:

- a cooling and subsequent recovery of SSTs over several years following the eruptions of El Chichòn in 1982 and Mount Pinatubo in 1991;
- a sharp warming and subsequent cooling caused by strong El Niño events in 1982/1983, 1997/1998 and 2015-2016;
- La Niña events in 1983-1985, 1988-1989, 1995-1996 and 2016-2017 and successive La Niñas from 1998-2001; and

- enhanced interannual variability related to a sequence of La Niña–El Niño–La Niña events over the period 2007–2012.

In addition, there has been a general warming of global SST over this period, as seen in global and hemispheric trends (Figure 3-10).

Figure 3-2 shows the global-average SST anomaly for each of the SST CCI products, the comparison data sets, and the SST CCI v1.0 products. We see generally good agreement, but a number of differences between the data sets is worth highlighting here.

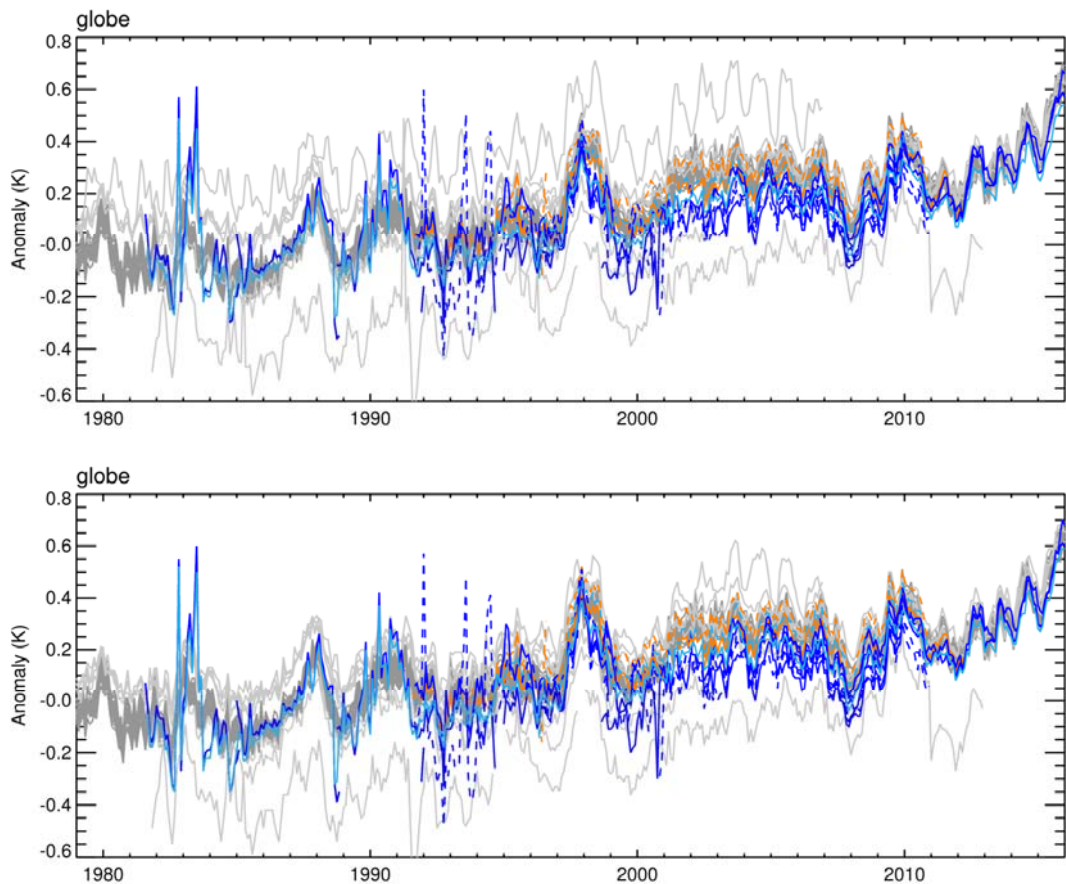


Figure 3-2. Top: Global average SST anomaly (K, relative to MyOcean OSTIA reanalysis climatology) for each of the comparison data sets (grey) and the SST CCI v2.0 products (solid lines) [SST CCI ATSR: orange, SST CCI AVHRR: blue, SST CCI analysis: cyan]. SST CCI v1.0 are shown as dashed lines. For SST CCI ATSR and SST CCI AVHRR there is one line for each individual satellite. Bottom: collocated comparison.

With the exception of a number of individual months, the SST CCI v2.0 AVHRR series retrievals provide an evolution of SST that is consistent with current understanding. Many of the comparison data sets (with the exception of the SST CCI v1.0 and 2.0 products) include measurements made *in situ*. The SST CCI v1.0 and 2.0 products do not, although the v2.0 products use *in situ* SST to aid the calibration of the AVHRR SSTs prior to 1991. Consequently, the generally good agreement between the different components of the observing system (satellite retrievals and *in situ* measurements) is reassuring.

In the SST CCI v1.0 products, there was a disagreement of order 0.1 K between the SST retrievals from the ATSR-series and the AVHRR-series over their period of overlap

(compare the dark blue and orange dashed lines). The SST CCI v1.0 analysis took values between these two input series. In the v2.0 SST CCI products, there is a much higher degree of consistency between the retrievals from the two sets of sensors (compare the dark blue and orange solid lines), particularly in the mean. Consequently, the SST CCI v2.0 analysis is more similar to both sets of retrievals.

The period of retrievals from the AATSR sensor, between 2002 and 2012, is one during which greater difference is observed between the SST CCI v2.0 products and the comparison data sets; the SST CCI v2.0 products are relatively cool then. This relative coolness continues thereafter and is particularly noticeable when comparing the non-collocated global mean SST anomaly from the SST CCI v2.0 analysis to the other data sets (Figure 3-2, lower panel) over the period 2014 onwards; the analysis is acting to reduce the global mean anomaly here (compare to the time series in the upper panel of Figure 3-2, which provides a comparison only where, for each pair, both the SST CCI product or the comparison data set and HadSST3 have information at any time).

The SST CCI v2.0 analysis tracks the retrievals from the AVHRR sensor on board MetOp-A more closely than the retrievals from the AVHRR on board NOAA-19. There is a relative drift between the retrievals from the NOAA-19 and MetOp-A AVHRRs (see Figure 3-3).

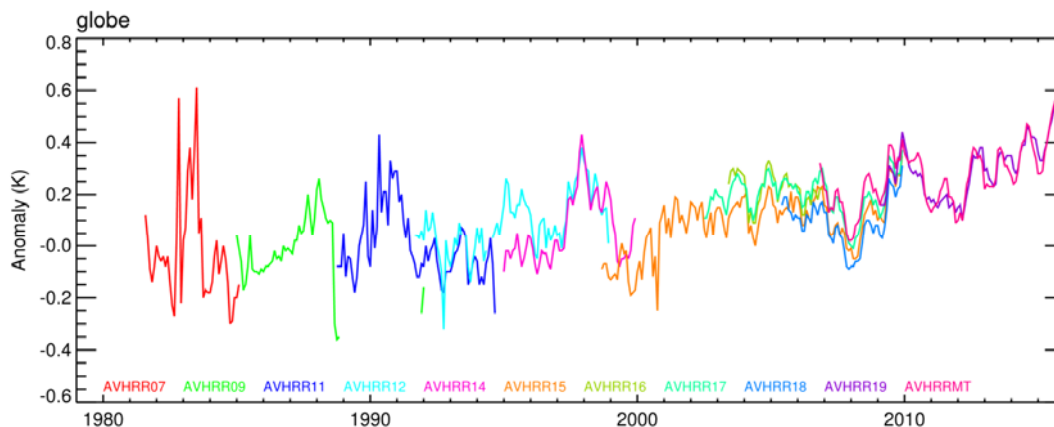


Figure 3-3. Global average SST anomaly (K, relative to MyOcean OSTIA reanalysis climatology) from successive AVHRR instruments. Colour-coded labels indicate the sensor, e.g. AVHRR07 = AVHRR onboard the NOAA-7 satellite and AVHRRMT = AVHRR onboard the MetOp-A satellite.

As mentioned above, there are individual months along the time series which demonstrate larger disagreements between the SST CCI v2.0 products and the comparison data. Most striking are November in 2000, October/November 1982, June/July 1983, together with some other outliers in late 1988 and perhaps May 1990.

Figure 3-3 demonstrates that the "spikes" in November 2000 are in the retrievals from the AVHRR onboard NOAA-15. In the case of November 2000, there are few retrievals from NOAA-15 in this month and the problem is one of sampling. The SST CCI v2.0 analysis is able to overcome the lack of data from NOAA-15 with the incorporation of the ATSR-2 retrievals and the use of statistical interpolation.

The period in 1982/3 is more complex to analyse because a number of factors which complicate the retrieval of SST and the interpretation of the results are at play at this time. In 1982, a very large volcanic eruption took place. El Chichòn erupted between March and September 1982, expelling a large quantity of sulphurous gases into the atmosphere. In the atmosphere, these gases formed sulphate aerosols which remained for many months after the eruption and are known to cause problems for the accurate retrieval of

SSTs from infrared instruments; particularly instruments like the AVHRR with only one view through the atmosphere to the surface (RD.299). Particular care was taken in producing the SST CCI version 2.0 products to try to overcome these difficulties. The associated infrared aerosol optical depth of volcanic eruptions has been estimated using additional information available from the HIRS instrument. This additional information was used in the SST retrieval and taken account of in the radiative transfer model to reduce the bias in the retrievals associated with the presence of the additional aerosol. Alongside the eruption of El Chichón, a large El Niño event took place between March/April 1982 and Sept/Oct 1983. Thus, we expect to see elevated SSTs over this period, but the size of the global average SST anomaly in the SST CCI v2.0 data sets is greater than that seen in the comparison data sets. Figure 3-6 demonstrates that part of the enhanced SST anomaly over this period in the SST CCI v2.0 data sets is likely erroneous and a consequence of calibration errors and the difficulty of retrieving accurate SSTs with a single-view sensor during a major volcanic eruption. Users should use the data for the period 01/10/1982-30/09/1983 with caution. Artefacts in the global mean are in the range of 0.1 to 0.5 K in October to December 1982, early August 1983 and late September 1983.

Since the SST CCI v2.0 analysis relies solely on the retrievals from the AVHRR onboard NOAA-7 at this time, it too follows the evolution of SST from that instrument. This effect was also seen in the SST CCI v1.0 AVHRR retrievals following the eruption of Mt Pinatubo in June 1991, but these errors have been corrected in the v2.0 products using the method outlined above.

The negative SST anomaly excursion in 1988 arises from the last few months of the retrievals from the AVHRR onboard NOAA-9 (Figure 3-3); this "spike" is visible in some regions, but not in others. Here too the SST CCI v2.0 analysis is unable to mitigate the impact of the erroneous retrievals and produces an enhanced cold anomaly.

3.4.1.2 HEMISPHERIC TIME SERIES

The same broad observations can be made for the hemispheric average time series as for the global average. Here though, it is apparent that the large spikes in 1982/3 are larger in the Southern Hemisphere.

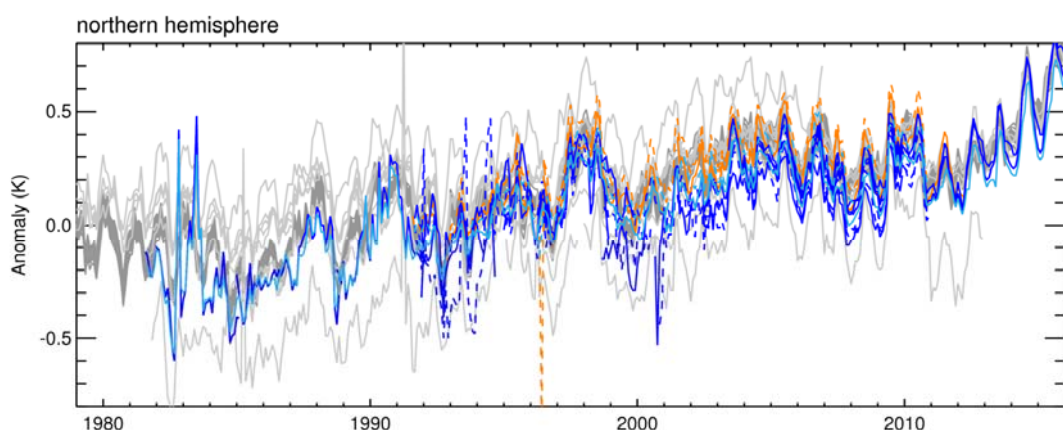


Figure 3-4. Northern Hemisphere average SST anomaly (K, relative to MyOcean OSTIA reanalysis climatology) for each of the comparison data sets (grey) and the SST CCI v2.0 products (solid lines) [SST CCI ATSR: orange, SST CCI AVHRR: blue, SST CCI analysis: cyan]. SST CCI v1.0 are shown as dashed lines. For SST CCI ATSR and SST CCI AVHRR there is one line for each individual satellite.

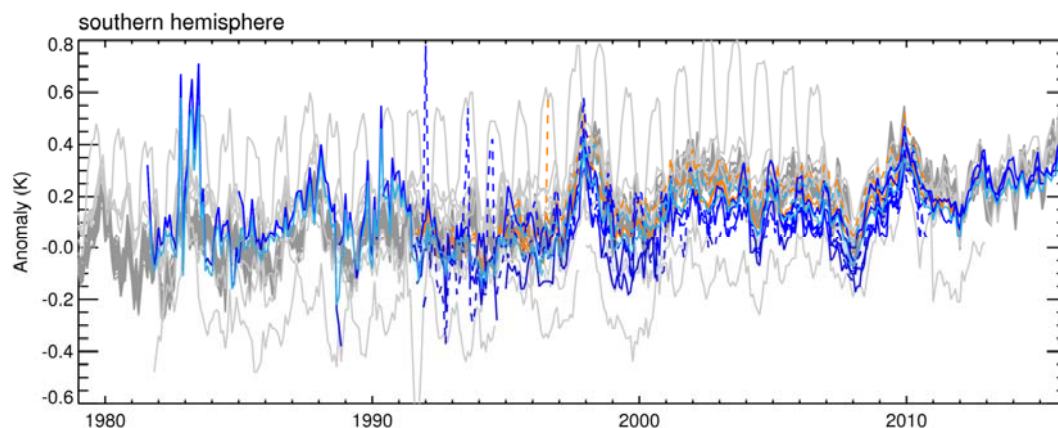


Figure 3-5. Southern Hemisphere average SST anomaly (K, relative to MyOcean OSTIA reanalysis climatology) for each of the comparison data sets (grey) and the SST CCI v2.0 products (solid lines) [SST CCI ATSR: orange, SST CCI AVHRR: blue, SST CCI analysis: cyan]. SST CCI v1.0 are shown as dashed lines. For SST CCI ATSR and SST CCI AVHRR there is one line for each individual satellite.

This feature is particularly prominent in the northern tropics, the Indian Ocean and the south Pacific (Figure 3-6). Although it is localised in time, specifically affecting 01/10/1982-30/09/1983, it also manifests as a clear hemispheric contrast pattern in the decadal average SST anomaly over the period 1982-1991 (see also Section, 3.4.2, Figure 3-18).

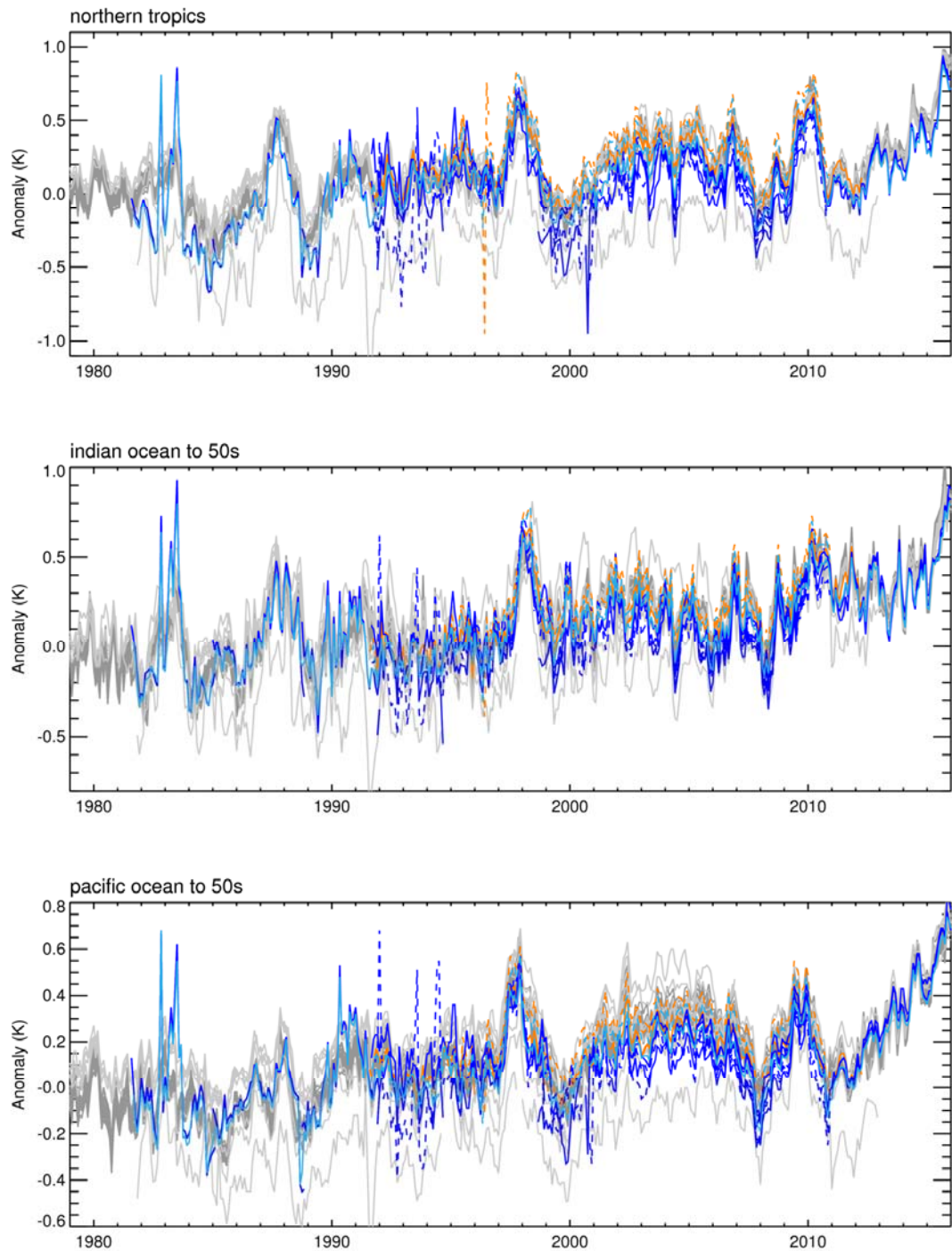


Figure 3-6. Average SST anomaly (K, relative to MyOcean OSTIA reanalysis climatology) in (top) northern tropics, (middle) Indian Ocean and (bottom) south Pacific for each of the comparison data sets (grey) and the SST CCI v2.0 products (solid lines) [SST CCI ATSR: orange, SST CCI AVHRR: blue, SST CCI analysis: cyan]. SST CCI v1.0 are shown as dashed lines. For SST CCI ATSR and SST CCI AVHRR there is one line for each individual satellite.

3.4.1.3 LINEAR TRENDS

Figure 3-7, **Figure 3-8**, Figure 3-10 and Figure 3-11 show linear trends for the SST CCI version 2.0 products, the different comparison data sets and the SST CCI v1.0 products for the various regions shown in Figure 3-1. The blue shaded area in Figure 3-10 and Figure 3-11 is an estimate of the measurement and sampling uncertainty as estimated from the HadSST3 data. This indicates the likely spread in trends attributable to weakly-correlated or uncorrelated measurement errors. The spread is generally small for large area averages (e.g. global and hemispheric averages) or for well-sampled regions such as the North Atlantic.

Figure 3-7 shows trends for the period 1982-2016. Figure 3-10 shows trends for 1992-2010 to allow comparison to the v1.0 products. Because some of the differences between the SST CCI products and the comparison data sets might arise from differences in large-scale sampling, **Figure 3-8** and Figure 3-11 show the trends over the same period after the coverage has been reduced to that of the *in situ*-only HadSST3 data set. The long-term warming during this period is comparable to the year-to-year variability, which is dominated by the period of high El Niño/La Niña activity around 1982-1985, 1997-2000, 2007-2010 and 2015-2017. Therefore, linear trends are not a good 'model' for temperature change over this period. Nonetheless they do highlight differences such as 'drifts' (or relative instabilities) between the data sets.

Over the period, 1982-2016, the SST CCI v2.0 products show linear trends (Figure 3-7) which are consistent with those of the comparison data sets in all regions except the North Pacific and the eastern tropical Atlantic. In the eastern tropical Atlantic, lower SSTs tend to be present in the SST CCI v2.0 products because of the impact of Saharan dust aerosols on the retrievals here (see also Figure 3-14). It is apparent that this affects the trends seen in the SSTs as well as their magnitude. The North Pacific is an area of extensive stratus cloud and is also an area where SST data sets tend to disagree (see also Figure 5-1).

Figure 3-10 provides linear trends in the different regions over the period 1992-2010. The trends in the SST CCI v2.0 products are broadly similar to those shown in the comparison data sets with a few exceptions. Linear trends in the global and Northern Hemisphere averages show relatively low spread between the data sets. The SST CCI v1.0 retrievals exhibit a relatively low trend over this period in the Southern Hemisphere and in many other regions (lighter blue symbol in Figure 3-10).

Trends are more uncertain in relatively poorly observed regions, such as around southern Greenland (Figure 3-9). Here, the SST CCI v2.0 analysis exhibits a lower trend over 1992-2010 than the SST CCI v2.0 ATSR and AVHRR retrievals, but this gap narrows when the data are collocated with HadSST3 (Figure 3-11). Changes in linear trend between the SST CCI v1.0 and v2.0 products vary in sign according to region.

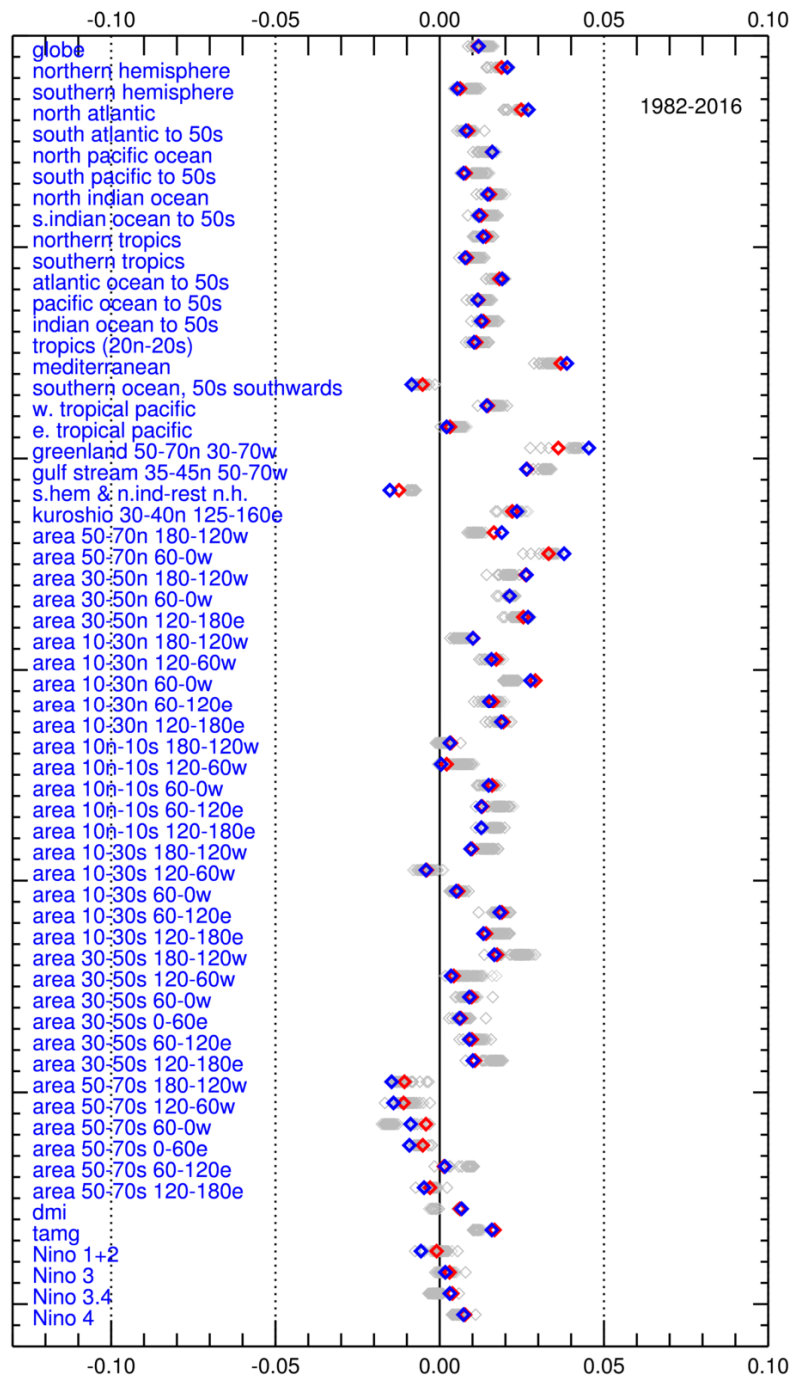


Figure 3-7. Linear trends (K/year) from January 1982 to December 2016 for each of the 61 regions and indices and each of the comparison data sets available over this period (grey) and the three SST CCI version 2.0 data sets: (red) SST CCI v2.0 analysis and (blue) SST CCI v2.0 AVHRR. Outlier comparison data sets are shown by grey dots.

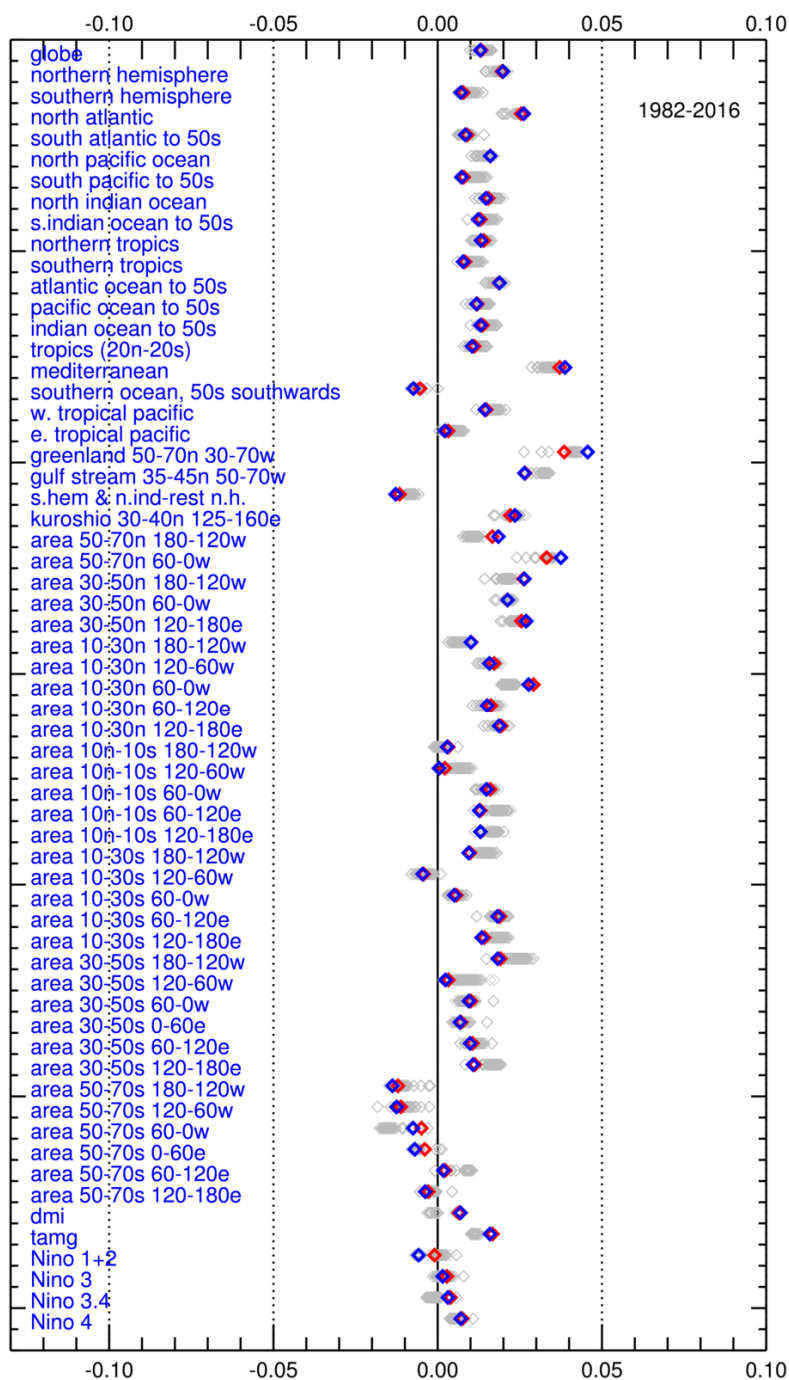


Figure 3-8. As for Figure 3-7 but each data set has been reduced to the coverage of HadSST3

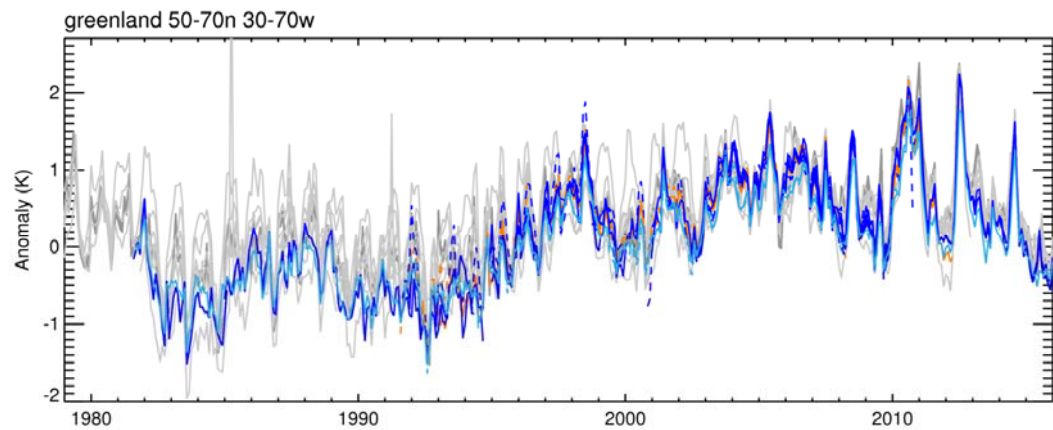


Figure 3-9. Average SST anomaly (K, relative to MyOcean OSTIA reanalysis climatology) for the area south of Greenland [50-70N, 30-70W] for each of the comparison data sets (grey) and the SST CCI v2.0 products (solid lines) [SST CCI ATSR: orange, SST CCI AVHRR: blue, SST CCI analysis: cyan]. SST CCI v1.0 are shown as dashed lines. For SST CCI ATSR and SST CCI AVHRR there is one line for each individual satellite.

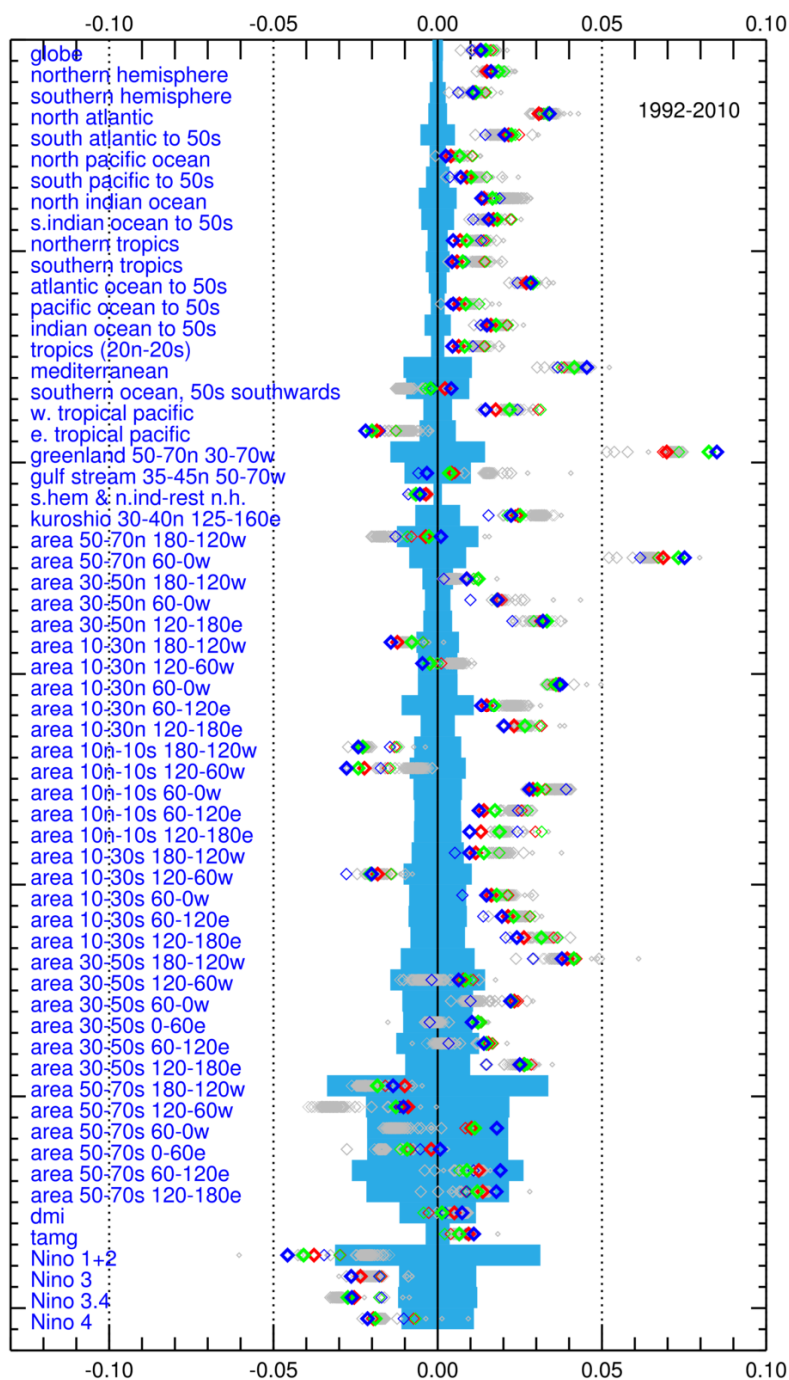


Figure 3-10. Linear trends (K/year) from January 1992 to December 2010 for each of the 61 regions and indices and each of the comparison data sets (grey) and the three CCI data sets: (red) SST CCI v2.0 analysis, (green) SST CCI v2.0 ATSR and (blue) SST CCI v2.0 AVHRR. The larger symbols correspond to the SST CCI v2.0 products, and the smaller green, blue and red symbols correspond to SST CCI v1.0 datasets. Outlier comparison data sets are shown by grey dots. The pale blue area is an estimate of the uncertainty in the trend arising from measurement and sampling errors in the HadSST3 data.

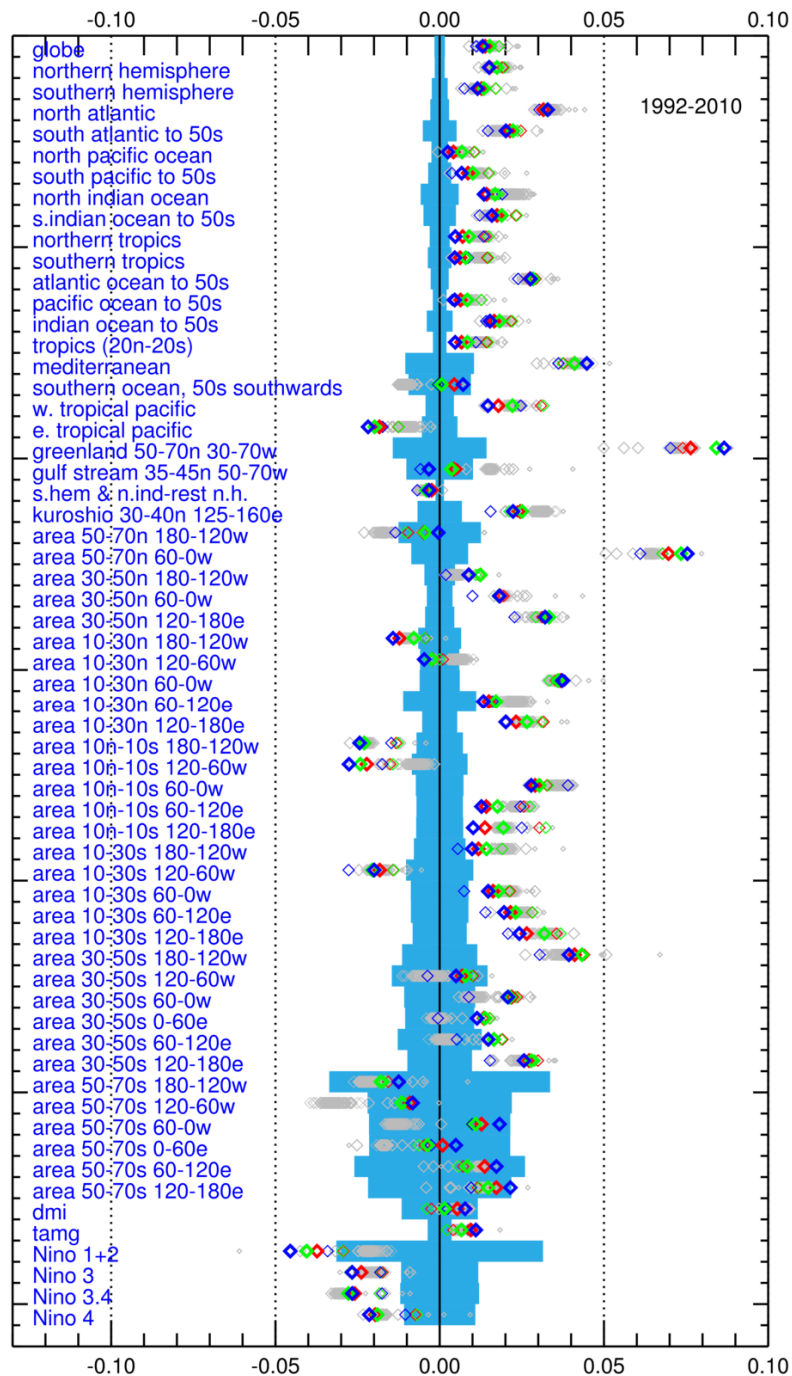


Figure 3-11. As for Figure 3-10 but each data set has been reduced to the coverage of HadSST3.

3.4.1.4 MODES OF VARIABILITY

Indices for some standard modes of variability are shown in Figure 3-12 and Figure 3-13. In Figure 3-12 the spread of estimates is relatively narrow for the Dipole Mode Index (DMI) and the Tropical Atlantic Meridional Gradient (TAMG), particularly after 1991, because the indices are calculated as the difference between two areas. This tends to reduce the effect of systematic offsets between the datasets. However, prior to 1991, the SST CCI v2.0 products are offset relative to the comparison datasets by a few tenths of a degree.

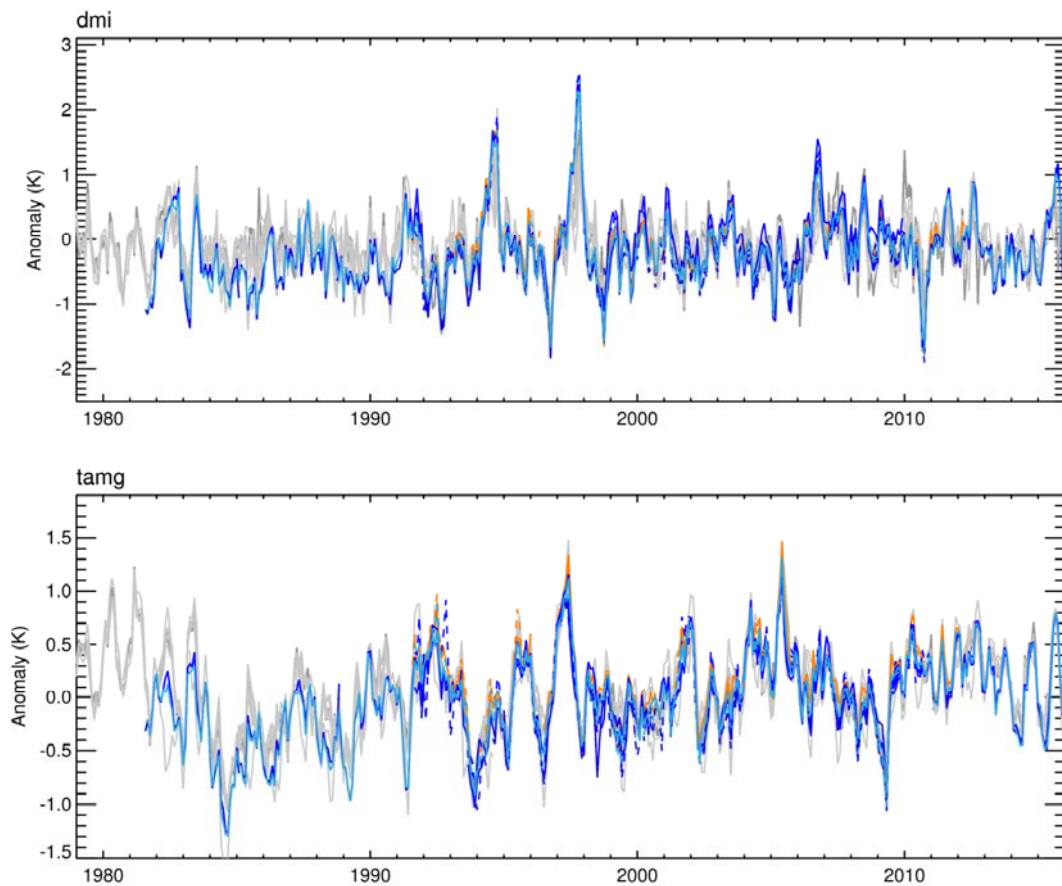


Figure 3-12. Dipole Mode Index (K, top) and Tropical Atlantic Meridional Gradient (K, bottom) for each of the comparison data sets (grey) and the SST CCI v2.0 products (solid coloured lines) [SST CCI ATSR: orange, SST CCI AVHRR: blue, SST CCI analysis: cyan]. SST CCI v1.0 products are shown as dashed lines. Units are in K because the indices are calculated as the difference between two simple area averages of temperature.

Happily, the apparent residual aerosol effects on the calibration of the SST CCI v2.0 AVHRR retrievals in 1982/3 do not seem to affect the Niño regions where the El Niño Southern Oscillation manifests in warmer (cooler) SST anomalies in El Niño (La Niña) years. Figure 3-13 shows the time series for the Niño 1+2, Niño 3, Niño 3.4 and Niño 4 regions. Apart from a spike at the peak of the Niño 1+2 time series in mid-1983, the SST CCI v2.0 AVHRR and SST CCI v2.0 analysis seem very consistent with the time series from the comparison data sets, including to large degree the SST CCI v1.0 products. This means that model simulations run from the SST CCI v2.0 products exhibit no ill-effects in their ENSO simulations from the residual aerosol effects seen elsewhere in the globe at that time (Section 3.4.1.1). In the time series for the Niño 1+2 region, in particular, we see in the SST CCI v1.0 AVHRR retrievals the signature of the atmospheric aerosol loading after the eruption of Mt Pinatubo in June 1991. This effect has been corrected in the v2.0 products.

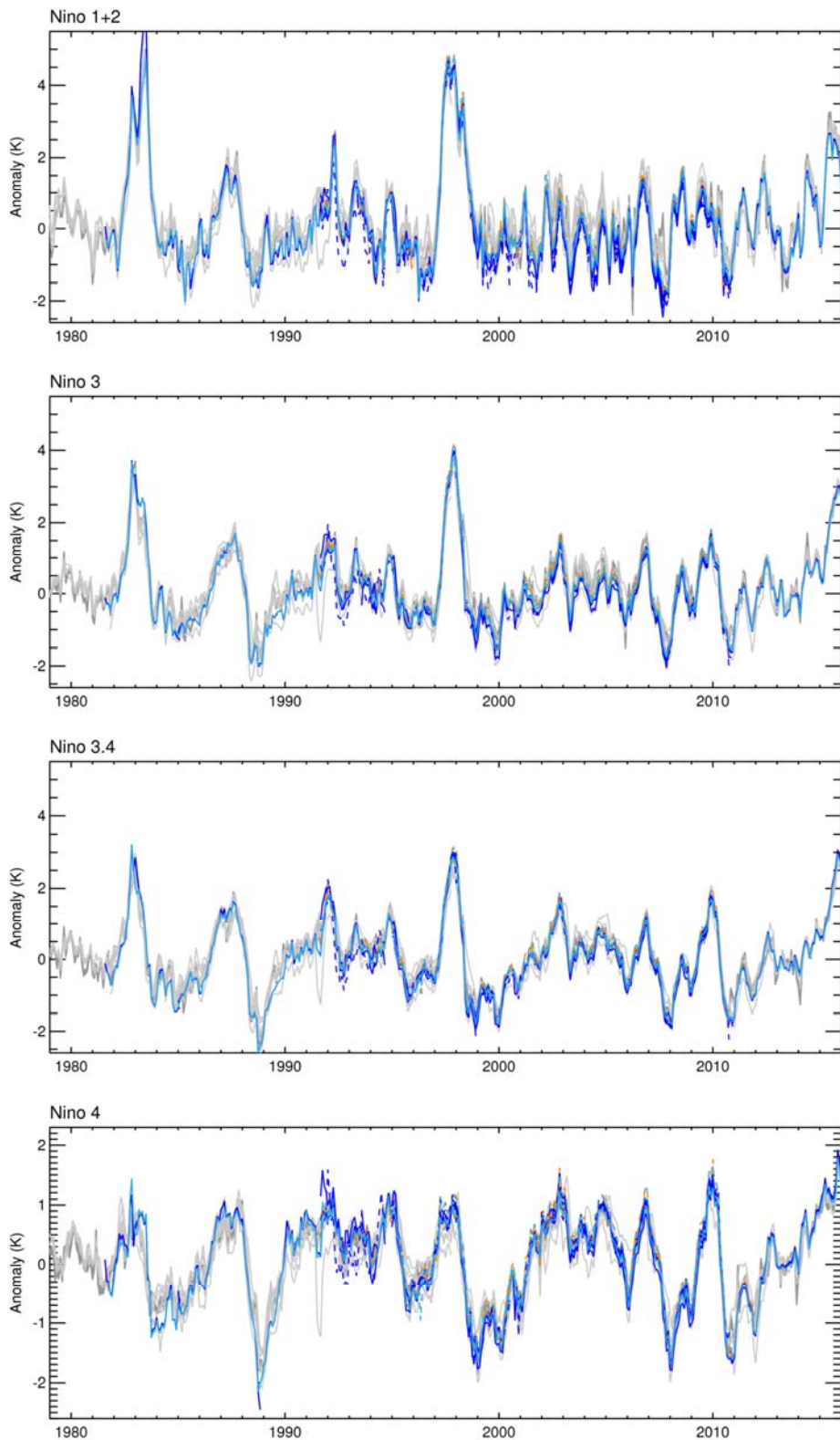


Figure 3-13. Niño indices. Area-average SST anomalies (K) for the four Niño regions described in Figure 3-1 for each of the comparison data sets (grey) and the SST CCI v2.0 products (solid lines) [SST CCI ATSR: orange, SST CCI AVHRR: blue, SST CCI analysis: cyan]. SST CCI v1.0 products are shown as dashed lines.

3.4.1.5 OTHER POINTS TO NOTE

Two regions in particular are strongly affected by the impact of dust aerosol on the SST retrievals, particularly when based only on the single-view AVHRR sensors.

The Arabian Sea and northern Indian Ocean is one and the area west of the Sahara in the eastern Atlantic [10-30N 60-0W] is the other. The impact of the relatively cool SST here in the SST CCI v2.0 products is discussed later (Section 5).

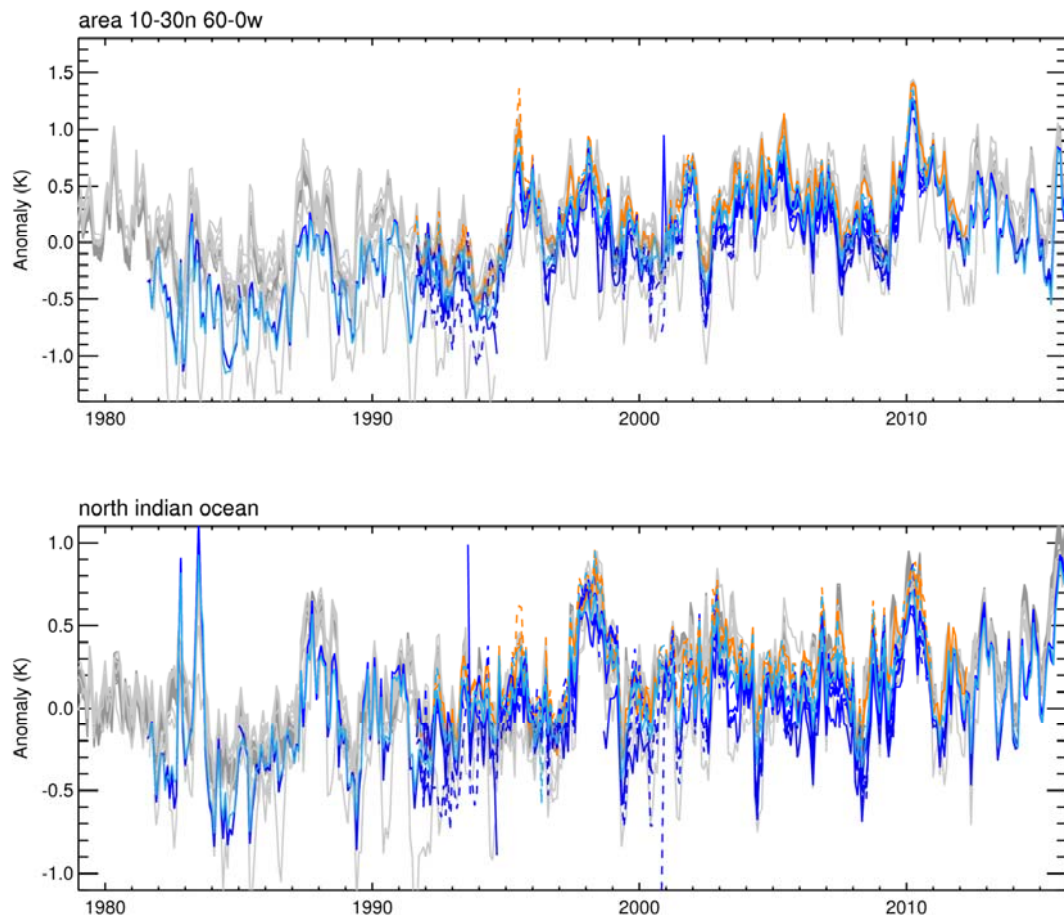


Figure 3-14. Average SST anomaly (K, relative to MyOcean OSTIA reanalysis climatology) in (top) eastern Atlantic [10-30N 60-0W] and (bottom) north Indian Ocean for each of the comparison data sets (grey) and the SST CCI v2.0 products (solid lines) [SST CCI ATSR: orange, SST CCI AVHRR: blue, SST CCI analysis: cyan]. SST CCI v1.0 are shown as dashed lines. For SST CCI ATSR and SST CCI AVHRR there is one line for each individual satellite.

A large shift in the relative position of the SST anomaly in the SST CCI v2.0 products can be seen in certain areas, e.g. the Southern Ocean (particularly the sector below the Indian Ocean) (Figure 3-15). Here, the comparison to the other datasets suggests a discontinuity in the SST CCI v2.0 time series in 1991-2, but these particular areas are poorly observed by non-satellite data sources and so interpretation of these time series is challenging. These areas also suggest a discontinuity in 2000.

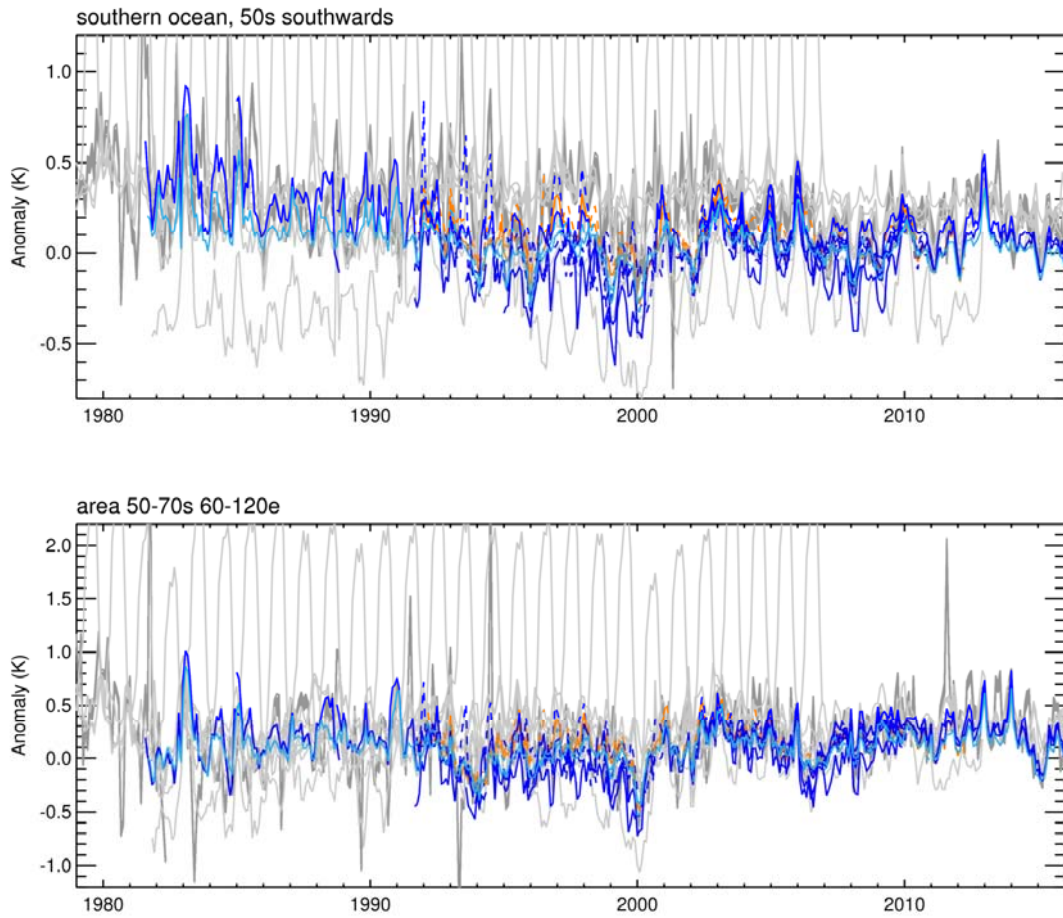
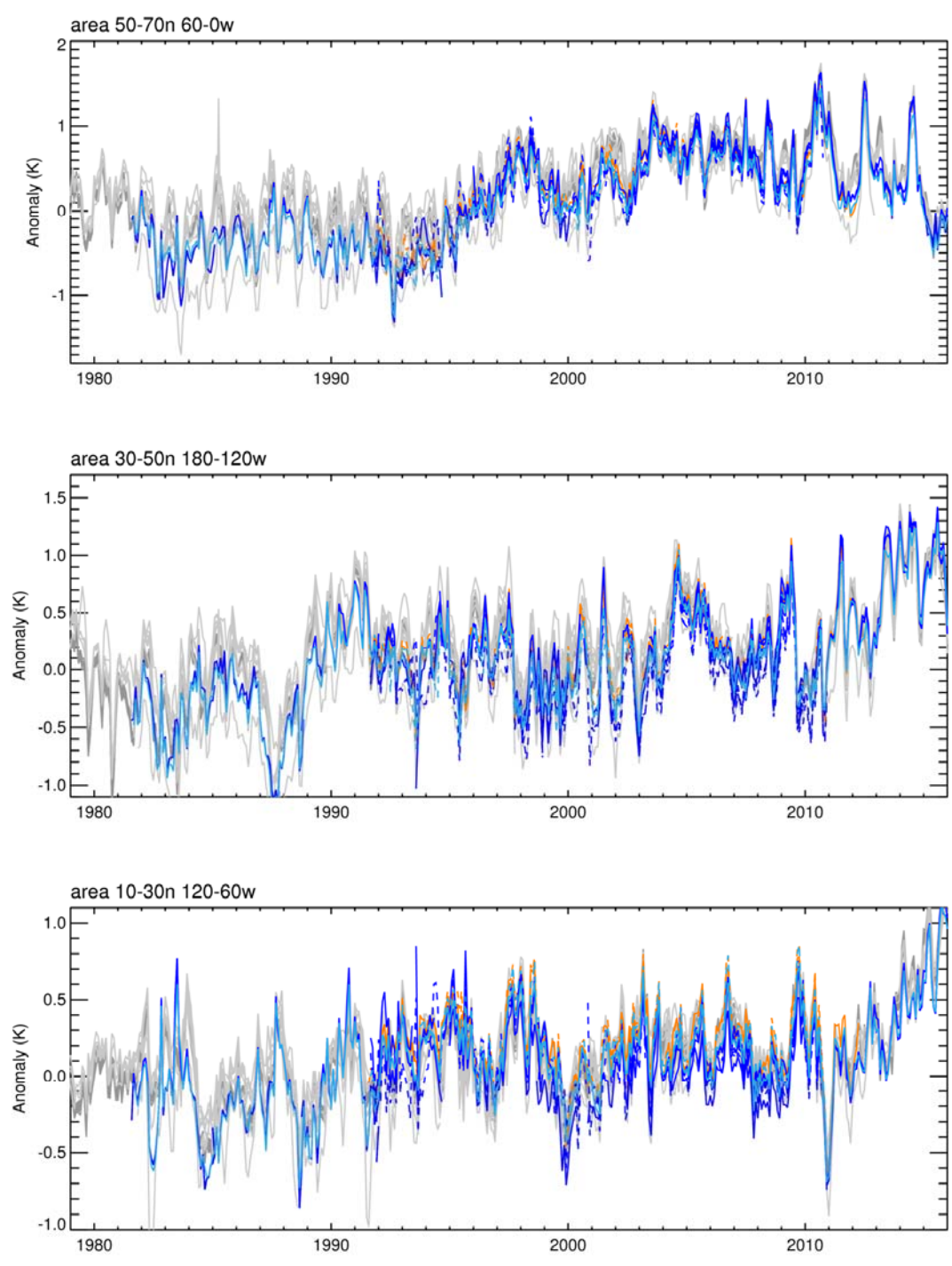


Figure 3-15. Average SST anomaly (K, relative to MyOcean OSTIA reanalysis climatology) in (top) Southern Ocean and (bottom) [50-70S, 60-120E] for each of the comparison data sets (grey) and the SST CCI v2.0 products (solid lines) [SST CCI ATSR: orange, SST CCI AVHRR: blue, SST CCI analysis: cyan]. SST CCI v1.0 are shown as dashed lines. For SST CCI ATSR and SST CCI AVHRR there is one line for each individual satellite.

In contrast to the areas just discussed, some Northern Hemisphere areas demonstrate relatively cool SSTs in the 1980s compared to the other datasets (Figure 3-16).

It should also be noted, however, that there is a clear improvement in the representation of the region [10N-10S, 60-0W] following the eruption of Mt Pinatubo (Figure 3-16).



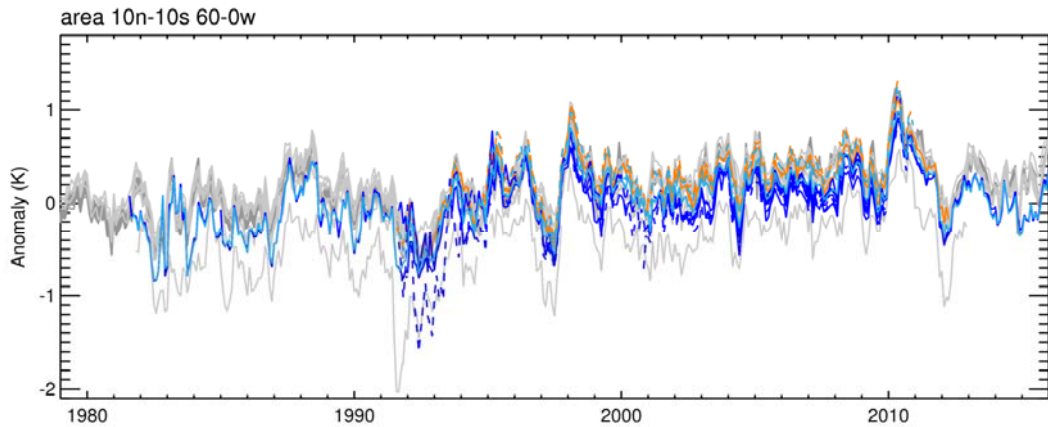
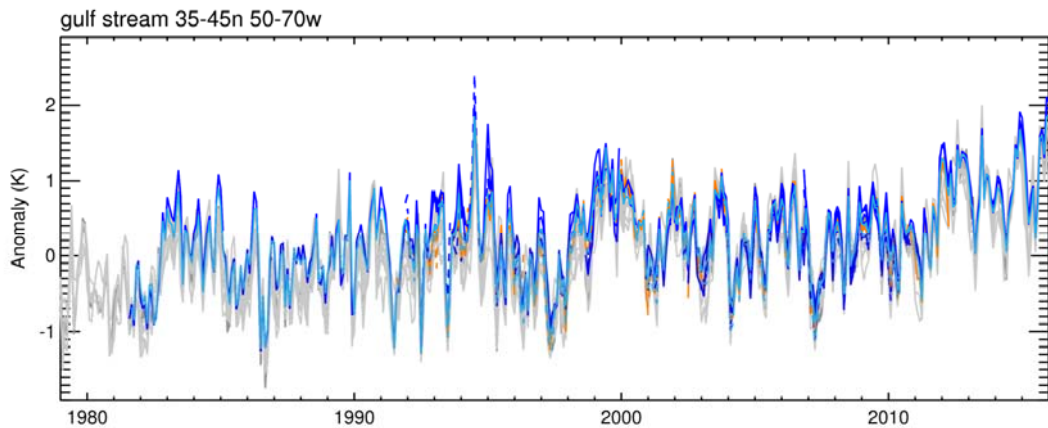


Figure 3-16. Average SST anomaly (K, relative to MyOcean OSTIA reanalysis climatology) in (top) [50-70N, 60-0W], (second) [30-50N, 180-120W], (third) [10-30N 120-60W] and (bottom) [10N-10S, 60-0W] for each of the comparison data sets (grey) and the SST CCI v2.0 products (solid lines) [SST CCI ATSR: orange, SST CCI AVHRR: blue, SST CCI analysis: cyan]. SST CCI v1.0 are shown as dashed lines. For SST CCI ATSR and SST CCI AVHRR there is one line for each individual satellite.

It is noted later in the report (Section 5) that the SST CCI v2.0 products are warmer than HadISST.2.2.0.0 in the Gulf Stream (Figure 5-1 and Figure 5-2). The same is apparent in (Figure 3-17) when comparing to other datasets, except over the period 2001-2012. In contrast, the SST CCI v2.0 products are consistent with the comparison data in the Kuroshio along the whole time series.



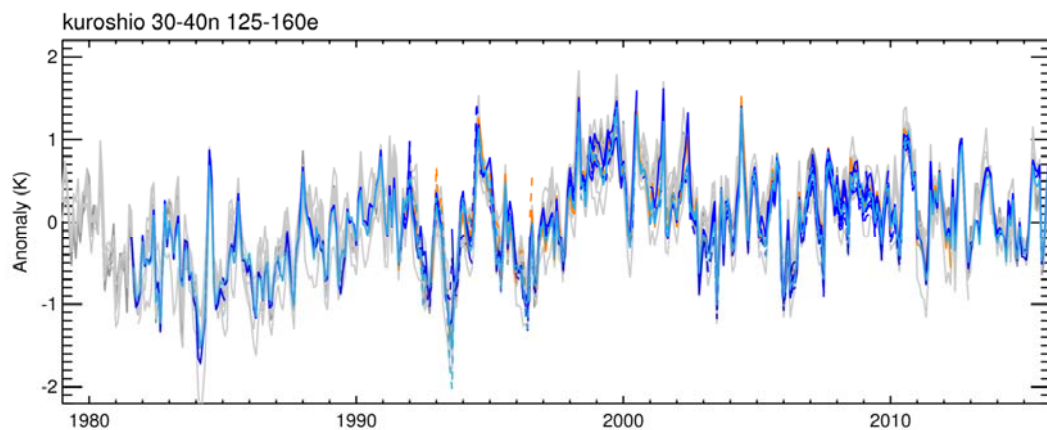


Figure 3-17. Average SST anomaly (K, relative to MyOcean OSTIA reanalysis climatology) in (top) the Gulf Stream and (bottom) the Kuroshio for each of the comparison data sets (grey) and the SST CCI v2.0 products (solid lines) [SST CCI ATSR: orange, SST CCI AVHRR: blue, SST CCI analysis: cyan]. SST CCI v1.0 are shown as dashed lines. For SST CCI ATSR and SST CCI AVHRR there is one line for each individual satellite.

3.4.2 MULTI-YEAR AVERAGES

Multi-year averages provide a useful means for assessing spatially the relative biases and multi-year variability in the different data sets considered. In particular, decadal averages expressed relative to a common climatology explore both the decadal variability and relative biases between datasets (Figure 3-18). Decadal averages are shown as anomalies relative to the MyOcean OSTIA reanalysis climatology. This mainly highlights the relative biases and trends amongst the data sets.

Decadal average SST anomalies for 1982-1991 in SST CCI v2.0 products display a hemispheric contrast with the Northern Hemisphere (on average) being cool and the Southern Hemisphere average being warm (Figure 3-18). Contrasting the averages in the SST CCI v2.0 products with the decadal averages in most of the other comparison data sets, e.g. HadISST1, COBE, ERSST, we see a much less hemispheric pattern and a decadal average which is more to be expected from a period with a strong El Niño event, such as that in 1982/3.

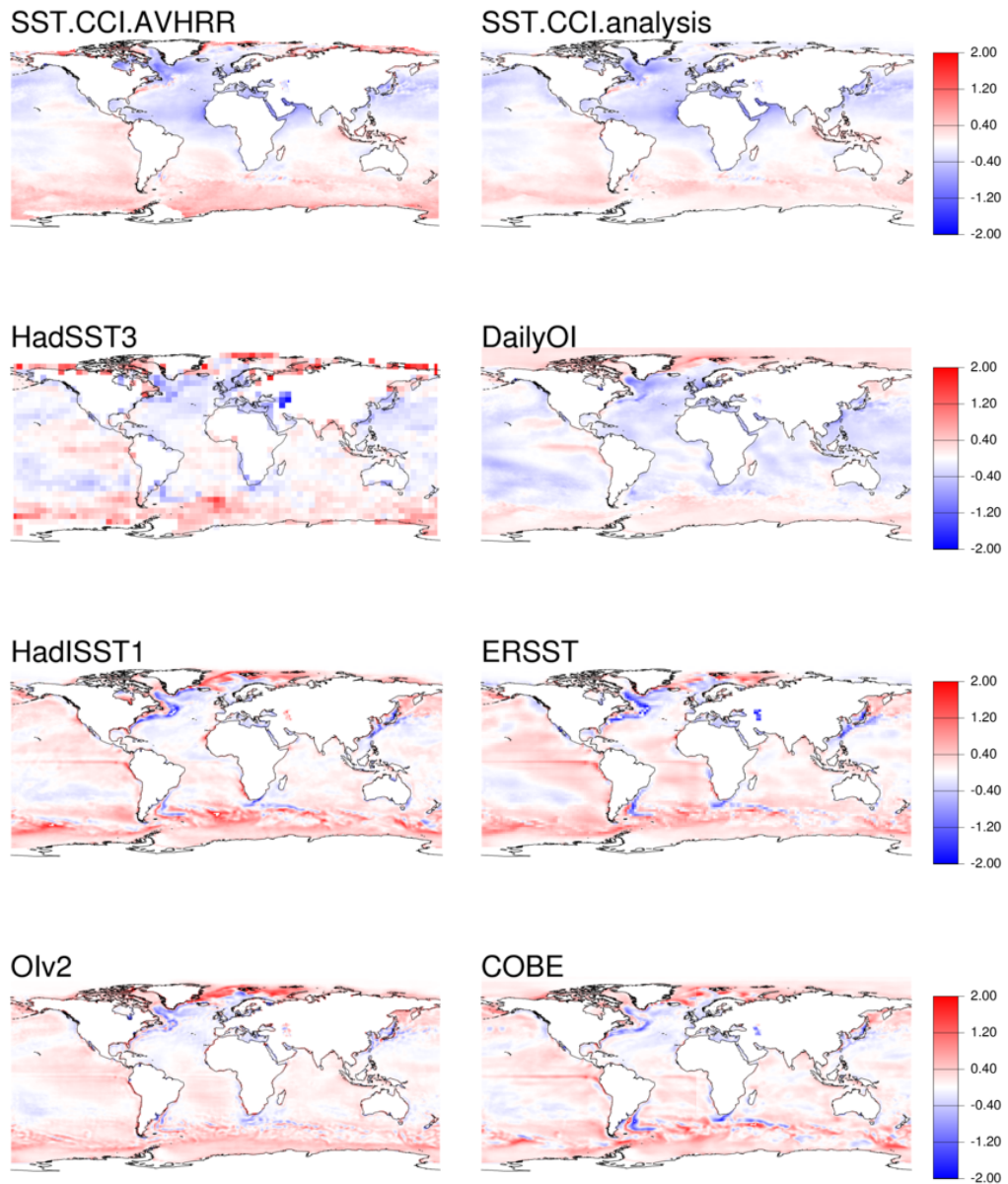
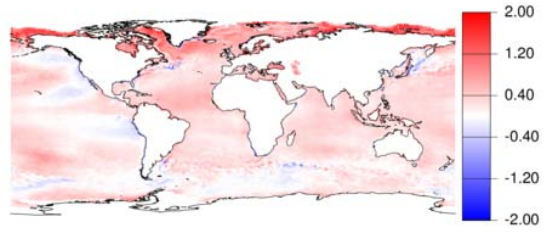
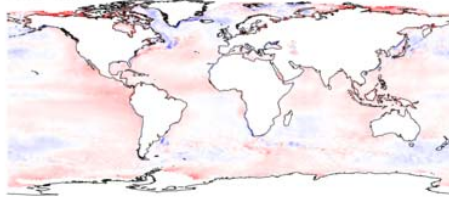


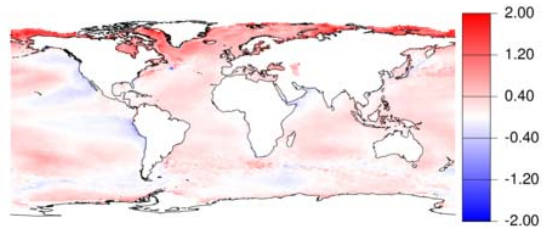
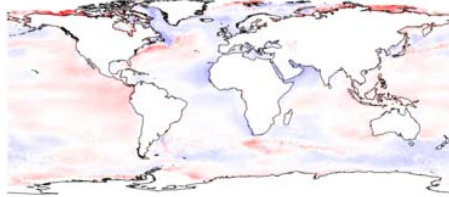
Figure 3-18. Decadal average SST anomalies (K) 1982-1991 for a selection of data sets. For a pixel to be filled, more than 30% of months need to have a valid SST.

In later periods (1991-2000 and 2001-2010, Figure 3-19), decadal averages are much more consistent with those of the comparison data. Here we also see the differences between the v1.0 and v2.0 SST CCI products seen earlier in the global mean time series; the SST CCI ATSR v2.0 product is cooler than the v1.0 product, particularly over 2001-2010, and the SST CCI AVHRR v2.0 product is a little warmer than the v1.0 product.

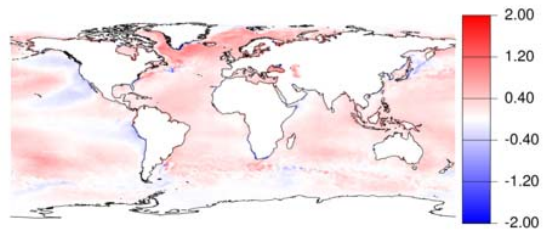
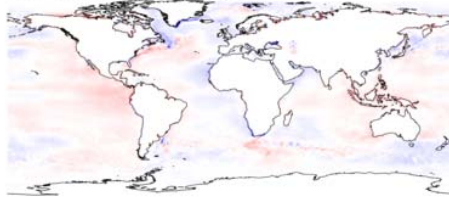
SST.CCI.ATSR



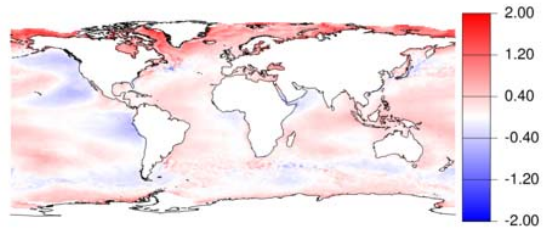
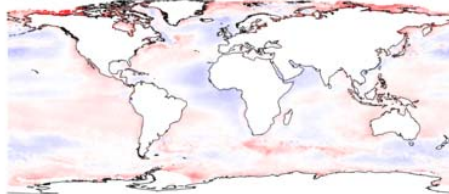
SST.CCI.AVHRR



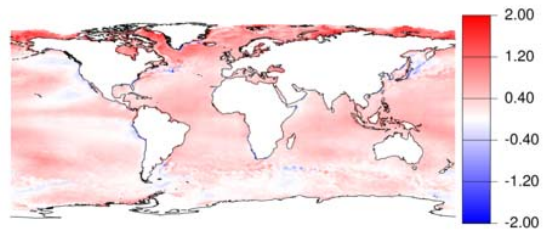
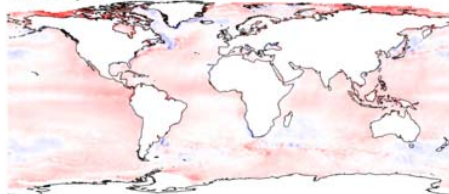
SST.CCI.analysis



L2p_phase1



L3u_phase1



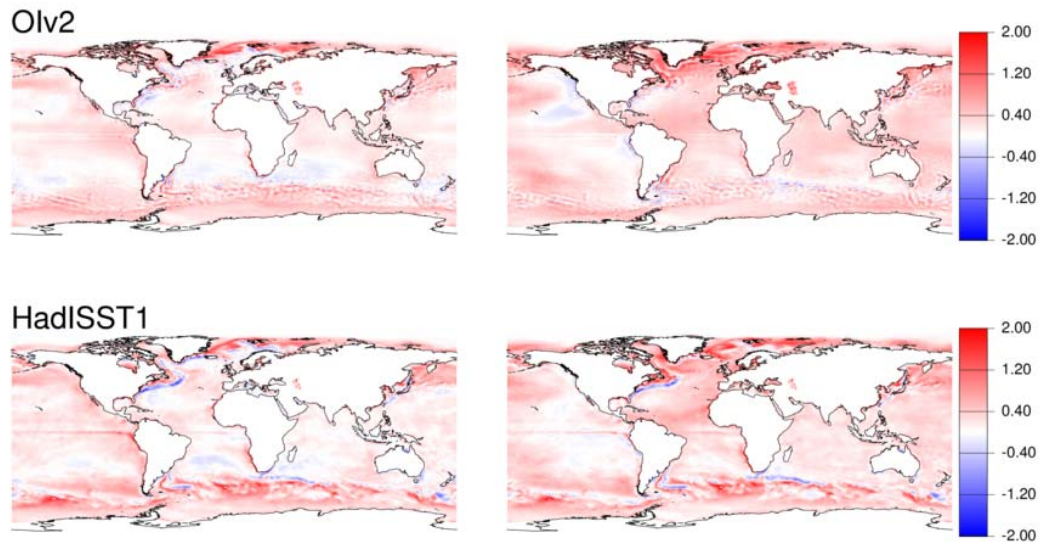


Figure 3-19. Decadal average SST anomalies (K) for a selection of data sets including SST CCI v1.0 products. From left to right the periods are 1991-2000 and 2001-2010. For a pixel to be filled, more than 30% of months need to have a valid SST.

3.4.3 AUTO-CORRELATIONS

Autocorrelation in the SST CCI v2.0 products over the whole period (Figure 3-20) is consistent with that of those comparison data sets which are infilled or based on plentiful observations. The outlier here is HadSST3, which grids only in situ measurements and performs no infilling; the impact of this is reduced autocorrelation.

Although it is useful to compare autocorrelation patterns, it is also difficult to judge which datasets are performing best as the true climatic autocorrelation fields are not known. In addition to autocorrelation due to true climatic variability, the datasets will suffer from biases which act to increase autocorrelation (by creating persistence in the sea surface temperatures) and random noise and sampling uncertainty which act to reduce the autocorrelation. It is difficult to say what combination of desirable and undesirable properties is causing any differences seen in autocorrelation seen between the datasets.

In the sub-period of the record with the best observational coverage, 1991-2010, the autocorrelation in the different SST CCI products is highly consistent (see Figure 3-21) and therefore probably does provide a good measure of the real persistence in the SST field.

The reduction in autocorrelation in the SST CCI analysis v2.0, relative to the AVHRR and ATSR products, is interesting and may indicate the addition of some extra noise in the new analysis; this requires further investigation. The MyOcean OSTIA reanalysis (which utilised an earlier version of the OSTIA analysis system) does maintain marginally higher persistence (see Figure 3-21).

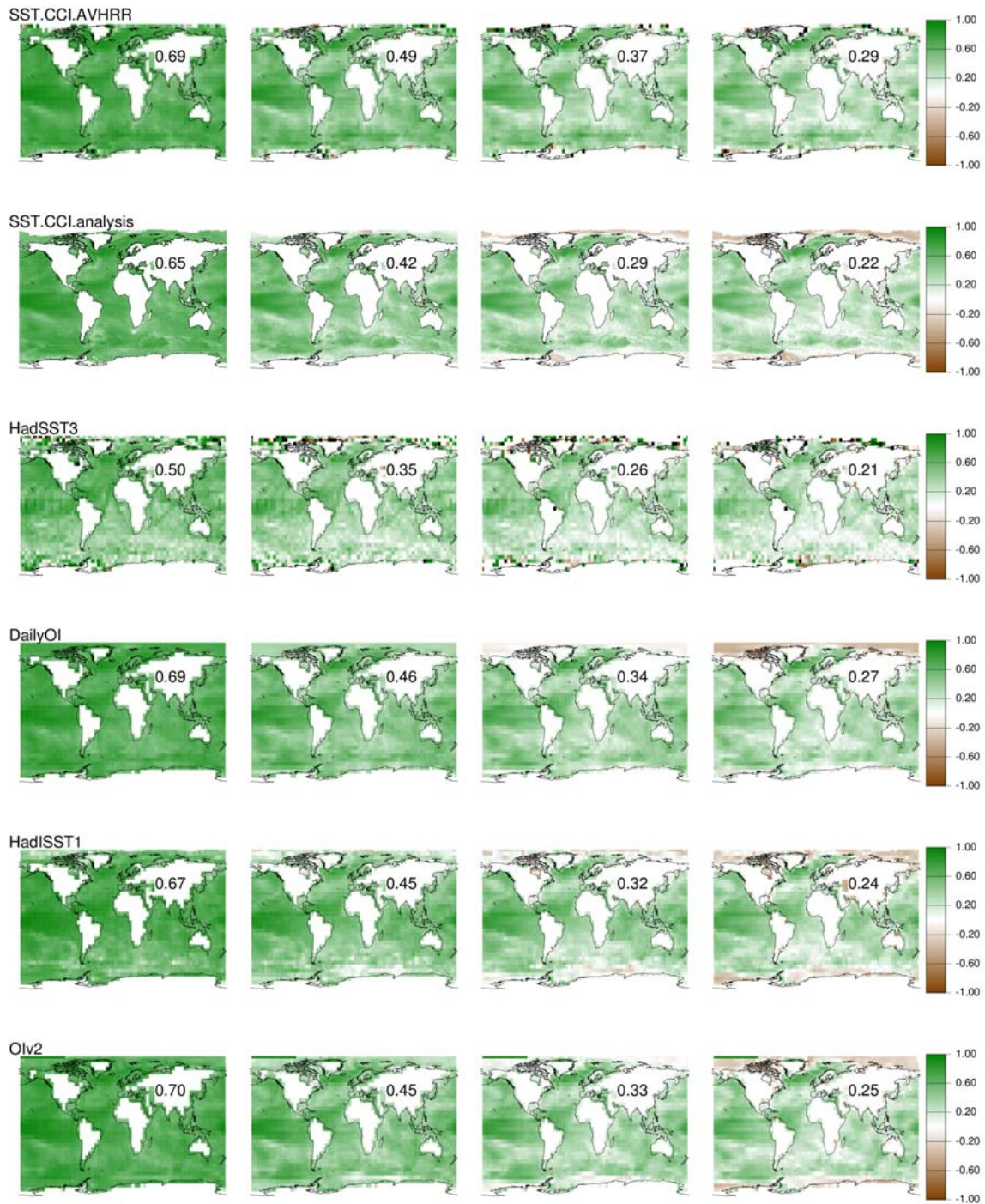


Figure 3-20. Lag correlations over 1982-2016 for lags from one to four months for a selection of datasets. In each subplot, the number shown over central Asia is the global median lag correlation.

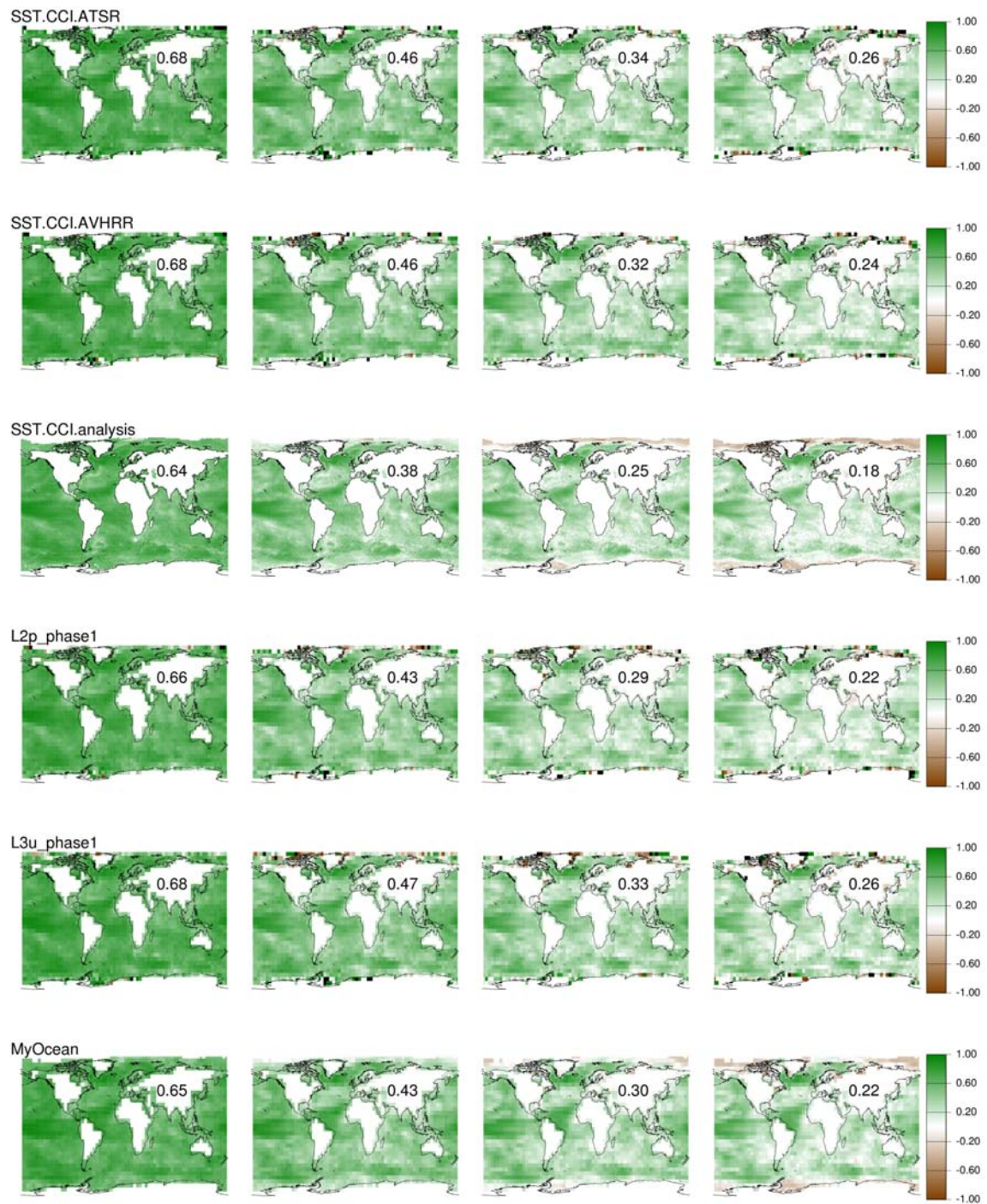


Figure 3-21. Lag correlations over 1991-2010 for lags from one to four months for a selection of datasets including SST CCI v1.0. In each subplot, the number shown over central Asia is the global median lag correlation.

4. SST CCI V2.0 PRODUCTS IN GHR SST MULTI-PRODUCT ENSEMBLE

4.1 Introduction

There are a number of level 4 products with long temporal span available to users, including the current and previous set of analyses produced within ESA SST CCI. The intercomparison of these can provide information on the strengths and weaknesses of each and give insight into the uncertainty in the analyses. The Group for High-Resolution SST (GHR SST) Multi-Product Ensemble (GMPE) system was designed to allow intercomparison of near real time analyses (Martin et al., 2012) and has previously been applied in Phase 1 of ESA SST CCI to facilitate the intercomparison of long-term analyses (Fiedler et al., 2019). Here, we update and extend the comparison to include the SST CCI analysis v2.0 back to 1982.

The GMPE system regrids all the input data on to a common 0.25° grid and generates the median and standard deviation of the analyses available on each day. Daily files are generated containing the median and standard deviation, as well as the differences between each individual analysis and the GMPE median. In addition, a map of gradients in the SST analyses (calculated on their original grids and regridded to the standard GMPE grid) is stored in the output files.

The analyses contained in the new GMPE files are listed in **Table 4-1** with their temporal extents, the type of SST they represent, from where they can be obtained and the applicable references. They include the current and previous versions of the ESA SST CCI analyses, both of which attempt to represent the daily average at 20 cm depth. HadISST.2.2.0.0 is also valid for a nominal depth of 20cm and is the analysis used in the comparison of model simulations documented in Section 5. A number of the analyses attempt to represent the foundation SST (the temperature from which the diurnal cycle grows), while AVHRR OI is bias corrected to in situ data and hence will be representative of their depths.

HadISST.2.2.0.0 is unique out of these datasets in that it attempts to represent uncertainty using an ensemble approach. By taking samples from a distribution of possible choices about things such as how bias corrections are done, a set of equally likely analyses ('realisations') are generated. This method allows complex error structures to be represented compared to the standard approach of providing a single uncertainty value at each grid point. Ten HadISST.2.2.0.0 realisations are included in the GMPE product. This allows the uncertainty assessed with HadISST.2.2.0.0 to be compared to the range of the other analyses. However, it does mean that HadISST.2.2.0.0 tends to dominate the GMPE median and standard deviation fields. This should be taken into account when using the data.

The outputs from the GMPE system have been evaluated in a number of ways. First differences to Argo reference data are analysed. Although the temporal extent of Argo data is relatively short (2002 onwards are analysed), by convention the data are not used in analyses and are reserved for validation. Near surface (3-5 m) Argo observations are used. These approximate the foundation SST (Fiedler et al., 2019), hence the type of SST each analysis tries to represent is important when interpreting these results. Second, Hovmöller plots of differences between the analyses and the GMPE median are compared, and third, examples of SST fields and gradients are shown.

Table 4-1. List of analyses included in the GMPE product.

Analysis	Time coverage	SST type	Available from	Reference
ESA SST CCI CDR2.0	01/09/1981 – 31/12/2016	Daily average at 20 cm	CCI data portal: http://cci.esa.int/data	Merchant et al. (2019)
ESA SST CCI CDR1.1 ¹	01/09/1991 – 31/12/2010	Daily average at 20 cm	CCI data portal: http://cci.esa.int/data	Merchant et al. (2014)
CMEMS OSTIA reprocessing	01/01/1985 – 31/12/2007	Foundation SST	CMEMS: http://marine.copernicus.eu/	Roberts-Jones et al. (2012)
AVHRR OI	01/09/1981 – 31/12/2016	In situ depths	PO.DAAC: https://podaac.jpl.nasa.gov/	Reynolds et al. (2007); NCEI (2016)
CMC 0.2°	01/09/1991 – 31/12/2016	Foundation SST	PO.DAAC: https://podaac.jpl.nasa.gov/	Brasnett (2008); CMC (2012)
HadISST.2.2.0.0 r0 – 9	01/09/1991 – 22/01/2016	20 cm	On request from the Met Office Hadley Centre: https://www.metoffice.gov.uk/hadobs/	Kennedy et al. (2018)
MGDSST	01/01/1982 – 31/12/2016	Foundation	JMA: https://ds.data.jma.go.jp/gmd/goos/data/rrtdb/file_list.php	Kurihara et al. (2006)

4.2 Argo validation statistics

Yearly values of mean and standard deviation differences between the analyses that are part of GMPE and the Argo matchups have been calculated. The statistics for the GMPE median were also calculated. The results for the global ocean are shown in **Figure 4-1**. The top panel shows the number of matchups in each year. These are very consistent between the different analyses and increase over time owing to the growth of the Argo array. Early in the time series the number of matchups is low. Hence results prior to ~2008 should be treated with caution.

The centre panel shows the median of the differences between the analyses and Argo. These are not necessarily expected to be zero since the analyses are not all designed to represent the foundation temperature, which is what the Argo data tries to approximate. Focussing on the period from 2008 onwards, when there are the largest number of matchups, the AVHRR OI and the SST CCI analysis v2.0 are cooler than Argo, while the MGDSST analyses are warmer. The HadISST.2.2.0.0 analyses have mean differences close to zero during the period 2010 - 2015, but are cooler prior to and after that time period. The change between 2009 and 2010 corresponds to a change in the input data used to generate it. The GMPE median mean difference is close to the HadISST.2.2.0.0 realisations, as would be expected as HadISST.2.2.0.0 is numerically dominant within the GMPE. CMC has a difference to Argo that stays close to zero through the time period, which is consistent with it representing foundation temperature.

¹ v1.1 was a minor update to v1.0 and conclusions in this section are compatible with those based on v1.0 products in other sections of this report.

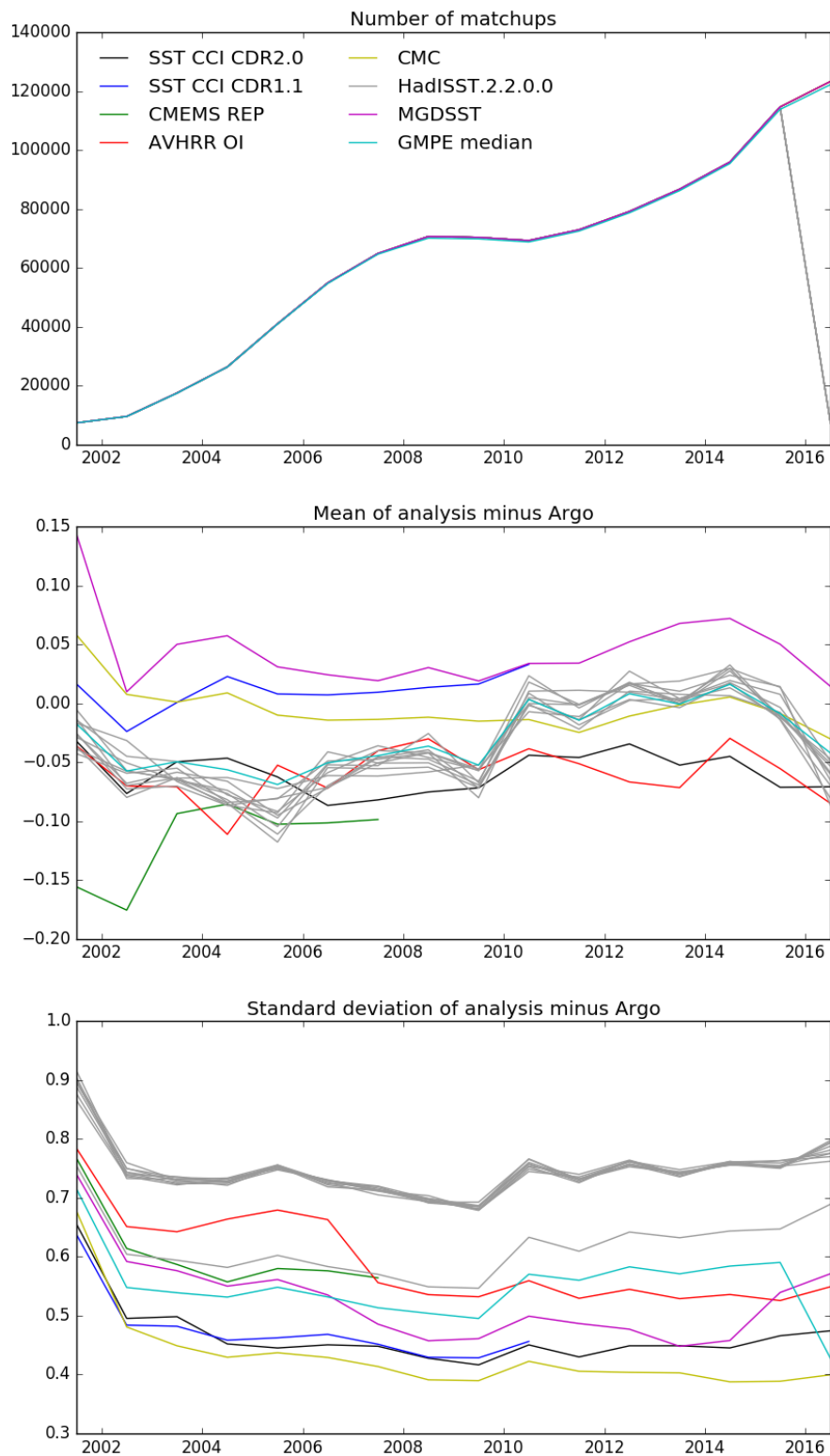


Figure 4-1. Top: number of matchups between each analysis and Argo data in each year of the analysis for the global ocean; middle: mean of analysis minus Argo matchups; bottom: standard deviation of analysis minus Argo matchups.

The bottom panel in Figure 4-1 shows the standard deviation of the differences between the analyses and Argo. CMC has consistently the lowest standard deviation of differences, which is perhaps to be expected since both Argo and CMC represent foundation temperature. The SST CCI analysis v1.1 and v2.0 have the second lowest standard deviations followed by MGDSST and AVHRR OI. In contrast to the results for the mean differences where the GMPE median and HadISST.2.2.0.0 were similar to each other, the GMPE median has a lower standard deviation of differences than the HadISST.2.2.0.0 realisations. The HadISST.2.2.0.0 realisations have the highest standard deviation of differences. One of the realisations (number 9) has a lower standard deviation than the others, though. The cause of this is not currently known but is under investigation.

Figure 4-2 shows the standard deviation of the analyses and Argo data for different regions of the ocean. Although there are regional differences in the magnitude of the standard deviation values, the relative performance of the analyses is fairly consistent with the global results.

Table 4-2 contains the standard deviation of differences between Argo and the individual analyses aggregated over the full time period for the globe and regions of the ocean. Each column is shaded so that the lowest value is green, the highest is red, with intermediate shades in between. This further emphasises the results reported above. CMC has the lowest standard deviation of difference to Argo with the SST CCI analysis v2.0 the second best, although with some regional variations. The table also emphasises the difference between HadISST.2.2.0.0 realisation 9 and the other realisations, which are all very similar to each other.

Table 4-2. Standard deviation of differences between the analyses and Argo matchups for the global ocean and regions of the ocean.

	Globe	N Atl	Trop Atl	S Atl	N Pac	Trop Pac	S Pac	Indian Ocean	S. Ocean
SST CCI analysis v2.0	0.45	0.53	0.38	0.49	0.47	0.30	0.36	0.41	0.48
SST CCI analysis v1.1	0.46	0.56	0.37	0.43	0.50	0.30	0.34	0.40	0.42
CMEMS REP	0.58	0.72	0.46	0.62	0.64	0.37	0.43	0.43	0.59
AVHRR OI	0.56	0.61	0.46	0.62	0.61	0.42	0.47	0.48	0.59
CMC	0.41	0.46	0.30	0.46	0.44	0.25	0.33	0.34	0.45
HadISST.2.2.0.0 r0	0.74	0.78	0.50	0.81	0.81	0.48	0.62	0.62	0.82
HadISST.2.2.0.0 r1	0.74	0.78	0.51	0.81	0.82	0.48	0.62	0.62	0.82
HadISST.2.2.0.0 r2	0.74	0.77	0.51	0.81	0.82	0.48	0.61	0.62	0.81
HadISST.2.2.0.0 r3	0.74	0.78	0.51	0.81	0.82	0.48	0.61	0.63	0.81
HadISST.2.2.0.0 r4	0.74	0.78	0.51	0.80	0.82	0.48	0.61	0.62	0.81
HadISST.2.2.0.0 r5	0.74	0.78	0.51	0.81	0.81	0.48	0.61	0.62	0.82
HadISST.2.2.0.0 r6	0.74	0.78	0.51	0.81	0.81	0.49	0.61	0.62	0.81
HadISST.2.2.0.0 r7	0.74	0.78	0.51	0.81	0.81	0.48	0.61	0.62	0.81
HadISST.2.2.0.0 r8	0.74	0.78	0.51	0.81	0.81	0.48	0.61	0.63	0.82
HadISST.2.2.0.0 r9	0.61	0.65	0.40	0.68	0.67	0.37	0.51	0.49	0.70
MGDSST	0.51	0.59	0.38	0.57	0.54	0.36	0.40	0.42	0.55
GMPE median	0.54	0.59	0.37	0.61	0.60	0.33	0.44	0.44	0.61

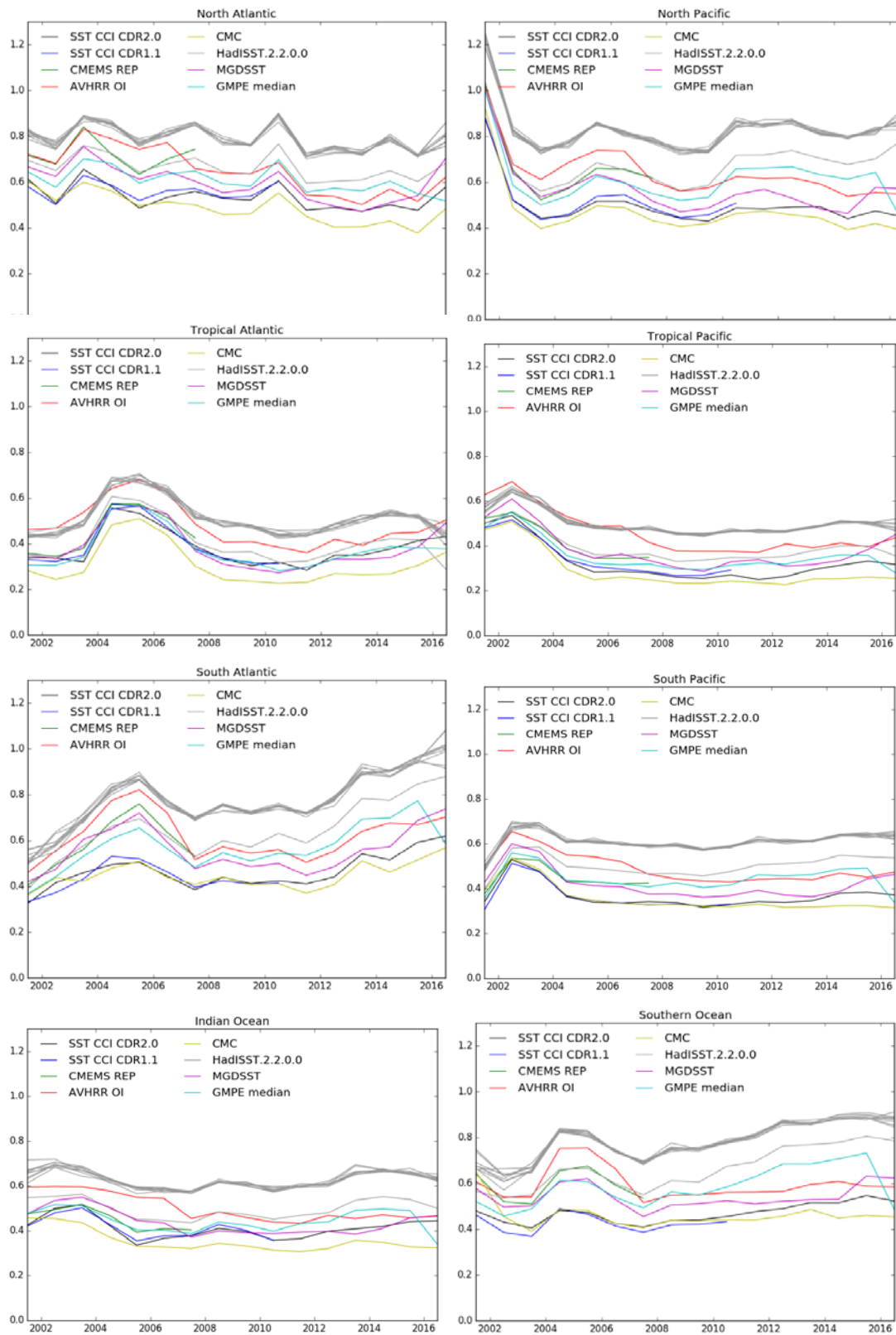


Figure 4-2. Yearly standard deviation of differences between analyses and Argo matchups for regions of the ocean.

4.3 Differences between the analyses and the GMPE median

Figure 4-3 shows Hovmöller diagrams of the differences between the analyses and the GMPE median. These were produced by first averaging anomalies over each month, then over longitude. These plots highlight where analyses differ strongly from the others, and where they are similar. As stated earlier, it should be noted when interpreting these results that the GMPE median is likely to be dominated by the HadISST.2.2.0.0 ensemble members because it makes up 10 out of the 16 analyses included in GMPE and these are relatively similar to each other.

The AVHRR OI analyses have generally positive values at high latitudes but are largely negative elsewhere. There is perhaps a trend towards smaller values towards the end of the time period. This is also seen for CMC, which has positive values at the beginning of the period and tends towards neutral values by the end. The CMEMS reprocessed product has distinct bands of differences. The most prominent occurs in the second half of the 1990s, which corresponds to the ATSR2 period.

The differences for HadISST.2.2.0.0 tend to be small compared to the other analyses, although some moderate differences can be seen. For example realisation 4 has larger positive differences at the beginning. Realisation 9, which was found to be unusual in the Argo comparisons, does not have large departures from the GMPE median.

MGDSST has positive differences to the median, which is consistent with the Argo matchup results. Similarly, the SST CCI analysis v1.1 can be seen to be warmer than v2.0. In SST CCI analysis v2.0, the period prior to 1991 looks noisier than 1991 onwards. This may be due to there being fewer analyses in the GMPE in the earlier period causing the median to be noisier, or could be related to the lack of ATSR data in the earlier period. From 1991, SST CCI analysis v2.0 seems relatively consistent with the median, compared to the other analyses.

4.4 SST features and gradients

The GMPE product contains gradient fields that can be used to compare the sharpness of features in the analyses. As an example, **Figure 4-4** shows plots of SSTs in the Gulf Stream region and SST gradients for an arbitrarily chosen day (1/7/2000) for each analysis. The representation of the SSTs is seen to be quite different in each analysis. For example, the CMEMS reprocessed product appears smooth with few recognisable features. The gradients are relatively small for this product. The CMEMS reprocessing and the SST CCI analysis v1.1 and v2.0 were each generated using the OSTIA analysis system. The benefits of the work done in both phases of the ESA SST CCI project can clearly be seen in the improvement in the sharpness of the SST features in the SST CCI datasets.

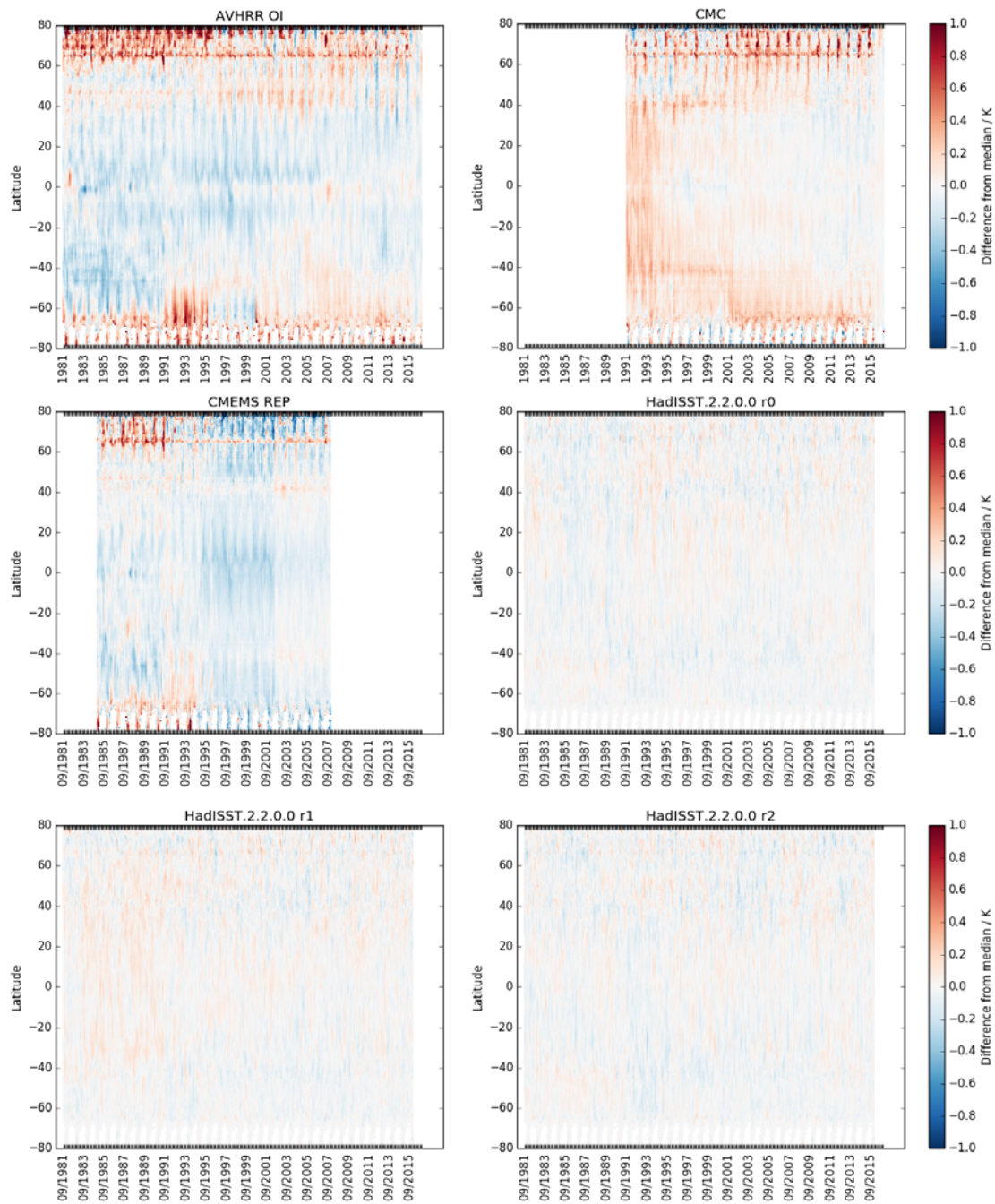


Figure 4-3. Hovmöller diagrams of the anomaly between each analysis included in the GMPE and the GMPE median.

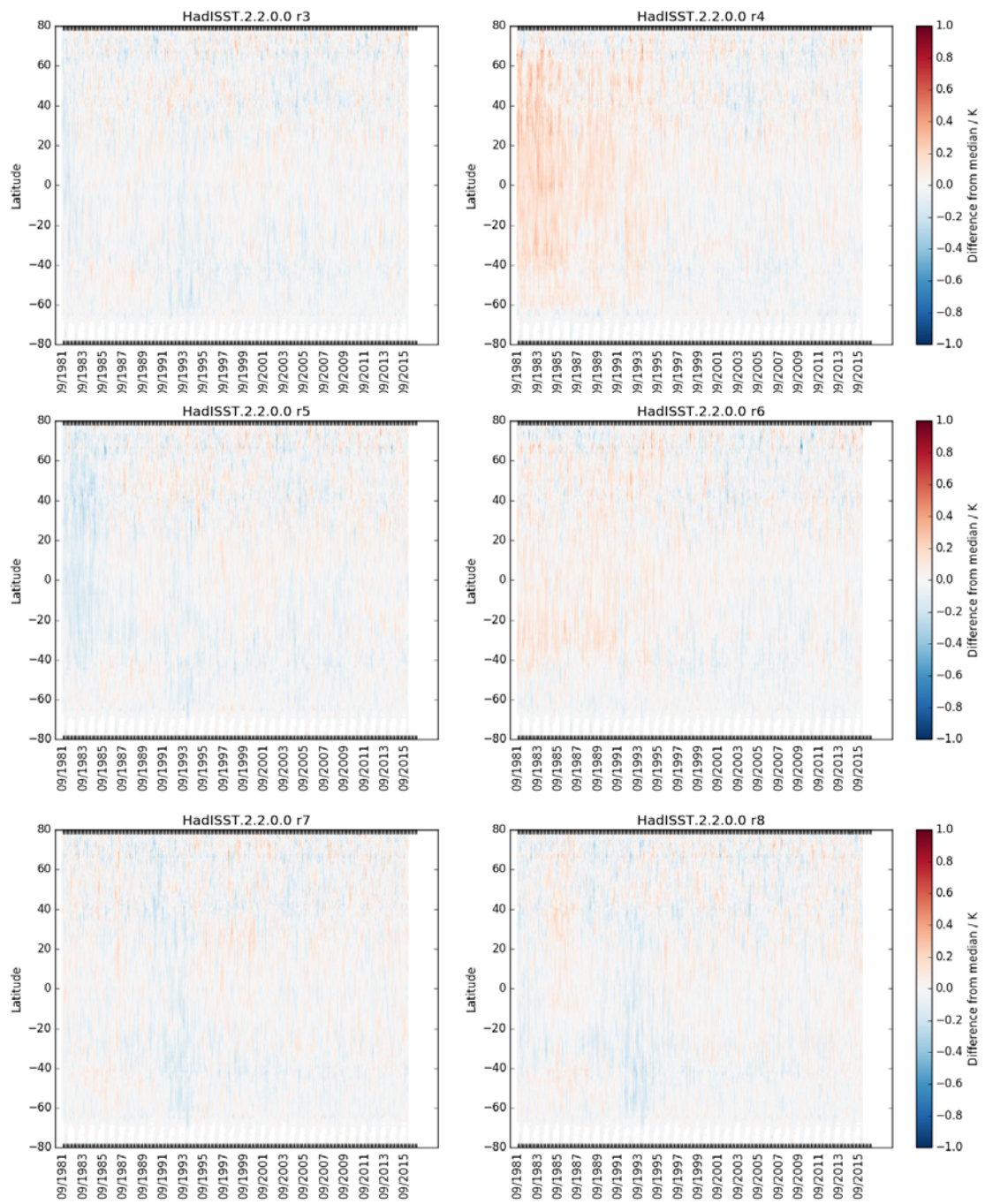


Figure 4-3 cont.

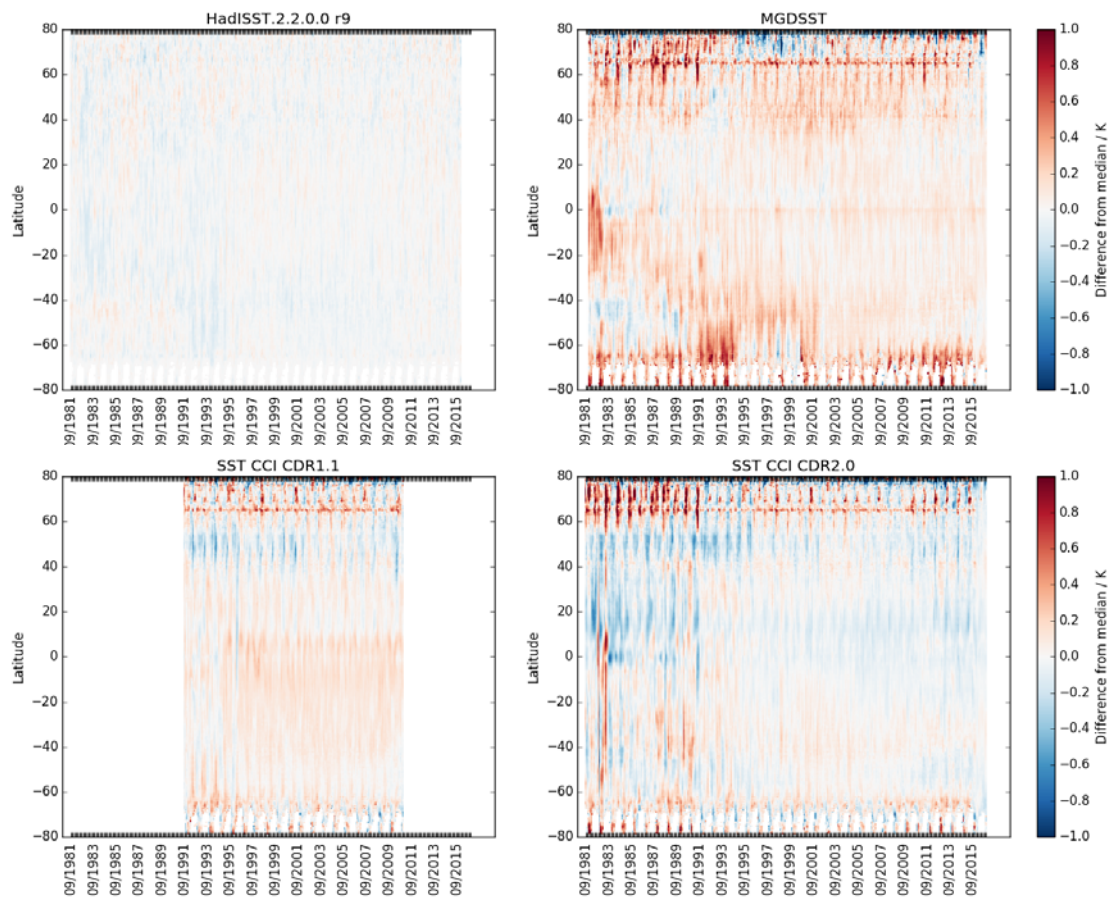


Figure 4-3 cont.

4.5 Conclusions

The GMPE outputs have been used to intercompare and assess different long-term analyses. Results relevant to the SST CCI analysis v2.0 are:

- Each analysis was compared to independent Argo data. The SST CCI analysis v2.0 was found to perform relatively well compared to other analyses in the analysis of the standard deviations of the differences. The CMC analysis performed best in this metric, but this may be partly because both it and the Argo data represent foundation temperature, while the SST CCI data represents 20 cm daily average. The SST CCI analysis v2.0 data were found to be cooler than the Argo data.
- Hovmöller plots of the differences between the analyses and the GMPE median showed that the SST CCI analysis v2.0 is relatively consistent with the median from 1991 onwards. Prior to that there are larger differences, which could be due to the GMPE median being noisier and/or the lack of ATSR data.
- Example plots of SSTs in the Gulf Stream region and their gradients showed the SST CCI analysis v2.0 analyses to be sharper and have larger gradients than the other analyses.

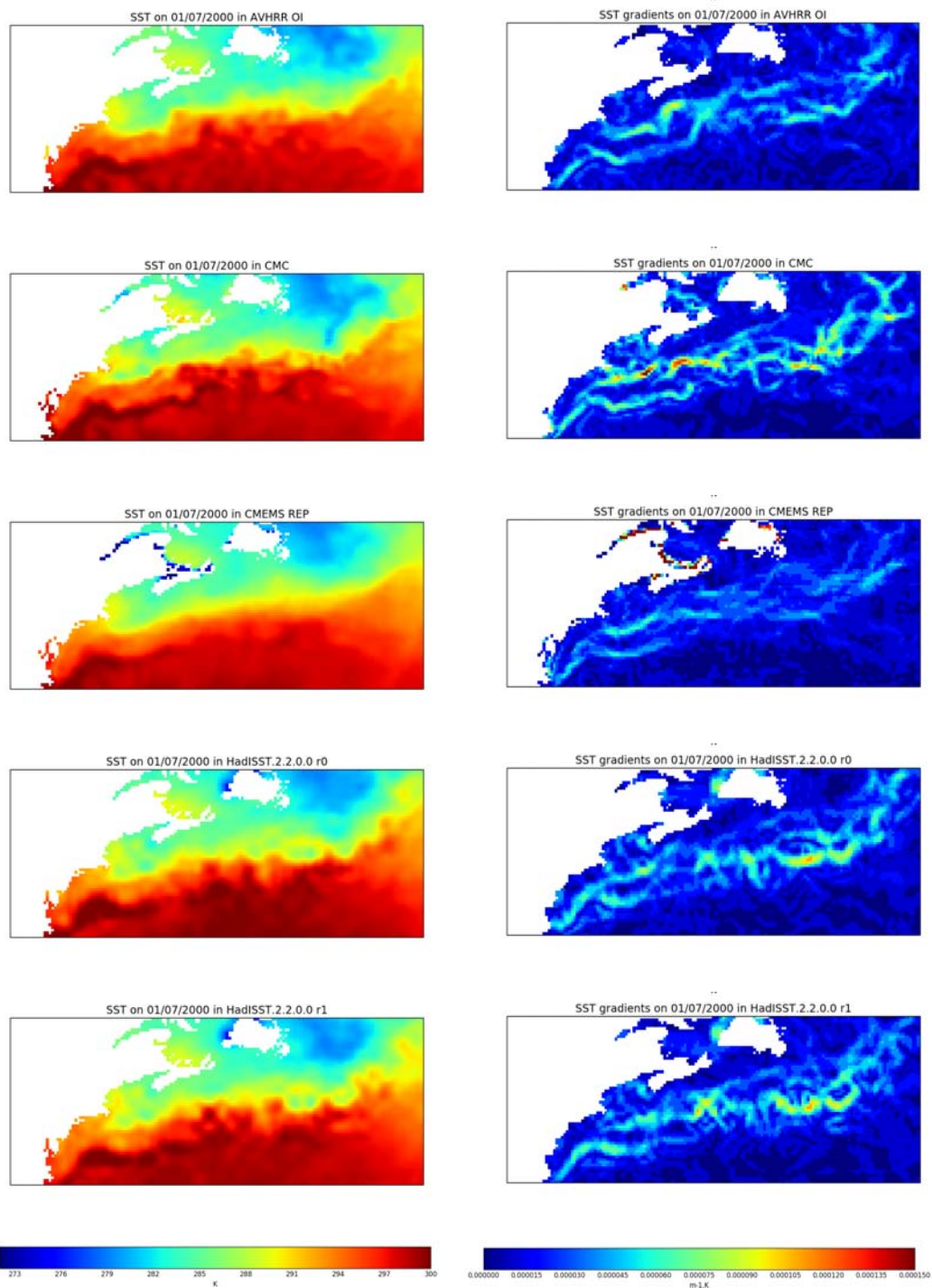


Figure 4-4. Example of SST fields and gradients from each analysis from the GMPE product for 01/07/2000.

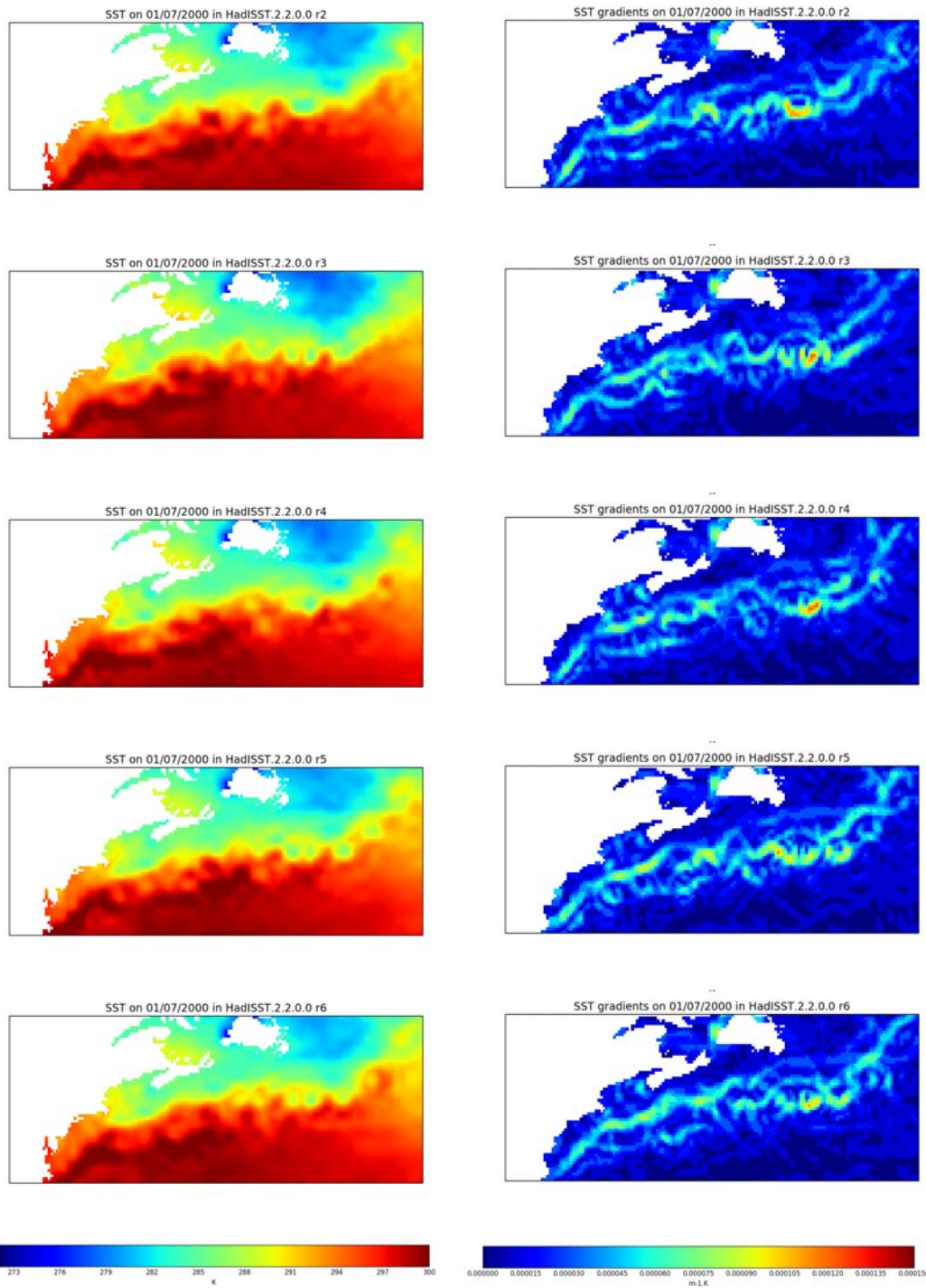


Figure 4-4 cont.

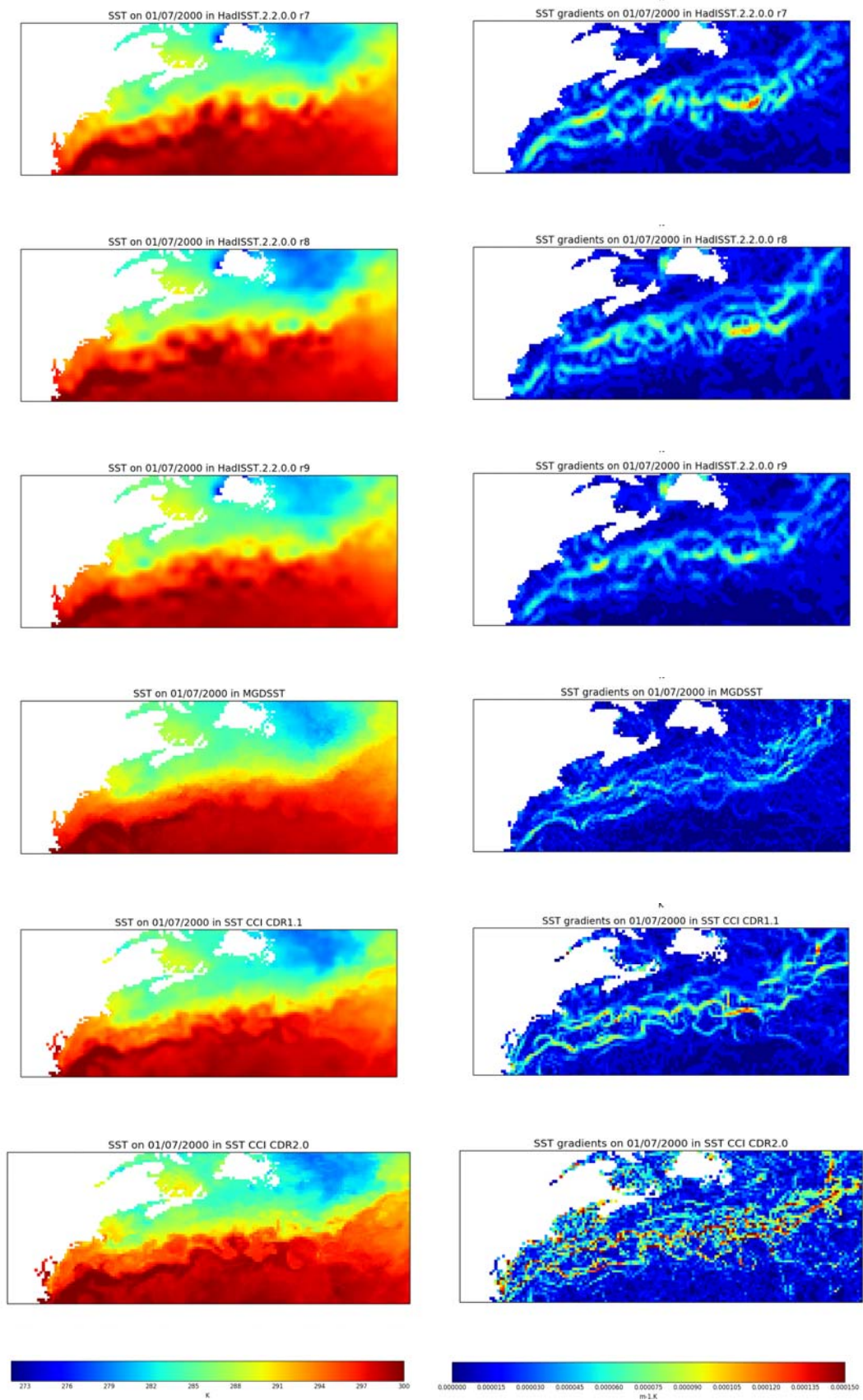


Figure 4-4 cont.

4.6 Acknowledgments

The GMPE products and this study have been generated/conducted using E.U. Copernicus Marine Service Information.

The Group for High Resolution Sea Surface Temperature (GHRSSST) AVHRR OI and CMC SST data were obtained from the NASA EOSDIS Physical Oceanography Distributed Active Archive Center (PO.DAAC) at the Jet Propulsion Laboratory, Pasadena, CA (<http://dx.doi.org/10.5067/GHAAO-4BC02> and <http://dx.doi.org/10.5067/GHCMC-4FM02>).

MGDSST data source was "NEAR-GOOS RRTDB" - https://ds.data.jma.go.jp/gmd/goos/data/rtrdb/file_list.php.

4.7 References

Brasnett B., 2008. The impact of satellite retrievals in a global sea-surface-temperature analysis. *Q.J.R. Meteorol. Soc.*, 134, 1745-1760. DOI: 10.1002/qj.319

Canada Meteorological Center. 2012. GHRSSST Level 4 CMC0.2deg Global Foundation Sea Surface Temperature Analysis (GDS version 2). Ver. 2.0. PO.DAAC, CA, USA. Dataset accessed [2018/19] at <http://dx.doi.org/10.5067/GHCMC-4FM02>

Fiedler, E.K., McLaren, A., Banzon, V., Brasnett, B., Ishizaki, S., Kennedy, J., Rayner, N., Roberts-Jones, J., Corlett, G., Merchant, C.J., Donlon, C., 2019, Intercomparison of long-term sea surface temperature analyses using the GHRSSST Multi-Product Ensemble (GMPE) system, *Remote Sensing of Environment*, 222, 18-33, doi: 10.1016/j.rse.2018.12.015.

Kennedy, J.J., Rayner, N.A., Millington, S.C., & Saunby, M. (2018). The Met Office Hadley Centre Sea Ice and Sea-Surface Temperature data set, version 2, Part 2: Sea Surface Temperature Analysis. *J. Geophys. Res. Atmos.* In prep.

Kurihara, Y., Sakurai, T., & Kuragano, T. 2006. Global daily sea surface temperature analysis using data from satellite microwave radiometer, satellite infrared radiometer and in situ observations. *Weather Bull.*, 73, 1–18. (in Japanese).

Martin, M., Dash, P., Ignatov, A. et al., 2012. Group for high resolution sea surface temperature (GHRSSST) analysis fields inter-comparisons. Part 1: A GHRSSST multi-product ensemble (GMPE). *Deep-Sea Research II* 77-80, 21-30, doi: 10.1016/j.dsr2.2012.04.013

Merchant, C. J., Embury, O., Roberts-Jones, J., Fiedler, E., Bulgin, C. E., Corlett, G. K., Good, S., McLaren, A., Rayner, N., Morak-Bozzo, S. and Donlon, C., 2014, Sea surface temperature datasets for climate applications from Phase 1 of the European Space Agency Climate Change Initiative (SST CCI). *Geoscience Data Journal*, doi: 10.1002/gdj3.20

Merchant, C.J. et al., 2019, Sea surface temperature datasets for climate applications from Phase 2 of the European Space Agency Climate Change Initiative (SST CCI). In preparation.

National Centers for Environmental Information. 2016. GHRSSST Level 4 AVHRR_OI Global Blended Sea Surface Temperature Analysis from NCEI. Ver. 2.0. PO.DAAC, CA, USA. Dataset accessed [2018/19] at <http://dx.doi.org/10.5067/GHAAO-4BC02>

Reynolds, R.W., Smith, T.M., Liu, C., Chelton, D.B., Casey K.S., Schlax, M.G., 2007, Daily High-resolution Blended Analyses for sea surface temperature. *J. Climate*, 20, 5473-5496, doi: 10.1175/2007JCLI1824.1

Roberts-Jones, J., Fiedler, E.K. and Martin, M, 2012, Daily, global, high-resolution SST and sea ice reanalysis for 1985-2007 using the OSTIA system, *J. Climate*, 25, 6215-6232, doi: 0.1175/JCLI-D-11-00648.1

5. ANALYSIS OF DEDICATED MODELLING EXPERIMENTS

5.1 Key messages

- We have analysed the influence of using the SST CCI analysis v2.0 (hereafter SST CCI) dataset as lower boundary forcing in atmosphere-only simulations at two horizontal resolutions, compared with the influence of using the HadISST.2.2.0.0 dataset.
- Overall, the impact of using SST CCI is relatively small, particularly in comparison with the influence of increasing the model's horizontal resolution.
- Where changes are seen, they are sometimes beneficial and sometimes detrimental.
- The warmer SST around the Maritime Continent, cooler SST at the equatorial Atlantic as well as the East Boundary Upwelling regions seem to reduce the bias in cloud regimes and radiation there. However, we do not know whether it is because these SST values are closer to reality, or these SST values are artefacts of aerosols and clouds which overcast the surface and such temperature is preferred by parameterizations for representing organized convection or boundary-layer clouds more realistically.
- The smaller sea ice cover in the SST CCI dataset reduces the overestimate of the frequency of clear-sky over the regions, which suggest that the sea ice fraction in the CCI dataset is more consistent with the International Satellite Cloud Climatology Project (ISCCP) sea ice product.
- No significant impact of the smaller sea ice fraction on atmospheric phenomena was found.
- Comparison of the atmospheric run with two different SST datasets was a good opportunity to investigate the influence of the range of uncertainty in observational SST data and estimate the local and remote impact.

5.2 Scientific analysis

5.2.1 AIMS OF THE STUDY

A new observational Sea Surface Temperature (SST) dataset based on satellite observations has been created (see earlier Sections in this report). The ESA SST CCI Analysis product version 2.0 (SST CCI analysis v2.0, hereafter SST CCI) is a daily satellite-only SST-depth analysis created by the OSTIA system from SST CCI ATSR and SST CCI AVHRR products. The data are provided at 0.05° resolution, in daily files covering 1981 – 2016.

Our aim is to investigate the response of an atmospheric model to the SST forcing provided by this dataset. We compare with the atmospheric model response to forcing from another daily SST dataset, HadISST.2.2.0.0 (Kennedy et al, in prep; Titchner and Rayner, 2014), which uses both satellite observations and ship observations.

We wanted to compare two daily SST forcing datasets, rather than a data sets where daily data are interpolated from monthly, such as the PCMDI AMIP forcing data set, which would not provide such a like-with-like comparison.

The versions of the satellite data used in SST CCI version 2.0 analysis are updated with respect to those used in HadISST.2.2.0.0 (SST CCI v1.0 AVHRR product and the ATSR Reanalysis for Climate). One dataset is not regarded a priori here to be better/worse than the other.

In this study we use four atmosphere-only experiments with two different SST and sea ice analyses, at two different horizontal resolutions. Our aim is to analyse large-scale differences in the atmosphere arising from relative differences in the average SST as well as from differences in SST variability. We also analyse how the differences are enforced or not in higher atmospheric resolution simulations with SST CCI.

5.2.2 METHOD

Our standard method of model evaluation is through the use of “Validation Notes” (which compare climatological fields from an “experiment” and a “control” simulation against observations and reanalyses of the real present-day climate) and “Auto-Assess” (which calculates process-based metrics relating to various regions and phenomena on a range of timescales). The four model simulations were each processed in this manner.

Atmospheric phenomena of interest, and corresponding regions, were selected based on the seasonal climatology of SST and sea ice, as well as various atmospheric variables in Validation Notes. Regions of interest here are: the Maritime Continent, Western Boundary Current regions, Eastern Boundary Upwelling regions and sea ice regions. To link the atmospheric phenomena related to the SST in the regions above, the effect of the different SST datasets on the following atmospheric phenomena are analysed: cloud regimes (section 5.2.3.3); tropical cyclones (section 5.2.3.4); South Asian summer monsoon (section 5.2.3.5); Madden-Julian Oscillation (MJO, section 5.2.3.6); El Niño Southern Oscillation (ENSO, section 5.2.3.7); and mid-latitude blocking, storms and North Atlantic Oscillation (NAO) (section 5.2.3.8).

In addition to the use of Auto-Assess, extra analyses are conducted for the variability of: surface temperature (time variance in the tropics, power spectrum over the West Boundary Current regions), cloud regimes, tropical cyclone tracks, NAO, and storm tracks.

Atmosphere-only simulations were conducted for the period 1982 to 2014 using the HadGEM3-GC3.1 model (Williams et al. 2018), configured for the CMIP6 HighResMIP experiments (Haarsma et al. 2016). The reference case uses HadISST.2.2.0.0 daily $\frac{1}{4}^{\circ}$ SST and sea-ice forcing (hereafter HadISST.2.2.0.0; Kennedy et al. in prep; Titchner and Rayner, 2014), to be compared with SST CCI analysis v2 (hereafter, in this report, SST CCI). Simulations at both 25-km (N512) and 130-km (N96) mid-latitude resolutions were completed for both SST forcing datasets.

5.2.3 RESULTS

5.2.3.1 SST

5.2.3.1.1 SST Annual Mean Climatology

First of all, the spatial distributions of the difference in the annual mean climatology in SST CCI from HadISST.2.2.0.0 are examined (Figure 5-1) and reveal the following:

1. SST CCI is lower in the Northern Hemisphere and higher in the Southern Hemisphere
2. SST CCI is higher along the West Boundary Current regions
3. SST CCI is lower in the East Boundary Upwelling regions

4. SST CCI is lower in the equatorial Atlantic
5. SST CCI is lower over the Arabian Sea
6. SST CCI is lower in the northern Pacific
7. SST CCI is higher around the Maritime Continent
8. SST CCI is lower in the equatorial central-east Pacific

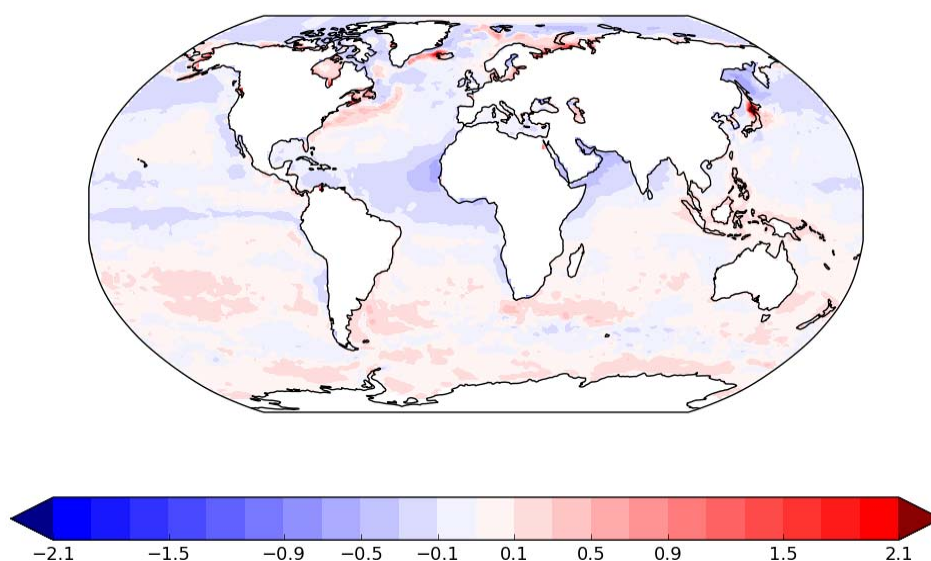


Figure 5-1. Climatological annual mean SST difference (K) of SST CCI analysis v2.0 from HadISST2.2.0.0 over the period 1982-2014. Plotted at N512 (~25km) resolution.

We note at this point that: 3) is a region of low stratocumulus; 4) and 5) tend to have impact from Saharan dust aerosols; 6) tends to be covered by stratus cloud; 7) tends to be a deep convective region. Although SST CCI introduced a new method to identify cloud-free conditions, these regions could either be contaminated by clouds/aerosols or the sampling of the cloud/aerosol free condition may be biased; we bear these points in mind as we continue.

5.2.3.1.2 SST Climatological Seasonal Variation

The characteristics of the seasonal variation of the SST difference in the two datasets (Fig 5.2) are: 1) the inter-hemispheric difference is stronger in MAM; 2) SST in West Boundary Current regions is higher in DJF; 3) SST in the East Boundary Upwelling regions is lower in JJA. Other notable features include a colder Arabian Sea throughout the year, but particularly in JJA, in SST CCI.

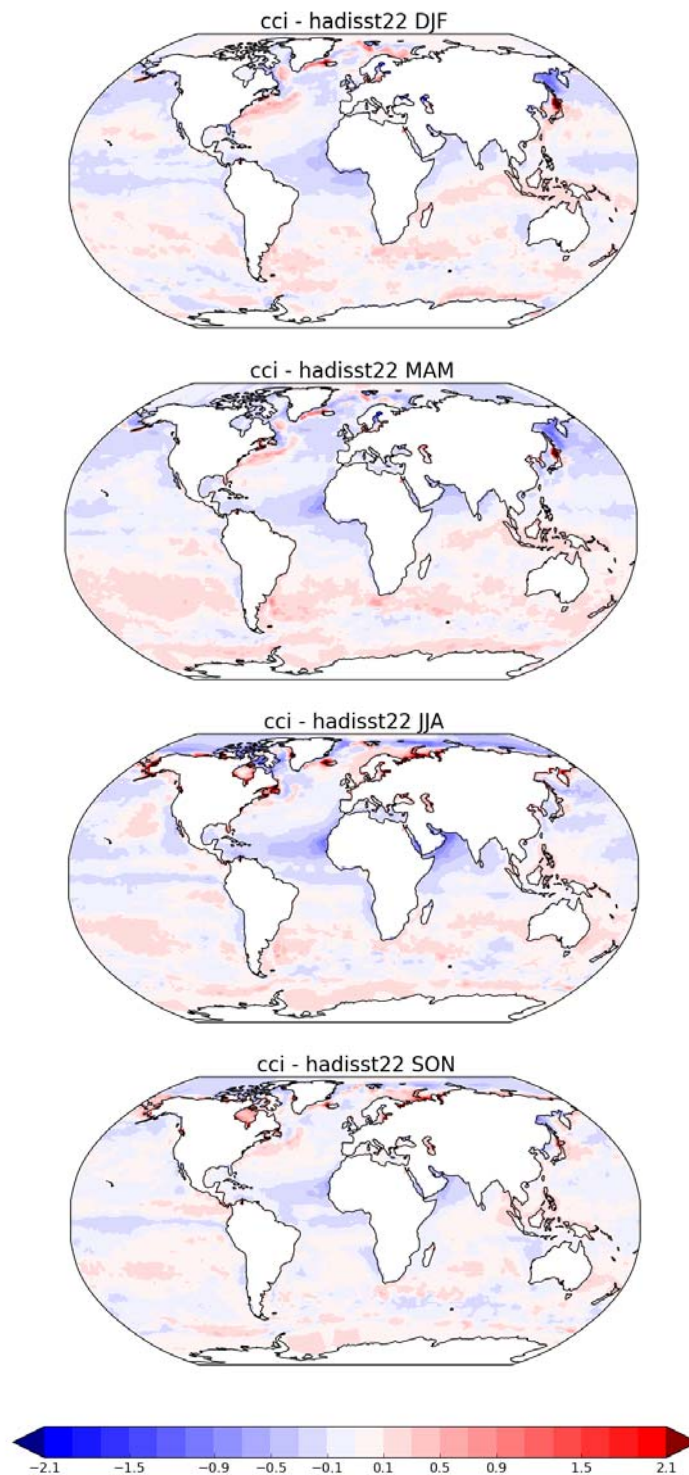


Figure 5-2. Climatological seasonal variation of the SST difference (K) in SST CCI analysis v2.0 from HadISST2.2.0.0. Plotted at N512 (~25km) resolution.

5.2.3.1.3 SST Variability

Variances of the tropical daily surface skin temperature data (Fig. 5.3) are found to be smaller in the SST CCI-forced simulations all over the ocean, except in the Eastern Pacific and Eastern Atlantic. This is also the case when the data are filtered to 10-90 days, which we do to highlight the intra-seasonal variability. In the N512 runs, small patchy areas over land including the Maritime Continent in SST CCI runs show larger variance, as does the northwest Arabian Sea.

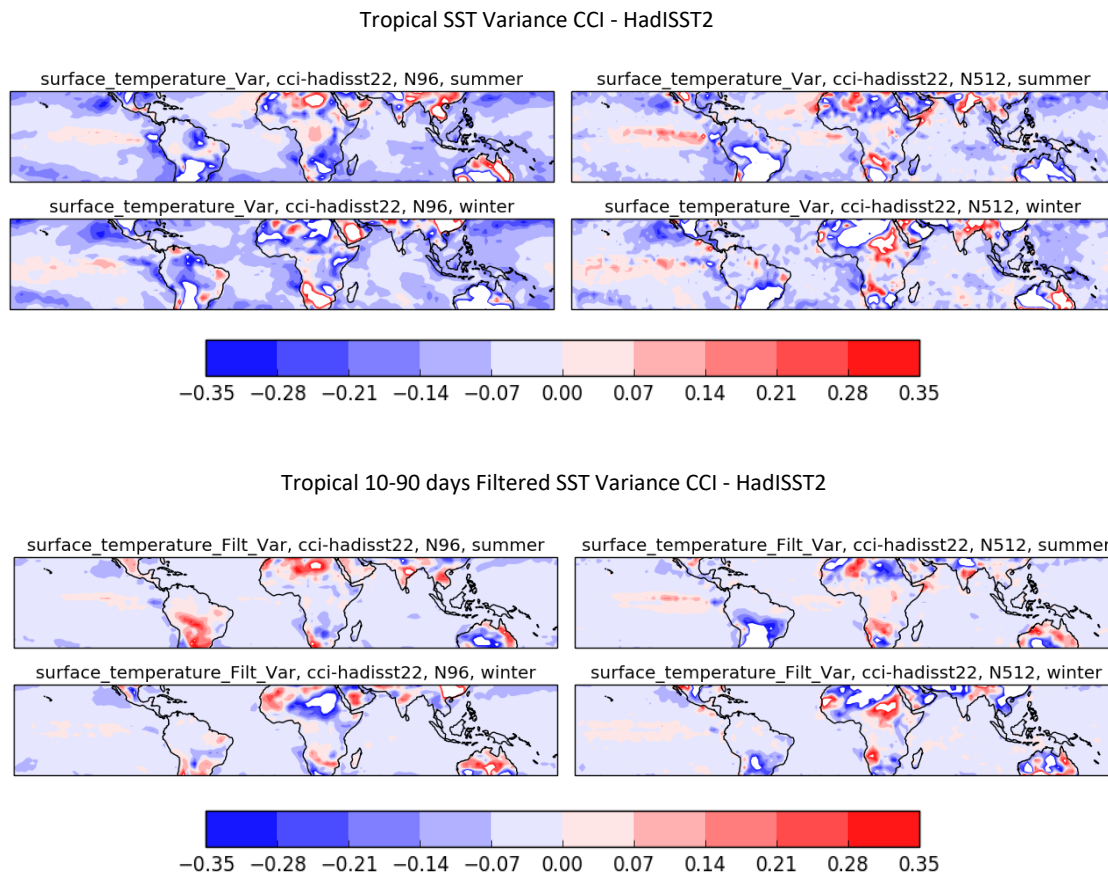


Figure 5-3. Spatial distributions of the difference in variance of the daily surface temperature data in SST CCI-forced simulation from HadISST2.0.0-forced simulation (CCI minus HadISST.2.2.0.0), (upper) non-filtered and (lower) filtered to isolate variability on 10-90 day timescale. In each 4-panel plot: (top left) N96 summer; (top right) N512 summer; (bottom left) N96 winter; (bottom right) N512 winter.

Power spectra of the surface skin temperature in the Western Boundary Current regions (Figure 5-4) show that both HadISST.2.2.0.0 and SST CCI analysis v2.0 capture signals between 100 and 10 km. These scales are better represented in SST CCI analysis v2.0, in the sense it exhibits a higher power density.

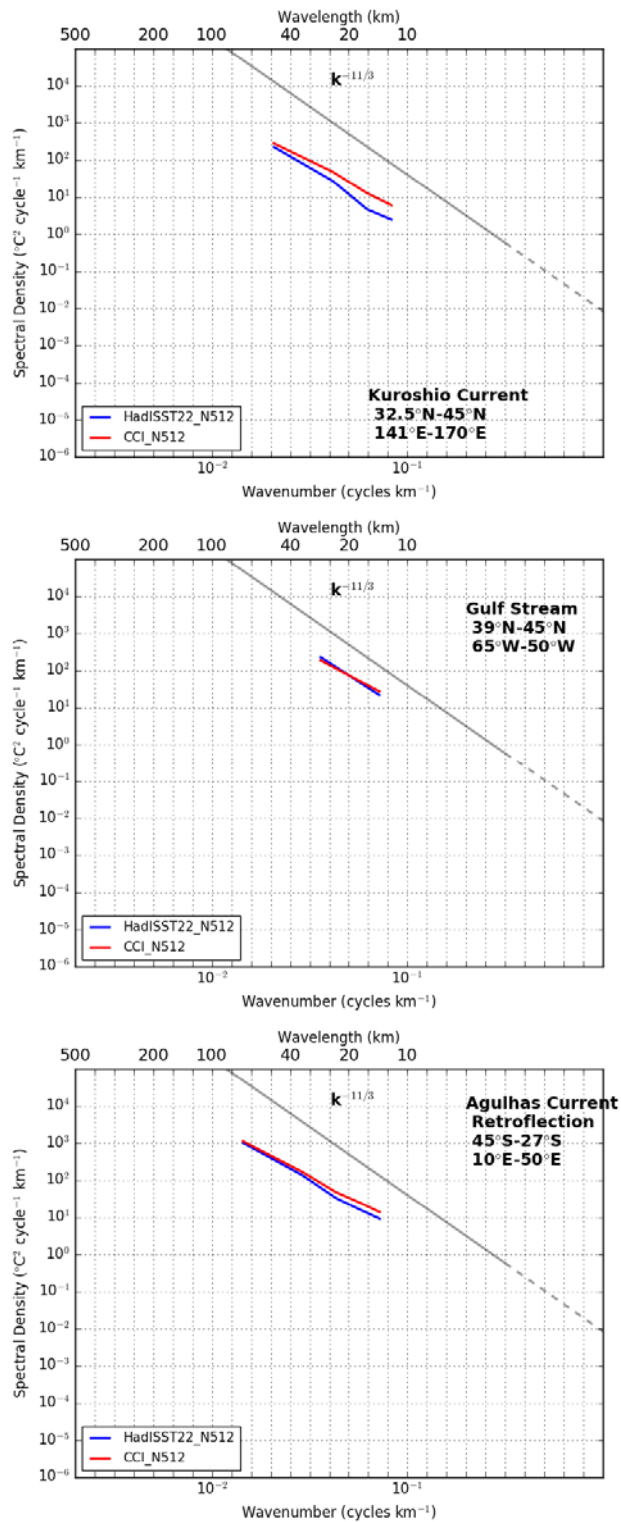


Figure 5-4. Power spectra in Western Boundary Current Regions: (upper) Kuroshio Current region, (middle) Gulf Stream region and (lower) Agulhas Current region. In each plot: blue for HadISST2.2.0.0, red for SST CCI analysis v2.0, grey represents theoretical power law.

5.2.3.2 SEA ICE

5.2.3.2.1 Sea Ice Annual Mean Climatology

Sea ice fraction in the SST CCI analysis v2.0 dataset is smaller, on average, than that in HadISST.2.2.0.0 (Fig 5.5). According to the validation notes, both simulations overestimate the outgoing shortwave radiation over the Arctic, but underestimate it over the Antarctic sea ice region in comparison with CERES-EBAF Edition 2.6r (Roeb et al., 2009)(not shown). Outgoing shortwave radiation is smaller in the SST CCI-forced simulation over the sea ice regions in both hemispheres (not shown). This is a reduction in the bias in the Arctic, but an increase in the bias over the Antarctic sea ice region.

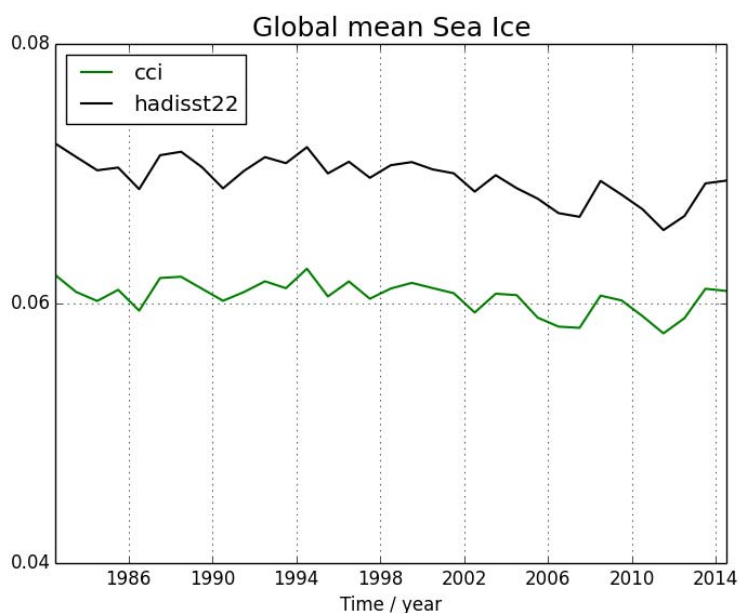


Figure 5-5. Time series of annual mean global coverage of the sea ice of SST CCI analysis v2.0 and HadISST2.2.0.0.

HadISST.2.2.0.0 applies bias adjustments to the passive microwave sea ice concentrations to make them consistent with historical ice chart data. The adjustments are quite large (see figures 5 and 6 in Titchner and Rayner, 2014). The SST CCI analysis v2.0 dataset uses passive microwave data without adjustments applied.

5.2.3.2.2 Sea Ice Climatological Seasonal Mean

The lower estimate of the sea ice fraction in the SST CCI analysis v2.0 is seen in all seasons (Fig 5-6).

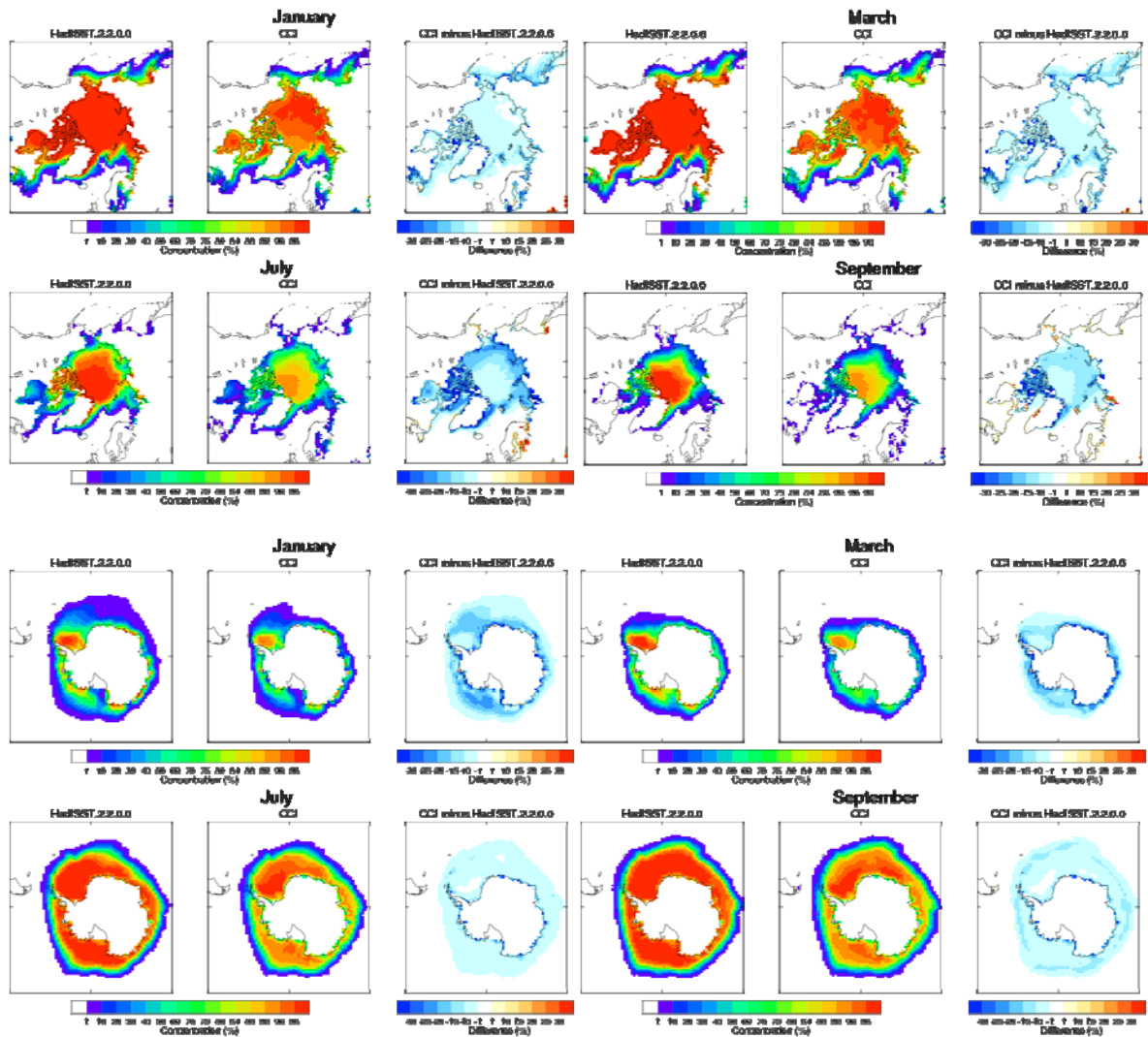


Figure 5-6. Climatological monthly mean (January, March, July, September) sea ice fraction (%) in SST CCI analysis v2.0, HadISST2.2.0.0 and the difference in SST CCI minus HadISST2.2.0.0 (top) in the Arctic, and (bottom) in the Antarctic.

5.2.3.2.3 Other comments relating to sea ice differences

The sea ice amount in SST CCI analysis v2.0 is smaller than that in HadISST2.2.0.0. Sea ice fraction in HadISST2.2.0.0 is much smaller after 1981 than in the period before (Titchner and Rayner, 2014). A climate feedback estimate derived using a historical simulation forced with HadISST2.1 sea ice dataset gives strong positive sea ice feedback (reduction in sea ice per global mean surface temperature change during the period), which does not have a physical explanation (Andrews et al 2018). Since the sea ice dataset incorporated into SST CCI analysis v2.0 has a smaller ice fraction than HadISST2.2.0.0 in the period from 1981 onwards, the sea ice estimated from the SST CCI dataset for the period with satellite observations, in combination with HadISST2.2.0.0 for pre-satellite period would be even larger than that using HadISST2.2.0.0 alone.

5.2.3.3 CLOUD REGIMES

5.2.3.3.1 Method and Data for Cloud regime projections

We apply the clustering method of Williams and Webb (2009) to daily International Satellite Cloud Climatology Project (ISCCP) observations and comparable Global Climate Model (GCM) output produced with the ISCCP simulator (Klein and Jakob 1999; Webb et al. 2001). A three-element vector of in-cloud mean cloud albedo (α), in-cloud mean cloud top pressure (CTP) and total cloud cover (TCC) is calculated for each daily mean GCM grid point. This is assigned to the closest observed regime based on the reference values of (CTP, α , TCC) in Tselioudis et al (2013) using a normalised minimum root-sum-square measure of distance. We define the relative frequency of occurrence (RFO) as the fraction of days on which each regime is assigned relative to the total number of data points. Annual and monthly climatological means of these quantities are calculated consistently for the models and observations. The period of the observed ISCCP data used is from 1984 to 2009. The RFO biases in the simulations are not sensitive either to the reference period or the length of the period of the observations.

5.2.3.3.2 Global Mean Climatology

Figure 5-7 shows global mean relative frequency of occurrence (RFO) of cloud regimes for July during 1982-2014. For the global average, the sign of the bias of the RFO of each cloud regime in HadISST.2.2.0.0-forced simulations remains in the SST CCI-forced simulations. This is consistent with the global summary seen in the validation notes that the global mean shortwave and longwave radiative fluxes are hardly different between the two simulations (within 0.2% difference). Slight changes in magnitude are seen between the HadISST.2.2.0.0-forced simulations and the SST CCI runs, but these are considerably smaller than the differences related to model resolution.



Figure 5-7. Global mean annual mean relative frequency of occurrence (RFO) of cloud regimes for the period 1982-2014. Shown as a difference from ISCCP, 1984-2009. HadISST.2.2.0.0-forced simulation at N96 (blue) and N512 (grey). SST CCI analysis v2.0-forced simulation at N96 (red) and N512 (yellow).

5.2.3.3.3 Global Distributions

The top panel of Figure 5-8 shows global maps of the difference in annual mean climatology of the RFO of cloud regimes between the HadISST.2.2.0.0-forced simulation and the observations. Different regimes have different distribution of errors. The Organized-convective regime is underestimated around the edges of the Maritime Continent but overestimated in the rest of the tropical ocean. Both the Anvil regime and the Cirrus regime are underestimated almost everywhere, especially over the Maritime Continent for the Anvil regime and over the subtropics for the Cirrus regime. Midlevel cloud regimes have positive bias in Medium-thick regime but negative bias in thin regime. The Fair-weather regime and the Shallow-cumulus regime are overestimated almost everywhere, especially the Fair-weather regime in the tropical ocean. Among the Stratocumulus regimes, the Low-Stratocumulus regime is overestimated over the East Boundary upwelling regions but the Thick-Stratocumulus regime is underestimated here. The RFO of the Clear-Sky regime suggests that the Eastern Boundary upwelling regions, land areas and sea ice regions all have too few cloud regimes and too much clear sky.

Differences in the spatial distributions of the RFO of the cloud regimes in the SST CCI runs are dominated by the tropical Organized-Convective-System regime, regimes associated with this regime (Anvil, Cirrus), and the Fair-Weather regime. With the increase in the RFO of the Organized-Convective-System regime over the Maritime Continent, the distributions of the regime shift southwards. This could be because of the difference in the spatial pattern of SST CCI in different seasons (Fig 5-2). There may be an impact of the warmer Southern Hemisphere SST, but it is not clear. The RFO of the Anvil regime and Cirrus regime are also larger over the Maritime Continent and their spatial patterns roughly agree with that of the Organized-Convective-System regime, with a wider spatial distribution in the Cirrus regime.

The changes in the Fair-Weather regime in the tropics are also suggested to be related to the changes in the tropical Organized-Convective-System regime. Over the regions where the RFO of the Organized-Convective-System system regime show big differences, the RFO difference the Fair-Weather regime is anti-correlated. One might suspect that the anti-correlation is an artefact of whether more (fewer) deep convective clouds overcast the regimes beneath and fewer (more) fair-weather clouds are identified by the ISCCP-simulator which sees radiative flux data at the top-of-the-atmosphere. Removing the impact of the masking effect would reduce the magnitude of the RFO difference of the fair-weather regime in the regions with organized convective systems. However, the anti-correlation remains, because the magnitude of the changes in the Fair-Weather regime tends to be much larger than the masking effect of the tropical organized convective clouds. This suggests that the changes in the Fair-Weather regime are related to the changes in the Organized-Convective-System regime in the tropics.

Although Western Boundary Current regions are one of the areas with the largest SST difference in SST CCI analysis v2.0 data relative to HadISST.2.2.0.0, the changes in clouds over these regions are subtle. They may be hidden by the remote changes caused by the SST differences over the Maritime Continent.

The RFO of the Clear-sky regime shows decreases over the sea ice regions in the SST CCI-forced simulation compared to the HadISST.2.2.0.0-forced simulation except a part of the edge of Greenland and the South Pole, and the positive biases are much smaller in the SST CCI runs. These smaller biases suggest that clouds occur more frequently over these regions in the SST CCI runs. Stratocumulus regimes contribute to the increase in the frequency of cloud regimes over the Eastern Boundary upwelling regions, especially the thick stratocumulus regime. Midlevel regimes, Shallow-Cumulus regime and the High- and Thick-Stratocumulus regimes contribute to the increase in the frequency of cloud regimes over the sea ice regions, but the changes in their contributions are different in different seasons and not all of the changes reduce biases (not shown). The RFO of Clear-sky regime also shows decrease over Eastern Boundary upwelling regions.

We next examine the seasonal variations in the Stratocumulus and Organized-Convective-Systems regimes in more detail.

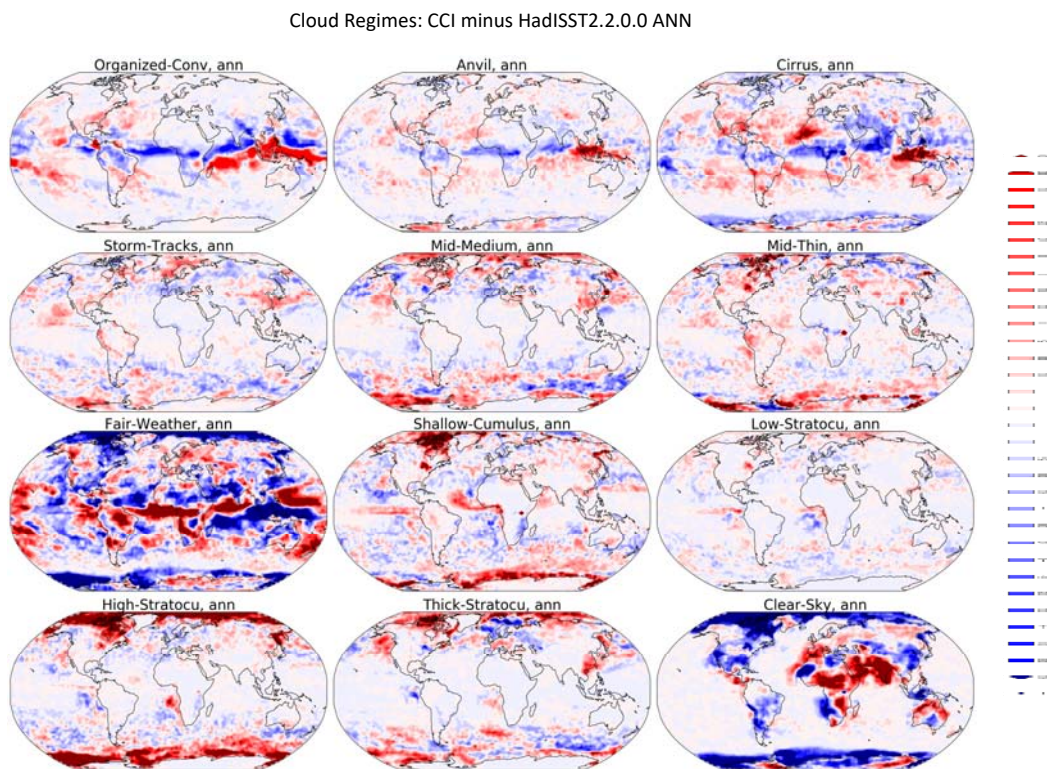
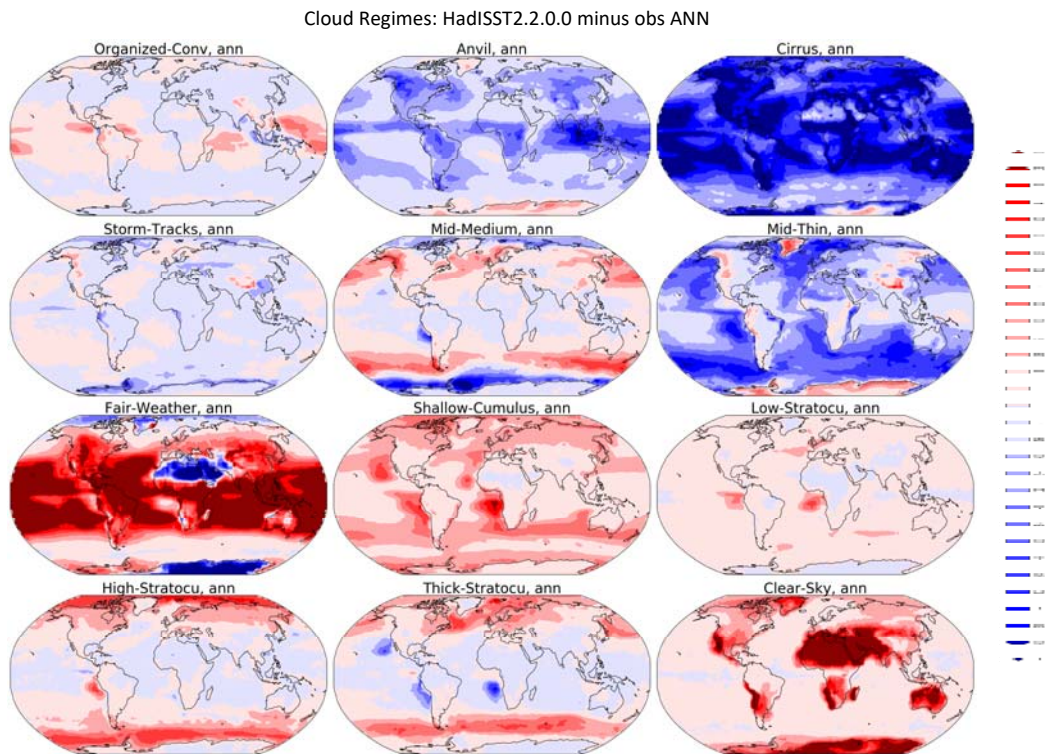


Figure 5-8. Global maps of the annual mean climatology of the RFO of cloud regimes, (upper) difference in HadISST.2.2.0.0-forced simulation from the observations, (lower) difference in SST CCI-forced simulation compared with the HadISST2.2.0.0 run (N96).

5.2.3.3.4 Stratocumulus

Although there is a spatial variation as well as monthly variation, larger thick-Stratocumulus regimes off the coast of California as well as Angola in July (Figure 5-9) contribute to the smaller RFO of clear-sky, as well as a reduction in the negative bias in the SST CCI-forced simulation in the outgoing shortwave over the region in the validation notes (not shown).

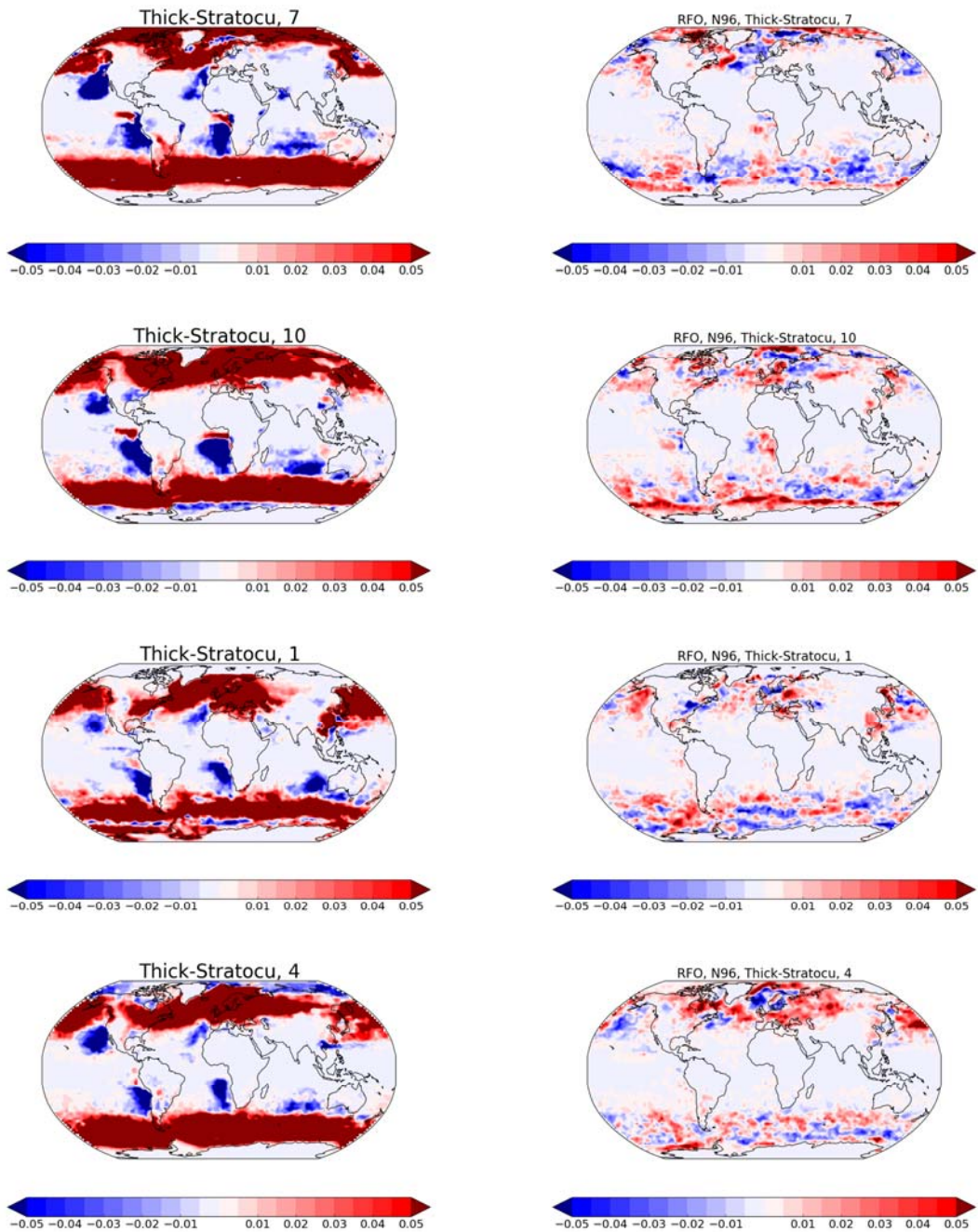


Figure 5-9. Global maps of the climatology of the RFO of thick stratocumulus regimes. From the top, July, October, January and April. (left) Biases in the RFO relative to ISCCP, and (right) the difference in the SST CCI-forced run compared with the HadISST2.2.0.0-forced run (N96).

Around the Eastern Boundary upwelling regions the RFO of the Stratocumulus regimes tends to be larger in the SST CCI runs in JJA, when the SST in the upwelling regions is lower in CCI data (Figure 5-2). According to Zhou et al. (2017), low cloud amount and outgoing shortwave flux increase with lower SST over the eastern boundary upwelling region (local effect) and with higher SST around the Maritime Continent (remote effect by the increase in subsidence). The SST CCI run has lower SST over the Eastern Boundary upwelling region and higher SST around the Maritime Continent (Figure 5-1). Both can contribute to the changes in stratocumulus regimes. Further study is necessary to understand how the difference in SST in each region affects different types of stratocumulus regimes.

5.2.3.3.5 Organized Deep Convective System regime

Spatial distributions of the differences between the RFO of the Organized-Convective-System regime in the two simulations show an increase over the Maritime Continent and a decrease over the Himalaya and India and the East Indian Ocean in the SST CCI-forced simulation. These changes reduce the bias. However, this regime also increases over the Equatorial Western Pacific and the Southern Indian Ocean, which increases the bias there. Further, the difference is slightly different in different seasons. The difference around the Maritime Continent is consistent with the seasonal difference between the two SST analyses (Fig 5.-2). In July (Fig. 5-10) the RFO of this regime also increases over the equatorial Western and Central Pacific and Thailand (increase in bias), but decreases in the north of the Philippine Sea and the West Pacific, Thailand and the subtropical Central Pacific (reduction in bias). In January and April, the increase in the regime around the Maritime Continent extends longitudinally, which reduces the bias over the Maritime Continent but increases the bias over the extended area. The regime decreases in the northern neighbouring area of the Philippine Sea and the Western Pacific Ocean, and also over the Congo Basin (reduction in bias).

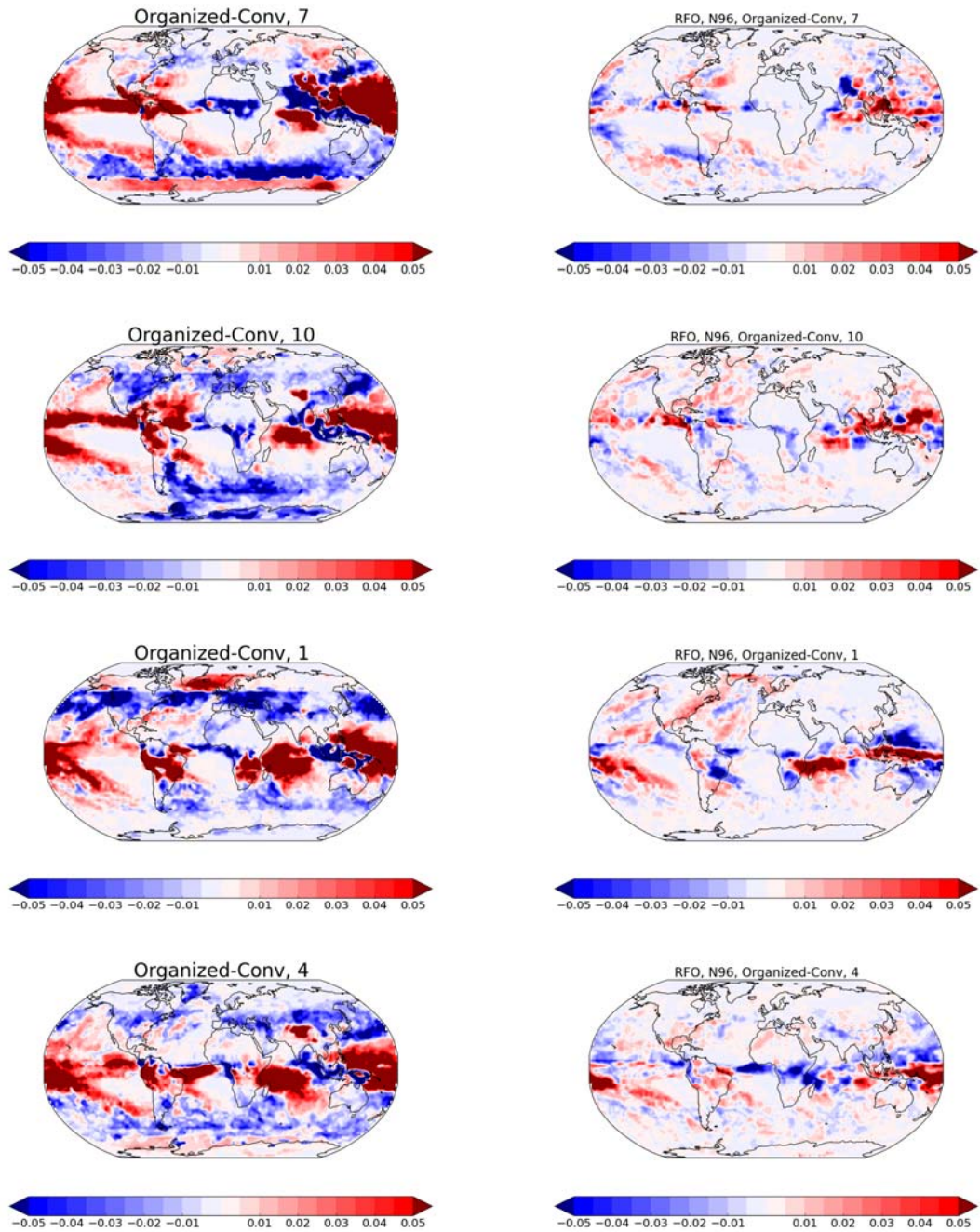


Figure 5-10. Global maps of the climatology of the RFO of Organized-Convective-System regimes. From the top, July, October, January and April. (left) Biases the RFO relative to ISCCP, and (right) the difference in the SST CCI-forced run compared with the HadISST2.2.0.0-forced run (N96).

5.2.3.3.6 Summary

The biases in the RFO of cloud regimes found in HadISST.2.2.0.0 runs remain in the SST CCI runs both in a global mean sense and in the spatial distributions. In this regard, the impact of the SST difference is subtle.

The result that cloud regime occurrence is underestimated over the sea ice regions and that the underestimate is smaller in the simulation forced with SST CCI analysis v2.0 suggests that the sea ice fraction in the SST CCI data is more consistent with the ISCCP sea ice dataset. We come to this conclusion because the ISCCP retrieved clouds are influenced by the sea ice data set used in the retrieval. The ISCCP Snow/Ice dataset contents are snow and sea ice fractional coverage deduced from ship/shore station reports and satellite visible, infrared, and microwave imagery data. Clouds over white surfaces are difficult to identify, especially low clouds. Hence whether the surface in a region is covered by snow/sea ice matters for cloud retrieval over the region.

The result that cloud regime occurrence is underestimated over the Eastern Boundary upwelling regions and that the underestimate is smaller in the SST CCI run implies that SST in the stratocumulus region given to the model could partly be responsible for the bias found in clouds.

The Organized Convective System regime is underestimated in the model simulations over the Maritime Continent. It is sensitive to the SST change and it affects the occurrence of the Fair Weather regime in the tropics more generally. The RFO increase for the Organized Convective System regime found in the SST CCI run is consistent with higher SST around the region and agrees better with the cloud observations. However, associated changes in neighbouring regions do not always improve the model bias there and are not necessarily consistent with the change in the local SST, which suggests that the change is caused by the change in the position of the convergence.

Despite the fact that the SSTs along the Western Boundary Current regions are distinctly higher in the SST CCI analysis v2.0, no clear RFO difference is found over these regions. Local and remote effects on the regimes over these regions could be cancelled out, but this cannot be distinguished in this study. We suggest that the impact of the SST over Western Boundary Current regions on clouds are relatively subtle compared with the remote impact of SST from other regions.

5.2.3.4 TROPICAL CYCLONES

5.2.3.4.1 Tropical cyclone tracking

We use the TRACK feature tracking software (Hodges et al. 2017) to identify and track tropical cyclone vorticity features using six-hourly simulated data for the period 1982-2014. In this analysis, we additionally compare with simulations forced by the monthly PCMDI dataset (Taylor et al. 2000, as used in the standard CMIP6 AMIP-II simulations, hereafter PCMDI-SST).

It should be noted that tropical cyclones (TCs) are extreme events, and as such there are not many globally each year (~100). Hence comparing the interannual variability in individual basins in single simulations does not give robust results. Here we use an ensemble of five simulations with the HadISST.2.2.0.0 dataset, to set against the one member with the other datasets, to see if there are systematic differences.

Observed TC tracks for the North Atlantic and Eastern Pacific basins are obtained from the National Oceanic and Atmospheric Administration (NOAA) National Hurricane Center's best-track Hurricane Database (HURDAT2 (Jan 2018 version); Landsea and Franklin, 2013). Observed TC data for all remaining basins are obtained from the US Navy's Joint Typhoon Warning Centre (JTWC) best-track database (Chu et al., 2002).

These will jointly be referred to as Observations in the following. We define an observed TC as having a 1-minute maximum sustained wind speed of 34 kt (17.5 m s⁻¹) or higher, to give a globally-uniform criterion, and we exclude subtropical storms from observations. We use Accumulated Cyclone Energy (ACE; Bell et al., 2000) as the main measure of tropical cyclone activity – it combines the number of storms each year with their lifetime and their windspeeds, and is a more robust measure than simple counts per year.

Ocean basins are defined: North Atlantic 100W-20E, 0-60N; East Pacific 140W-75W, 0-40N; North West Pacific 265W-180W, 0-60N.

5.2.3.4.2 Mean tropical cyclone activity per ocean basin

The mean tropical cyclone activity (as measured by ACE) is shown in Figure 5-11 for each (single member) simulation driven by the different SST datasets. In the northern hemisphere, there is slightly more TC activity in the SST CCI simulation, which is a combination of increased activity in the Pacific (East and North West) together with a slight reduction in the Atlantic – however all of these changes are within the interannual standard deviation (measured by the black line). For the Southern Hemisphere, there is a clearer increase in activity with SST CCI, particularly in the South Indian and South Pacific basins.

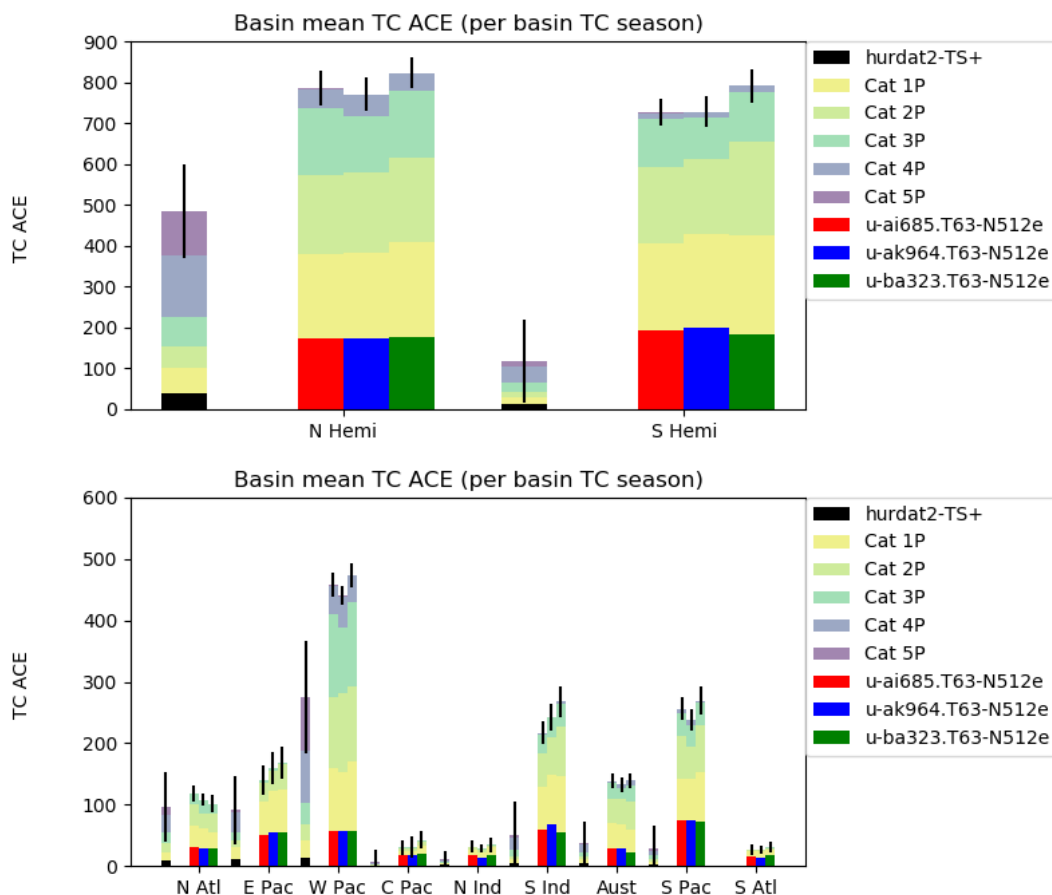


Figure 5-11. Mean tropical cyclone activity (ACE) in (top) Northern and Southern Hemispheres and (bottom) each ocean basin over the period 1982-2014. The colours in each bar show the proportion of ACE related to particular storm strengths. The initial colour indicates the N512 model (red is the HadISST2.2.0.0-forced simulation, blue is PCMDI-SST-forced, green is SST CCI-forced, black is observations) and corresponds to the weakest storms. The Cat xP shadings indicate how strong the tropical cyclone was (in terms of minimum sea level pressure), from weak (Cat 1P) to strong (Cat 5P).

5.2.3.4.3 Tropical cyclone interannual variability

The tropical cyclone interannual variability in the North Atlantic (NA), East Pacific (EP) and North West Pacific (WP) are shown in Figure 5-12 (for the 25km simulations only) over 1982-2014 for each of the simulations. These figures show the (ACE) per year.

It is clear that the interannual variability is quite noisy, and this is a combination of forced variability (for example driven by the SST forcing, by large-scale phenomena such as El Niño), as well as weather-type variability that the model (and the real world) produces. Hence, we would not expect the model simulations to agree perfectly with observations, and the five-member ensemble gives an idea of the range of variability using the HadISST.2.2.0.0 forcing dataset with slightly perturbed initial conditions.

The overall impression from these time series is that for the North Atlantic, ACE activity in the SST CCI simulation is generally a little lower than the HadISST.2.2.0.0-forced ensemble mean, while for the East Pacific the activity is slightly higher. The NW Pacific does not show a significant difference. There are often large differences between simulated and observed ACE, with a clear systematic offset between the simulations over the western Pacific and the JTWC observations.

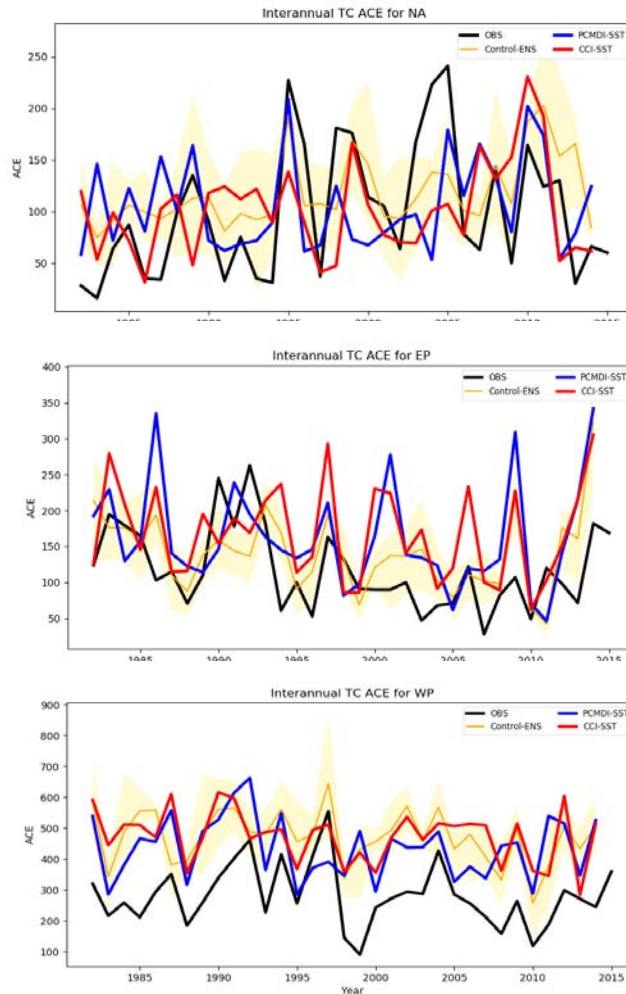


Figure 5-12. Tropical cyclone interannual variability in (top) North Atlantic (NA); (middle) East Pacific (EP); (bottom) North West Pacific (WP). Control-ENS (orange) is the ensemble of five members using HadISST.2.2.0.0. (Blue), PCMDI-forced simulation. (Red) SST CCI-forced simulation. (Black) observations.

5.2.3.4.4 Tropical cyclone track density

The tropical cyclone track density (number of storms moving through a 4° cap centred at each point per month) is shown in Figure 5-13. The left-hand column shows the bias in the different models against observations, and the right-hand column shows the impact of using a different SST forcing compared to the control HadISST.2.2.0.0 dataset. There is a clear reduction in the low bias (blue regions) seen at N96-130km in the North Atlantic when we move to N512-25km using either CCI SST or PCMDI-SST, while for the North West Pacific the model is rather over-active at N512 (left column). Comparing both these datasets with HadISST.2.2.0.0 (right column), we see they both have slightly reduced activity in the North Atlantic, more activity in the Eastern Pacific, and a more mixed signal in the North West Pacific. It is hypothesised that the reduced Atlantic and increased Eastern Pacific activity may be related, perhaps because easterly waves are prevented from becoming tropical cyclones in the Atlantic due to the cooler SSTs, and then are able to form later on in their lifetime. The excessive activity in the Southern Hemisphere (as seen earlier) is slightly enhanced in the South Indian Ocean with PCMDI-SST and CCI SST. It should be noted that this overall Southern Hemisphere excess is sensitive to the particular tracking algorithm used.

5.2.3.4.5 Conclusions

There is considerable variability in the tropical cyclone climatology, making it difficult to draw clear conclusions from just one model simulation using the different SST datasets (compared to the control ensemble using HadISST.2.2.0.0). However, there are indications that using the SST CCI does have some impact, though this is considerably smaller in magnitude than existing model biases against the observed climatology.

There are several systematic differences notable at both 130km and 25km resolutions in the SST CCI-forced simulation compared to the HadISST.2.2.0.0-focused simulations:

1. For the most part, the impact of different SST forcing is smaller than the bias, and the impact is consistent at both 130km and 25km simulations;
2. There seems to be some indication of a reduction in storms in the North Atlantic (particularly in the western part), and an increase in the East Pacific;
3. The NW Pacific signal is more complex, with perhaps a reduction to the south and an increase further north.
4. Southern Hemisphere activity generally increases with the SST CCI simulation.

For (2) and (4), these changes would be consistent with the SST differences shown in Section 5.2.3.1 (cooler in the Atlantic and warmer in the East Pacific). SST is certainly not the only driver of tropical cyclones, but warmer SSTs are conducive to their genesis.

The reduction further south in the NW Pacific is consistent with differences noted for the monsoon (see Section 5.2.3.5), where a slightly stronger jet is found in flow from the Indian Ocean towards the NW Pacific – this would act to reduce (or steer northwards) tropical cyclones, and hence prevent them from making landfall in this region.

However, more detailed analysis would be required to be certain about these hypotheses. The understanding of model biases against observations has many components (model bias, forcing bias, observational bias, tracking bias), and separation of these is complex. This exercise can help to suggest how sensitive model simulations are to the SST forcing, and hence give some idea of the uncertainties in present day simulations (and hence future projections).

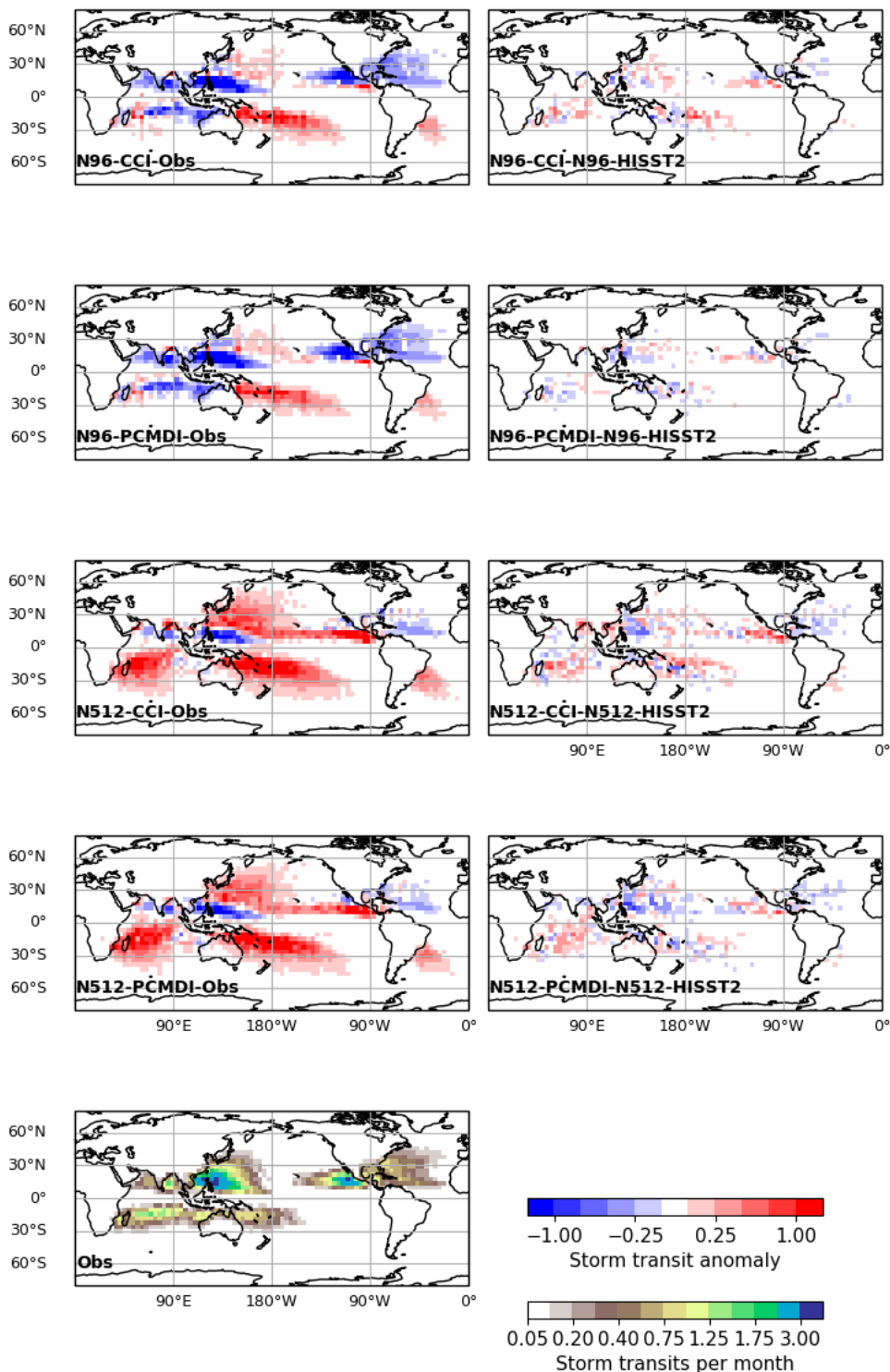


Figure 5-13. Tropical cyclone track density (number of storms per month passing over a 4-degree cap at each point). Lower left is the observed track density. The left column shows the difference between the given model simulation and observations, while the right column shows the difference between that same model simulation and the control (driven by HadISST.2.2.0.0).

5.2.3.5 EFFECTS ON SOUTH ASIAN SUMMER MONSOON

5.2.3.5.1 Climatology

Seasonal mean precipitation differences (Figure 5-14) show less rainfall (smaller bias when compared against Tropical Rainfall Measuring Mission 3B42 product, version 7-7A (hereafter referred to as TRMM; Kummerow et al. 1998, Huffman et al. 2010, Huffman et al. 2013) over the equatorial Indian Ocean and less over the Himalayan foothills, at both horizontal resolutions, in the runs forced by SST CCI. However, at N96 there is a decrease in rainfall over northern/central India, while at N512 there is an increase. At both resolutions, there is also a detrimental reduction in rainfall over the southern and eastern Arabian Sea.

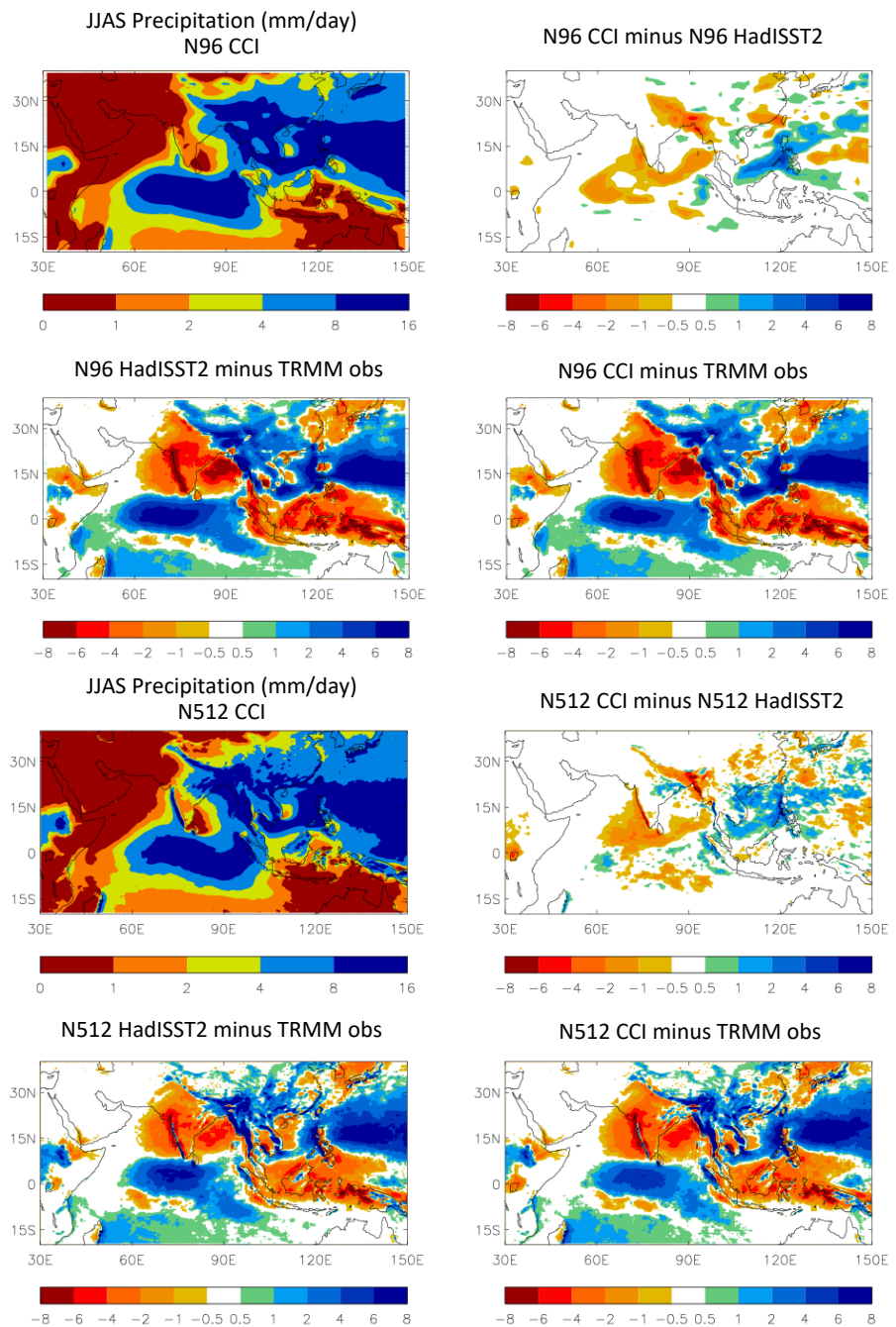


Figure 5-14. JJAS mean rainfall (mm/day) in the (upper) N96 and (lower) N512 simulations. In each 4-panel plot: (top left) precipitation in run forced by SST CCI; (top right) difference between runs forced by CCI and HadISST.2.2.0.0; (bottom left) error in precipitation (against TRMM observations) in run forced by CCI; (bottom right) error in run forced by HadISST.2.2.0.0.

The reduction in rainfall over the Arabian Sea when using SST CCI may be related to colder SSTs over the northern and western Arabian Sea in this dataset. Levine and Turner (2012) showed that colder Arabian Sea SSTs are related to reduced moisture fluxes and therefore affect Indian monsoon rainfall, particularly in the early part of the season. The seasonal cycle of rainfall (Figure 5-15) shows reduced rainfall in June and July with the SST CCI, and maps of the monthly rainfall differences (not shown) indicate that the changes along the western Ghats and eastern Arabian Sea occur in June. This is consistent with the study of Levine and Turner (2012) and Levine et al. (2013), although the SST differences in the current case are rather smaller than those tested in those studies. The reason for the reduction in the equatorial Indian Ocean rainfall bias is unclear, although it may be related to the colder Arabian Sea SSTs via the other changes in circulation.

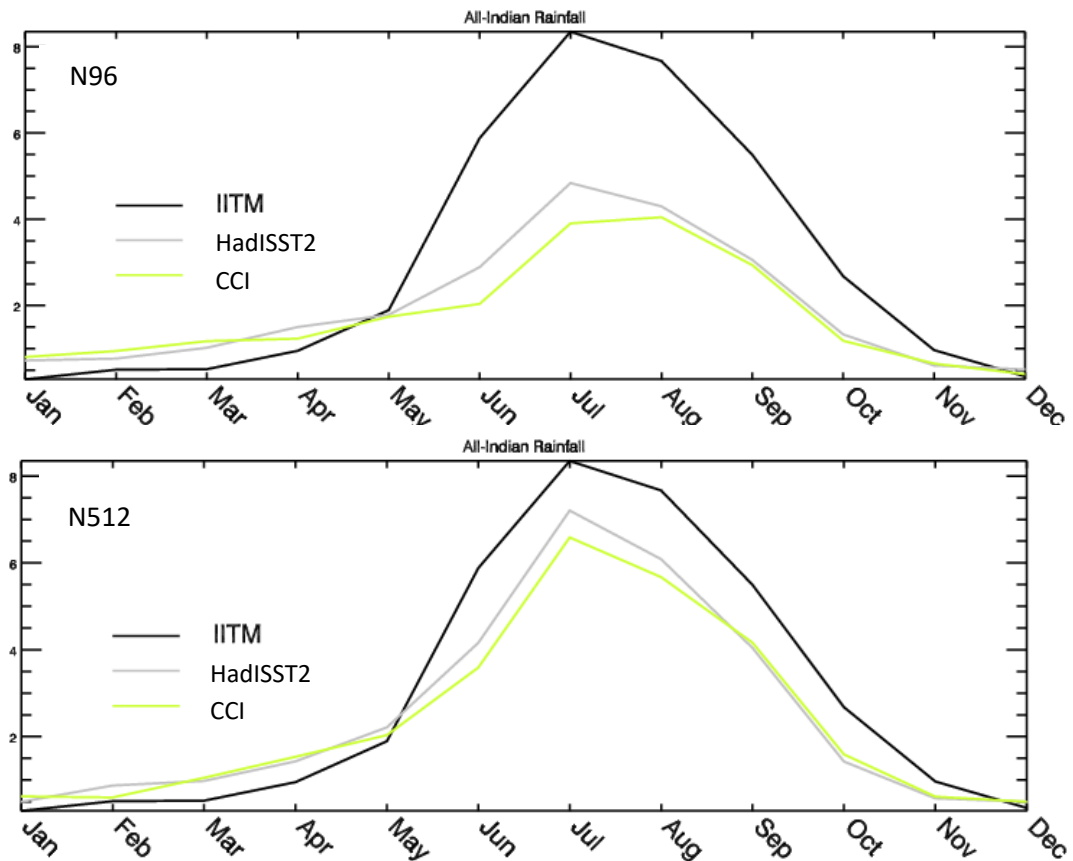


Figure 5-15. Seasonal cycle of monthly All-India rainfall from the four simulations, forced by (green) SST CCI and (grey) HadISST.2.2.0.0, at (top) N96; (bottom) N512 resolution. The black line shows All-India rainfall climatology provided by the Indian Institute of Tropical Meteorology (IITM; https://tropmet.res.in/static_pages.php?page_id=53)

In both cases, the rainfall changes over central and northern India appear to be related to differences in the rainfall contribution from monsoon depressions and low-pressure systems (Figure 5-16). These systems are the main contributors to rainfall in this region, but are often underestimated in models, particularly at lower resolutions (Levine and

Martin, 2017). Therefore, it might be argued that the changes between the runs at N512 resolution could be more indicative of the effects of the SST changes.

It is notable that, at N96, the decrease in rainfall contribution appears to be related to a decreased number of monsoon lows and depressions, while at N512 the total number of events is similar while the rainfall contribution is increased, indicating perhaps that some of the systems are stronger with the SST CCI. However, there is also a suggestion in Figure 5-16 (lower panels) that the rainfall contribution from monsoon lows and depressions in the N512 run with SST CCI has shifted location, with more concentration over the northern Bay of Bengal and fewer tracks extending to northwest India than with HadISST.2.2.0.0. Levine and Turner (2012) showed that cold SST biases in the Arabian Sea affect the structure of the monsoon trough as well as the moisture supply into the region. However, further work is needed in order to understand the changes seen in these simulations.

Figure 5-14 also shows more rainfall in the South China Sea (SCS) and western Pacific (degrading the simulation in both regions when forced by SST CCI). This is related to a slight acceleration of the mean westerly 850 hPa wind and therefore convergence here, particularly at N512 resolution (Figure 5-17), which itself is related to a larger anomalous cyclonic flow over China. These indicate a weaker and/or more displaced Western North Pacific Subtropical High (WNPSH), which is thought to be related to errors over the Maritime Continent and the SCS. In a current hypothesis, errors over the Maritime Continent push more southerly flow and convergence into the SCS during the seasonal transition (in May), leading to excessive convection over the SCS and West Pacific which spins up the westerly wind bias in a positive feedback. Such a process would be exacerbated by warmer SSTs, such as are seen in the CCI dataset. Levine and Martin (2017) and Saha et al. (1981) also showed evidence that the precursors for many monsoon depressions and low-pressure systems occur over the South China Sea and the Western Pacific.

Figure 5-18 shows the latitudinal progression of monthly rainfall over the annual cycle for the Indian region. For both SST datasets this progression is represented better at N512 resolution. With the SST CCI, the northward progression is slightly more abrupt, possibly related to the colder SSTs over the Arabian Sea. The southward retreat at the end of the monsoon season is similar in all four model runs, while the slightly improved equatorial Indian Ocean rainfall amount with SST CCI is apparent at both resolutions.

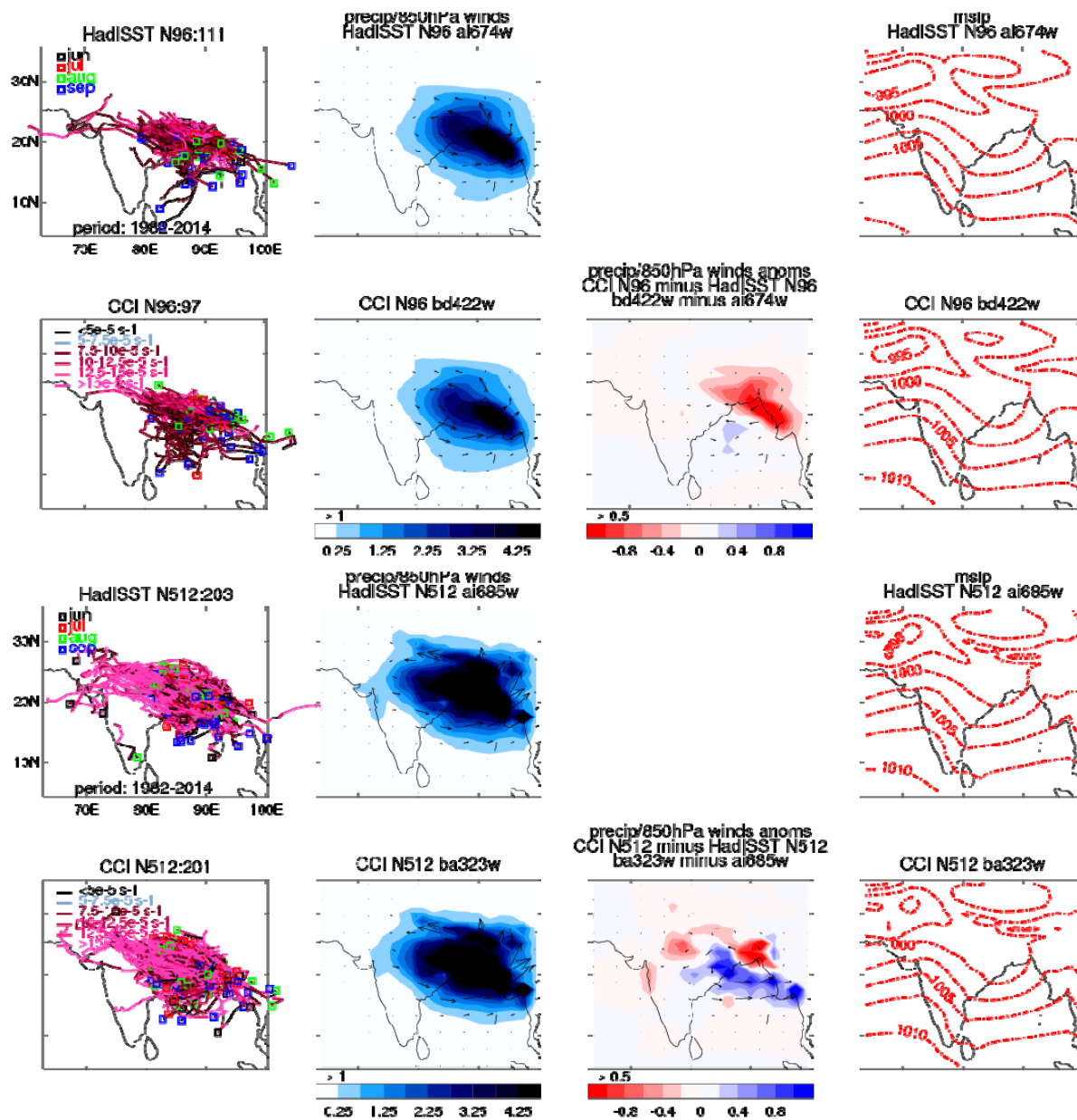


Figure 5-16. Composite analysis of monsoon depressions in the four experiments: (1st column) individual depression tracks; (2nd column) precipitation and 850 hPa winds; (3rd column) difference in precipitation and winds; (4th column) mean sea level pressure. Results are shown for N96 runs (upper) and N512 runs (lower).

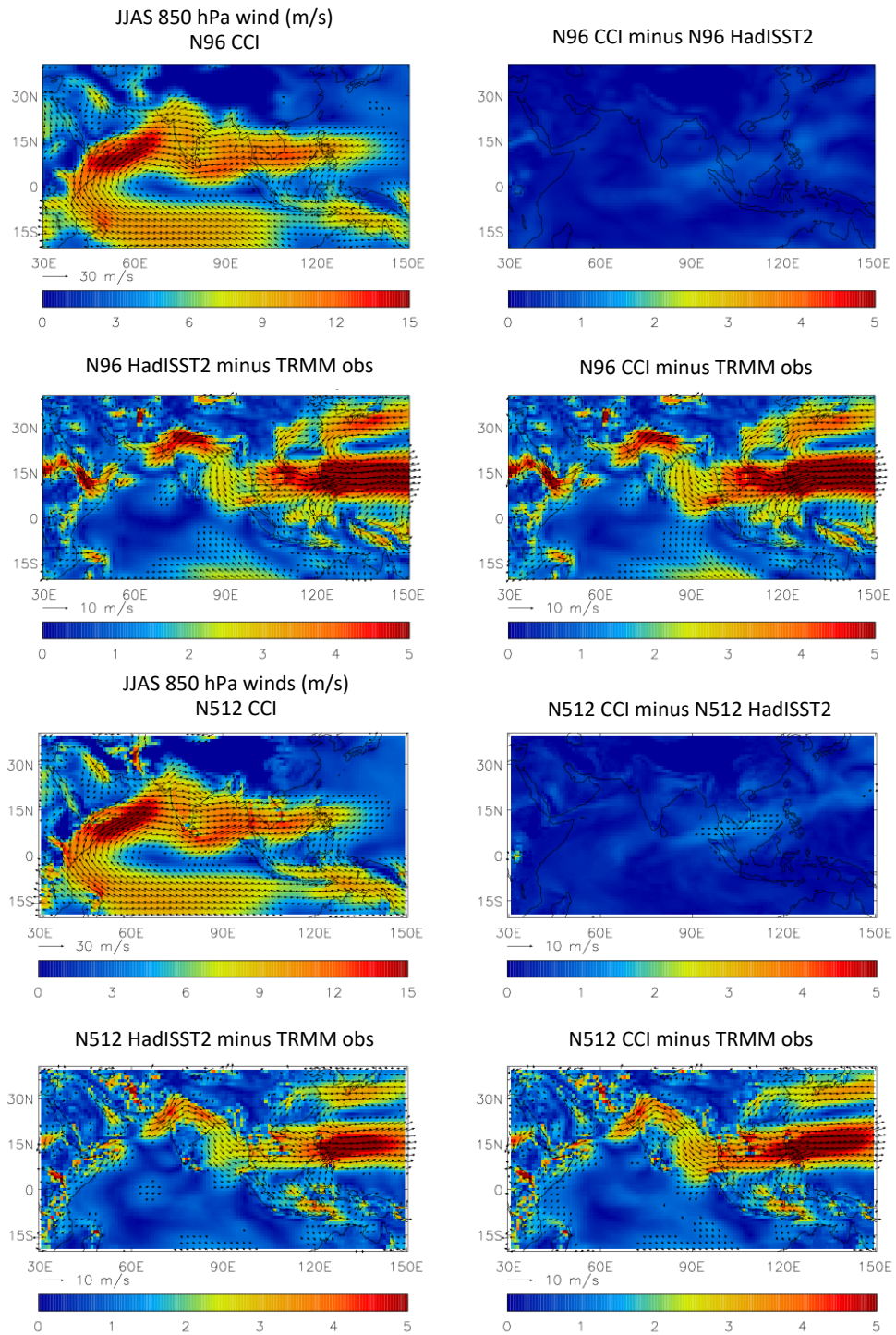


Figure 5-17. As Figure 5-14 but for JJAS mean 850 hPa winds, compared against ERA-Interim reanalyses.

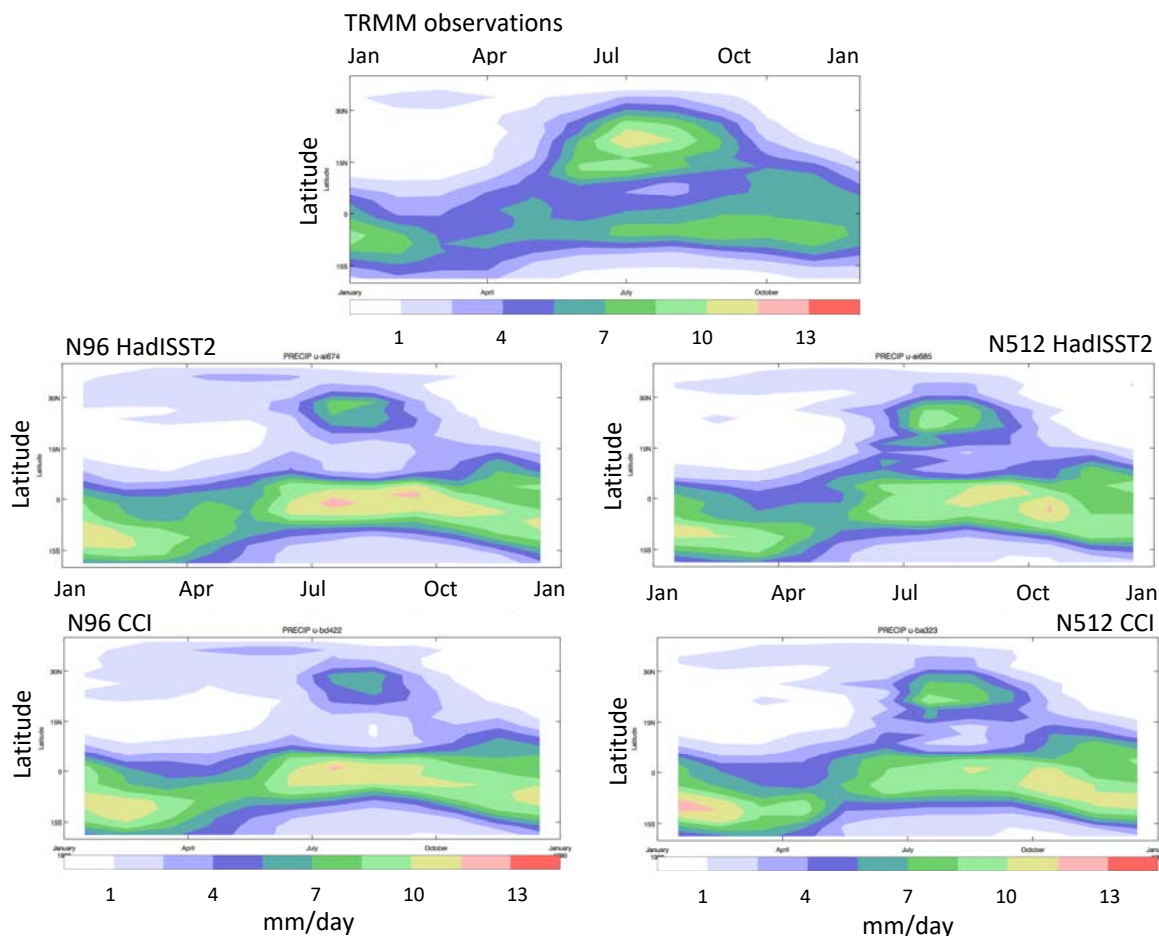


Figure 5-18. Latitude – time Hovmöller plots of monthly climatological rainfall averaged between 70-90E, indicating the arrival and northward progression of rainfall over India. (top) TRMM observations; (left) N96 runs forced by (upper) HadISST.2.2.0.0, (lower) SST CCI. (right) as (left) but for N512 runs

5.2.3.5.2 Interannual variability

Changes in the teleconnections between All-India Rainfall (AIR) and SST (Figure 5-19, left) should be viewed with caution as only 20 years of each simulation was analysed. However, the SST CCI-forced simulations consistently show a reduced correlation with northern Arabian Sea SSTs (possibly because they are colder) and a southward shift of the location of the maximum correlation into the central Arabian Sea. At N512 there is an increased positive correlation in the SST CCI-forced simulation with Bay of Bengal, the eastern Indian Ocean, SCS, Western Pacific and the Maritime Continent, which may be related to the effects of the warmer climatological SSTs in these regions in the CCI dataset on the large-scale Asian monsoon circulation. However, these changes are opposite to those found at N96 (not shown) so they may not be robust. Correlations between Nino3.4 SSTs and tropical rainfall are consistently similar in the simulations to those in observations for both SST datasets with very little change between the SST CCI and HadISST.2.2.0.0-forced simulations.

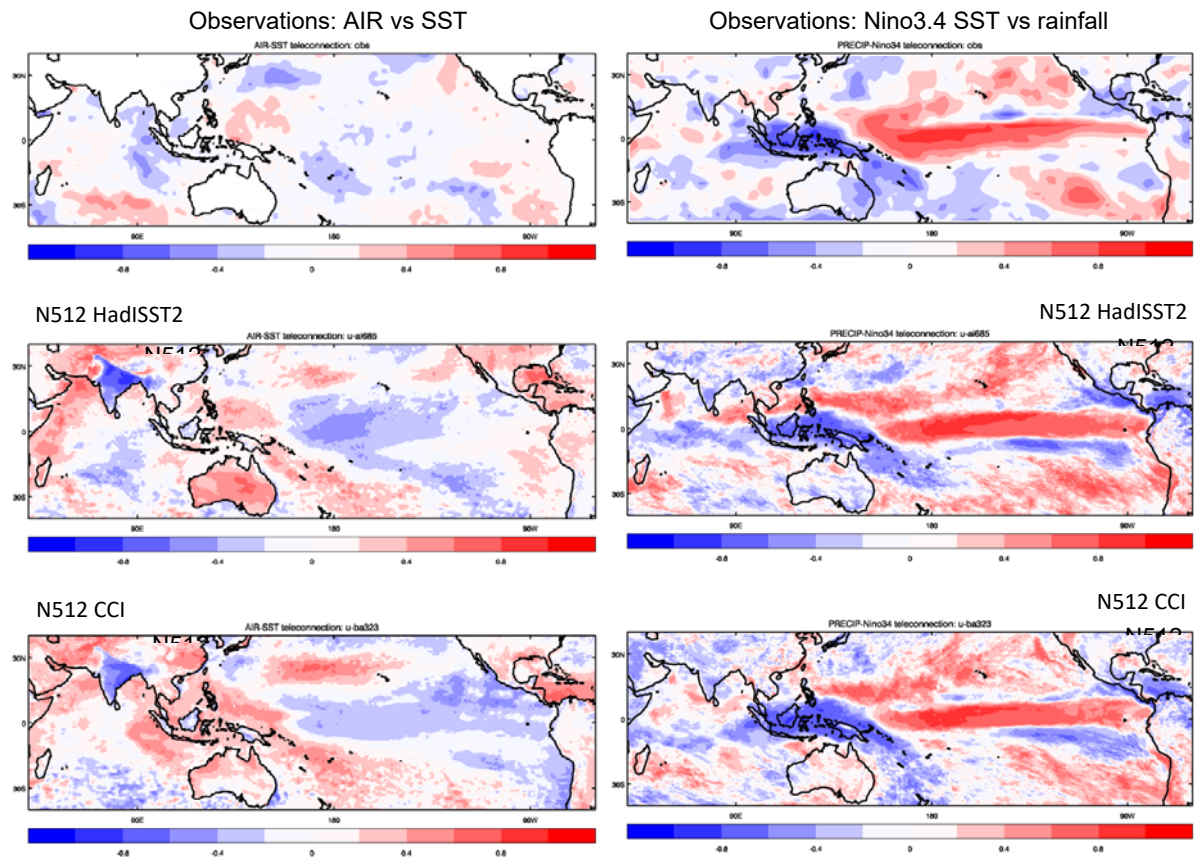


Figure 5-19. Correlations between (left) All-India Rainfall (AIR) and surface temperatures, and (right) Nino3.4 SSTs and rainfall, in JJAS for (top) GPCP rainfall observations and HadISST1.1 SSTs; (middle) model rainfall from N512 run with HadISST.2.2.0.0 SSTs; (bottom) model rainfall from N512 run with SST CCI.

5.2.3.5.3 Intraseasonal variability

Analysis of intraseasonal variability of the monsoon examines the eastward and northward propagating modes of the Boreal Summer Intraseasonal Oscillation (Lee et al., 2013) is shown in Figures 5-20 and 5-21. The active (positive) phase of the northward propagating mode is slightly stronger at both resolutions with the CCI SSTs, but this mode is coherent with the HadISST2.2.0.0 SSTs. The models tend to have a propagation speed that is slightly too slow, and this is not really affected by the SST forcing. The eastward propagating mode (Figure 5-20) is poorly represented in all four simulations. Most of the activity occurs at around 95E and there is little evidence of propagation. The lack of influence of the SST forcing on this is consistent with the results for the MJO.

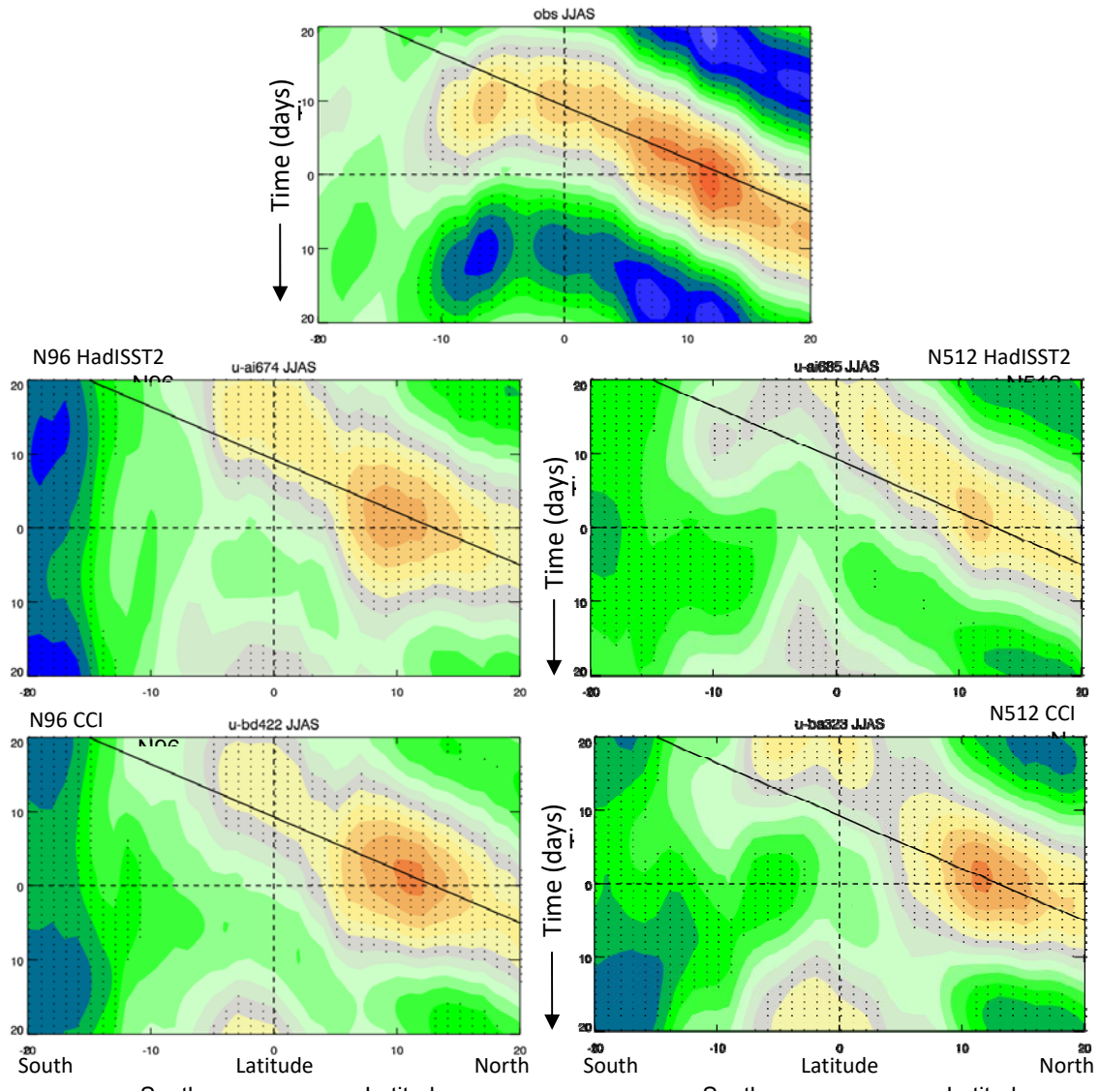


Figure 5-20. Composite lead/lag analysis of the northward propagating phase of the Boreal Summer Intra-Seasonal Oscillation (BSISO) in the South Asian monsoon region. Top: observations from TRMM; middle: N96 (left) and N512 (right) runs forced by HadISST.2.2.0.0 SSTs; bottom: N96 (left) and N512 (right) runs forced by SST CCI. Diagonal lines indicate the propagation speed as determined from the observations.

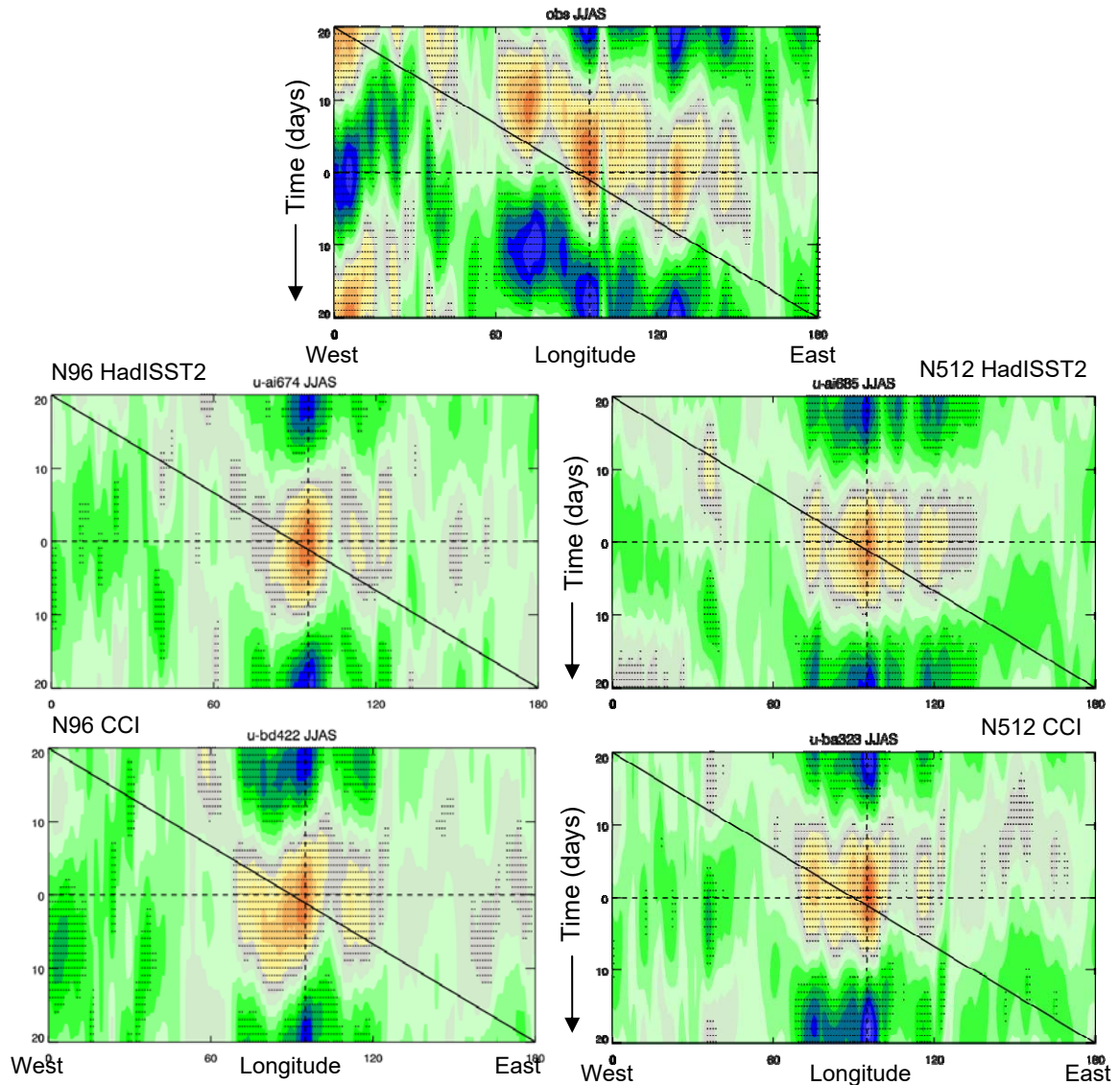


Figure 5-21. As Figure 5-20 but for the eastward-propagating mode.

5.2.3.5.4 Summary

The South Asian summer monsoon simulation shows some changes when the SST CCI are used, at both resolutions. Colder SSTs in the Arabian Sea appear to be related to reduced moisture fluxes and rainfall over the eastern Arabian Sea and western Ghats mountains, and may also contribute to changes in the characteristics of the monsoon trough that affect the passage of monsoon lows and depressions across northern and central India. There are detrimental increases in rainfall in the South China Sea and western Pacific that are related to increased convergence here. We hypothesise that this is related to the warmer SSTs in this region in the CCI dataset.

Changes in monsoon inter-annual variability are hard to judge given the number of years analysed, but the southward shift in the region of positive correlation of All-India rainfall with the Arabian Sea SST is evident at both resolutions. Impacts of the SST forcing on monsoon intraseasonal variability are minimal.

5.2.3.6 MADDEN-JULIAN OSCILLATION

The convective phase of the Madden-Julian Oscillation (MJO) and its propagation are well represented in both sets of simulations, perhaps slightly better in those forced with SST CCI analysis v2.0. Both sets of simulations however do not produce much of the suppressed regions and their propagation seen in the observations (Figure 5-22).

Equatorial ($10^{\circ}\text{S} - 10^{\circ}\text{N}$) Outgoing Longwave Radiation (OLR) wave spectra zoomed in on the MJO time (30 days to 80 days) and space scales are calculated for the years of 1988 to 2008 and are shown in Figure 5-22. The spectra between 30 days and 80 days (vertical lines on Figure 5-22) correspond to MJO. Neither of the simulations represents the amplitude for this timescale strongly enough, and not much has changed in SST CCI runs. The analysis across timescales also indicates very little change between the datasets (not shown).

Equatorial power spectra

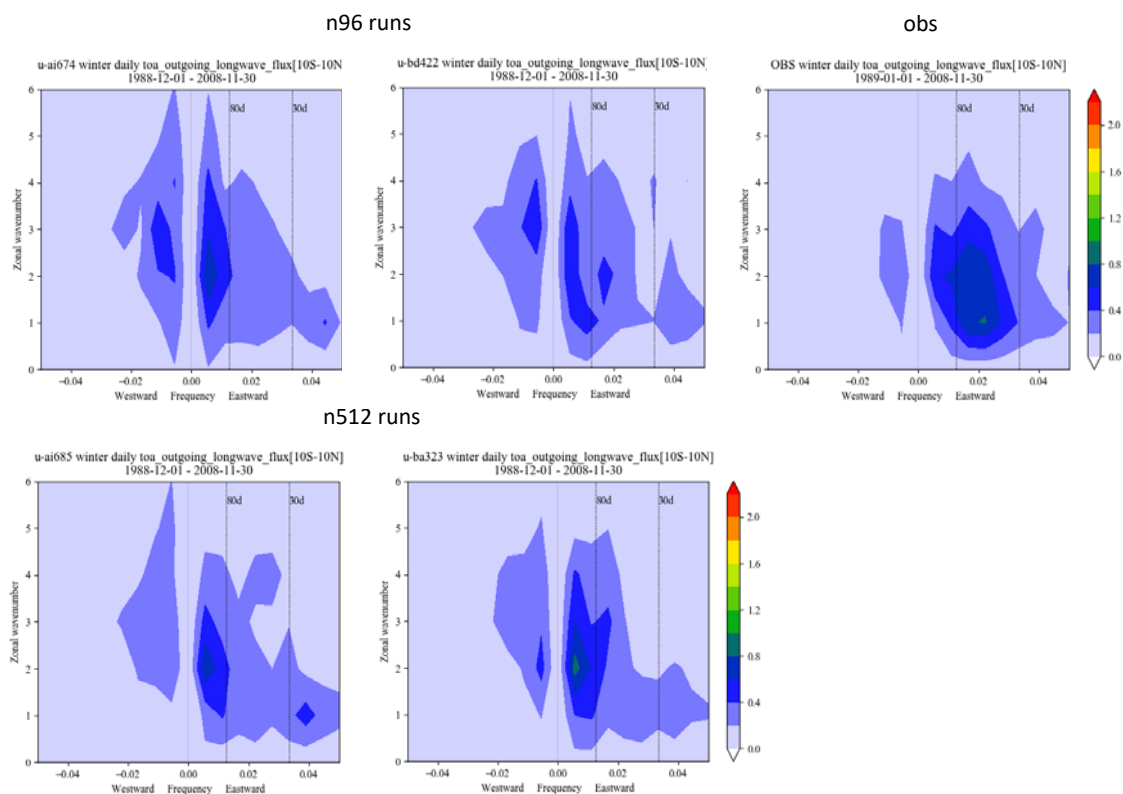


Figure 5-22. Equatorial OLR wave spectra zoomed in on the MJO time and space scales (Nov-Apr). (left) HadISST2.2.0.0-forced simulation, (middle) SST CCI runs and (right) the observations (NOAA-OLR, Rieberman and Smith, 2016). For model runs: (top) N96; (bottom) N512.#

5.2.3.7 EL NIÑO SOUTHERN OSCILLATION

El Niño Southern Oscillation (ENSO) is the atmospheric interannual variability which has the longest timescale among those analysed here. Consequently, there is a caveat that twenty years of the analysis is not long enough to provide robust characterisation of the interannual variability, especially from only one ensemble member. In addition, the SST observations used in AutoAssess² for ENSO evaluation are from HadISST1 (Rayner et al, 2003) and cover a different, longer, period than that of the model simulations.

Table 5-1. Standard deviation of precipitation in Nino4 and absolute correlation coefficient between the Southern Oscillation Index (SOI) and Nino3 SST in the observations and runs with SST CCI analysis v2.0 and HadISST2.2.0.0

	observations	N96		N512	
		SST CCI	HadISST.2.2.0.0	SST CCI	HadISST.2.2.0.0
Stdev Nino4 PPTN [mm/day]	2.7 ± 0.54	2.8	3.0	2.9	3.1
Abs correlation SOI/Nino3 SST	0.6 ± 0.1	0.53	0.54	0.54	0.58

Among the ENSO metrics in AutoAssess, notable differences between the simulations forced by different SSTs are summarized in **Table 5-1**. The standard deviation of precipitation in Nino4 tends to be overestimated in the simulations (although consistent with the range given by the uncertainty estimate), but the value in the SST CCI runs is 10% smaller than the HadISST.2.2.0.0 runs, which is closer to the best estimate from the observations. Also, the absolute correlation between the Southern Oscillation Index and Nino3 SST is 5% smaller in the SST CCI runs than HadISST.2.2.0.0 runs. These suggest that either the variance of the SST is lower here or the atmospheric interaction with the SST is smaller in SST CCI runs. Nonetheless, the correlation in all cases is consistent with the range given by the uncertainty in the observed relationship.

The composites of the two SST analyses during El Niño and La Niña (Figure 5-23) show that, in DJF, El Niño anomalies are warmer in the Eastern/Central Pacific in SST CCI (both are warmer than HadISST1 but SST CCI by more) but HadISST.2.2.0.0 has colder anomalies in the West Pacific. In JJA during La Niña the West Pacific is warmer in HadISST.2.2.0.0; HadISST.2.2.0.0 also has warmer anomalies in the East Pacific, however. The impact of the SST on precipitation in the West Pacific is much bigger than in the East Pacific, and relatively smaller SST anomalies in SST CCI in the West Pacific in DJF in El Niño, and JJA in La Niña, could be responsible for the smaller standard deviation of the Nino4 precipitation and smaller correlation between the Southern Oscillation Index and Nino3 SST.

² AutoAssess is a framework used at the Met Office for evaluating weather and climate models against observations

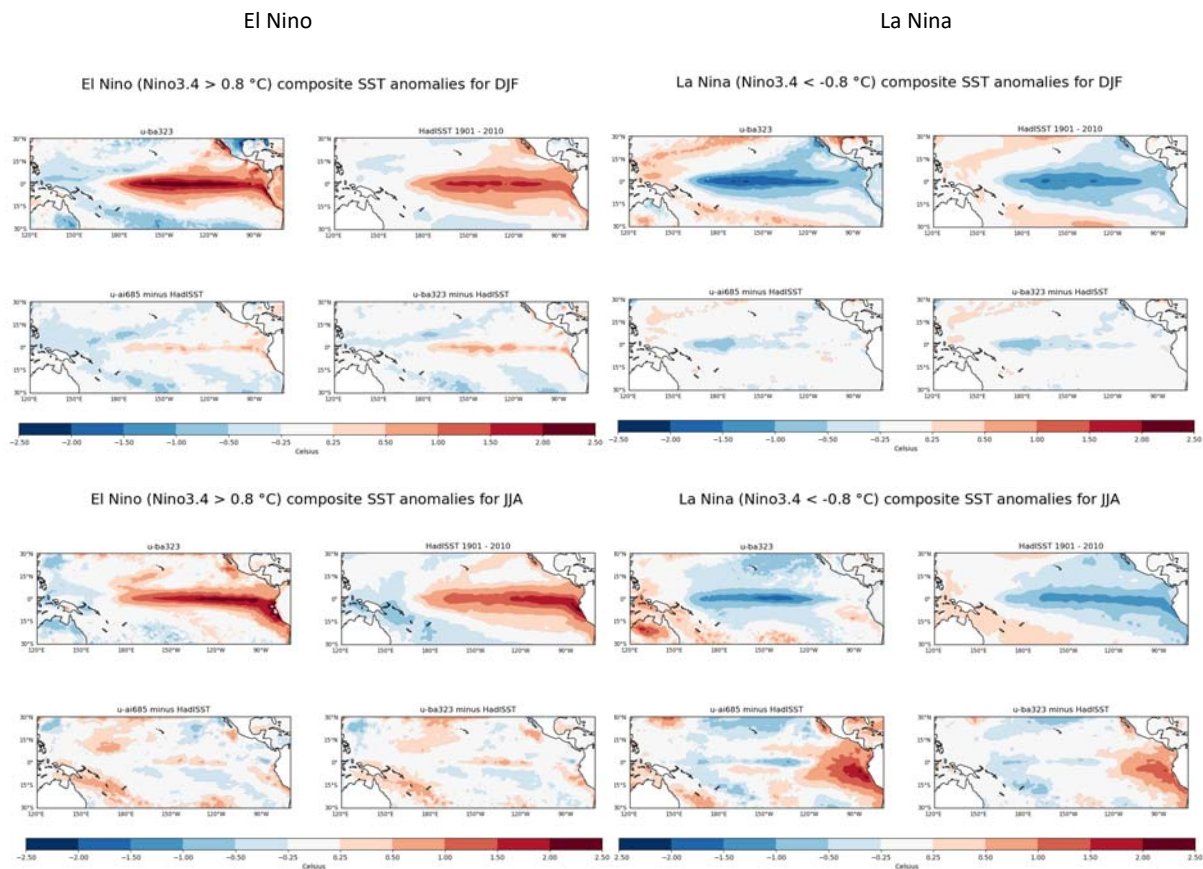


Figure 5-23. SST composite during El Niño and La Niña (upper) DJF (lower) JJA. In each 4-panel plot: (top left) SST CCI analysis v2.0 at N512; (top right) HadISST1; (bottom left) HadISST2.2.0.0 minus HadISST1; (bottom right) SST CCI minus HadISST1.

ENSO teleconnections with precipitation are defined by the number of El Niño years with top tercile rainfall divided by the number of El Niño years. The teleconnections are shown in Figure 5-24 and they are generally well represented in both simulations, but SST CCI runs are consistently better in two regions at both resolutions. The positive bias in the precipitation over Sahel in summer (JAS) in the HadISST.2.2.0.0 runs disappeared in the SST CCI runs. Precipitation over South East Asia in early spring (FMA) is underestimated in HadISST.2.2.0.0 runs, but the negative bias almost disappeared in SST CCI runs. For the Sahel, SST over the equatorial Atlantic is lower in SST CCI. The consequence of this is that moisture transport from there to the Sahel would reduce in amount but the variability could also reduce. Future work will be necessary to test whether the disappearance of the bias in precipitation over the Sahel is linked to lower SST over the equatorial Atlantic.

It is also noted that the strength of the teleconnection over South Africa in DJF and North-East Australia in NDJ is systematically lower in higher resolution both in HadISST.2.2.0.0 runs and SST CCI runs; examples of differences with resolution that are consistent in both simulations.

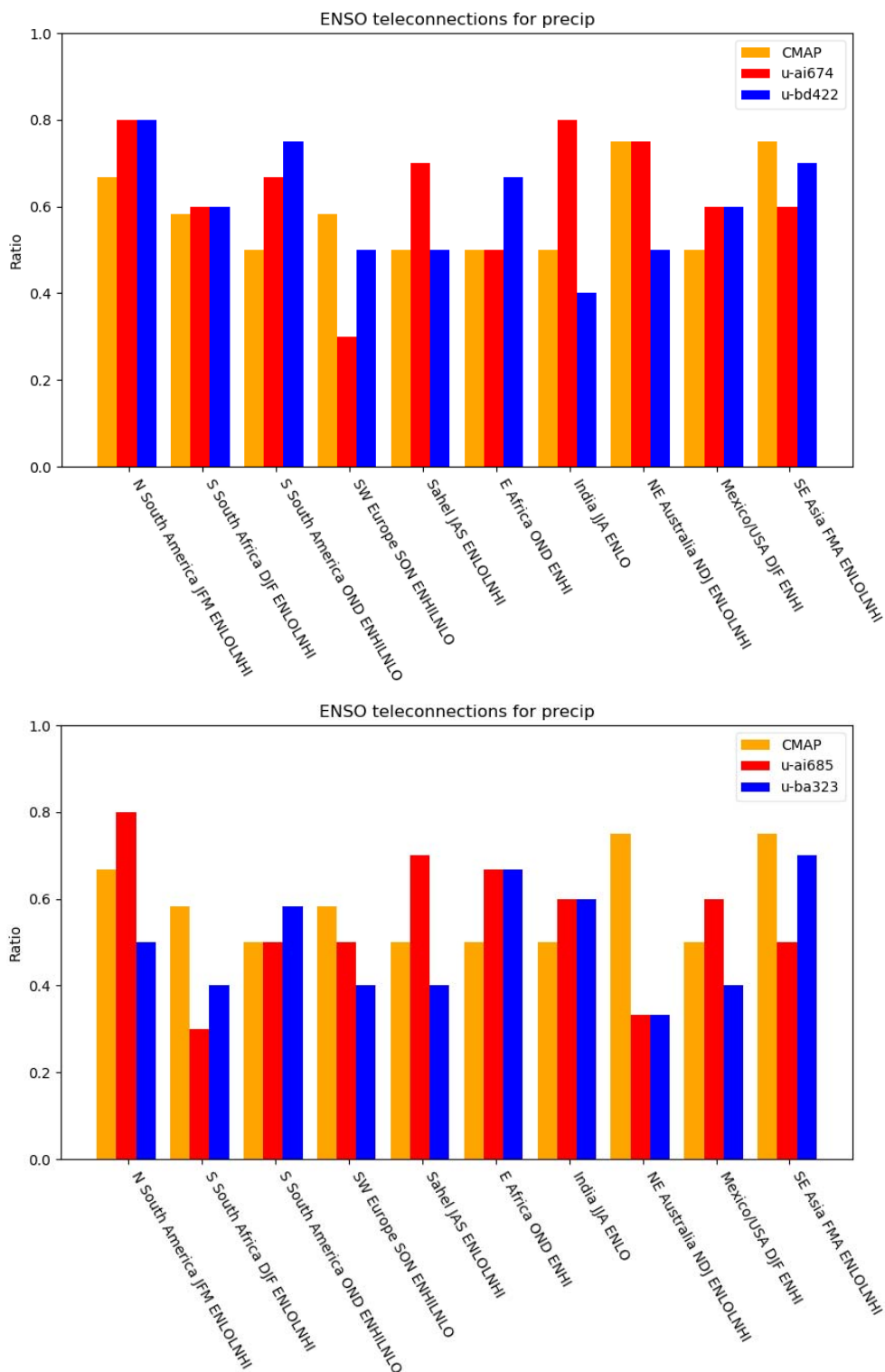


Figure 5-24. ENSO teleconnections for a set of different regions and selected seasons, examining precipitation. (Top) Simulations at N96; (bottom) at N512. Red: HadISST.2.2.0.0-forced. Blue: SST CCI-forced. Orange: observations from CMAP.

5.2.3.8 MID-LATITUDE WEATHER SYSTEMS

5.2.3.8.1 Storm Tracks

The following analysis has been performed using Kevin Hodges' TRACK algorithm (see Hodges, 1994; 1995; 1996; Hoskins and Hodges, 2002; Hodges et al., 2011), which objectively identifies and tracks positive and negative vorticity features from genesis to lysis. Figure 5-25 shows the cyclone (positive vorticity) track density (i.e. the number of cyclones passing through a given region) for the Northern Hemisphere winter (December, January and February – DJF) season.

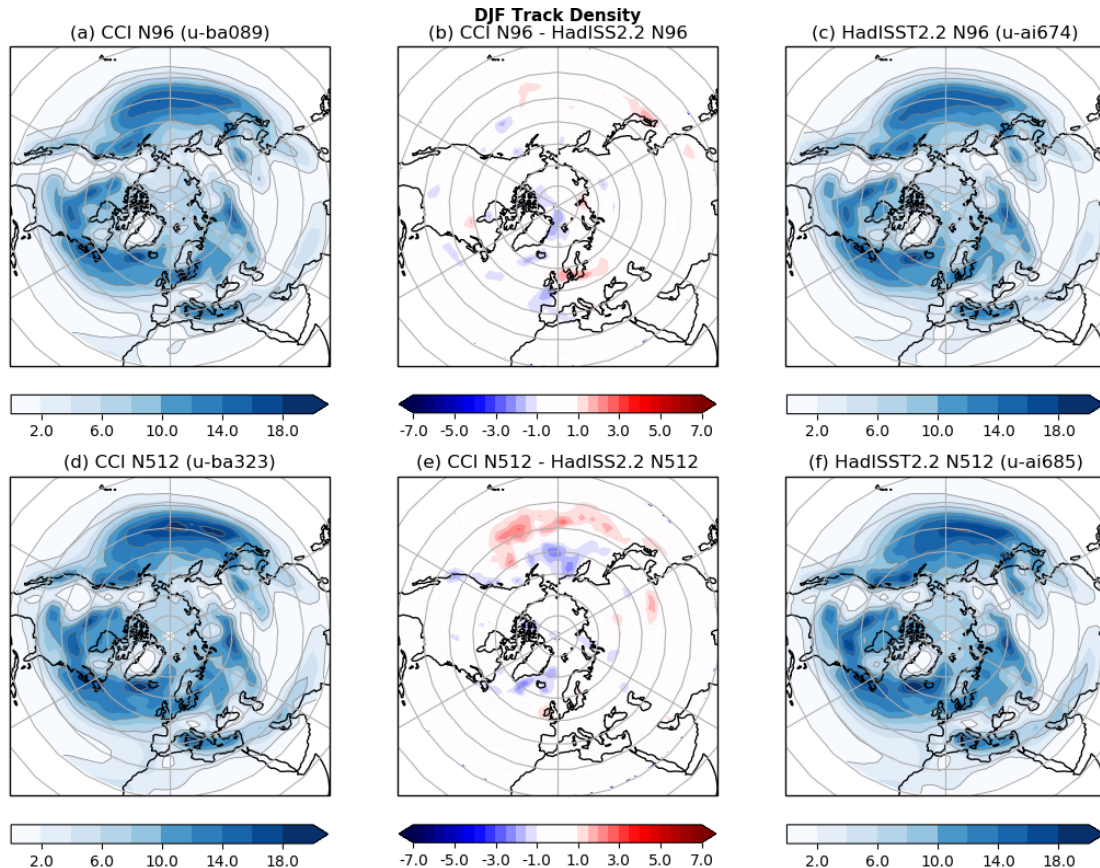


Figure 5-25. Northern Hemisphere cyclone track density (number of storms per month passing through a 4-degree cap centred at each point) from the (a) SST CCI N96, (c) HadISST.2.2.0.0 N96, (d) SST CCI N512 and (f) HadISST.2.2.0.0 512 simulations datasets. The difference in cyclone track density between (b) CCI N96 and HadISST.2.2.0.0 N96, and (e) SST CCI N512 and HadISST.2.2.0.0 N512.

Differences between the results from the SST CCI and HadISST.2.2.0.0 runs are shown in the middle panels in Figure 5-25:

- The mean track densities are very similar in all four simulations with the main storm tracks all present (North Pacific, North American, North Atlantic, Mediterranean, Siberian and Middle East) in Figs. 5-25(a), (c), (d) and (f).
- N96: Very small reductions in track density over the Greenland Sea and around the Bay of Biscay and small increases over northern Europe (Fig. 5-25b) for SST CCI relative to HadISST.2.2.0.0.

- N512: Similar small reductions in track density over the Greenland Sea for SST CCI relative to HadISST.2.2.0.0; however, increased (decreased) track density around 30N-40N (50-60N) in the North Pacific (Fig. 5.25c).

In order to determine whether these changes are relevant, we now compare against reanalyses.

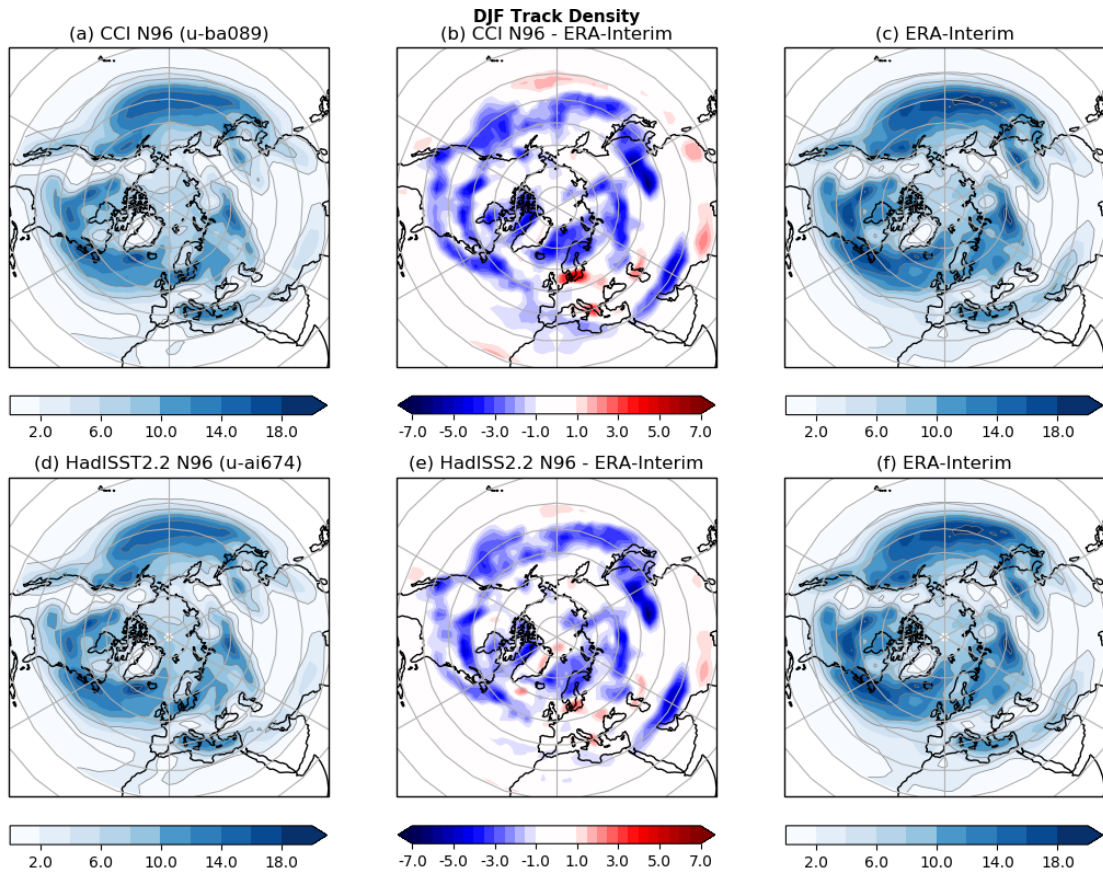


Figure 5-26. Northern Hemisphere cyclone track density from the (a) SST CCI N96, (c) ERA-Interim, (d) HadISST.2.2.0.0 N96 and (f) ERA-Interim datasets. The difference in cyclone track density between (b) SST CCI N96 and ERA-Interim, and (e) HadISST.2.2.0.0 N96 and ERA-Interim.

Figure 5-26 shows differences between the N96 simulations and ERA-Interim:

- It is clear that the main storm tracks are present in both N96 simulations (Figs. 5-26a and d), as present in ERA-Interim (Figs. 5-26c and f).
- There is a clear negative bias in cyclone track density relative to ERA-Interim in all the major storm tracks, however (Figs 5-26b and e).
- The negative biases relative to ERA-Interim in both simulations (SST CCI N96 and HadISST.2.2.0.0 N96) are considerably larger in magnitude than the differences resulting from the change to the SST/sea ice datasets (compare Figs 5-26b and e with 5-25b and e).

The SST CCI dataset therefore has little or no impact on the overriding systematic model biases.

Figure 5-27 shows differences between the N512 simulations and ERA-Interim:

- Again, the main storm tracks are present in the N512 simulations as those presented in the ERA-Interim dataset (Figs. 5-27a, c, d and f).
- The pattern and magnitudes of the track density biases for SST CCI (Fig. 5-27b) and HadISST.2.2.0.0 (Fig. 5-27e) relative to ERA-Interim are very similar (i.e. the different SST/sea ice datasets have little impact).
- Therefore, it appears most of the improvement (almost all) in the cyclone track density is driven by the increase to N512 resolution from N96 (see next section for confirmation).

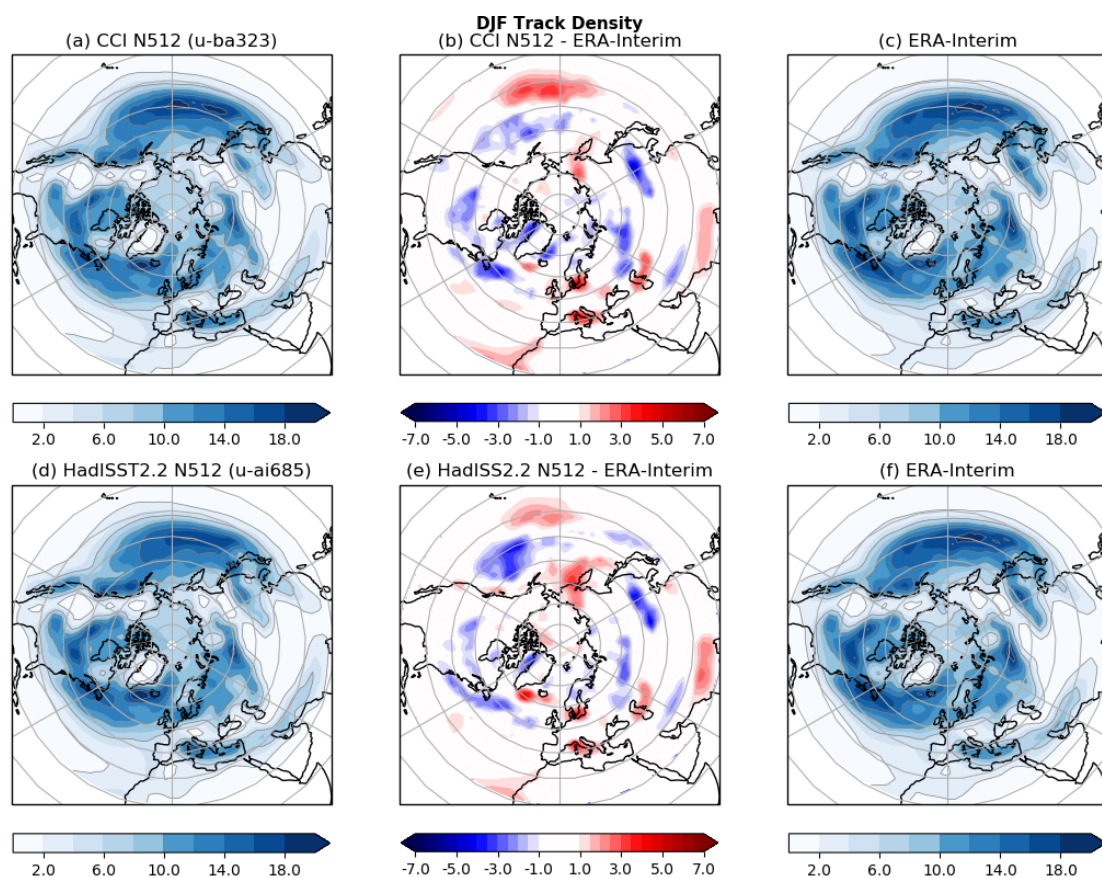


Figure 5-27. Northern Hemisphere cyclone track density from the (a) SST CCI N512, (c) ERA-Interim, (d) HadISST.2.2.0.0 N512 and (f) ERA-Interim datasets. The difference in cyclone track density between (b) SST CCI N512 and ERA-Interim, and (e) HadISST.2.2.0.0 N512 and ERA-Interim.

Figure 5-28 shows the impact of resolution (N96 vs N512). The middle figures (Figs. 5-28b and e) clearly show there is a marked increase in the cyclone track density that is purely the result of increasing the resolution. The increases in track density that result from running the model at N512 (Figs. 5-28b and e) are much larger than the differences that result from using SST CCI instead of HadISST.2.2.0.0 (Figs. 5-25b and e).

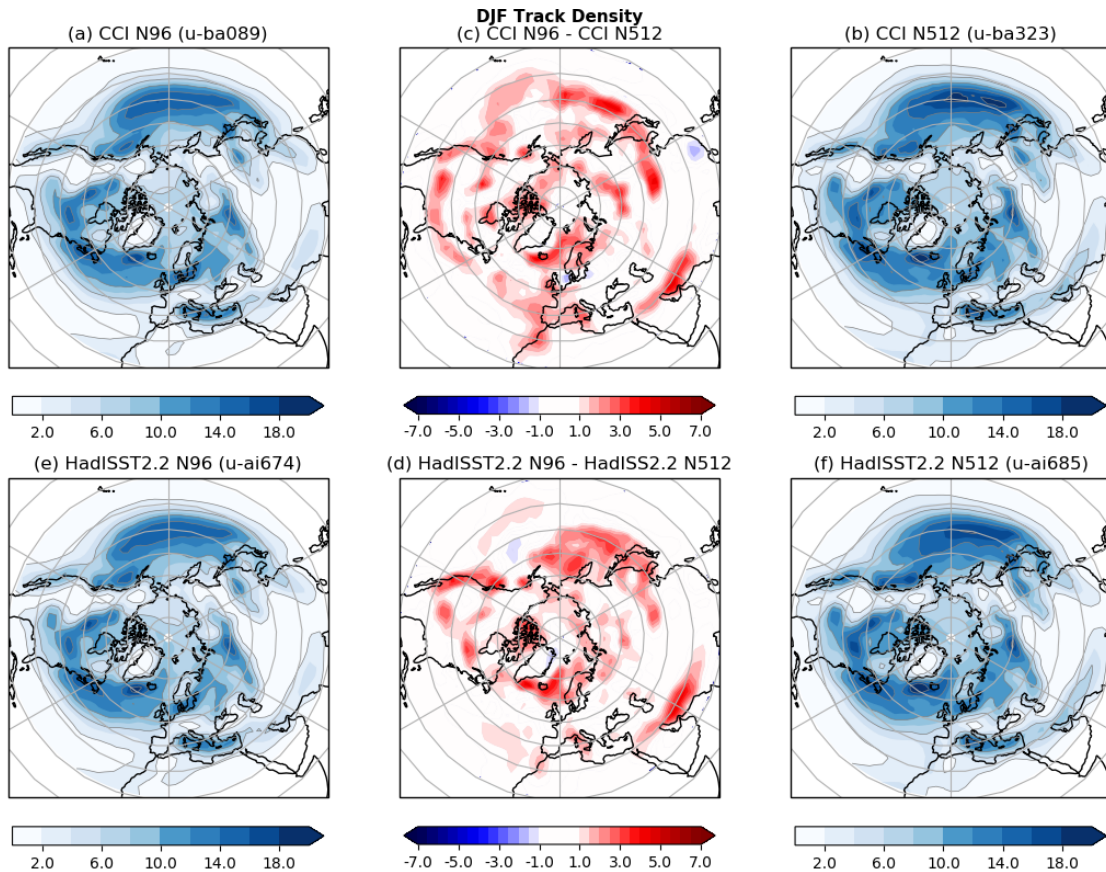


Figure 5-28. Northern Hemisphere cyclone track density from the (a) SST CCI N96, (c) SST CCI N512, (d) HadISST.2.2.0.0 N96 and (f) HadISST.2.2.0.0 N512 datasets. The difference in cyclone track density between (b) SST CCI N96 and SST CCI N512, and (e) HadISST.2.2.0.0 N96 and SST CCI N512.

The SST CCI dataset has a negligible impact on the storm tracks relative to the HadISST.2.2.0.0 dataset. A much larger improvement in the storm tracks results from increasing the resolution. Nevertheless, there appears to be no degradation in performance when using the SST CCI.

5.2.3.8.2 Blocking

The following analysis has been performed using the method outlined in Pelly and Hoskins (2003) and Berrisford et al. (2007), where atmospheric blocking frequency is identified from time periods where the upper-level (the PV=2 surface i.e. the dynamical tropopause) meridional temperature gradient is reversed. The overall seasonal (DJF) frequency of occurrence of such reversals is presented in the figures below.

N96 simulations compared to MERRA

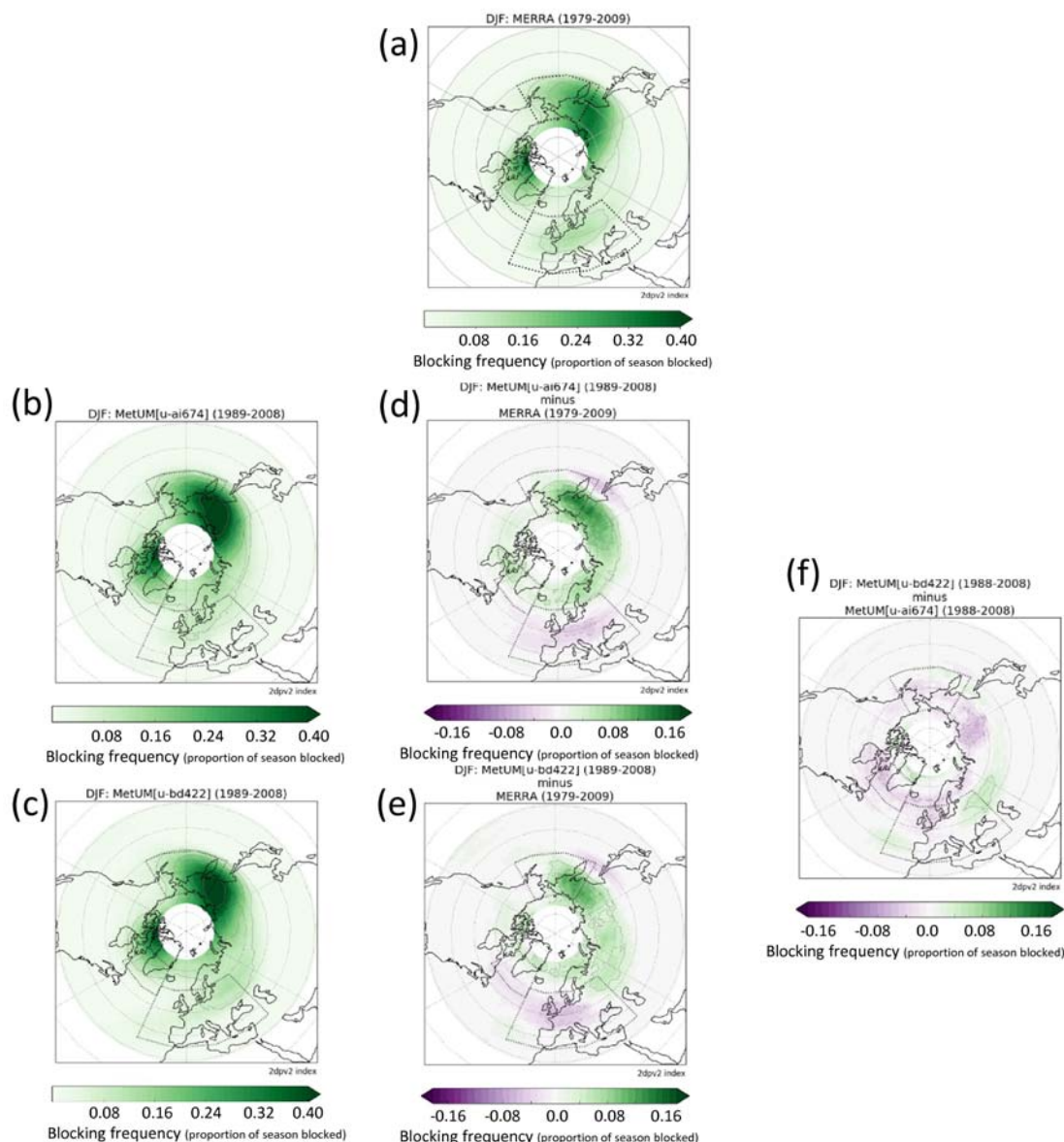


Figure 5-29. DJF mean blocking frequency taken from (a) MERRA, (b) HadISST.2.2.0.0 N96 and (c) SST CCI N96 simulations. The difference in blocking frequency between (d) HadISST.2.2.0.0 N96 and MERRA, and (e) SST CCI N96 and MERRA. Finally, the difference between SST CCI N96 and HadISST.2.2.0.0 N96 in (f).

- The main focus of atmospheric blocking is over north-east Asia/north-west Pacific, Greenland and western Europe (Fig. 5-29a), which is broadly represented in both the HadISST.2.2.0.0 and SST CCI simulations (Figs. 5-29b and c, respectively).

- The frequency of blocking events is too high relative to MERRA poleward of 60N in both simulations and too low over Europe (Figs. 5-29d and e), whose difference is roughly 30% of the absolute magnitude of the blocking in MERRA.
- The blocking biases are reduced slightly in the SST CCI simulation relative to HadISST.2.2.0.0 (Fig 5-29f); however, the effect is relatively small (at most 10% of the absolute magnitude of the blocking in MERRA) and the overall pattern of the bias in the SST CCI simulation (relative to MERRA) still clearly resembles the error in HadISST.2.2.0.0 N96.

N512 simulations compared to MERRA

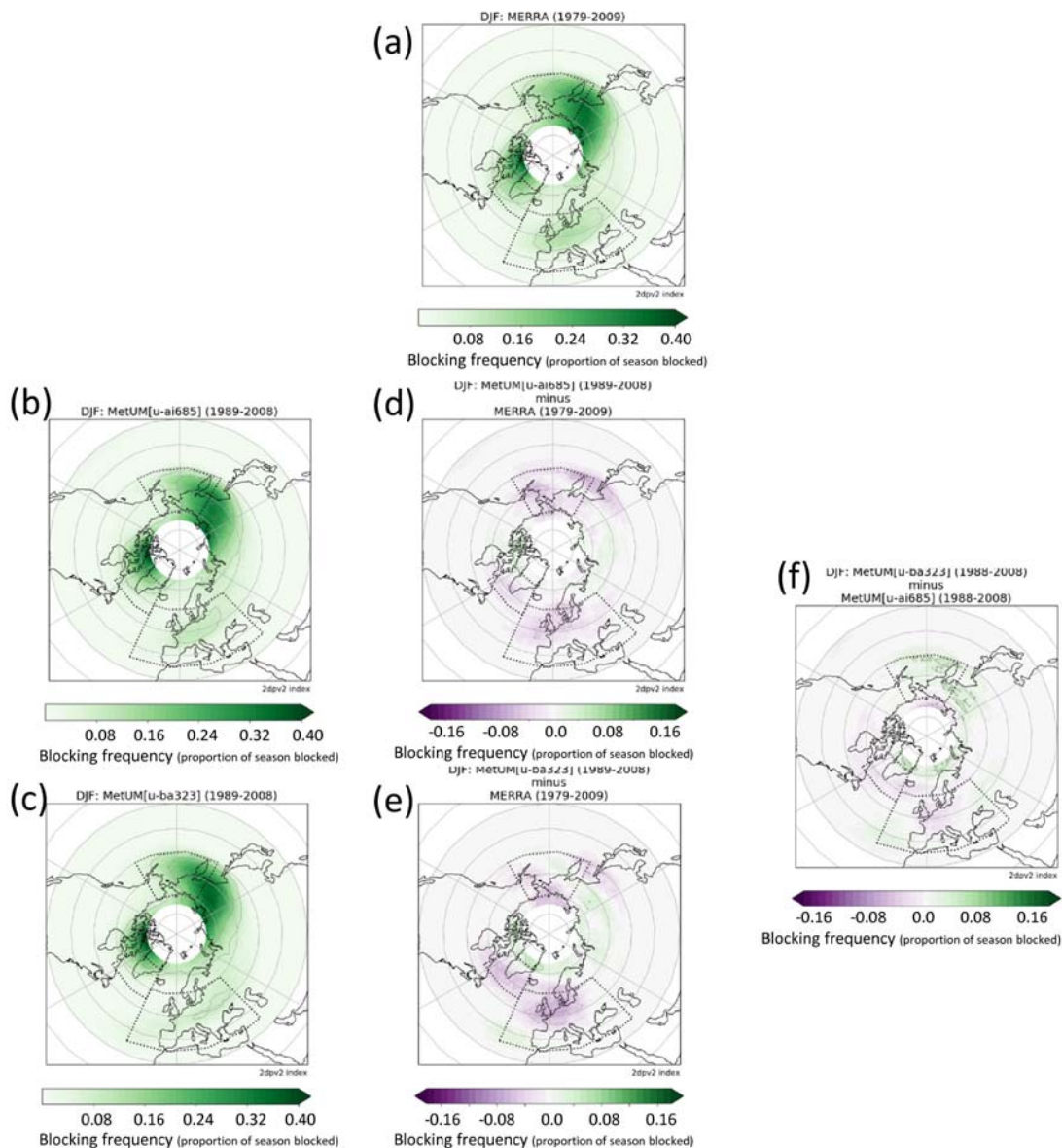


Figure 5-30. DJF mean blocking frequency taken from (a) MERRA, (b) HadISST.2.2.0.0 .2 N512 and (c) CCI N512 simulations. The difference in blocking frequency between (d) HadISST.2.2.0.0 N512 and MERRA, and (e) CCI N512 and MERRA. Finally, the difference between CCI N512 and HadISST.2.2.0.0 N512 in (f).

- As with the N96 simulations, the regions of relatively high, seasonal mean blocking frequency in the SST CCI N512 and HadISST.2.2.0.0 N512 simulations correspond well with those of MERRA (compare Figs 5-30b and c with a).
- The positive bias in blocking frequency relative to MERRA poleward of 60N visible in the N96 simulations is almost non-existent in the N512 simulations (compare Figs. 5-29d and e with Figs. 5-30d and e).
- It is clear that the high-latitude blocking bias is more sensitive to (and improves more with) increased resolution than changing SST/sea ice datasets.
- Conversely, the negative bias in blocking frequency over Europe remains unchanged in all simulations (i.e. it is not sensitive to resolution or the SST/sea ice configuration).
- Overall, there is very little difference in blocking frequency between the SST CCI N512 and HadISST.2.2.0.0 N512 simulations (Fig. 5-30f).

There is slight evidence that the simulation of blocking at high latitudes in the Northern Hemisphere winter is better with the SST CCI data rather than HadISST.2.2.0.0 at N96; however, the improvement is small and the overall patterns of the systematic biases over the Arctic (and Europe) do not change. There is almost no impact of using SST CCI over HadISST.2.2.0.0 in the N512 simulations. As with the storm tracks, the real improvement in the representation of blocking comes from increasing the resolution and not from changing the SST/sea ice field. Nevertheless, it appears that there is no degradation in performance when using the SST CCI dataset (as was the case with the cyclone tracking).

5.2.3.8.3 North Atlantic Oscillation

A hypothesis that the sea ice difference between SST CCI and HadISST.2.2.0.0 causes a difference in simulated North Atlantic Oscillation (NAO) is tested by calculating the NAO Index. The index was estimated for 1982-2014. Statistical significance tests for the difference between two datasets in the mean (t-test) and the standard deviation (f-test) suggests that the difference between the two simulations are not significant. Only the differences in the standard deviation between the two resolutions are significant. Therefore, there is no evidence from this length of simulation that the sea ice difference causes a difference in simulated NAO.

5.2.4 CONCLUSIONS

We have analysed the influence of using the SST CCI dataset as forcing in atmosphere-only simulations at two horizontal resolutions, compared with the influence of using the HadISST.2.2.0.0 dataset. Overall, the impact of using SST CCI is relatively small, particularly in comparison with the influence of increasing the model's horizontal resolution. Where changes are seen, they are sometimes beneficial and sometimes detrimental.

The SST CCI dataset has a significant impact on spatial distributions of cloud regimes, especially Organized-Convective-System, Anvil, Cirrus, Fair-Weather regimes. SST differences over the Western Pacific, warmer SST around the Maritime Continent and cooler SST in the surrounding area are regarded to be mainly responsible for the changes, with some contribution from the cooler Equatorial Atlantic also. Changes in the spatial distributions of tropical cyclones and South Asia Monsoon are consistent with the changes in the Organized-Convective-Systems regime. Both analysis of surface skin temperature and ENSO indicate that SST variability decreases over the Western Pacific but increase over the Eastern Pacific. The standard deviation of precipitation in Nino4 and absolute correlation coefficient between the SOI and Nino3 SST are closer to the observations, but both values are within the range given by the uncertainty in the observed relationship.

Although the warmer SST around the Maritime Continent, cooler SST at the equatorial Atlantic as well as the East Boundary Upwelling regions seem to reduce the bias in cloud regimes and radiation there, we do not know whether it is because these SST values are closer to reality, or these SST values are artefacts of aerosols and clouds which overcast the surface but such temperature is preferred by parameterizations for representing organized convection or boundary-layer clouds more realistically.

Although quantitatively smaller than the changes in the above regimes, the frequency of stratocumulus regimes also changes, especially Thick-Stratocumulus regime at the East Boundary Upwelling regions which becomes more frequent. Not only lower SST at these regions but also the Western Pacific SSTs are regarded to be responsible for this increase. No significant impact of the higher SST at the Western Boundary Current regions is found. Compared with the impact of horizontal resolution, the SST dataset itself has a negligible impact on atmospheric phenomena. Overall, there appears to be no degradation in performance when using the SST CCI dataset.

The influence of the differences in sea ice cover are perhaps more significant. The reduction in sea ice cover in SST CCI significantly reduces the outgoing shortwave radiation and changes the frequency of different cloud regimes over the sea ice regions. The result that cloud regime occurrence tends to be underestimated over the sea ice regions in the simulations, and that the underestimate is smaller in SST CCI runs, suggests that the sea ice fraction in the SST CCI data is more consistent with the ISCCP satellite sea ice observations. Whether the surface in a region is covered by snow/sea ice matters for cloud retrieval over the region. Hence the retrieved clouds are influenced by the sea ice data set used.

5.2.5 FUTURE POTENTIAL AREAS OF STUDY

In carrying out the analysis described above, we have identified several possible areas of study using the current SST CCI dataset:

- Strong deep convection is sensitive to the SST, but also sensitive to orography, which changes the regime in neighbouring regions via circulation changes. It would be interesting to conduct an atmospheric experiment, forcing the

atmospheric model with SST CCI analysis v2.0 at the original gridded data resolution (0.05-degree grid).

- Because SST CCI dataset has different spatial pattern of the SST in some key regions (Maritime Continent and the neighbouring regions, East Boundary Upwelling region and West Boundary Current region), patterned patch SST experiments of these regions using SST CCI dataset as well as other dataset would be useful to quantify the local and remote impact of the SST on the atmosphere.
- While we have compared the influence of two daily SST and sea-ice datasets in this work, the usage of daily SST is not necessarily common in climate model community, e.g. standard Coupled Model Intercomparison Project atmosphere-only experiments (including those for the current CMIP6) are forced with interpolated monthly SSTs. Klingaman et al (2008) conducted atmosphere-only (AGCM) experiments with daily SST, analysed the active/break cycles of the monsoon and showed that “high-frequency SST anomalies not only increased variance in intra-seasonal rainfall but helped to organize and maintain coherent convective events, such as northward-propagating intra-seasonal oscillation (NPISO). Further, the results indicate that an AGCM can respond to realistic and frequent SST forcing to generate an NPISO that closely resembles observations. These results have important implications for simulating the NPISO in AGCMs and coupled climate models, as well as for predicting tropical intra-seasonal variability in short- and medium-range weather forecasts.” Their results suggest that daily SSTs do make a difference to shorter-timescale variability, and which may affect longer timescales too. This could be investigated in future work to further investigate the value of using daily data, like SST CCI dataset.
- The Stratocumulus regime is the biggest source of cloud feedback uncertainty. Many metrics/diagnostics have been developed to investigate this (Tsushima et al., 2017). The Stratocumulus regime in climate models is less frequent than observed but too bright (Nam et al., 2013, Tsushima et al., 2013). SST in the stratocumulus region given to the model could partly contribute to the biases in models. The SST dataset used in CMIP Model Intercomparison projects has a different spatial pattern from the SST CCI. Examination of the impact of these differences will be useful for the community.

5.2.6 RECOMMENDATIONS FOR FUTURE DEVELOPMENTS OF THE SST CCI PRODUCTS

Variance of the SST are implied to be smaller over the tropical ocean, except the Eastern Pacific in various timescales (daily, intra-seasonal, inter-annual). Construction of the dataset with a longer time period would be useful to verify the results on the interannual timescale.

Studies such as Klein and Hartmann (1993), Qu et al (2014), Brient and Schneider (2016) produced metrics to evaluate the seasonal variation/interannual variation of the stratocumulus regime with the local SST variation. Accurate observations of the SST over the region, as well as the Maritime Continent and the surrounding region, is critical for such metrics.

It would be useful to examine the regions in which the SST CCI product has cooler SST than other datasets (in the tropical-subtropical Atlantic, Indian Ocean) that are hypothesised to be due to dust. The tropical cyclone analysis suggests that this can impact on simulation performance, and hence it would be useful to know which dataset should be trusted more.

The retrieval of the ISCCP clouds are influenced by the snow and sea ice data set used. Snow and sea ice data set which are retrieved using information (wavelength) which is not sensitive to clouds would be useful.

5.2.7 ACKNOWLEDGMENTS

We thank Sarah Ineson for useful comments for writing the ENSO section and Paul Earnshaw for supports to obtain results from the AutoAssess.

5.2.8 REFERENCES

Andrews, T., Gregory, J. M., Paynter, D., Silvers, L. G., Zhou, C., Mauritsen, T., ... Titchner, H. (2018). Accounting for Changing Temperature Patterns Increases Historical Estimates of Climate Sensitivity. *Geophysical Research Letters*, 45 (16), 8490–8499. doi:10.1029/2018GL078887

Bell, G. D., Halpert, M. S., Schnell, R. C., Higgins, R. W., Lawrimore, J., Kousky, V. E., Tinker, R., Thiaw, W., Chelliah, M., Artusa, A., 2000: Climate assessment for 1999. *Bull. Amer. Meteor. Soc.* 81 (6), s1-s50. URL [http://dx.doi.org/10.1175/1520-0477\(2000\)81%5Bs1:caf%5D2.0.co;2](http://dx.doi.org/10.1175/1520-0477(2000)81%5Bs1:caf%5D2.0.co;2)

Berrisford, P., B.J. Hoskins, and E. Tyrlis, 2007: Blocking and Rossby Wave Breaking on the Dynamical Tropopause in the Southern Hemisphere. *J. Atmos. Sci.*, 64, 2881–2898, <https://doi.org/10.1175/JAS3984.1>

Brient, F., and Schneider, T.: Constraints on Climate Sensitivity from Space-Based Measurements of Low-Cloud Reflection, *Journal of Climate*, 29, 5821-5835, 10.1175/JCLI-D-15-0897.1, 2016.

Chu, J. H., Sampson, C. R., Levine, A. S., Fukada, E., 2002: The Joint Typhoon Warning Center tropical cyclone Best-Tracks, 1945-2000. Tech. rep., naval Research Laboratory Tech. Rep. NRL/MR/7540-02-16.

Haarsma, R. J., and Coauthors, 2016: High Resolution Model Intercomparison Project (HighResMIP). *Geosci. Model Dev.*, 9, 4185–4208, <https://doi.org/10.5194/gmd-9-4185-2016>.

Hodges, K.I., 1994: A General Method for Tracking Analysis and its Application to Meteorological Data, *Mon. Weather Rev.*, 122, 2573-2586.

Hodges, K.I., 1995: Feature Tracking on the Unit Sphere, *Mon. Weather Rev.*, 123, 3458-3465.

Hodges, K.I., 1996: Spherical Nonparameteric Estimators Applied to the UGAMP Model Integration for AMIP, *Mon. Weather Rev.*, 124, 2914-2932.

Hodges, K., Cobb, A., & Vidale, P. L., 2017: How well are tropical cyclones represented in reanalysis datasets? *Journal of Climate*, 30(14), 5243–5264. <https://doi.org/10.1175/JCLI-D-16-0557.1>

Hodges, K.I., Lee, R.W. and Bengtsson, L., 2011: A Comparison of Extratropical Cyclones in Recent Reanalyses ERA-Interim, NASA MERRA, NCEP CFSR, and JRA-25 , *J. Clim.* , 24, 4888-4906.

Hoskins, B.J., and Hodges, K.I., 2002: New Perspectives on the Northern Hemisphere Winter Storm Tracks, *J. Atmos. Sci.*, 59, 1041-1061

Huffman, G. J. and co-authors, 1997: The Global Precipitation Climatology Project (GPCP) combined data set. *Bull. Amer. Meteor. Soc.*, 78, 5-20.

Huffman G.J., Adler R.F., Bolvin D.T., Nelkin E.J. (2010) The TRMM Multi-Satellite Precipitation Analysis (TMPA). In: Gebremichael M., Hossain F. (eds) *Satellite Rainfall Applications for Surface Hydrology*. Springer, Dordrecht

Huffman, G. J., and D. T. Bolvin (2013), TRMM and other data precipitation data set documentation, Laboratory for Atmospheres, NASA Goddard Space Flight Center and Science Systems and Applications. ftp://precip.gsfc.nasa.gov/pub/trmmdocs/3B42_3B43_doc.pdf. Klein S, Jakob C (1999) Validation and sensitivities of frontal clouds simulated by the ECMWF model. *Monthly Weather Review* 127 (10):2514-2531. doi:10.1175/1520-0493(1999)127<2514:VASOFC>2.0.CO;2

Kennedy, J.J., N.A. Rayner, S.C. Millington, M. Saunby (in prep) The Met Office Hadley Centre Sea Ice and Sea-Surface Temperature data set, version 2, part 2: sea-surface temperature analysis

Klein, S. A., and D. L. Hartmann, 1993: The seasonal cycle of low stratiform clouds. *J. Climate*, 6, 1587–1606.

Klingaman, N. P., P. M. Inness, H. Weller, and J. M. Slingo, 2008: The importance of high-frequency sea surface temperature variability to the intraseasonal oscillation of Indian monsoon rainfall. *J. Climate*, 21, 6119–6140, <https://doi.org/10.1175/2008JCLI2329.1>.

Kummerow, C., W. Barnes, T. Kozu, J. Shiue, and J. Simpson, 1998: The Tropical Rainfall Measuring Mission (TRMM) Sensor Package. *J. Atmos. Oceanic Technol.*, 15, 809–817, [https://doi.org/10.1175/1520-0426\(1998\)015<0809:TTRMMT>2.0.CO;2](https://doi.org/10.1175/1520-0426(1998)015<0809:TTRMMT>2.0.CO;2)

Landsea, C. W., Franklin, J. L., 2013: Atlantic hurricane database uncertainty and presentation of a new database format. *Mon. Wea. Rev.* 141 (10), 3576-3592. URL <http://dx.doi.org/10.1175/mwr-d-12-00254.1>

Lee, JY., Wang, B., Wheeler, M.C. et al., 2013: Real-time multivariate indices for the boreal summer intraseasonal oscillation over the Asian summer monsoon region. *Clim Dyn* (2013) 40: 493. <https://doi.org/10.1007/s00382-012-1544-4>

Levine, R.C. & Martin, G.M., 2017: On the climate model simulation of Indian monsoon low pressure systems and the effect of remote disturbances and systematic biases. *Clim Dyn* (2018) 50: 4721. <https://doi.org/10.1007/s00382-017-3900-x>

Levine, R.C. & Turner, A.G., 2012: Dependence of Indian monsoon rainfall on moisture fluxes across the Arabian Sea and the impact of coupled model sea surface temperature biases. *Clim. Dyn.*, 38, 2167. <https://doi.org/10.1007/s00382-011-1096-z>

Levine, R.C., Turner, A.G., Marathayil, D., and Martin, G.M., 2013: The role of northern Arabian Sea surface temperature biases in CMIP5 model simulations and future predictions of Indian summer monsoon rainfall, *Clim. Dyn.*, doi:10.1007/s00382-012-1656-x

Liebmann B. and C.A. Smith, 1996: Description of a Complete (Interpolated) Outgoing Longwave Radiation Dataset. *Bulletin of the American Meteorological Society*, 77, 1275-1277.

Loeb, N. G., B. A. Wielicki, D. R. Doelling, G. L. Smith, D. F. Keyes, S. Kato, N. Manlo-Smith, and T. Wong (2009), Toward optimal closure of the Earth's TOA radiation budget, *J. Clim.*, 22, 748–766.

Nam, C., and Quaas, J.: Evaluation of Clouds and Precipitation in the ECHAM5 General Circulation Model Using CALIPSO and CloudSat Satellite Data, *Journal of Climate*, 25, 4975-4992, 10.1175/JCLI-D-11-00347.1, 2012.

Pincus, R., Platnick, S., Ackerman, S., Hemler, R., and Hofmann, R.: Reconciling Simulated and Observed Views of Clouds: MODIS, ISCCP, and the Limits of Instrument Simulators, *Journal of Climate*, 25, 4699-4720, 10.1175/JCLI-D-11-00267.1, 2012.

Pelly, J.L. and B.J. Hoskins, 2003: A New Perspective on Blocking. *J. Atmos. Sci.*, 60, 743–755, [https://doi.org/10.1175/1520-0469\(2003\)060<0743:ANPOB>2.0.CO;2](https://doi.org/10.1175/1520-0469(2003)060<0743:ANPOB>2.0.CO;2)

Rayner, N. A.; Parker, D. E.; Horton, E. B.; Folland, C. K.; Alexander, L. V.; Rowell, D. P.; Kent, E. C.; Kaplan, A. (2003) Global analyses of sea surface temperature, sea ice, and night marine air temperature since the late nineteenth century *J. Geophys. Res.* Vol. 108, No. D14, 4407 10.1029/2002JD002670

Reynolds, R. W., 1988: A real-time global sea surface temperature analysis. *J. Climate*, 1, 75-86.

Saha, K., F. Sanders, and J. Shukla, 1981: Westward Propagating Predecessors of Monsoon Depressions. *Mon. Wea. Rev.*, 109, 330–343, [https://doi.org/10.1175/1520-0493\(1981\)109<0330:WPPOMD>2.0.CO;2](https://doi.org/10.1175/1520-0493(1981)109<0330:WPPOMD>2.0.CO;2)

Spencer, R. W., 1993: Global oceanic precipitation from the MSU during 1979-91 and comparisons to other climatologies. *J. Climate*, 6, 1301-1326.

Taylor, K.E., D. Williamson and F. Zwiers, 2000: The sea surface temperature and sea ice concentration boundary conditions for AMIP II simulations. PCMDI Report 60, Program for Climate Model Diagnosis and Intercomparison, Lawrence Livermore National Laboratory, 25 pp. Available online: <http://www-pcmdi.llnl.gov/publications/pdf/60.pdf>

Titchner, H. A., and N. A. Rayner (2014), The Met Office Hadley Centre sea ice and sea surface temperature data set, version 2: 1. Sea ice concentrations, *J. Geophys. Res. Atmos.*, 119, 2864-2889, doi: 10.1002/2013JD020316.

Tselioudis G, Rossow W, Zhang Y, Konsta D (2013) Global Weather States and Their Properties from Passive and Active Satellite Cloud Retrievals. *J Clim* 26 (19):7734-7746. doi:10.1175/JCLI-D-13-00024.1

Tsushima, Y., Ringer, M., Webb, M., and Williams, K.: Quantitative evaluation of the seasonal variations in climate model cloud regimes, *Climate Dynamics*, 41, 2679-2696, 10.1007/s00382-012-1609-4, 2013.

Tsushima, Y., Brient, F., Klein, S. A., Konsta, D., Nam, C. C., Qu, X., Williams, K. D., Sherwood, S. C., Suzuki, K., and Zelinka, M. D.: The Cloud Feedback Model Intercomparison Project (CFMIP) Diagnostic Codes Catalogue – metrics, diagnostics and methodologies to evaluate, understand and improve the representation of clouds and cloud feedbacks in climate models, *Geosci. Model Dev.*, 10, 4285-4305, <https://doi.org/10.5194/gmd-10-4285-2017>, 2017

Webb M, Senior C, Bony S, Morcrette J (2001) Combining ERBE and ISCCP data to assess clouds in the Hadley Centre, ECMWF and LMD atmospheric climate models. *Clim Dyn* 17 (12):905-922. doi:10.1007/s003820100157

Williams KD, Webb MJ (2009) A quantitative performance assessment of cloud regimes in climate models. *Clim Dyn* 33(1):141–157.

Williams, K. D., Copsey, D., Blockley, E. W., Bodas-Salcedo, A., Calvert, D., Comer, R., et al. (2018). The Met Office Global Coupled model 3.0 and 3.1 (GC3.0 & GC3.1) configurations. *Journal of Advances in Modeling Earth Systems*, 10, 357–380. <https://doi.org/10.1002/2017MS001115>

Qu, X., A. Hall, S. A. Klein, P. M. Caldwell, 2014: On the spread of changes in marine low cloud cover in climate model simulations of the 21st century. 42: 2603-2626. DOI 10.1007/s00382-013-1945-z.

Xie P., and P. A. Arkin, 1997: Global precipitation: a 17-year monthly analysis based on gauge observations, satellite estimates, and numerical model outputs. *Bull. Amer. Meteor. Soc.*, 78, 2539-2558.

Zhou, C., M. D. Zelinka, and S. A. Klein, 2017: Analyzing the dependence of global cloud feedback on the spatial pattern of sea surface temperature change with a Green's Function approach, *J. Adv. Model. Earth Syst.*, 9, 2174-2189, doi:10.1002/017MS001096.

6. VOLUNTARY REPORTS BY TRAILBLAZER USERS

6.1 Inter-comparison of High-Resolution SST Climatology data sets over the Australian region

Yuwei Hu^{1,2}, Helen Beggs³ and Xiao Hua Wang^{1,2}

1. *Sino-Australian Research Centre for Coastal Management, University of New South Wales, Canberra, Australia*
2. *School of Science, University of New South Wales, Canberra, Australia*
3. *Bureau of Meteorology, Melbourne, Australia*

6.1.1 KEY MESSAGES

- The SST CCI analysis v2.0 data provided a relatively flexible and accurate reference to the climatology comparison studies.
- The long reference period of SST CCI analysis v2.0 data provides a convincing SST climatology through this study.
- The SST climatology datasets derived from SST CCI analysis v2.0 data are highly consistent with the in-situ tropical mooring measurements.
- The SST CCI analysis v2.0 data files are well organised and contain essential information, thus very easy to use.
- It will be much more convenient for downloading the data if an FTP server is available.
- Monthly mean SST CCI analysis v2.0 files are suggested together with the daily files.
- Producing a night-only SST CCI analysis v2.0 would enable it to be used for applications that require a consistent night-time SST, such as coral bleaching studies.

6.1.2 SCIENTIFIC ANALYSIS

6.1.2.1 AIMS OF THE STUDY

Sea surface temperature (SST) climatology datasets provide the reference for observations of ocean anomalous events such as coastal upwelling and Marine Heat Waves (MHWs), which may have detrimental effects on the local marine ecosystem. The representativeness of the SST climatology datasets of the historical and current ocean surface states is essential to identify and predict anomalous events. Here we compare four high resolution SST climatology datasets around the Australian coast to investigate the uncertainty introduced by the reference SSTs to current estimates of SST trends in anomalous events. The datasets studied are: (i) 0.05-degree SST Climate Change Initiative (CCI) global daily climatology for 1981-2016 and 1992-2016, calculated by this study from the ESA SST CCI Analysis product version 2.0, a satellite-only SST-depth analysis created by OSTIA system from SST CCI ATSR and SST CCI AVHRR products (1981-2016); (ii) 0.02-degree SST Atlas of the Australian Regional Seas (SSTAARS), a pixel-wise daily climatology for 1992-2016 (Wijffels et al., 2018), based on the 0.02-

degree bias-corrected version 2 Integrated Marine Observing System (IMOS) one-day composite night-time AVHRR SST; (iii) 0.05-degree NOAA Coral Reef Watch (CRW) global monthly climatology for 1985–2012³, derived from the MyOcean OSTIA Reanalysis (1985-2002) and NOAA Geo-Polar Blended SST reanalysis (2002–2012)(Maturi et al., 2017) and (iv) 0.1 degree BRAN SST daily climatology for 1994-2016, derived from the BRAN_2016 ocean reanalysis data generated by the OFAM3 ocean model (Oke et al.,2013).

6.1.2.2 METHOD

The method section will contain the method to generate the SST climatology and the comparison method of the climatology dataset groups, followed by the density distribution analysis of each comparison group and in-situ data validation of the main climatology datasets.

6.1.2.2.1 Climatology Datasets

There are two SST climatology products used in this study which are the atlas of the Australian regional seas (SSTAARS) and Coral Reef Watch (CRW). Apart from SSTAARS and CRW, three climatology datasets are generated by this study based on the SST CCI analysis v2.0 and BRAN_2016 ocean reanalysis. They are CCI_A daily climatology derived from SST CCI analysis v2.0 data for 1981-2016 using the conventional averaging method, CCI_1992 daily climatology derived from SST CCI analysis v2.0 data for 1992-2016 using the same method as CCI_A but over a different reference period. The last is BRAN_A daily climatology derived from BRAN_2016 ocean reanalysis data for 1994 - 2016. In order to compare against the CRW climatology, monthly resolution CCI_A, CCI_1992, SSTAARS and BRAN_A are also calculated using monthly averaging. Details of the climatology datasets used in this study are listed in Table 6-1. The SSTAARS data files are set as the spatial coverage reference, and therefore only the grid cells with valid SSTAARS values over the Australian domain (20°N-70°S, 70°E-170°W) are included in the climatology datasets used by this study. Note that the SSTAARS spatial coverage is dictated by the coverage of the High Resolution Picture Transmission (HRPT) AVHRR SSTs used to form the SSTAARS climatology (Wijffels et al., 2018).

In this report we define CCI_A as the reference to compare with other climatology datasets. An additional comparison group of CCI_1992 – SSTAARS is conducted to deeper investigate the potential of SSTAARS to be a convincing climatology dataset. The comparison groups are listed in Table 6-2 together with the main control factors of the comparison.

Table 6-1. Main attributes of the climatology datasets.

Climatology Datasets	Attributes				
	Spatial Resolution	Temporal Resolution	Reference Period	Data Source	Calculation Algorithm
CCI_A	0.05° (~5 km)	Daily Monthly	1981-2016 (36 years)	Climate Change Initiative (CCI) SST version 2 analyses (daily SST0.2m)	Daily and Monthly averaging

³ <https://coralreefwatch.noaa.gov/satellite/coraltemp.php>

CCI_1992	0.05° (~5 km)	Daily Monthly	1992-2016 (25 years)	Climate Change Initiative (CCI) SST version 2 analyses (daily SST0.2m)	Daily and Monthly averaging
CRW	0.05° (~5 km)	Monthly	1985-2012 (28 years)	OSTIA Reanalysis (1985 - 2002) NOAA Geo-Polar Blended SST reanalysis (2002 – 2012) (daily night-time SST0.2m)	<ul style="list-style-type: none"> • Linear interpolation • Monthly averaging • Bias adjustment
SSTAARS	0.02° (~2 km)	Daily Monthly	1992-2016 (25 years)	Bias corrected version 1 and version 2 IMOS one-day composite night-time AVHRR SST0.2m L3S data (quality level ≥ 4)	<ul style="list-style-type: none"> • Parametric model fitting • Climatology reconstruction
BRAN_A	0.1° (~10 km)	Daily Monthly	1994-2016 (23 years)	BRAN_2016 ocean reanalysis (daily SST2.5m)	Daily and Monthly averaging

Table 6-2. Experiment groups of the climatology comparison and the main control factors of the differences (match: √ and mismatch: ×).

Experiment Groups	Control Factors			
	Day and Night Input Data	Reference Period	Central Year	Calculation Algorithm
CCI_A – SSTAARS	×	×	×	×
CCI_1992 – SSTAARS	×	√	√	×
CCI_A – CRW	×	×	√	√
CCI_A – BRAN_A	√	×	×	√

The datasets are pre-processed to reduce the mismatch of temporal and spatial resolution. Then, the differences of corresponding time in each experiment group are produced, followed by the temporal bias and Standard Deviation (STD) and three kinds of statistical analysis based on the data distribution pattern along latitude, longitude and time bins. The daily files of CCI_A climatology datasets from corresponding months are averaged at each pixel to form the monthly files. The SSTAARS climatology are regridding from 0.02° resolution to 0.05° resolution using the area weighted averaging method. Regridding using the nearest neighbour method from 0.1° to 0.05° has been

applied to the BRAN_A climatology. The 0.05° resolution is the optimal choice, with the advantage of retaining the greatest amount of original data combined with lower computation time.

6.1.2.2.2 Density Distribution of the Differences

The differences of each comparison group are first calculated along with the temporal relative bias and standard deviation (STD) in each valid SSTAARS grid cell. The histogram distribution of the differences within different bins (latitude, longitude, time) is calculated based on equation 1 to 3.

$$N_{SST\ Difference} = \sum_{i=1}^k BIN\ count_i \quad (1)$$

$$N_{BIN\ count} = \sum_{i=1}^l SST\ count_i \quad (2)$$

$$\sigma_{count_i} = STD(BIN\ count_i) \quad (3)$$

The $BIN\ count_i$ in each bin (1°N latitude, 1°E longitude and time interval) of the $SST\ Difference$ of each group as shown in equation 1 are first calculated. The histogram $SST\ count_i$ within an interval of 0.01°C of each $BIN\ count_i$ are then calculated based on equation 2. Furthermore, the data value at both edges of the $BIN\ count_i$ are removed using the $4.5\sigma_{count_i}$ threshold as shown in equation 3 to filter out the outliers of the differences. This may extract the cold or warm tails in the high temperature zone and makes the histogram of each $BIN\ count_i$ close to the normal distribution.

6.1.2.2.3 Climatology validation using tropical mooring data

There are no common criteria for quantifying the accuracy of the climatology datasets in this study. Hence the long-term in-situ hourly SST mooring measurements from the NOAA Pacific Marine Environmental Laboratory (PMEL) Global Tropical Moored Buoy Array (GT MBA, <https://www.pmel.noaa.gov/gtmba/taotriton-collaboration>) are used here to validate the accuracy of the climatology datasets. The CRW climatology is not included in the validation as the number of qualified values for monthly files are not sufficient for a convincing statistical analysis. There are 16 platforms from the TAO/TRITON array available in the SSTAARS valid data domain (Figure 6-1). However, due to the time period limitation, platform 52087 (2001-2018) will not be included in the validation. The SST measured by the TAO/TRITON mooring platforms represent 1 m SST_{depth}.

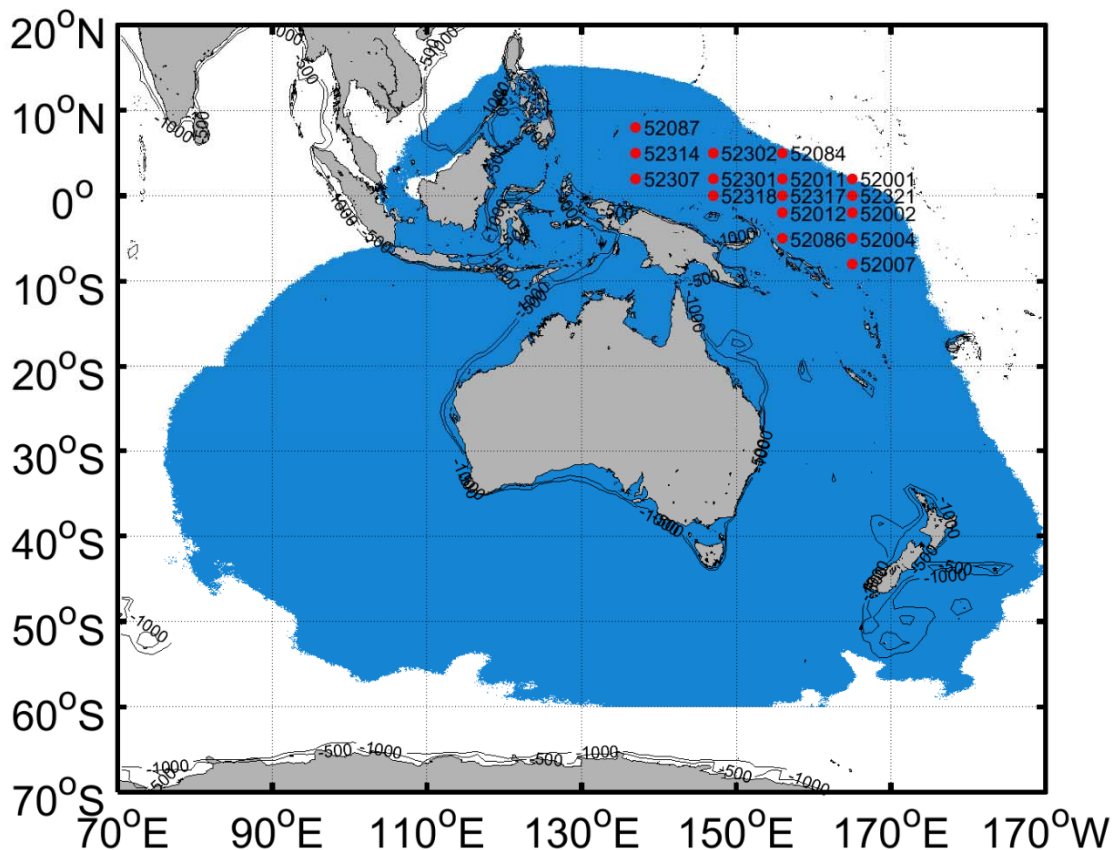


Figure 6-1. TAO/TRITON Platform Code and location (red) and SSTAARS domain (blue).

Details of the TAO/TRITON platform and SST data used in this study are described in Table 6-3. The hourly mooring data are pre-processed based on different time periods that are close to each of the reference periods of the CCI_A, SSTAARS and BRAN_A climatology datasets to achieve an effective validation. For comparisons with SSTAARS, the in-situ climatology reference period starts at 1992, and for BRAN_A the reference period starts at 1994. There are no platforms that have a similar measurement period to the CCI_A climatology dataset (1981-2016). Therefore, any mooring platform that has a reference period longer than the SSTAARS climatology dataset (1992-2016) are included in the CCI_A validation. Note that both day and night-time mooring data were used in this study.

A daily mooring climatology time series is generated at each platform location using the averaging method and only data values with high quality code (QC) 1 and 2 are included. 'QC=1' represents the highest quality, and means the measurements of the mooring that are pre or post-deployment calibrated agree to within sensor specifications. 'QC=2' indicates default quality and only pre-deployment calibrations are applied on the measurements (McPhaden et al., 1998). The values of the four grid cells nearest the location of the mooring in the gridded climatology data are averaged to compare with the in-situ measurement.

For CCI_A, SSTAARS and BRAN_A climatology datasets, a group of time series at the same location as the TAO/TRITON array platforms are generated. Differences from TAO/TRITON mooring measurements are generated by subtracting the corresponding time series of each gridded climatology. Then mean bias, STD and correlation coefficient (R value) are calculated at each platform location.

Table 6-3. TAO/TRITON Details.

Order	Platform Code	Latitude (°N)	Longitude (°E)	Maximum Qualified days (QC=1&2)	Time Period
1	52318	0	147	7813	1994/04/28 – 2016/12/09
2	52317	0	156	8578	1991/08/29 – 2016/12/31
3	52321	0	165	8775	1986/12/13 – 2016/12/31
4	52307	2	137	8189	1992/04/22 – 2016/12/07
5	52301	2	147	6841	1990/02/18 – 2016/12/10
6	52011	2	156	8574	1991/08/30 – 2016/12/12
7	52001	2	165	9178	1985/07/09 – 2016/12/31
8	52012	-2	156	8833	1991/08/28 – 2016/12/16
9	52002	-2	165	9497	1985/07/06 – 2016/12/31
10	52314	5	137	5694	1993/05/01 – 2016/12/06
11	52302	5	147	7954	1990/02/19 – 2014/02/18
12	52084	5	156	7450	1991/09/01 – 2015/01/01
13	52086	-5	156	8034	1991/08/26 – 2014/12/24
14	52004	-5	165	9686	1987/01/30 – 2016/12/31
15	52007	-8	165	7661	1991/08/11 – 2016/12/31

6.1.2.3 RESULTS

6.1.2.3.1 Mean Difference and STD of Residual Difference

Figure 6-2 and Figure 6-3 plot the spatial distribution of mean difference (Figure 6-2) and STD (Figure 6-3) at each grid cell of the comparison group in Table 6-2.

Most regions of the group CCI_A – SSTAARS (Figure 6-2a) has mean difference close to zero except the warm relative bias in the southeast and cold bias in the northwest coastal seas of Australia. This pattern of differences is only found in this group, and is possibly caused by differences in the original input data and the reference period.

The group CCI_1992 – SSTAARS (Figure 6-2b) is warmer in most of the regions compared to group CCI_A – SSTAARS (Figure 6-2a) as the reference period is changed from 1981 – 2016 to 1992 – 2016. This relative warmth is consistent with the rising trend of in-situ SST over the Australian region since 1981⁴. The warm mean relative bias in the north-east is evident in both Figure 6-2(a) and (b).

⁴

http://www.bom.gov.au/climate/change/index.shtml#tabs=Tracker&tracker=timeseries&tQ=graph%3Dsst%26area%3Daus%26season%3D0112%26ave_yr%3D0

The group CCI_A – CRW (Figure 6-2c) has the same centre year which suggests the large relative bias seen in this group is mainly caused by differences in the original data. The group CCI_A – BRAN_A (Figure 6-2d) has no regions of large relative bias like group CCI_A – SSTAARS (Figure 6-2a), except off the north-west coast of Australia, but horizontal artefacts are found. The nearest neighbour method used for the spatial resolution adjustment applied on the BRAN_A climatology may be the cause of these horizontally distributed differences.

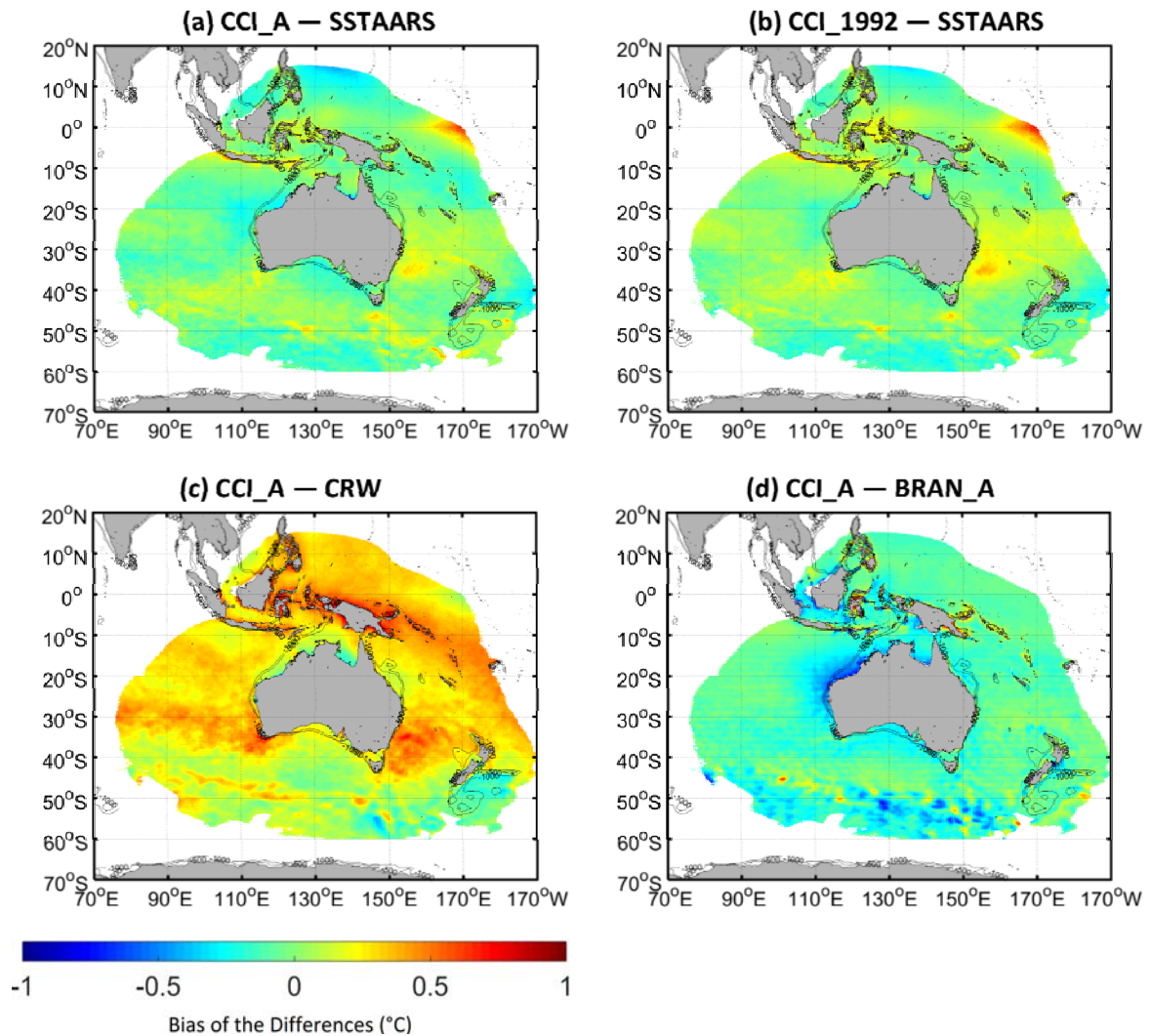


Figure 6-2. Spatial distribution of the temporal relative bias (°C) of group (a) CCI_A – SSTAARS, (b) CCI_1992 – SSTAARS, (c) CCI_A – CRW and (d) CCI_A – BRAN_A.

For all groups, most of the regions have STD smaller than 0.5°C. The groups containing CRW (Figure 6-3c) show dappled STD over most regions. To test that the dappled values are not caused by the spatial resolution adjustment, the resolution adjustment process was reversed. The upgrading process was converted to a degrading process. However, the dappled values still appeared in the STD plots of group CCI_A – CRW.

The group of CCI_1992 – SSTAARS (Figure 6-3b) has a similar time span for the input data, which may cause the smaller STD than for group CCI_A – SSTAARS (Figure 6-3a) over the whole domain. This smaller STD indicates the CCI_1992 and SSTAARS climatology datasets represent similar seasonal cycles over the same reference period.

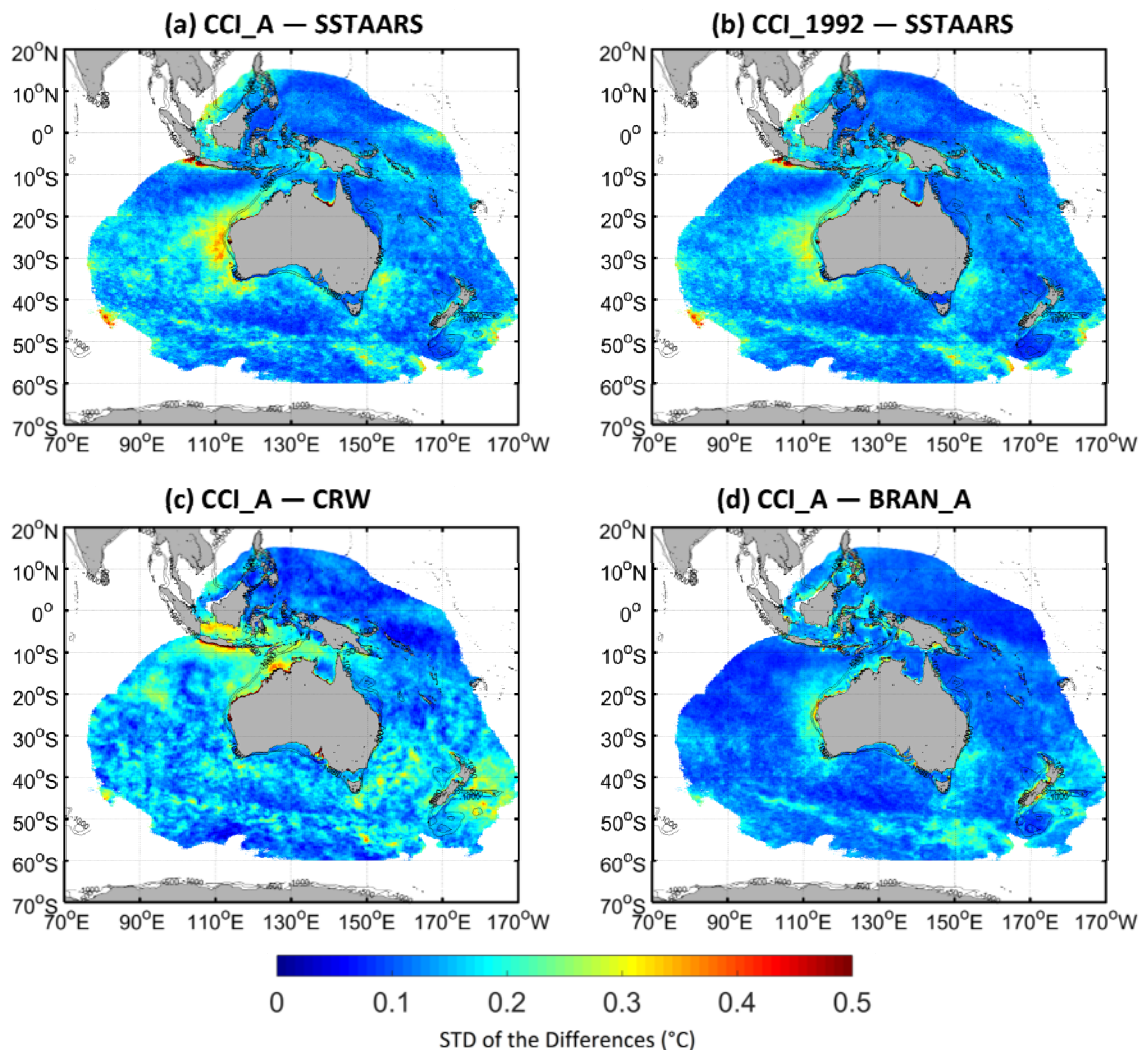


Figure 6-3. Spatial distribution of the temporal STD (°C) of group (a) CCI_A – SSTAARS, (b) CCI_1992 – SSTAARS, (c) CCI_A – CRW and (d) CCI_A – BRAN_A.

6.1.2.3.2 Density Distribution of the Differences

Figure 6-4 to Figure 6-6 show the density distributions along the 1°N latitude bin (Figure 6-4), 1°E longitude bin (Figure 6-5) and within the 1-day or 1-month time bin (Figure 6-6) for each comparison group. The plots are scaled in a logarithmic colour bar to achieve a better view of the data density.

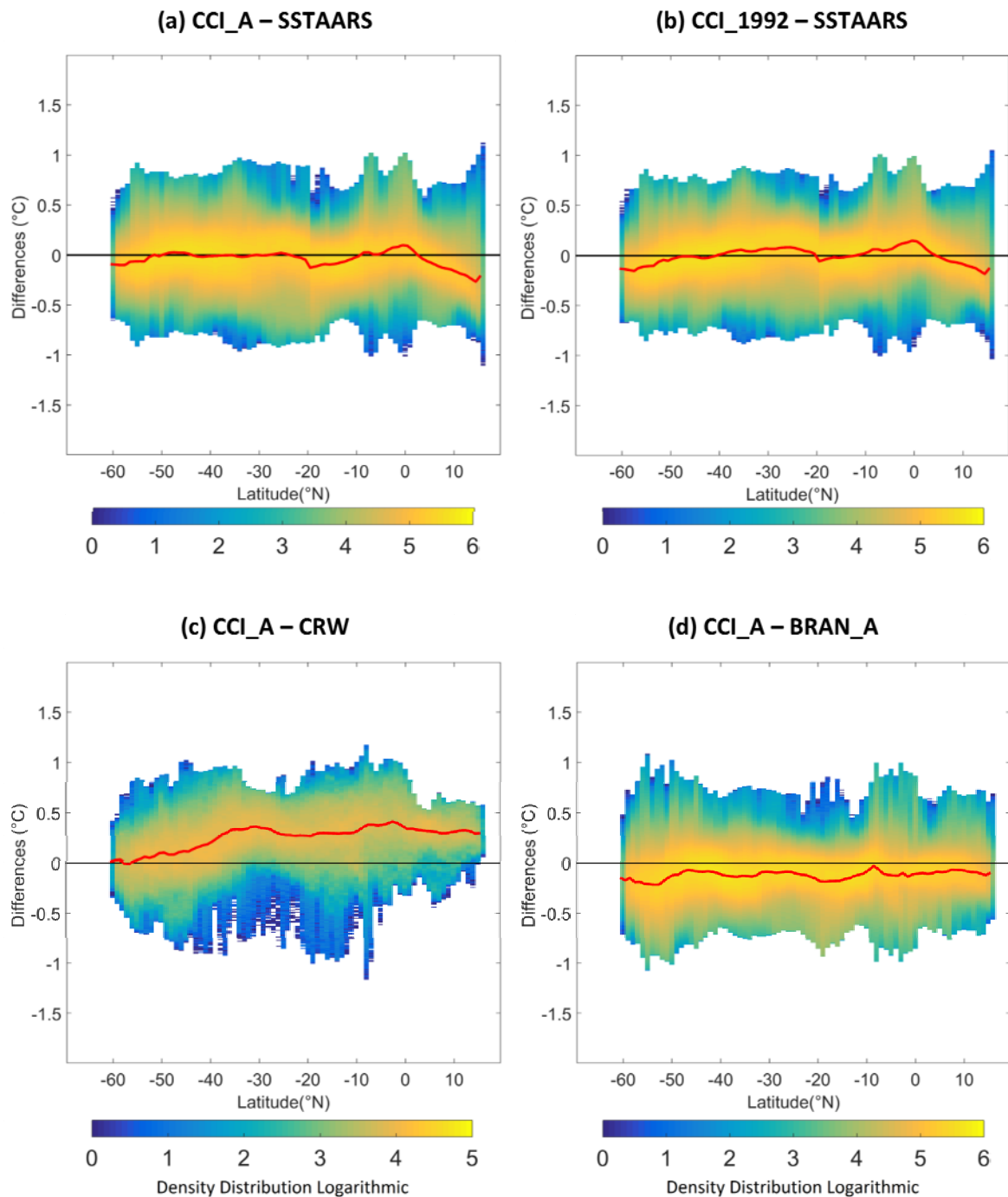


Figure 6-4. The density distribution of (1) CCI_A – SSTAARS, (2) CCI_1992 – SSTAARS, (3) CCI_A – CRW and (4) CCI_A – BRAN_A within each 1°N (latitude) × 0.01°C (Temperature) bin (°C). The red line is the relative bias in each latitude bin. A logarithmic density distribution is used.

The group CCI_A – SSTAARS (Figure 6-4a) shows the smallest relative bias within each latitude bin in the southern hemisphere around Australia. The relative bias increased up to -0.3°C from 0°N to 20°N. This increased difference in the north tropical regions may indicate biases in the input data in this region. Compared to group CCI_A – SSTAARS (Figure 6-4a), the group CCI_1992 – SSTAARS (Figure 6-4b) has a similar density distribution pattern but with a mean relative bias closer to zero. The group CCI_A – BRAN_A (Figure 6-4d) has a mean relative bias of -0.2°C over the latitude bands. This

relative bias may be partly attributed to the different reference periods as CCI_A starts 13 years before BRAN_A.

The group CCI_A – CRW (Figure 6-4c) shows relative bias with a mean value around 0.4°C. The main reason for this relative bias is possibly the different reference periods as the enhanced rate of ocean warming around Australia for the period 2013 – 2016 are not included in the CRW climatology. If the SST trends increased rapidly in this four-year period, the CRW climatology may have a cold bias compared to other climatology datasets, which is consistent with Figure 6-4.

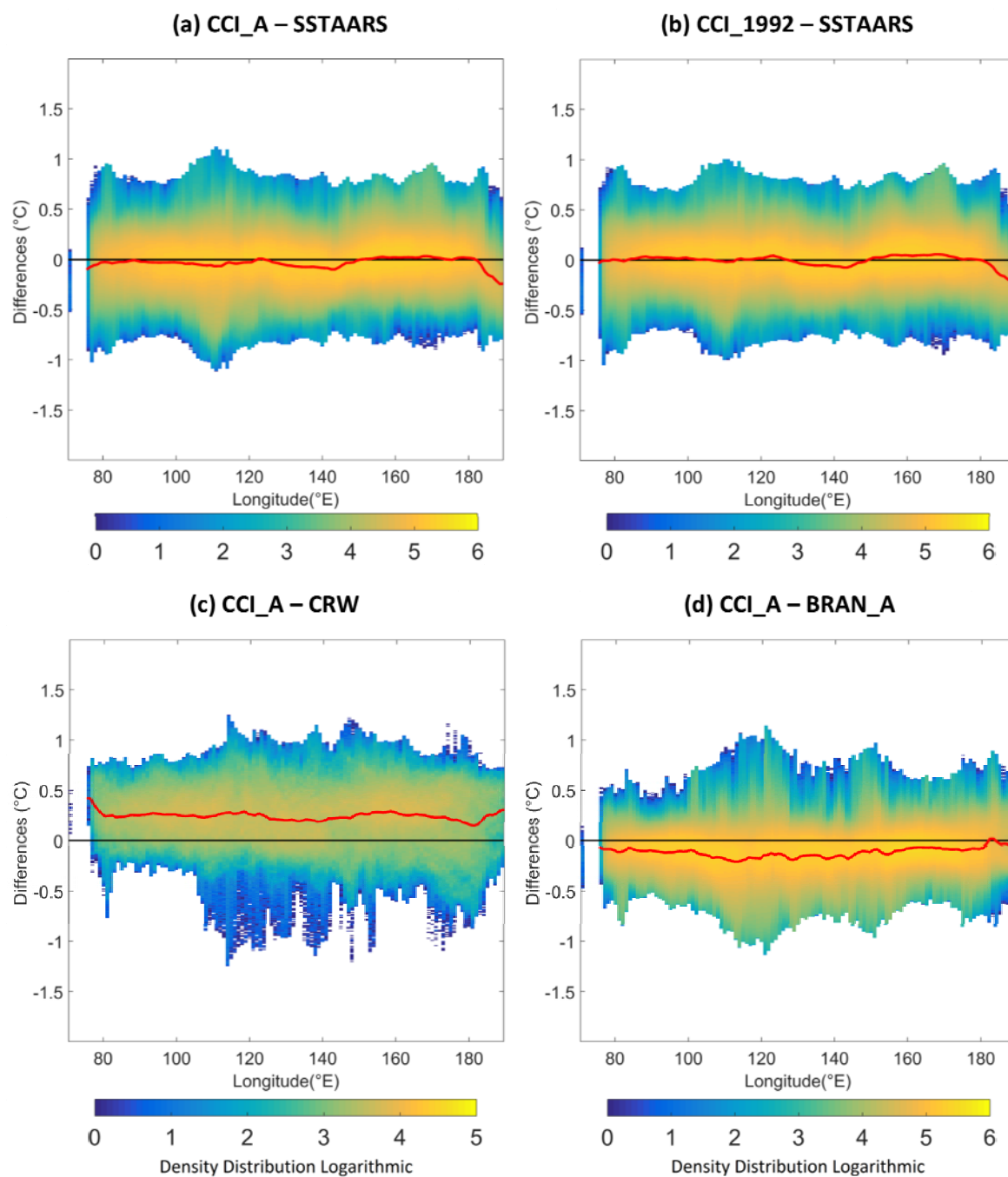


Figure 6-5. The density distribution of (1) CCI_A – SSTAARS, (2) CCI_1992 – SSTAARS, (3) CCI_A – CRW and (4) CCI_A – BRAN_A within each 1°E (longitude) × 0.01°C (Temperature) bin (°C). The red line is the bias in each longitude bin. A logarithmic density distribution is used.

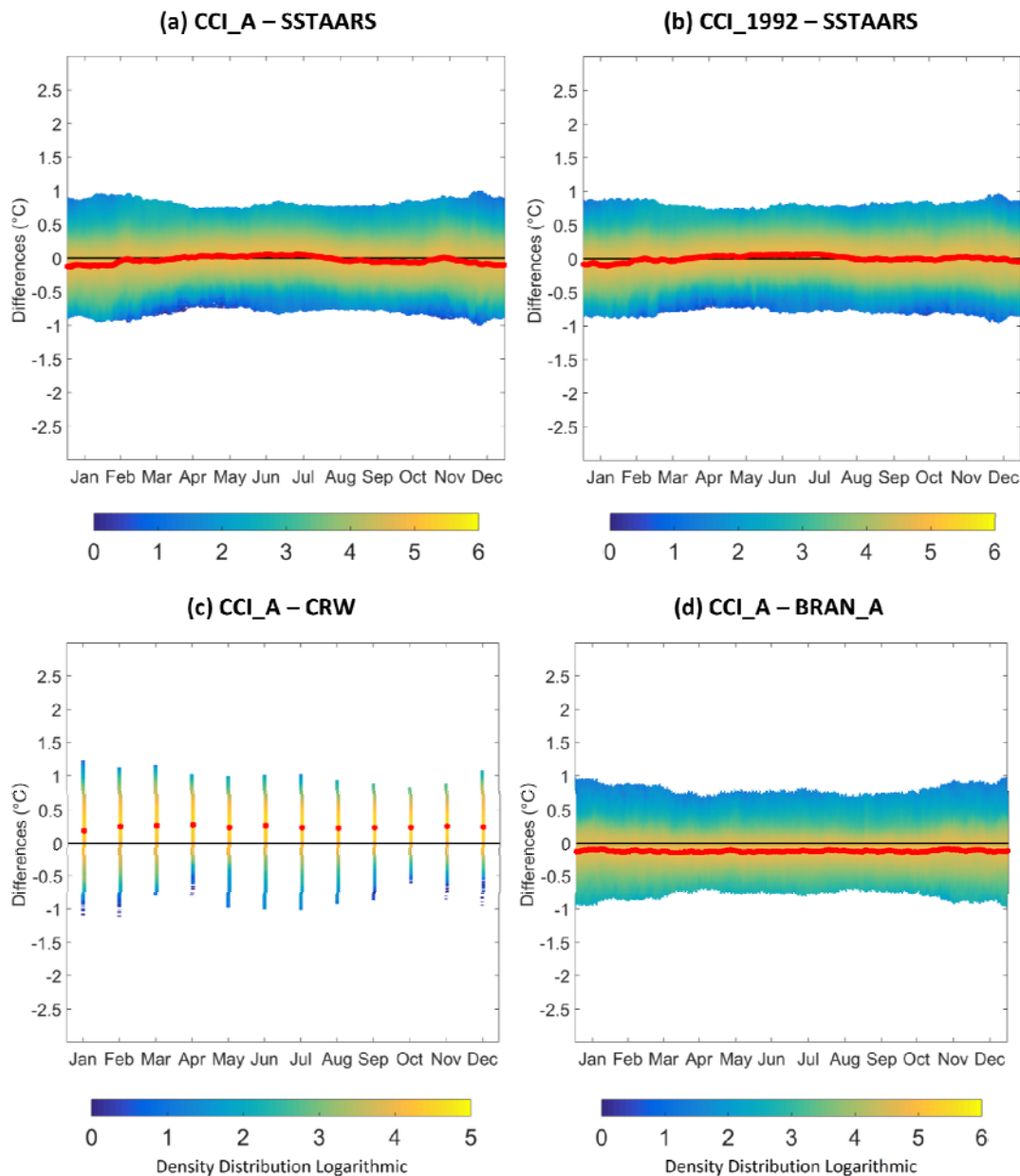


Figure 6-6. The density distribution of (1) CCI_A – SSTAARS, (2) CCI_1992 – SSTAARS, (3) CCI_A – CRW and (4) CCI_A – BRAN_A within time interval $\times 0.01^{\circ}\text{C}$ (Temperature) bin ($^{\circ}\text{C}$), the red line is the bias in each time interval bin. A logarithmic density distribution is used.

The longitude distribution has a similar overall pattern as the latitude distribution. The group CCI_1992 – SSTAARS (Figure 6-5b) has the best agreement among all comparison groups.

Like the latitude distribution, the density distribution within each time interval of CCI_1992 – SSTAARS (Figure 6-6b) has near-zero relative bias over most days in the year. It is worthwhile to point out that although the group CCI_A – BRAN_A (Figure 6-6d) shows a mean bias around 0.1°C , the bias is evenly distributed and exhibits a lack of seasonality which may be attributable to the properties of the input data, as they are both gap-free analyses that are less affected by cloud than SSTAARS.

Overall, the group CCI_1992 – SSTAARS has the best agreement, which means the differences of group CCI_A – SSTAARS are mostly caused by the reference period and

the input data. The parametric model fitting algorithm used by SSTAARS (Wijffels et al., 2018) did not appear to induce large bias.

6.1.2.3.3 In-situ Measurement Validation

Differences to the TAO/TRITON mooring SST1m climatology at each site are generated by subtracting the in-situ climatology from the corresponding time series of each gridded climatology. Mean bias, STD and correlation coefficient (R value) for the gridded climatology minus in-situ climatology are calculated at each platform location and presented in Table 6-4.

Table 6-4. Statistical analysis (Bias, STD and Correlation Coefficient R at 95% confident level) of gridded climatology minus in-situ climatology. Coloured numbers highlight discrepancies, discussed in the text.

Platform Code	Latitude (°N)	Longitude (°E)	CCI_A			SSTAARS			BRAN_A		
			Bias	STD	R	Bias	STD	R	Bias	STD	R
52318	0	147							-0.03 0.87		0.07
52317	0	156	-0.09 0.80		0.07	-0.16 0.66		0.13	-0.03 0.81		0.07
52321	0	165	-0.09 0.84		0.09	-0.47 0.84		0.21	-0.03 0.74		0.11
52307	2	137				-0.16 0.79		0.14	-0.04 0.86		0.08
52301	2	147	-0.11 0.78		0.09	-0.07 0.52		0.14	-0.07 0.81		0.07
52011	2	156	-0.07 0.83		0.07	-0.05 0.70		0.13	-0.04 0.89		0.05
52001	2	165	-0.09 0.92		0.07	-0.33 0.85		0.16	-0.00 0.93		0.08
52012	-2	156	-0.07 0.84		0.07	-0.08 0.71		0.11	0.01	0.06	0.86
52002	-2	165	-0.09 0.85		0.07	-0.34 0.70		0.22	-0.04 0.84		0.07
52314	5	137							-0.05 0.95		0.08
52302	5	147	-0.05 0.93		0.09	0.01	0.10	0.90	-0.03 0.91		0.07
52084	5	156	-0.11 0.85		0.11	-0.05 0.74		0.11	-0.05 0.90		0.06
52086	-5	156	-0.06 0.94		0.10	-0.05 0.86		0.11	-0.02 0.96		0.06
52004	-5	165	-0.06 0.86		0.06	-0.13 0.80		0.09	-0.01 0.82		0.07
52007	-8	165	-0.08 0.95		0.10	0.05	0.10	0.92	-0.05 0.97		0.06
Total			-0.08 0.92		0.09	-0.14 0.72		0.20	-0.03 0.93		0.07

Mooring platforms 1 (52318), platform 4 (52307) and platform 10 (52314) are not considered in the CCI_A climatology validation because the mooring reference periods start in 1994, 1992 and 1993, respectively. The CCI_A climatology has a mean bias of -0.08°C with STD of 0.09°C and correlation coefficient of 0.92. This small cold mean bias may be partly attributable to the longer reference period of CCI_A climatology (1981 – 2016). Comparison with most of the platforms indicates biases close to the mean value. Comparisons to the mooring platforms 2 (52317, 0°N , 156°E) and 5 (52301, 2°N , 147°E), as green-marked in Table 6-4, have lower R values compared to those with other platforms, which may be a consequence of lower density of valid infra-red satellite observation data during the monsoon season in the tropical regions, although the monsoons affect all mooring sites in this study.

Mooring platforms 1 (52318) and platform 10 (52314) are not considered in the SSTAARS climatology validation based on the criteria of the reference period. The SSTAARS climatology has a mean bias of -0.14°C with a correlation coefficient of 0.72 (Table 6-4). This mean cold bias may be partly attributable to diurnal warming affecting the daytime mooring SST1m observations, since SSTAARS is formed from night-time data only (Wijffels et al., 2018). The three highest differences occur at platforms 3 (52321, 0°N , 165°E), 7 (52001, 2°N , 165°E) and 9 (52002, 2°S , 165°E), red-marked in Table 6-4. The location of these three platforms corresponds to the 0.4°C warm relative bias of CCI_A – SSTAARS in Figure 6-2a. Note that CCI_A is based on both day and night-time infra-red satellite data, so is more likely than SSTAARS to include the effect of diurnal warming of the surface ocean. Another possible reason for the larger bias is the low density of the SSTAARS input data at these sites (see Figure 1, Wijffels et al., 2018). The relatively low correlation coefficient occurs at platform 2 (52317, 0°N , 156°E) and 5 (52301, 2°N , 147°E), as green-marked in Table 6-4. The low coefficient indicates an unmatched seasonal cycle, possibly linked to the low density of the SSTAARS input data over platforms 2 and 5. Similar to the CCI_A climatology, the lower R values are mostly caused by fewer valid tropical IMOS AVHRR L3S SST values input into SSTAARS during the monsoon months. Comparisons with other platforms show biases close to the mean value and reasonable R values.

The BRAN_A climatology (Table 6-4) has a mean cold bias of -0.03°C with STD of 0.07°C and correlation coefficient of 0.93. It has the best performance, which is mainly due to the BRAN_2016 analysis ingesting all available TAO/TRITON mooring temperature data (Oke et al., 2013)

6.1.2.4 CONCLUSIONS

Based on the statistical analysis and in-situ validation, the SST CCI analysis v2.0 daily climatology (CCI_A) and SSTAARS have the best general agreement, especially over similar time periods, with the SST climatology from BRAN_2016 being warm over the west and south and the CRW climatology generally cold. There are a few spatially local areas where disagreement is more pronounced, and for CCI_1992 minus SSTAARS, this includes a region near the north-east of the domain as well as a region off the coast of eastern Australia. The largest and most pronounced region of difference, in the north-east, is corroborated by the TAO/TRITON array SST observations which points to a discrepancy in favour of CCI_A. However, the fact that the same artefact appears in CCI_A minus CRW indicates further investigation is required. BRAN_A being strongly influenced by the TAO/TRITON buoy measurements means it may not provide much light on this situation. CCI_A displays much closer agreement with the climatology formed from the TAO/TRITON mooring SSTs than does SSTAARS.

This regional inter-comparison study of high-resolution SST climatology data sets indicates that a 5 km daily 1981 – 2016 climatology formed from the SST CCI analysis v2.0 would be suitable for use as a high-resolution reference for Marine Heat Wave studies over the Australian region. However, for smaller spatial scales or where a night-only SST climatology is required, the 2 km daily 1992 – 2016 SSTAARS would also be

suitable, noting that the feature resolution of the optimally interpolated SST CCI analysis v2.0 will be significantly coarser than that of the 2 km composite-based SSTAARS climatology.

6.1.2.5 REFERENCES

Wijffels, Susan E., Helen Beggs, Christopher Griffin, John F. Middleton, Madeleine Cahill, Edward King, Emlyn Jones, Ming Feng, Jessica A. Benthuyssen, Craig R. Steinberg and Phil Sutton (2018). A fine spatial scale sea surface temperature atlas of the Australian regional seas (SSTAARS): seasonal variability and trends around Australasia and New Zealand revisited, *J. Marine Systems*, 187, 156-196.

<https://doi.org/10.1016/j.jmarsys.2018.07.005>

Maturi, E., Harris, A., Mittaz, J., Sapper, J., Wick, G., Zhu, X., . . . Koner, P. (2017). A New High-Resolution Sea Surface Temperature Blended Analysis. *Bulletin of the American Meteorological Society*, 98(5), 1015-1026. doi:10.1175/bams-d-15-00002.1

Oke, P., Sakov, P., Cahill, M. L., Dunn, J. R., Fiedler, R., Griffin, D. A., et al. (2013). Towards a dynamically balanced eddy-resolving reanalysis: BRAN3. *Ocean Modelling*, 67, 52–70. <https://doi.org/10.1016/j.ocemod.2013.03.008>

McPhaden, M.J., A.J. Busalacchi, R. Cheney, J.R. Donguy, K.S. Gage, D. Halpern, M. Ji, P. Julian, G. Meyers, G.T. Mitchum, P.P. Niiler, J. Picaut, R.W. Reynolds, N. Smith, K. Takeuchi (1998). The Tropical Ocean-Global Atmosphere (TOGA) observing system: A decade of progress. *J. Geophysical Research*, 103(14), 169-240.

6.1.3 FEEDBACK ON SCIENTIFIC UTILITY OF THE SST CCI PRODUCTS

- The SST CCI analysis v2.0 data provided a relatively flexible and accurate reference for the climatology comparison study.
- The long reference period of SST CCI analysis v2.0 data provides a convincing SST climatology through this study.
- The SST climatology datasets derived from SST CCI analysis v2.0 data are highly consistent with the in-situ day and night tropical mooring measurements.
- Producing a night-only SST CCI analysis v2.0 would enable it to be used for applications that require a consistent night-time SST, such as coral bleaching studies, and allow for more accurate comparisons with other night-only or foundation SST analyses.

6.2 Using gridded sea surface temperature products to estimate the temperature experienced by tropical corals: Implications for coral reef monitoring

Georgios Margaritis

University of Southampton

6.2.1 KEY MESSAGES

- Provided a longer time span of data than ESA SST CCI analysis v1.0 enabling the inclusion of more sites and *in situ* data in the study
- ESA SST CCI analysis v2.0 and the NOAA CoralTemp gridded SST products both provide a good representation of daily subsurface temperatures, by comparison to near-coral logger temperature data at depths 3 – 6 m.
- Differences in trends exist between the products that will lead to different estimates of coral stress due to changing temperatures.

6.2.2 SCIENTIFIC ANALYSIS

6.2.2.1 AIMS OF THE STUDY

This study constitutes the first chapter of my PhD project, and is entitled: 'Using gridded sea surface temperature products to estimate the temperature experienced by tropical corals: Implications for coral reef monitoring.' The study aims to:

- Investigate the relationship between *in situ* water temperature measured close to coral reefs and gridded Sea Surface Temperature (SST) products from satellites.
- Quantify the uncertainty of inferring the temperature experienced by the corals in tropical coral reefs, using various gridded SST products.
- Investigate the ability of the SST product used by NOAA Coral Reef Watch to monitor coral reefs, and predict coral bleaching events; and compare it to the new ESA SST CCI Analysis version 2.

6.2.2.2 METHOD

6.2.2.2.1 In situ data

Logger temperature data were collected from two regions, Belize and Florida Keys, and a total of seven sites. Loggers in Belize were installed by collaborators from the University of North Carolina at Chapel Hill. Full description of the installation process is available in Castillo and Lima (2010). *In situ* data in Florida Keys were provided by the U.S. Geological Survey Coral Reef Ecosystems Studies project. A more detailed description is available at Kuffner et al. (2013).

Belize

HOBO Water Temperature Pro Data Loggers (accuracy $\pm 0.2^{\circ}\text{C}$ and resolution 0.2°C) were installed between 3 and 5 m depth at East Snake Caye (16.193, -88.627) within the inner lagoon reef (inshore), and at White Reef (16.083, -88.333) on the outer barrier reef (offshore) (Figure 6-7). They recorded temperatures at 10, 15 or 30-min intervals from June 2002 to December 2007 (Castillo and Lima, 2010).

Florida Keys

Subsurface temperature data were also collected at five off-shore coral reefs along the length of the Florida Keys. From northeast to southwest the sites are: Fowey Rocks, Molasses Reef, Crocker Reef, Sombrero Reef, and Pulaski Shoal (Figure 6-8). Temperatures were recorded from 2009 to 2017 with Onset HOBO Water Temp Pro V2 data loggers, placed at depths 4 to 6 m (Kuffner et al., 2013).

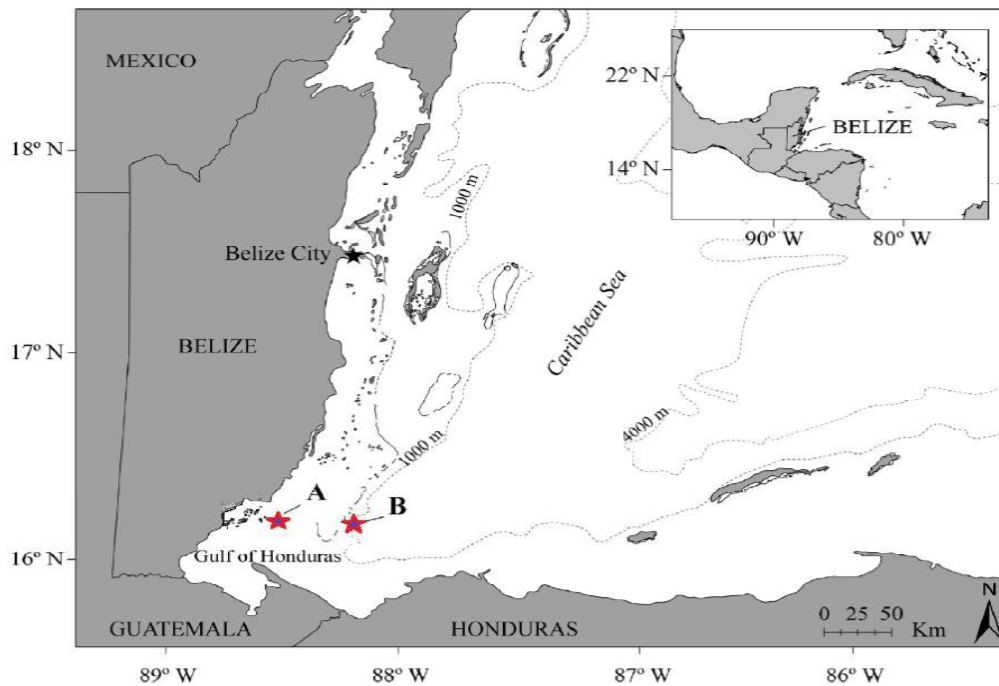


Figure 6-7. Map showing the locations where loggers were installed for in situ measurements at the mesoamerican barrier reef off Belize. (A) Port Honduras Marine Reserve, inshore, and (B) Sapodilla Cayes Marine Reserve, offshore. Adapted from (Castillo and Lima, 2010).

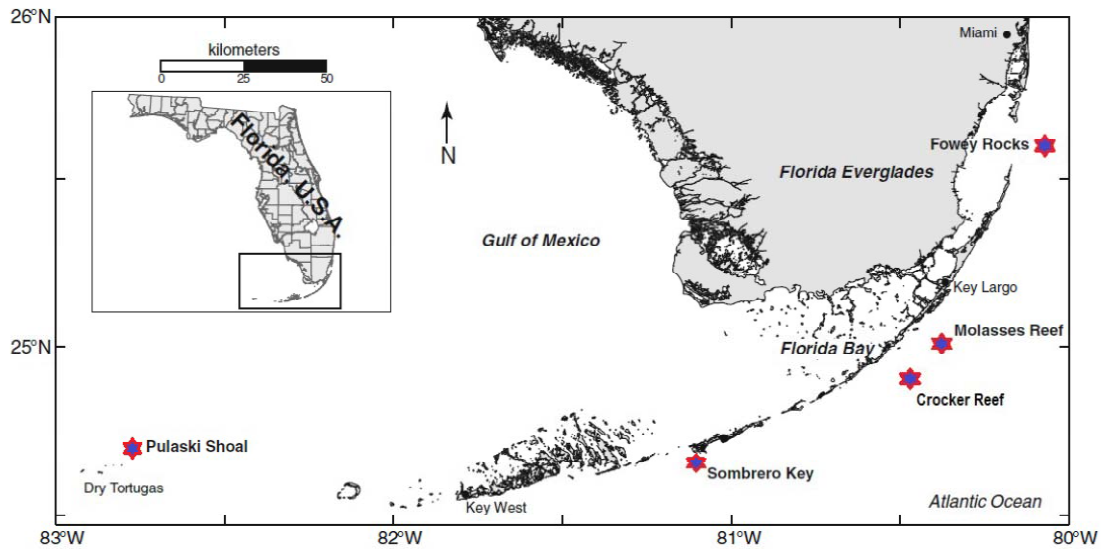


Figure 6-8. Map of the Florida Keys, USA, showing the five locations where loggers were installed (red stars). Site names used are those of the adjacent National Data Buoy Center stations: Fowey Rocks (Fowey), Molasses Reef (Molasses), Crocker reef (Crocker), Sombrero Key (Sombrero) and Pulaski Shoal (Pulaski). Adapted from (Kuffner et al., 2013).

Table 6-5. *In situ* data temporal span and exact locations for all seven sites used in this study.

Site	Fowey	Molasses	Sombrero	Crocker	Pulaski	Belize inshore	Belize offshore
Start	Aug-09	Apr-09	Jul-09	Jun-13	Jun-09	Jun-02	Jun-02
Finish	Oct-17	Apr-13	Nov-17	Nov-17	Nov-17	Dec-07	Dec-07
Latitude	25.590°N	25.010°N	24.627°N	24.909°N	24.694°N	16.193°N	16.083°N
Longitude	80.096°W	80.375°W	81.109°W	80.527°W	82.773°W	88.627°W	88.333°W

6.2.2.2.2 Gridded SST products

Level 4 data from four daily gridded SST products were acquired and compared. Two of the products were then also compared with *in situ* observations from the loggers at the 7 different sites. The products used were:

- NOAA Coral Reef Watch Version 1.0 Daily Global 5-km Satellite Virtual Station Time Series Data (CoralTemp) (Maturi et al., 2017)⁵
- ESA SST CCI Analysis product version 2.0

⁵ Downloaded on 11 Jan 2019 from <ftp://ftp.star.nesdis.noaa.gov/pub/sod/mech/crw/data/coraltemp/v1.0/nc>

Satellite-only SST-depth analysis created by OSTIA system from SST CCI ATSR and SST CCI AVHRR products, 0.05 degrees resolution, daily files covering 1981 – 2016.

- NOAA High Resolution SST, daily, 0.25° spatial resolution SST analysis (Banzon et al., 2016, NOAA High Resolution SST data provided by the NOAA/OAR/ESRL PSD, Boulder, Colorado, USA, from their Web site at <https://www.esrl.noaa.gov/psd/>)
- ESA SST CCI Analysis product version 1, daily, 0.05° spatial resolution, estimated at a depth of 20 cm (Merchant et al., 2014).

6.2.2.2.3 Statistical analysis methodology

Statistical analysis was carried out to investigate the mean differences between gridded SST observations and *in situ* measurements at different temporal and spatial scales.

The U.S. National Oceanic and Atmospheric Administration's Coral Reef Watch (NOAA CRW) program has developed coral-specific satellite-based tools to monitor thermal stress causing bleaching events around the world (Liu et al., 2006). Coral Bleaching Hot Spots product is one of these tools and is used to identify sites where temperatures are abnormally high for the area. It is an anomaly product based on the climatological mean SST of the hottest month for the site, or maximum monthly mean (MMM). A Hot Spot has been defined as an area where daily SST exceeds the monthly climatology temperature of the warmest month of the year for the region, by 1 °C or more (Liu et al., 2014).

The logger time series are fairly short (

Table 6-5), so we must rely on gridded products to provide longer time series to indicate how much warming the corals have experienced. These products need therefore to provide accurate information on both decadal and daily timescales. The eventual aim is to examine the ability of the satellite SST product used by NOAA CRW to predict coral bleaching events, and compare its estimates using SST CCI analysis v2.0.

6.2.2.3 RESULTS

September 2003 was identified as a month when coral at the Belize inshore site was likely to have experienced anomalously warm conditions likely to have triggered a hotspot alert. Monthly mean regional SST is shown in Figure 6-9 for each of the 4 SST data products.

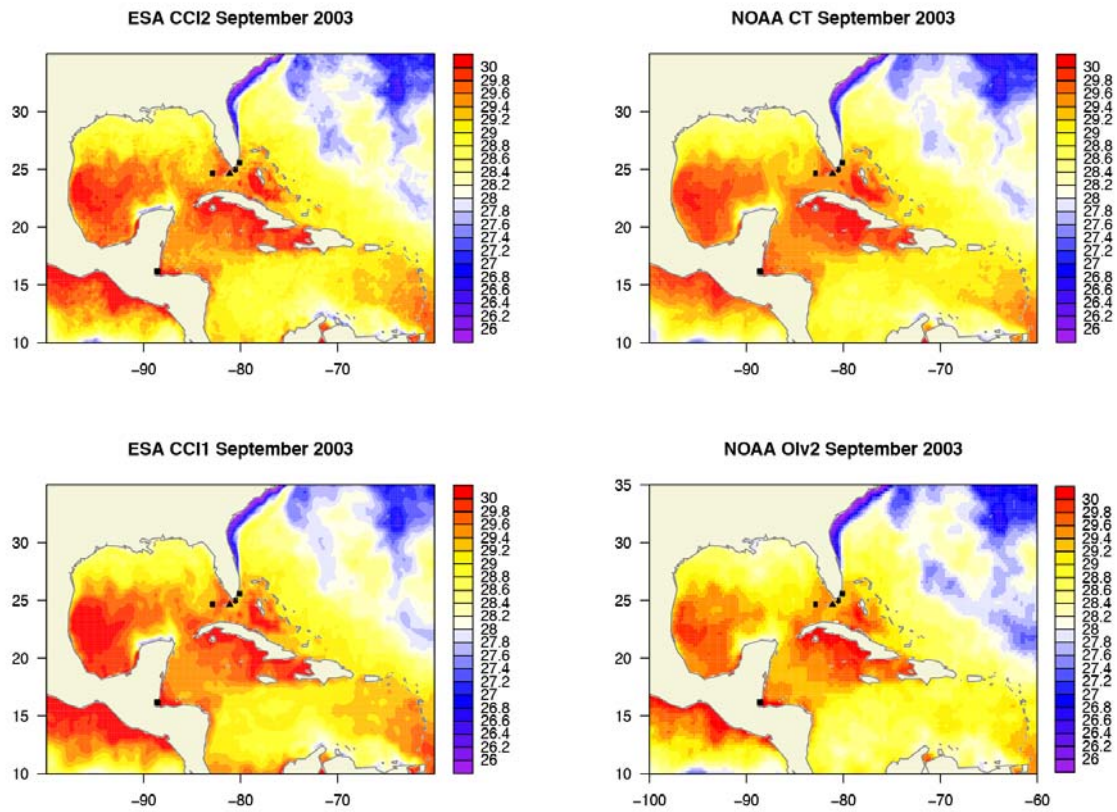


Figure 6-9. Monthly mean SST (°C) for September 2003 for each of 4 satellite-derived gridded data products. Top left - SST CCI analysis v2.0; top right - NOAA Coral Temp; lower left - SST CCI analysis v1.0; lower right - NOAA High Resolution SST.

The lower spatial resolution of the NOAA High Resolution SST product (0.25°, lower right) compared to the other products (0.05°) is clear. SST CCI analysis v2.0 shows finer resolution detail than the other high spatial resolution products, and that detail appears to be physically reasonable. Anomalies (relative to 1992 to 2010 monthly means) are shown in Figure 6-10. This suggests that the elevated temperatures seen at the Belize site are not particularly widespread.

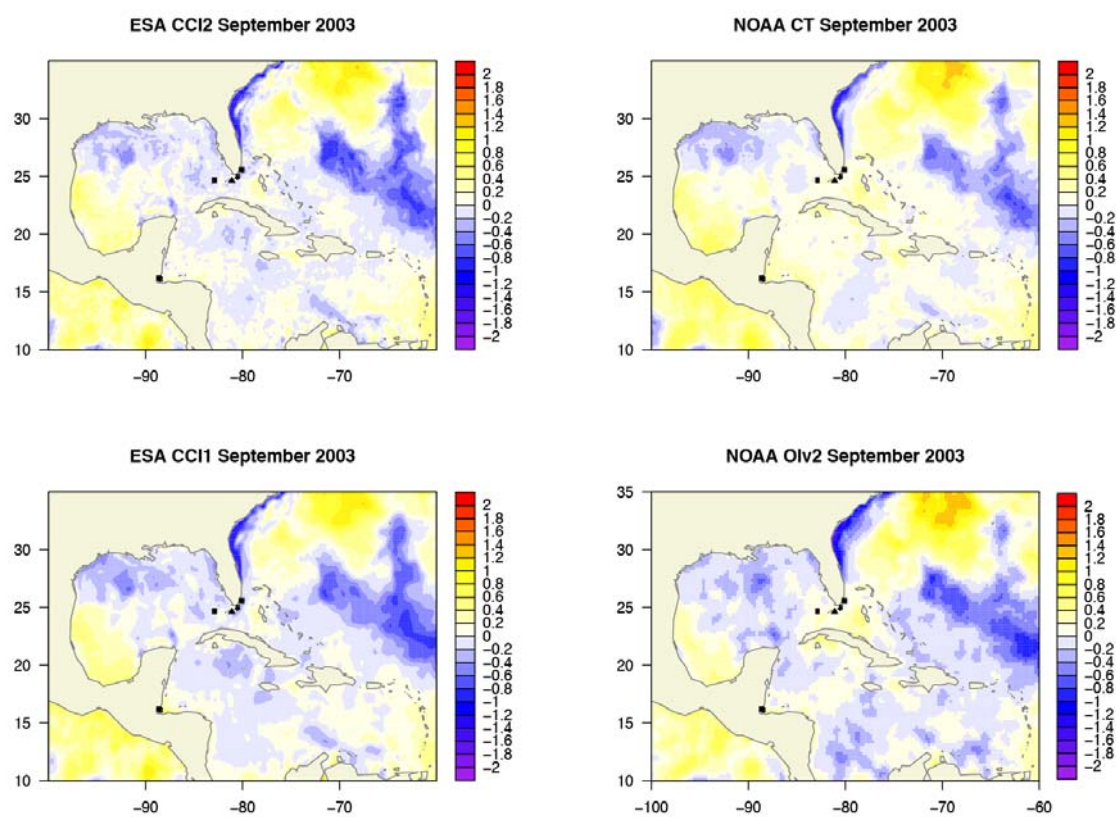


Figure 6-10. Monthly mean SST anomaly relative to 1992-2010 ($^{\circ}\text{C}$) for September 2003 for each of 4 satellite-derived gridded data products. Top left - - SST CCI analysis v2.0; top right - NOAA Coral Temp; lower left -SST CCI analysis v1.0; lower right - NOAA High Resolution SST.

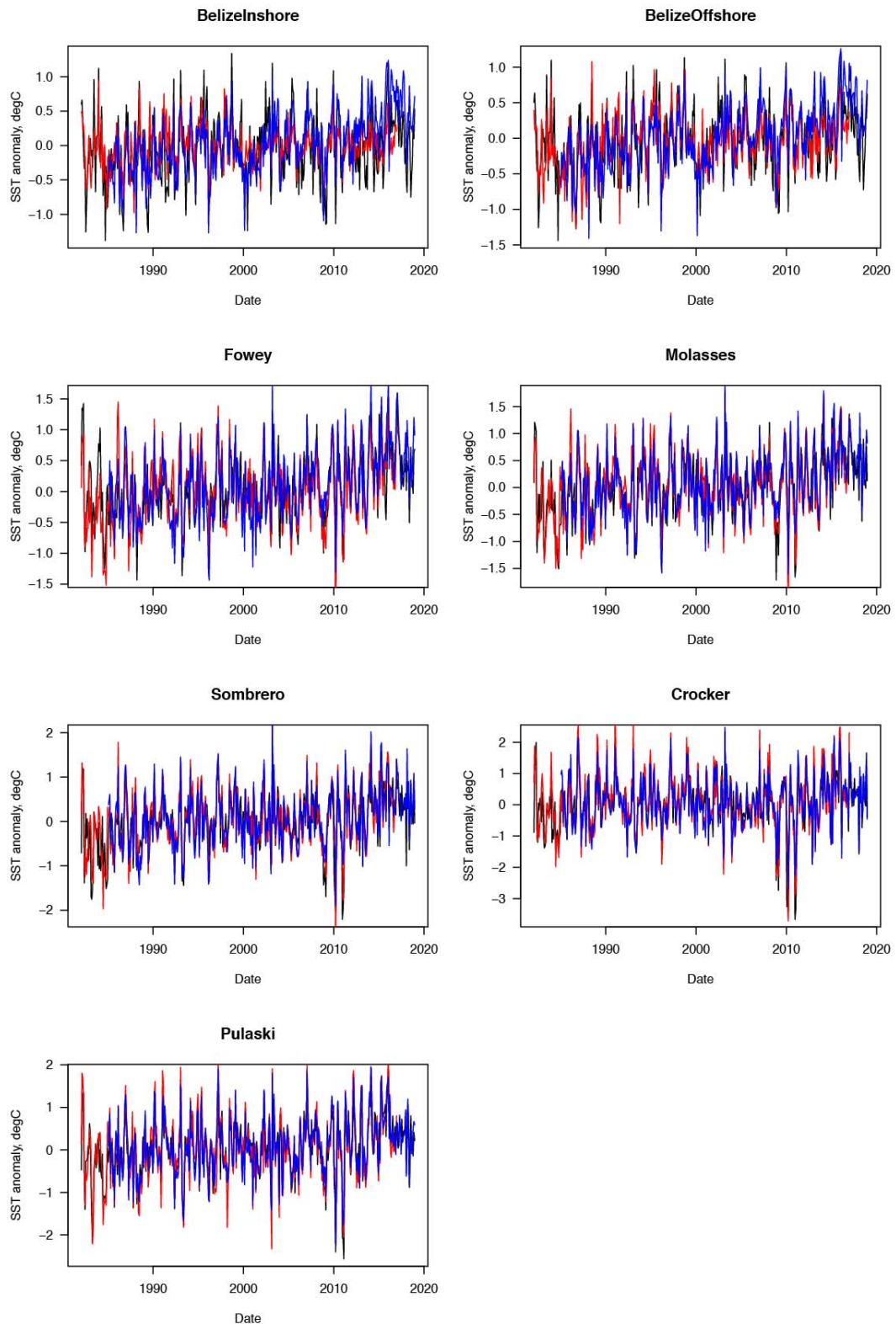


Figure 6-11. Monthly mean SST anomalies (relative to monthly means for 1992-2010) for NOAA High Resolution SST (black); SST CCI v2.0 (red) and NOAA CoralTemp (blue) for each of the 7 sites (as subplot labels)

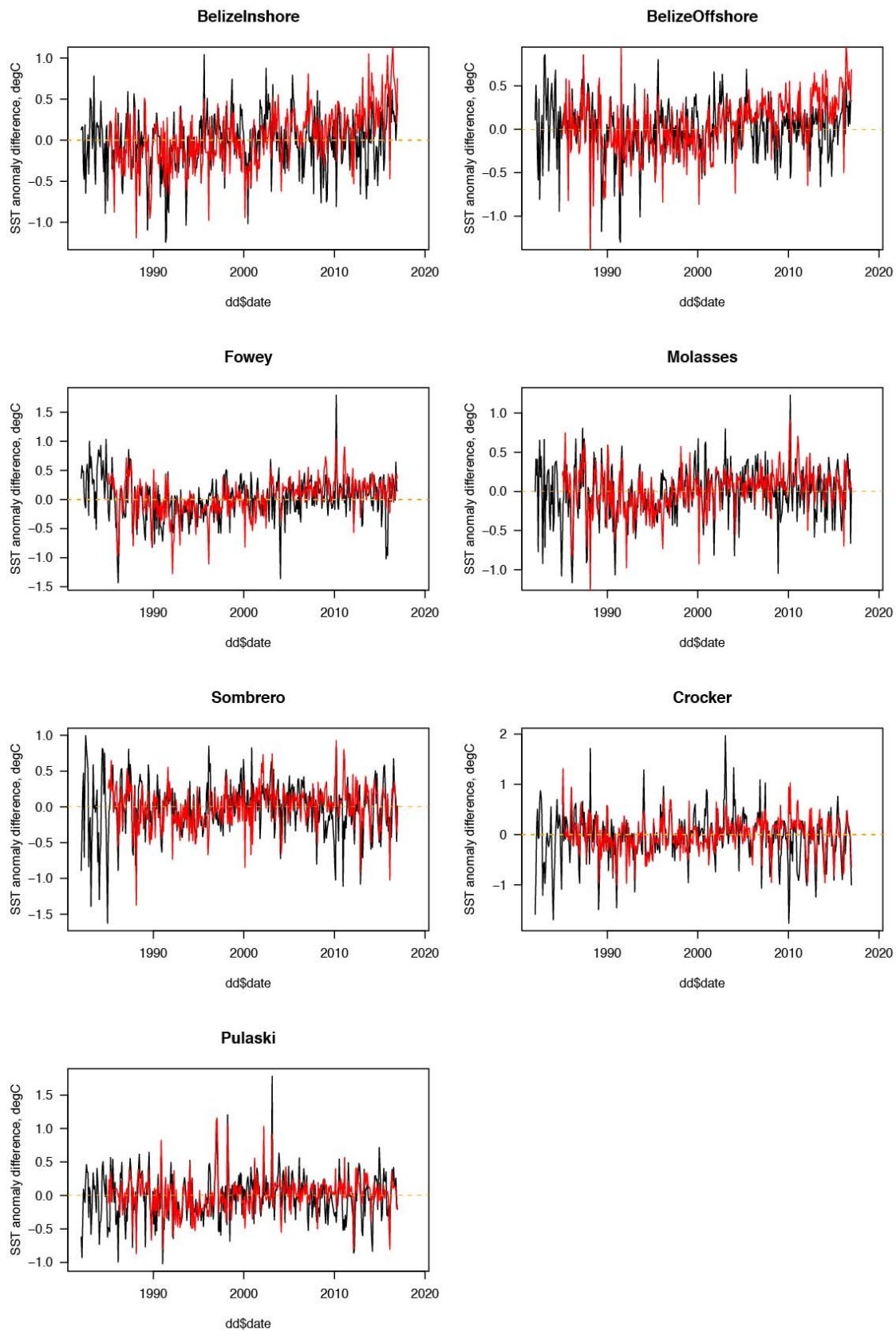


Figure 6-12. As Figure 6-11 but for differences of NOAA High Resolution SST (black) and NOAA CoralTemp (red) from SST CCI v2.0.

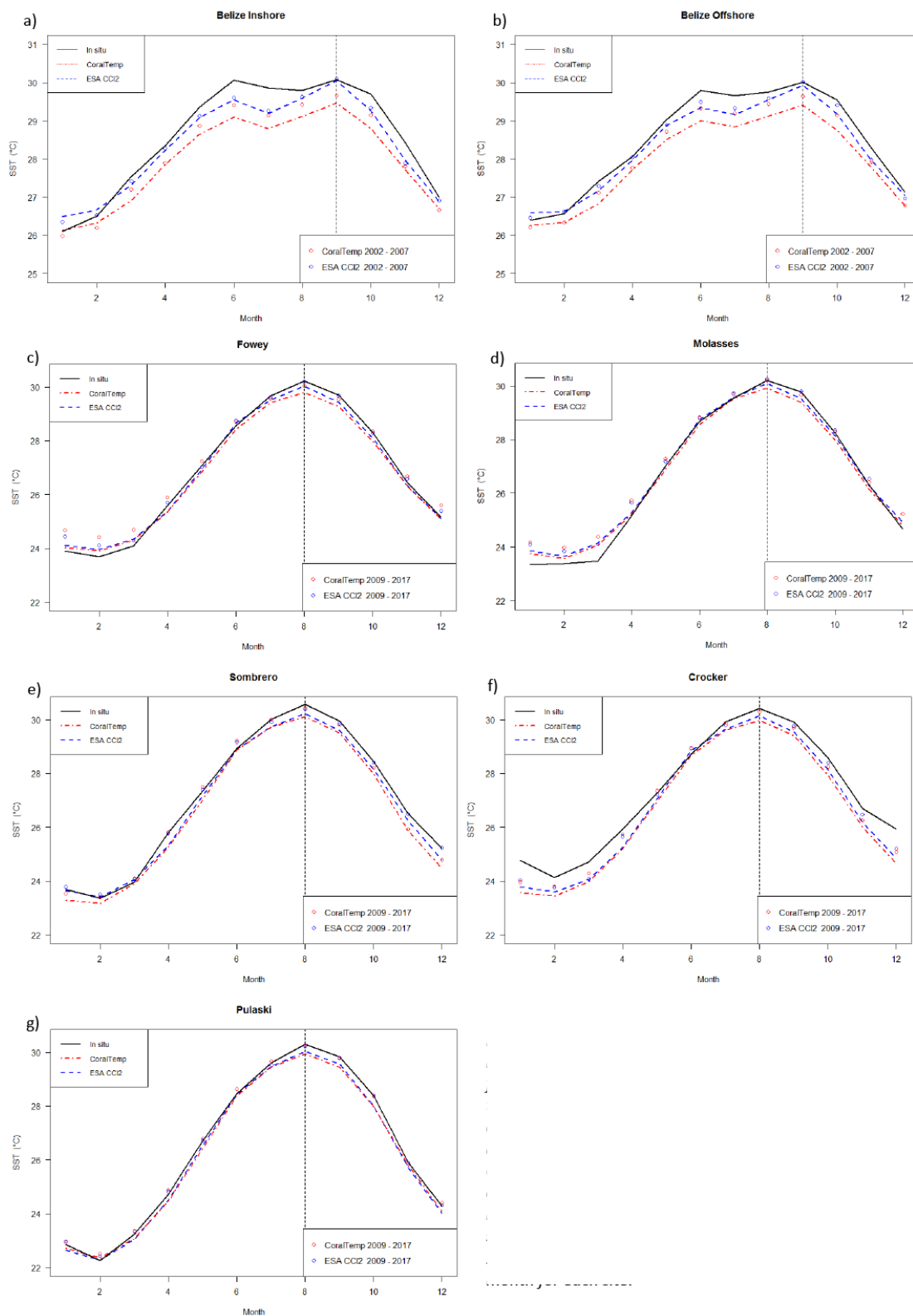


Figure 6-13. Mean monthly temperatures (annual cycle, °C) for the Belize region as measured by in situ and gridded SST products for the a) inshore and b) offshore site. c)-g) mean monthly temperatures for all 5 sites in the Florida region. Climatologies were calculated for the full common period of available satellite data (1985-2015). Points show reduced climatologies derived from the periods when in

situ data were available (2002-2007 Belize and 2009-2017 Florida Keys). Vertical lines indicate the hottest month for each site.

Figure 6-12 shows that there are some differences between the satellite temperatures at all scales. Particularly at the Belize sites there is a trend difference between the SST CCI v2.0 and the NOAA products. At Crocker in particular there are variations in annual cycle. There also periods at all sites (not shown) where there are common differences across all the products suggesting that surface conditions as seen by the satellites are not representative of subsurface conditions.

Figure 6-13 shows that the satellite products mostly show similar seasonal variations to the logger data. Where there are differences, the satellite may underestimate (e.g. Molasses) or overestimate (e.g. Crocker) seen in the logger data.

Table 6-6. Standard deviations of anomaly differences (product - logger, °C) for each of the logger sites.

	NOAA CoralTemp	SST CCI v2.0	Number of days
Belize Inshore	0.38	0.46	1603
Belize Offshore	0.33	0.38	3086
Fowey	0.55	0.52	1350
Molasses	0.50	0.48	1599
Sombrero	0.59	0.53	2996
Crocker	0.42	0.43	1467
Pulaski	0.35	0.38	3027

6.2.2.4 CONCLUSIONS

There are differences in trend between the SST CCI analysis v2.0 and the NOAA CoralTemp product that are large enough to be important for the prediction of the stress experienced by corals, particularly for the locations near Belize. Both products show similar scatter at the daily scale compared with logger temperatures.

6.2.3 FEEDBACK ON SCIENTIFIC UTILITY OF THE SST CCI PRODUCTS

SST CCI analysis v2.0 compare well with the *in situ* observations at the locations considered. We will therefore further investigate its suitability for monitoring coral reefs and predicting bleaching events.

Although the temporal span (1991–2010) of ESA SST CCI analysis 1.0 was incompatible with the logger data from Florida (2009 – 2017), the new SST CCI analysis v2.0 extended the available data enabling our comparison to include the 5 sites in Florida.

6.2.4 REFERENCES

- BANZON, V., SMITH, T. M., CHIN, T. M., LIU, C. & HANKINS, W. 2016. A long-term record of blended satellite and in situ sea-surface temperature for climate monitoring, modeling and environmental studies. *Earth System Science Data*, 8, 165.
- CASTILLO, K. D. & LIMA, F. P. 2010. Comparison of in situ and satellite-derived (MODIS-Aqua/Terra) methods for assessing temperatures on coral reefs. *Limnology and Oceanography: Methods*, 8, 107-117.
- KUFFNER, I., HICKEY, T. & MORRISON, J. 2013. Calcification rates of the massive coral *Siderastrea siderea* and crustose coralline algae along the Florida Keys (USA) outer-reef tract. *Coral Reefs*, 32, 987-997.
- LIU, G., HERON, S. F., EAKIN, C. M., MULLER-KARGER, F. E., VEGA-RODRIGUEZ, M., GUILD, L. S., DE LA COUR, J. L., GEIGER, E. F., SKIRVING, W. J. & BURGESS, T. F. 2014. Reef-scale thermal stress monitoring of coral ecosystems: new 5-km global products from NOAA Coral Reef Watch. *Remote Sensing*, 6, 11579-11606.
- LIU, G., STRONG, A. E., SKIRVING, W. & ARZAYUS, L. F. Overview of NOAA coral reef watch program's near-real time satellite global coral bleaching monitoring activities. *Proc 10th Int Coral Reef Symp*, 2006. 1783-1793.
- MATURI, E., HARRIS, A., MITTAZ, J., SAPPER, J., WICK, G., ZHU, X., DASH, P. & KONER, P. 2017. A New High-Resolution Sea Surface Temperature Blended Analysis. *Bulletin of the American Meteorological Society*, 98, 1015-1026.
- MERCHANT, C. J., EMBURY, O., ROBERTS-JONES, J., FIEDLER, E., BULGIN, C. E., CORLETT, G. K., GOOD, S., MCLAREN, A., RAYNER, N. & MORAK-BOZZO, S. 2014. Sea surface temperature datasets for climate applications from Phase 1 of the European Space Agency Climate Change Initiative (SST CCI). *Geoscience Data Journal*, 1, 179-191.

6.3 Regional ocean reanalysis for the North-West European Shelf Seas

Richard Renshaw

Met Office

6.3.1 KEY MESSAGES

- Reprocessed SSTs are a key data source for our regional ocean reanalysis. Our requirement is for SST observations with small bias, good coverage, and with consistent processing (no jumps) over a long period.
- To date, we have used the ESA CCI L2P ESA SST CCI ATSR and AVHRR products version CDR2.0 for 2011-2017

6.3.2 SCIENTIFIC ANALYSIS

6.3.2.1 AIMS OF THE STUDY

We produce a regional ocean reanalysis for the North-West European Shelf Seas, funded by CMEMS. The aim is to produce a record of ocean fields from 1993 to the present day that is comprehensive, physically coherent, and homogeneous in time.

6.3.2.2 METHOD

The reanalysis combines model and observations in a statistically optimal way. CCI SST data provides the bulk of the observations that we assimilate.

6.3.2.3 RESULTS

We assess the quality of the reanalysis by evaluating it against observations, to produce a CMEMS QuID (Quality Information Document). These are available on the CMEMS website <http://marine.copernicus.eu/>

Compared against *in situ* profile observations, reanalysis temperature biases are generally smaller than $\pm 0.5^{\circ}\text{C}$ at all depths over the North West Shelf. Correlations between V4 and mooring data are generally greater than 0.98, with V4 representing well the annual temperature cycle. Figure 6-14 shows mean and RMS difference against *in situ* observations from the World Ocean Database 2013 for the current (v4) and previous (v2) reanalyses.

V2 assimilated just SST observations (*in situ* and ESA CCI SST). V4 also assimilated *in situ* profile. For 2011 onwards, V4 differs from V2 in that it used the second release of the ESA CCI SST dataset.

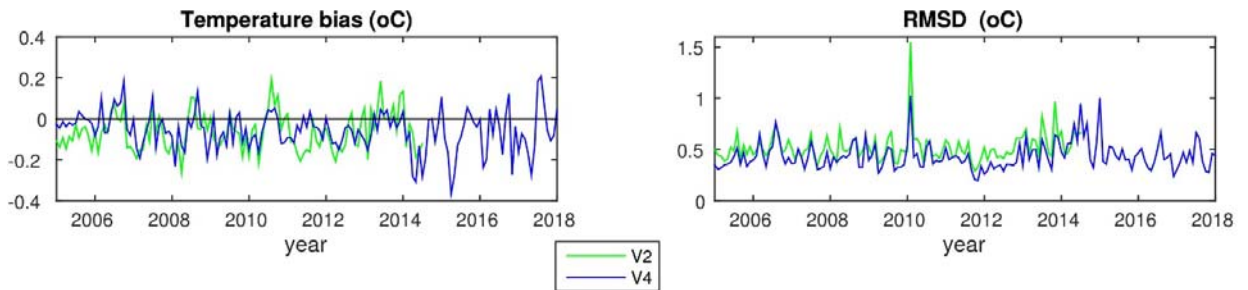


Figure 6-14. Time-series of near-surface (0-5m depth) temperature, Reanalysis minus WOD13 observations. Green is previous reanalysis (v2), blue is latest reanalysis (v4).

6.3.2.4 CONCLUSIONS

We don't assess the quality of the CCI SST product directly, but the quality of the reanalysis overall is an indicator of the quality of its inputs.

6.3.3 FEEDBACK ON SCIENTIFIC UTILITY OF THE SST CCI PRODUCTS

The SST CCI product is the major source of observation data in this reanalysis. It ensures that the reanalysis sea surface temperature is realistic and coherent geographically and through time. Well-constrained temperatures at the surface influence the full 3D ocean dynamics and so also contribute to the accuracy of the reanalysis at depth.

6.4 Feedback from the ESA SST CCI v2.0 product over the Eastern Atlantic

Luísa Lamas¹ (luisa.lamas@hidrografico.pt)

Rita Esteves¹ Sara Almeida¹

Eduardo de Azevedo² Cecília Correia³ Francisco Reis⁴

1. Instituto Hidrográfico, Rua das Trinas 49 1249-093 Lisboa, Portugal, luisa.lamas@hidrografico.pt
2. Universidade dos Açores, DCA - Centro do Clima, Meteorologia e mudanças Globais, Rua Capitão João D'Ávila, Pico da Urze, 9700-042, Angra do Heroísmo, Portugal, eduardo.mv.azevedo@uac.pt
3. Administração dos Portos da Região Autónoma da Madeira, S.A., Gare Marítima do Porto do Funchal, 9004-518 Funchal, Portugal, ceciliacorreia@apram.pt
4. Observatory for the Environment of the Azores, Rua Gaspar Corte Real, Freguesia da Sé, 9700-033, Angra do Heroísmo

6.4.1 KEY MESSAGES

- ESA SST CCI analysis product provides a spatial and temporal coverage of the sea surface temperature field that is essential for climate studies over the Eastern Atlantic where in-situ data is sparse and insufficient.
- ESA SST CCI analysis product was accurate within 0.3 to 0.4°C for the oceanic (offshore) buoys and 0.3 to 0.8°C for the coastal buoys.
- The temporal and spatial resolution of the ESA SST CCI analysis product are sufficient for open ocean studies, but with finer spatial resolution the data could be extended to coastal and shelf areas. A spatial resolution of 1 km could considerably improve the results in shallower areas (less than 100m depth).
- Inter-annual, seasonal and spatial variability still needs to be further analysed.

6.4.2 SCIENTIFIC ANALYSIS

6.4.2.1 AIMS OF THE STUDY

Sea surface temperature is a key parameter that influences many environmental processes, including ocean dynamics, biology and climate. Thermal gradients at the upper ocean are directly relatable with the heat budget between the ocean and atmosphere which has a crucial role in the global climate. The accurate knowledge of SST regarding not only its variability, but its short- and long-time trends is imperative to understand the ocean's role on a changing climate. Good assessment of the SST across the Atlantic is essential to understand the ocean's contribution to climate change and will contribute for the effectiveness of protective and preventive initiatives and political decisions.

Although sea surface temperature data is one of the oldest available datasets, mainly from research ships, drifting and moored buoys, they represent sparse and sporadic data points. Satellite observations, however, can provide a continuous and global coverage of the ocean surface temperature, but still need to be calibrated and validated against in situ data.

Here, the European Space Agency's Sea Surface Temperature Climate Change Initiative (ESA SST CCI) Analysis Product Version 2.0 (hereinafter **ESA SST CCI analysis v2.0**) is compared against in-situ SST data collected by 14 moored buoys located in the eastern Atlantic. The main objective of this study is to validate **ESA SST CCI analysis v2.0** data and assess the product's utility for ocean and climate studies over the Portuguese marine waters, and in particular for shallower waters, where some of the coastal buoys are moored.

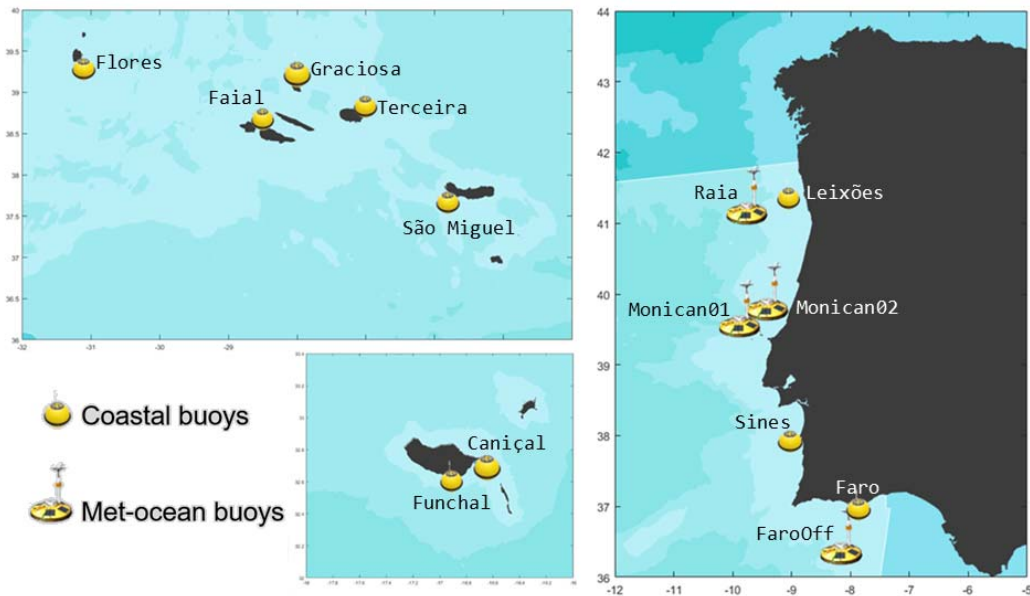


Figure 6-15. Portuguese marine waters showing the 14 coastal and oceanic mooring buoys. Top left : Azores; bottom left: Madeira; right: Portugal mainland

6.4.2.2 METHODS

The **ESA SST CCI analysis v2.0** used in this study consists of daily files, covering the period between 1981 and 2016, of satellite-only SST-depth analysis created by OSTIA system from SST CCI ATSR and SST CCI AVHRR products at 0.05° resolution.

Daily values of SST from the **ESA ST CCI analysis v2.0** were compared against in-situ data acquired by 14 coastal buoys operated by the Hydrographic Institute (IHPT), the University of Azores (UA) and Observatory for the Environment of the Azores (OAA) and the Ports Administration of the Madeira Autonomous Region (*Administração dos Portos da Região Autónoma da Madeira – APRAM*) providing a significant coverage across the eastern Atlantic, in an area of relatively scarce in situ data (**Figure 6-15**).



Figure 6-16. Oceanographic Datawell Waverider (left) and Meteo-oceanographic Oceanor Wavescan (right) buoys (photo © Instituto Hidrográfico).

There are currently two types of buoys - Meteo-oceanographic Oceanor Wavescan and Datawell Waverider. Both types are equipped with a trans-receiver GPS (Global Positioning System). The Wavescan buoys, equipped with Aanderaa 4050 temperature sensors, measure SST at approximately 1 m depth and ensure real-time access to the data through their INMARSAT-C satellite link communication system. The Waveriders are equipped with internal temperature sensors located at 0.7 m depth and have a HF link communication system installed (**Figure 6-16**). Information about the name, location, depth and start date of collecting temperature data is shown in Table 6-7.

The Datawell Waverider SST data were acquired at a sample rate of 30 minutes, whereas the Oceanor Wavescan data were acquired at a sample rate of 1 hour. Upon reception, data follow a validation procedure at the contributing institutions, the IHPT, the UAC and the APRAM, process after which data are loaded into transactional local databases.

In-situ data were daily averaged to compare with the daily datasets of **ESA SST CCI analysis v2.0**. Then, **ESA SST CCI analysis v2.0** data points were extracted at each buoy location using the nearest neighbour. Future work will include a spatial analysis using the surrounding pixels (3x3) to analyse the uncertainties associated with point-to-pixel match-up and sensitivity of the results for different match-up techniques.

Results will be discussed using determination coefficients (R^2) and root mean square error (RMSE), to assess the differences between both datasets. Results from the years between 2010 and 2016, with sporadic gaps of in situ data, are shown and discussed in the next section.

Table 6-7. Position, depth, type and start date of SST measurements for each buoy. Shaded colours were added to mark different locations: red: Coastal Portugal (PT) mainland; green: Oceanic PT; blue: Coastal Madeira; orange: Coastal Azores.

Station Name	Position (WGS 84)	Depth (m)	Buoy Type	Start Date
--------------	-------------------	-----------	-----------	------------

Leixões	41°19.00'N 08°59.00'W	83	Waverider	1998
Sines	37°55.27'N 08°55.73'W	97	Waverider	1988
Faro	36°54.28'N 07°53.90'W	93	Waverider	1986
Raia	41°08.92'N 09°34.90'W	1622	Wavescan	2010
Monican01	39°30.94'N 09°38.24'W	1850	Wavescan	2009
Monican02	39°33.61' N 09°12.60' W	80	Wavescan	2010
FaroOff	36°23.90'N 08°04.10'W	1334	Wavescan	2014
Funchal	32°37.1'N 16°56.5'W	100	Waverider	1996
Canical	32°43.2'N 16°43.7'W	100	Waverider	2002
Terceira	38° 45.04'N 27° 00.60'W	100	Waverider	2005
São Miguel	37° 43.89'N 25° 43.46'W	90	Waverider	2005
Flores	39° 21.86'N 31° 10.00'W	80	Waverider	2006
Faial	38° 35.26'N 28° 32.26'W	110	Waverider	2007
Graciosa	38° 05.21'N 27° 57.73'W	97	Waverider	2007

6.4.2.3 RESULTS

In general, the **ESA SST CCI analysis v2.0** represents well the variability and magnitude of the sea surface temperature measured at each buoy location, for both coastal and oceanic, located along Portugal mainland, Azores and Madeira islands (**Figure 6-17** through **Figure 6-20** showing the analysis for 4 different buoys, one representing each location).

Determination coefficients, which quantify the relation between both datasets in terms of variability, were higher than 0.95 for all the buoy locations, with lower values for Coastal PT buoys and higher values for Azores and Oceanic PT buoys.

Generally, the **ESA SST CCI analysis v2.0** seems to overestimate the temperature for most buoy locations. Differences between both datasets rarely exceeded 0.5°C, with generally higher RMSE during summer months (April to October), however, further analysis needs to be performed to assess the seasonal variability of the **ESA SST CCI analysis v2.0**.

ESA SST CCI analysis v2.0 data at the location of Azores buoys showed both the highest and lowest deviations, with Graciosa and Flores showing lowest RMSE values, 0.30 and 0.36°C respectively, and Terceira and Faial the highest RMSE, 0.76 and 0.66°C, respectively. The R^2 , however, was high for all of the buoys. At the oceanic PT buoys location, the RMSE between both datasets was smaller than 0.34°C and at the coastal PT buoys location, the R^2 was the lowest (Figures 6-21 through 6-24). These results suggest that **ESA SST CCI analysis v2.0** is more accurate for the open ocean.

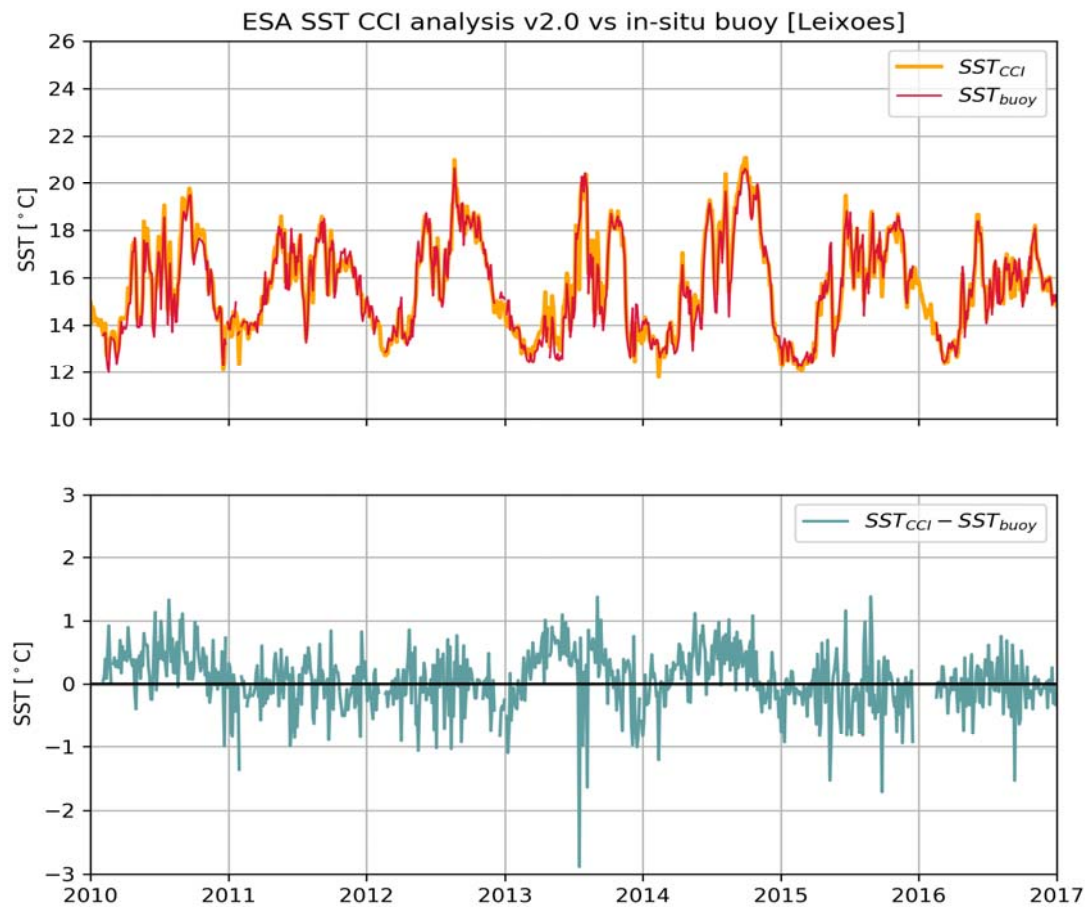


Figure 6-17. Top: Sea surface temperature from ESA SST CCI analysis v.2 at the location of Leixões (Coastal Portugal Mainland) buoy against Leixões buoy data from 01.01.2010 until 31.12.2016 at 3-day intervals. Bottom: Difference between ESA SST CCI analysis v.2 (SST_{CCI}) at the location of Leixões buoy and SST data from the Leixões buoy (SST_{buoy}).

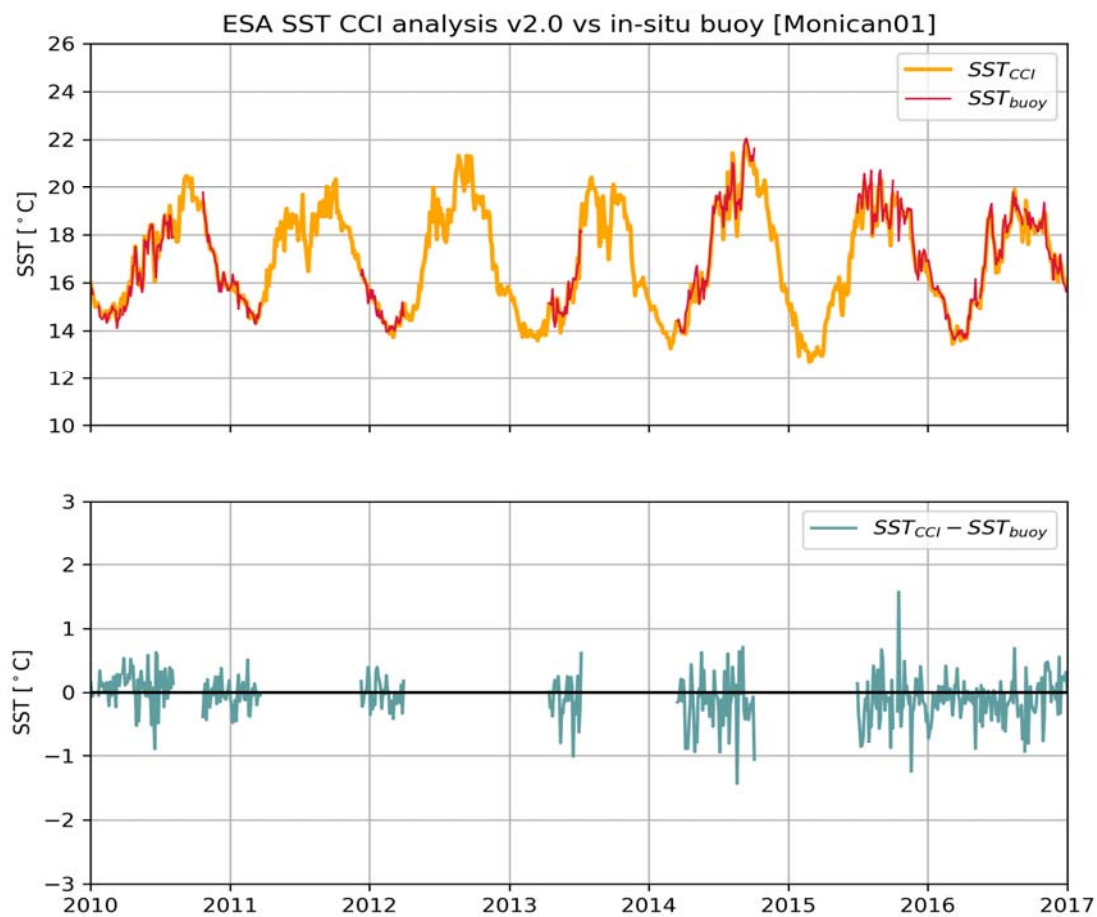


Figure 6-18. Same as Figure 6-17 for Monican01 buoy (Oceanic Portugal mainland).

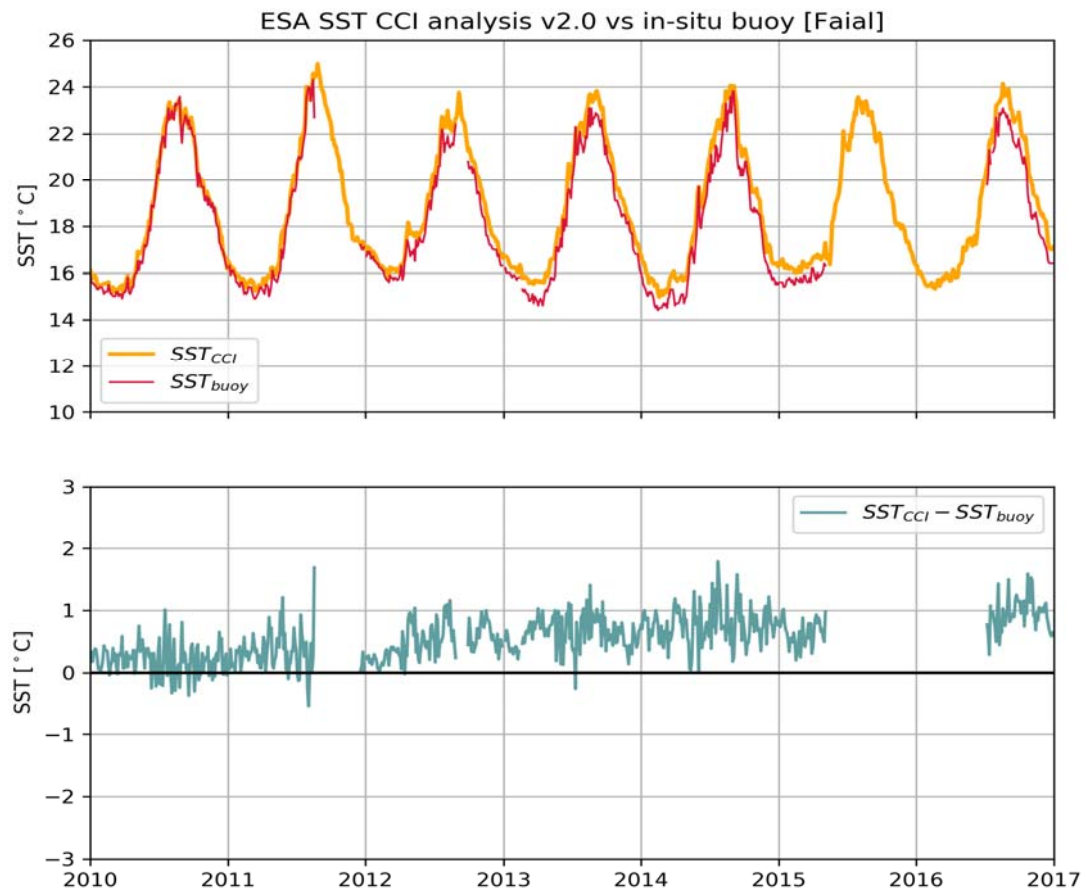


Figure 6-19. Same as Figure 6-17 for Faial buoy (Coastal Azores).

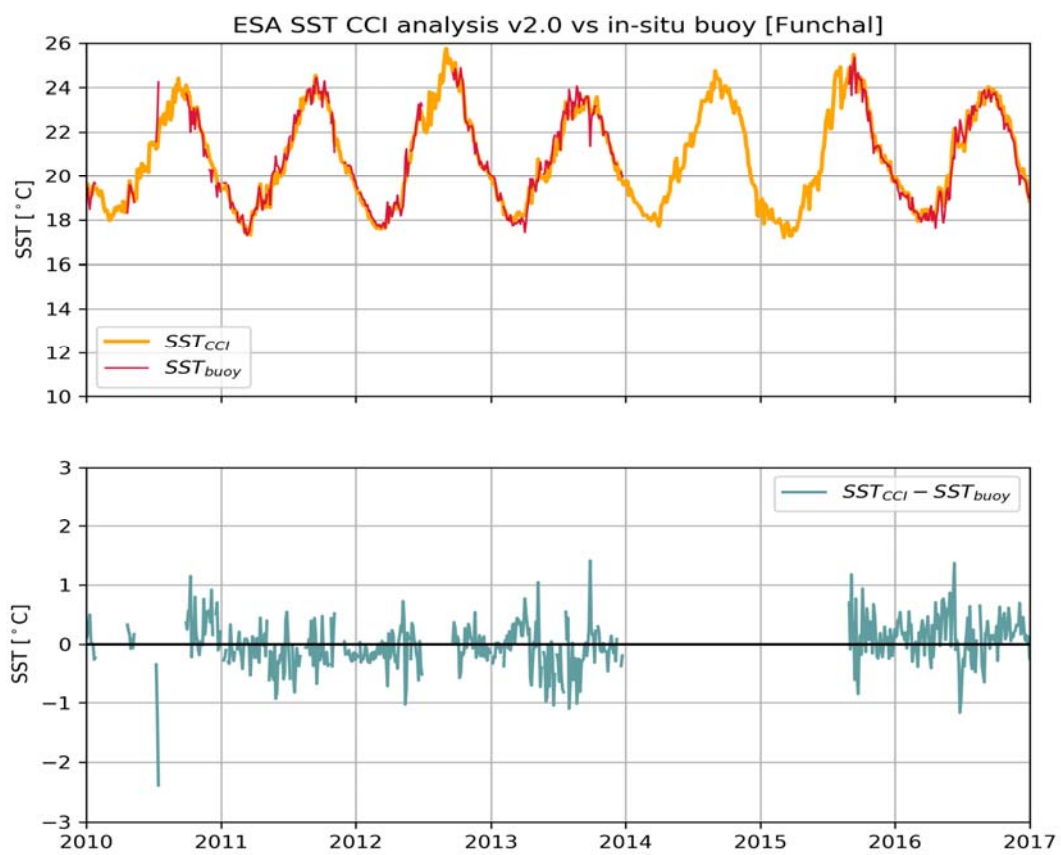


Figure 6-20. Same as Figure 6-17 for Funchal buoy (coastal Madeira).

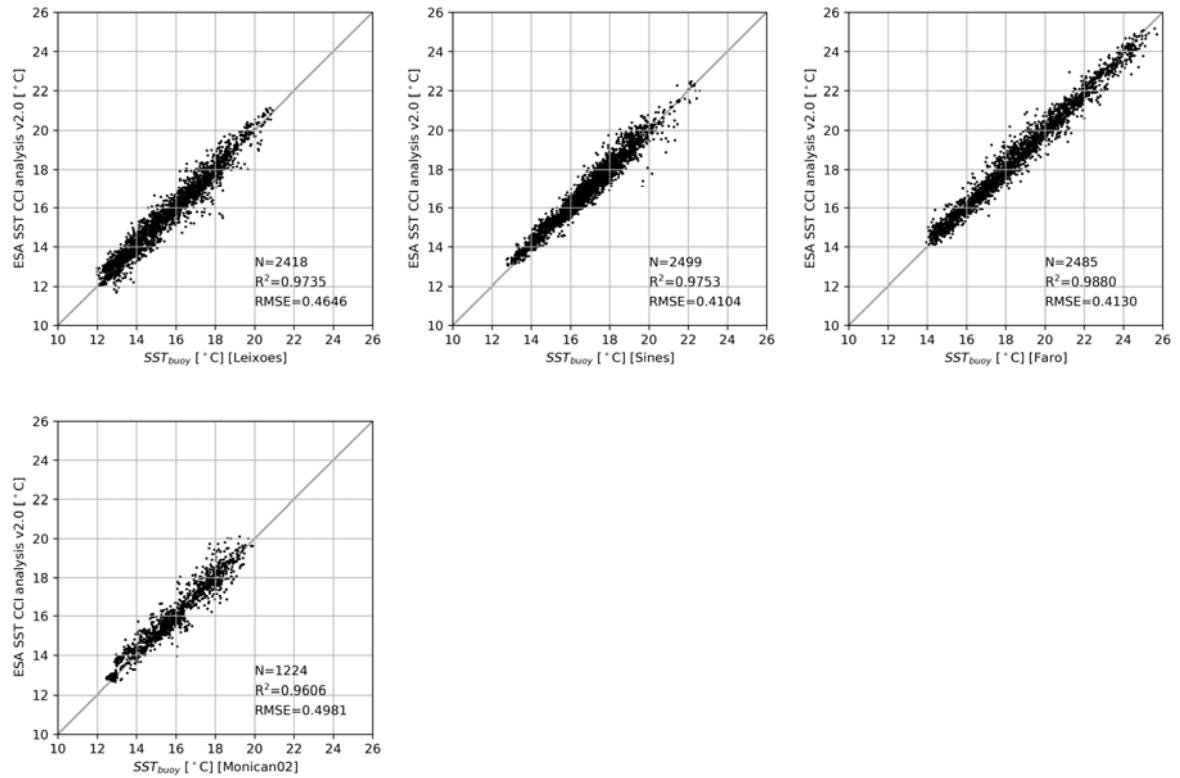


Figure 6-21. Scatter plot of the SST CCI analysis v2.0 against in situ SST data for the 4 coastal buoys located at Portugal mainland. N represents the data sample, R² is the coefficient of determination between both datasets and RMSE the root mean square error between both datasets.

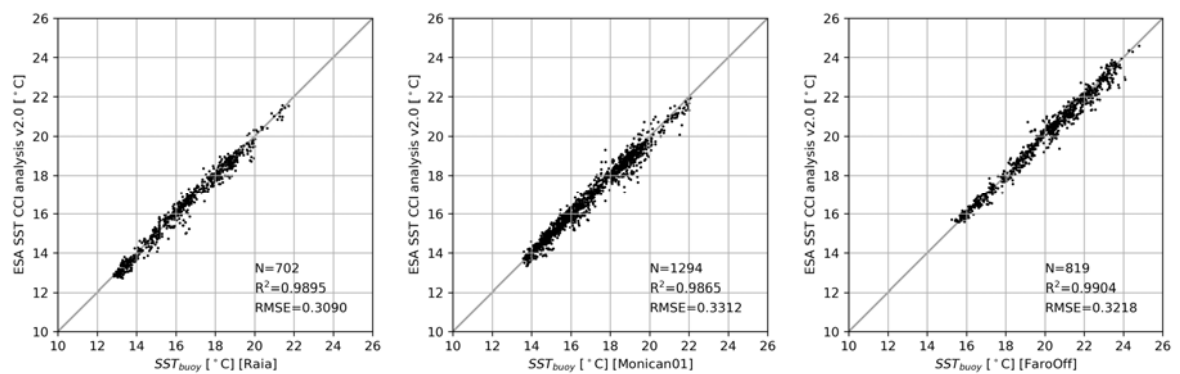


Figure 6-22. Same as Figure 6-21 for the 3 oceanic buoys at Portugal Mainland

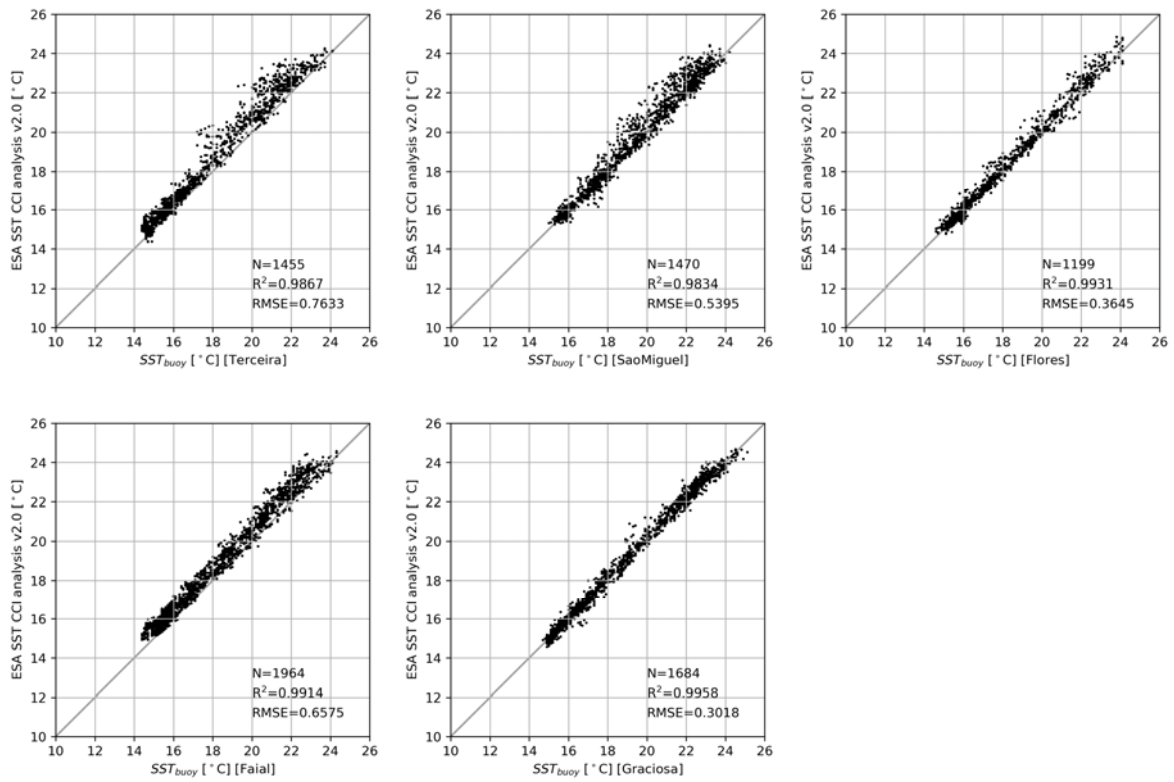


Figure 6-23: Same as Figure 6-21 for the 5 coastal buoys at Azores.

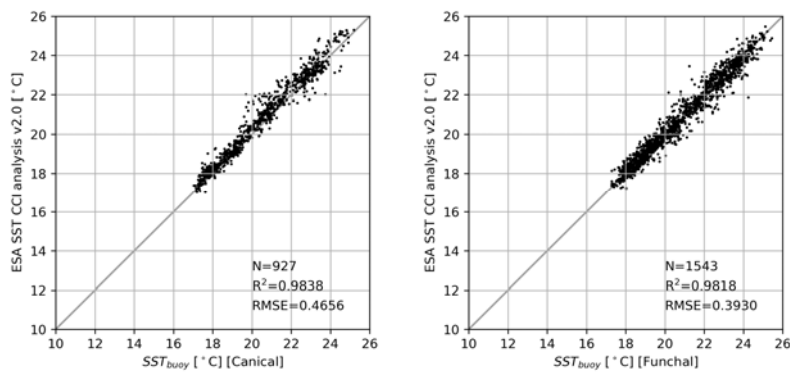


Figure 6-24. Same as Figure 6-21 for the 2 coastal buoys at Madeira.

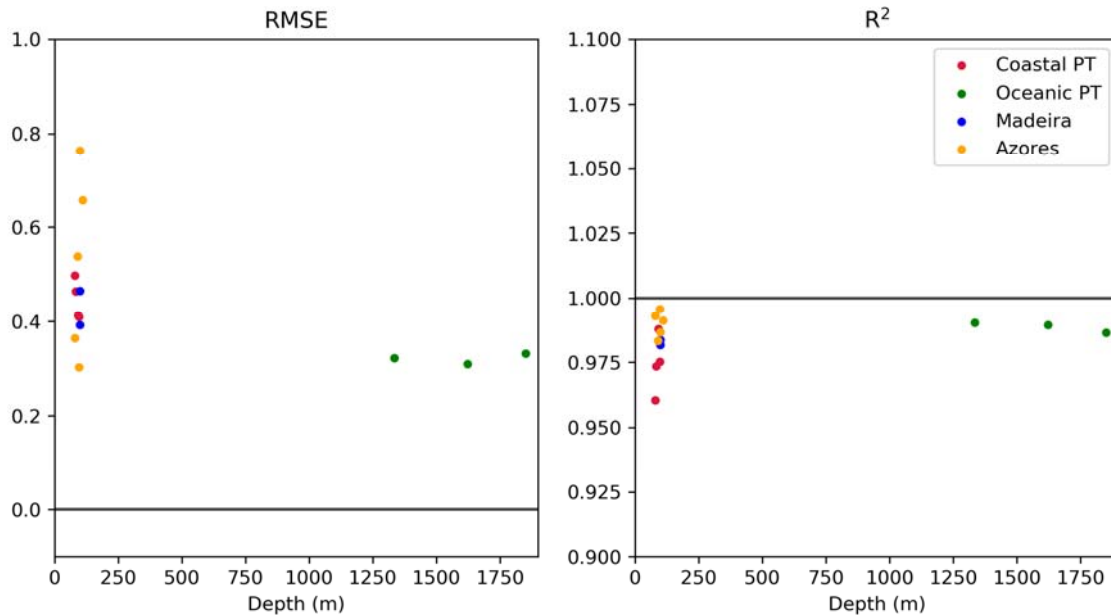


Figure 6-25. RMSE and R^2 (obtained for the ESA SST CCI analysis v.2 product versus buoy data for the period between 01.01.2010 and 31.12.2016) plotted against depth (m) for each buoy. Coastal PT includes Leixões, Monican02, Sines and Faro buoys; Oceanic PT includes Monican01, Raia and FaroOff; Azores includes São Miguel, Terceira, Graciosa, Flores and Faial; and Madeira includes Caniçal and Funchal.

6.4.2.4 CONCLUSIONS

The preliminary work exposed in this report shows that the data looks promising, showing generally the spatial and seasonal variability of the surface temperature with an accuracy of 0.3 to 0.5°C at most of the buoy locations. Overall, the oceanic buoys showed smaller RMSE, which suggests that the **ESA SST CCI analysis v2.0** is more accurate in the open ocean, as expected, and still needs some tuning for coastal ocean. [This discrepancy could also arise from diurnal differences at different depths and will be explored in further work by the author.]

Further analysis should be performed for inter-annual, seasonal and spatial variability.

6.4.3 FEEDBACK ON SCIENTIFIC UTILITY OF THE SST CCI PRODUCTS

This preliminary work showed that the data looks promising, with errors of less than 0.5°C even at the coastal buoy locations (depth < 100m). The data also captured the overall seasonal and inter-annual variability and magnitude of the surface temperature measured by the moored buoys. **ESA SST CCI analysis v2.0** can be particularly important to analyse the spatial and temporal variability of the sea surface at the Eastern Atlantic Ocean for the past 30 years. This product provides an important source of information, especially for the open ocean, where surface temperature measurements are scarce and sporadic.

6.5 Evaluating coupled climate model EC-Earth3-Veg

Ulrika Willén

SMHI, Swedish Meteorological and Hydrological Institute

6.5.1 KEY MESSAGES

- A first evaluation of ENSO in the coupled climate model EC-Earth3-Veg using with SST CCI analysis v2.0, showed that the model has a substantially reduced cold tongue bias and the seasonal variability has improved compared to EC-Earth2. However the eastern tropical Pacific Ocean warm bias remains and the variability for this region is underestimated.
- We find the new SST CCI analysis v2.0 data very useful for investigating ENSO variability for the last 30+ years and for evaluation of climate models. For longer perspective of ENSO the CCI data can be used in combination with HadISST1.1 data.
- It is beneficial to have high temporal and spatial resolution consistent SST data with uncertainties, for process studies, evaluation of climate models and for initialisation of seasonal and decadal climate predictions – even if in this study we did not use the uncertainties and only looked at coarse resolution models.
- It would help users if short information is supplied in the data access folder, e.g. a README file describing the data sets, L4 etc.

6.5.2 SCIENTIFIC ANALYSIS

6.5.2.1 AIMS OF THE STUDY

The El Niño Southern Oscillation (ENSO) is the most important coupled ocean-atmosphere phenomenon affecting global climate variability on seasonal to inter-annual time scales. It is an irregularly periodical variation in winds and sea surface temperatures (SST) over the tropical eastern Pacific Ocean, affecting much of the tropics and subtropics. The warm (El Niño) phase is associated with large positive SST anomalies in eastern to central Pacific occurring on 3-7 years times-scales and the cold phase (La Niña) occurring every 2-4 years is less intense but longer lasting. The phases can be classified by calculating SST anomalies for different regions of the Equatorial Pacific, most typically the Niño3.4 region (190E-240E, 5S-5N).

The short time scale, large amplitude and multiple ECV's affected by ENSO makes it an ideal natural forcing to focus on for cross-assessment of multiple satellite records as the CCI data sets, albeit the records are too short for sampling the ENSO diversity and the decadal ENSO variability. Climate models capture the basic ENSO features but the amplitude, life cycle and frequency are not properly reproduced and most models' variability extends too far into the Western Pacific. To further understand model performances and biases, evaluating models with observational constraints derived from multiple variables can give new perspectives.

In this user report we examine ENSO variability in SST satellite observations from the ESA Climate Change Initiative and in the coupled climate model EC-Earth3-Veg historical simulations. We also use the HadISST1.1 long term SST observations. A paper including parts of this study and the inclusion of other ECV's from ESA-CCI as well as other satellite datasets is ongoing.

6.5.2.2 METHOD

We compare monthly mean SST values from observations and an atmosphere-ocean coupled climate model for the Tropical Pacific Ocean from 1870 to 2014. We have used the ESA SST CCI Analysis product version v2.0 created by OSTIA system from SST CCI ATSR and SST CCI AVHRR products, 0.05-deg resolution, daily files covering 1981 – 2016. We made monthly means for the period 1982 to 2014 (without using the CCI SST simulator) and re-gridded the data to the climate model resolution. We also used HadISST1.1 for the period 1870 to 2014.

The model data come from six EC-Earth3-Veg historical simulations starting from different initial states for the time period 1870 to 2014. The runs have not yet been given their CMIP6 names so we use the run numbers; t605, t606, t607, t608, t611 and t612.

We divided the analysis into two periods, 1870-1981 and 1982-2014, respectively. We choose the break at 1981 since before then there was no satellite data in HadISST and the break at 2014 since that is the end year of the CMIP6 historical simulations.

6.5.2.3 RESULTS

Figure 6-26 shows the time–longitude cross section of the monthly mean anomalies of SST over the equatorial Pacific Ocean (averaged between 5°S and 5°N) for SST CCI analysis v2.0 and one EC-Earth3-Veg member (t607) for 1982 to 2014. The distinct El Niño and La Niña phases are clearly visible in the observations e.g. 1997 to 2000. The climate model simulation has a realistic SST variability, but it is not in phase with the observations as expected for an atmosphere-ocean coupled model. This member (t607) has a power spectrum of the Niño3.4 time series similar to that of HadISST1.1 for the full historical simulation (1870-2014, not shown).

Most CMIP3 and CMIP5 (including EC-Earth2) coupled models have an excessive cool equatorial Pacific cold tongue bias and an accompanied deterioration of the El Niño–Southern Oscillation (ENSO) variability. All EC-Earth3-Veg CMIP6 simulations have small cold biases of less than 0.2K compared to HadISST1.1 between 180E to 240E as can be seen in Figure 6-27a for the period 1870-1981. Near the coast of South America (260E-280E) the EC-Earth3 simulations all have warm biases of about 1.K. For present day (1982-2014) Figure 6-27b, the model simulations are too warm (0.1-0.5K) compared to SST CCI analysis v2.0 and HadISST1.1 between longitudes 180E-240E. Near South America the SST overestimations are higher (~1.5K). This eastern Pacific Ocean bias is also common for CMIP3/CMIP5 models and could be linked to the lack of stratiform clouds and/ or too small ocean mixing.

All EC-Earth3 simulations have larger variability (0.1-0.2K) than HadISST1.1 for the historical period 1870-1981 (Figure 6-27c). For present day (Figure 6-27d) the models compare well with the SST CCI analysis v2.0 standard deviations for the cold tongue region (within +/- 0.1K), except member t612 that has a much lower variability of 0.6K compared to the observed 0.9K for the 180E to 240E plateau region. The model simulated variabilities are underestimated near the coast (260E-280E) coinciding with the warm bias region.

To investigate the seasonal variations in SST we plot the monthly SST mean values and standard deviations in Figure 6-28 for SST CCI analysis v2.0. The western warm pool and eastern cold tongue are clearly seen both peaking in August to October (Figure 6-28a). The variability is largest for the Niño3.4 region in October to February and largest for the coastal region from March to July (Figure 6-28b). SST CCI analysis v2.0 is slightly colder (Figure 6-28c) and the variability is slightly larger in Western and Eastern Pacific Ocean (Figure 6-28d) than HadISST1.1. The increase in variability is expected due to the higher spatial and temporal resolution of SST CCI analysis v2.0 than HadISST1.1.

To corresponding EC-Earth seasonal variations are shown in Figure 6-29 for one of the simulations, t607. The mean and variability patterns are similar to the SST CCI analysis v2.0. The difference plots show again that the model is too warm especially over the eastern part of the Pacific Ocean but the bias also extends into the Niño3.4 region. The model variability is smaller than in the observations especially along the South American coast in March to August.

In Figure 6-30 we show the monthly mean biases for all the six EC-Earth3-Veg model simulations. The pattern is similar for all simulation with a small positive bias (0.5K, as previously noted in Figure 6-27b) except for the warm Eastern bias region where the bias reach >2K from August to December. This bias stretches westwards in boreal winter. Finally, in Figure 6-31 we show the monthly mean std biases for all the six EC-Earth3-Veg model simulations. The variability is underestimated for the coastal region from April to July for all members, and there is also an underestimation varying between the simulations for the Niño3.4 region in October to January. The largest negative bias is seen for t612, which explains the underestimation in the standard deviation previously noted in Figure 6-27d.

The reasons for the SST biases will be investigated further looking into the cloud and radiation fields and ocean temperature at deeper levels.

6.5.2.4 CONCLUSIONS

A first evaluation of ENSO in the coupled climate model EC-Earth3-Veg using with SST CCI analysis v2.0, showed that the model has a substantially reduced cold tongue bias and the seasonal variability has improved compared to EC-Earth2. However, the eastern tropical Pacific Ocean warm bias remains and the variability for this region is underestimated

We found small differences between SST CCI analysis v2.0 and HadISST1.1 for present day, which we assume can be due to the higher temporal and spatial resolution of SST CCI analysis v2.0.

6.5.3 FEEDBACK ON SCIENTIFIC UTILITY OF THE SST CCI PRODUCTS

We find the new SST CCI analysis v2.0 data very useful for investigating the ENSO variability for the last 30+ years and for evaluation of climate models. For longer perspective of ENSO the CCI data can be used in combination with HadISST1.1 data.

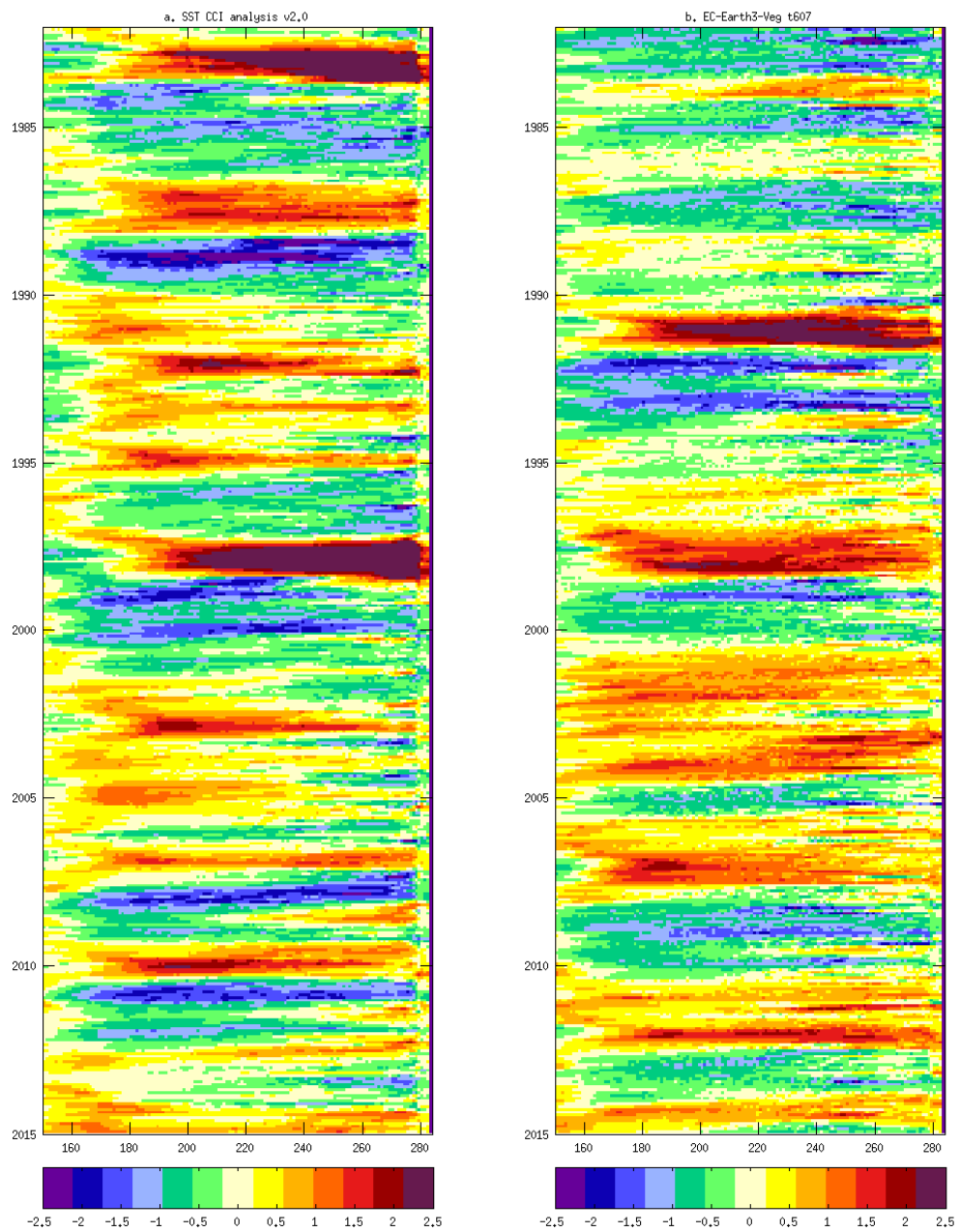


Figure 6-26. Hovmöller plots of SST averaged for 5S to 5N between 150E to 285E from 1982 to 2014 for a. SST CCI analysis v2.0 and b. EC-Earth3-Veg t607.

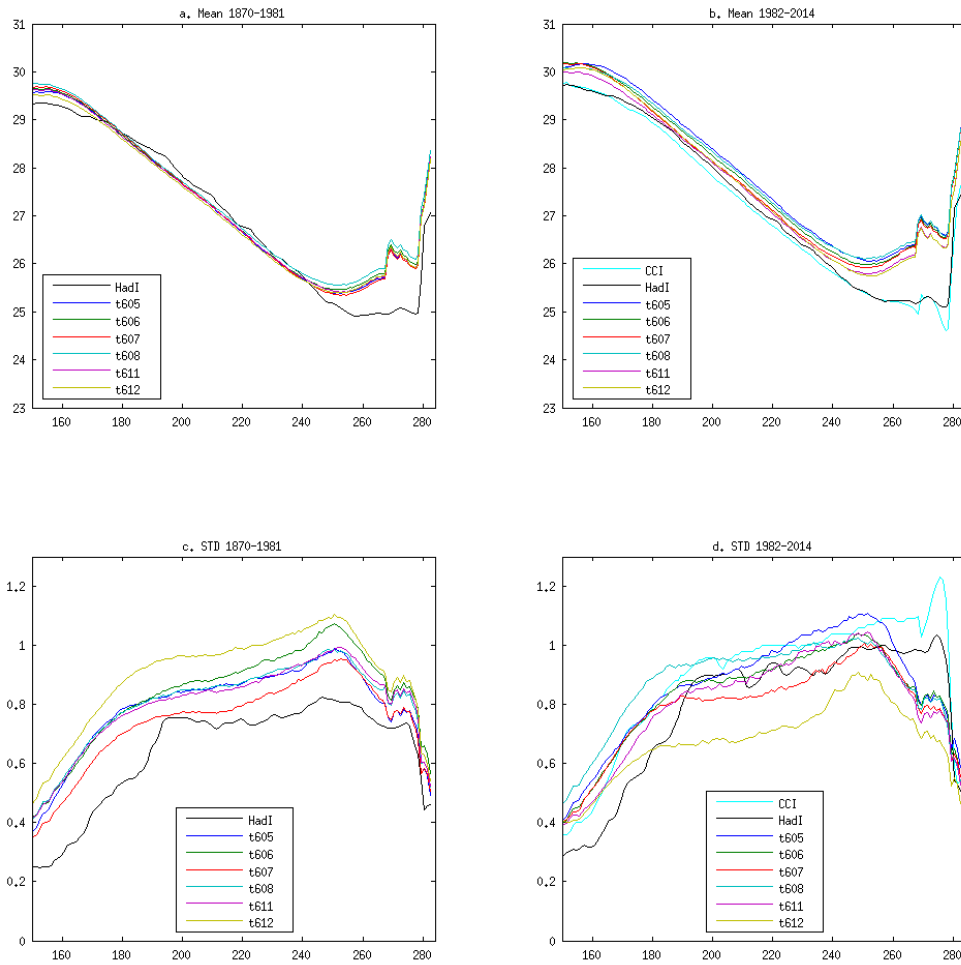


Figure 6-27. Monthly mean (top row) and standard deviations (bottom row) for SST for observations SST CCI analysis v2.0 (cyan) and HadISST (black) and for EC-Earth3-Veg, averaged for 5S to 5N between 150E to 285E for 1870-1981 (left column) and 1982 -2014 (right column).

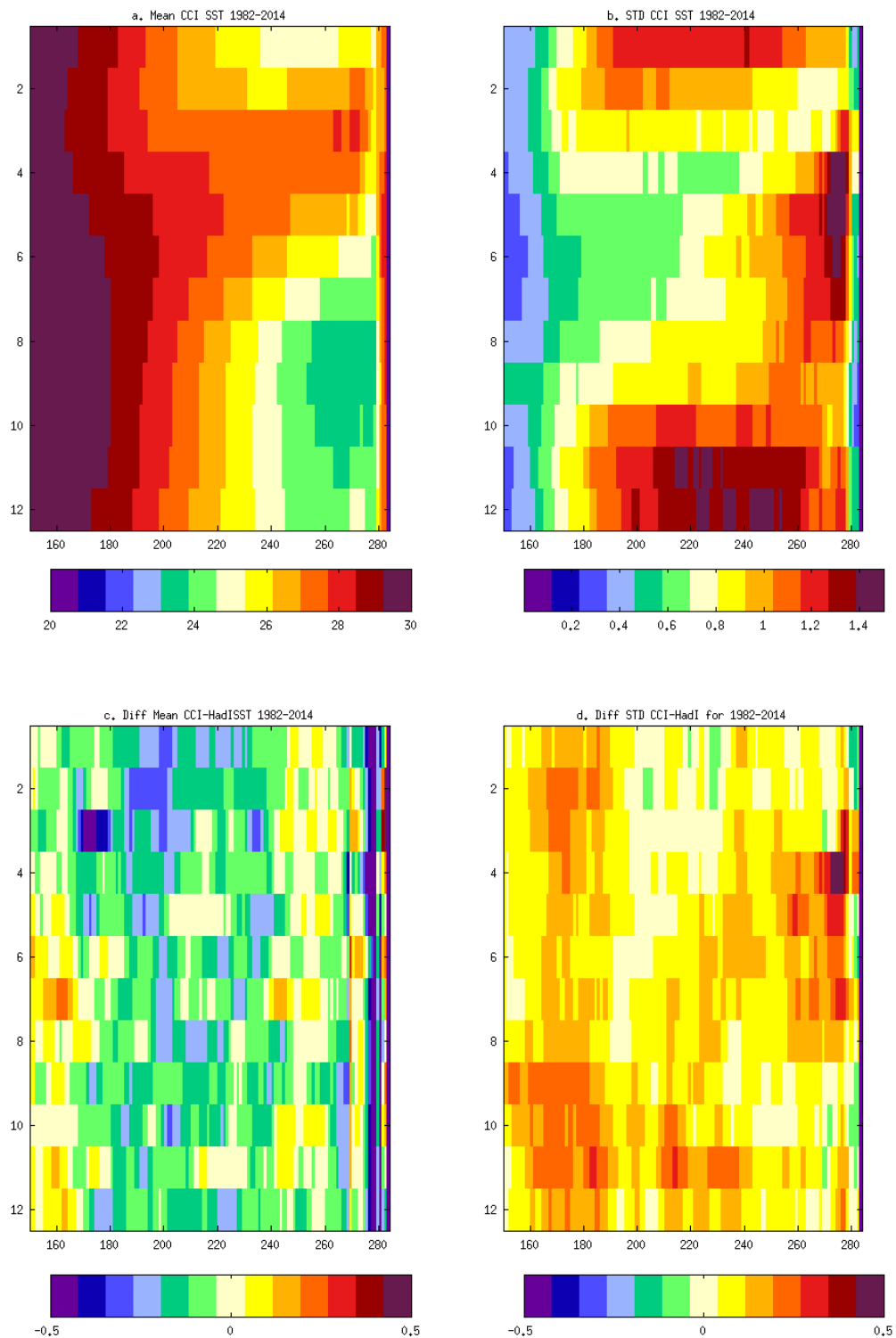


Figure 6-28. Zonal month-longitude cross sections between 150E and 285E of SST CCI analysis v2.0 averaged for 5S to 5N and 1982 to 2014, for a. Mean SST and b. standard deviation of SST and differences between SST CCI analysis v2.0 and HadISST1.1 for c. Mean SST and d. STD SST.

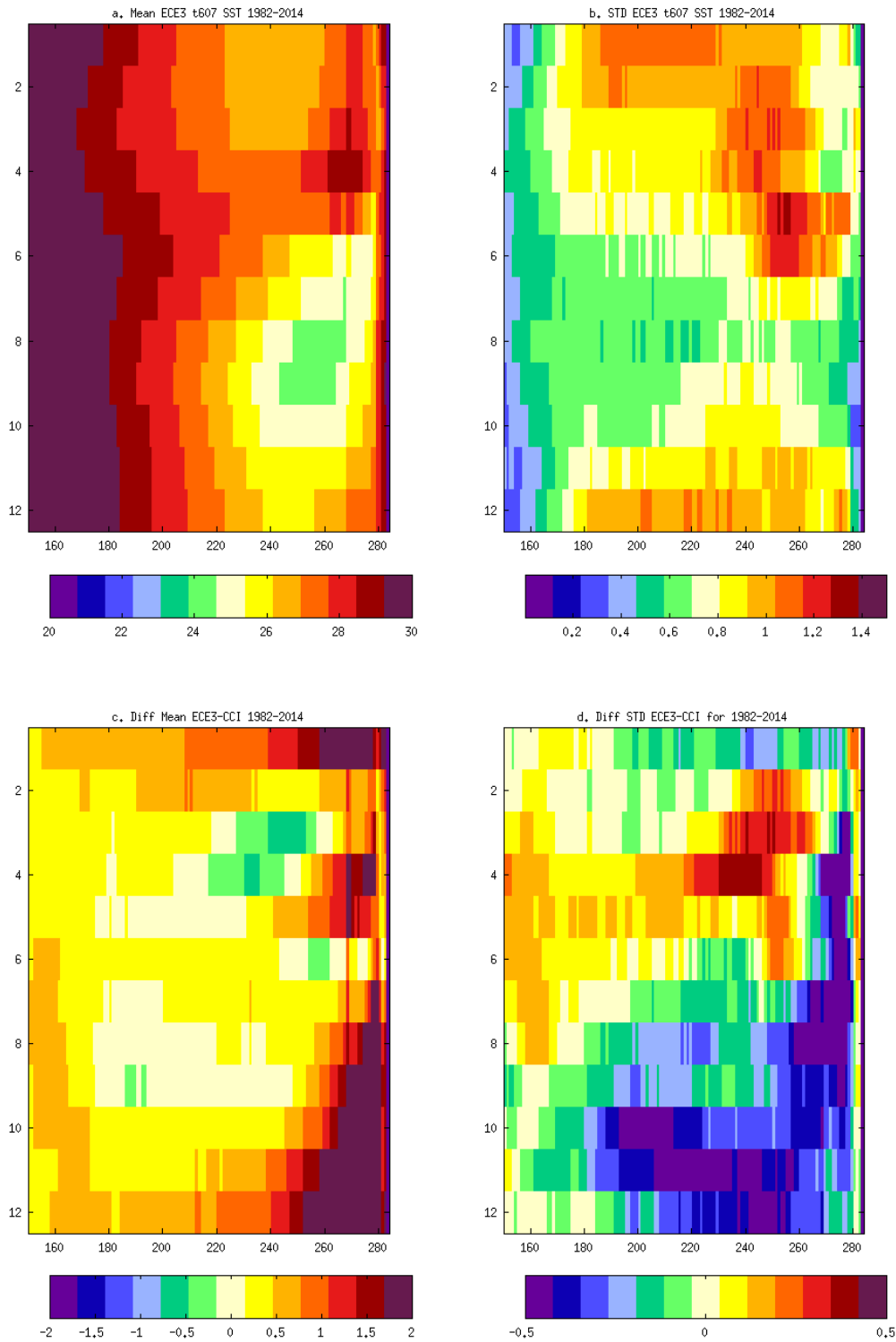


Figure 6-29. Zonal month-longitude cross sections between 150E and 285E of EC-Earth3-Veg, t607 SST averaged for 5S to 5N and 1982 to 2014, for a. Mean SST and b. standard deviation of SST and the differences between EC-Earth3-Veg t607 and SST CCI analysis v2.0 for c. Mean SST and d. STD SST.

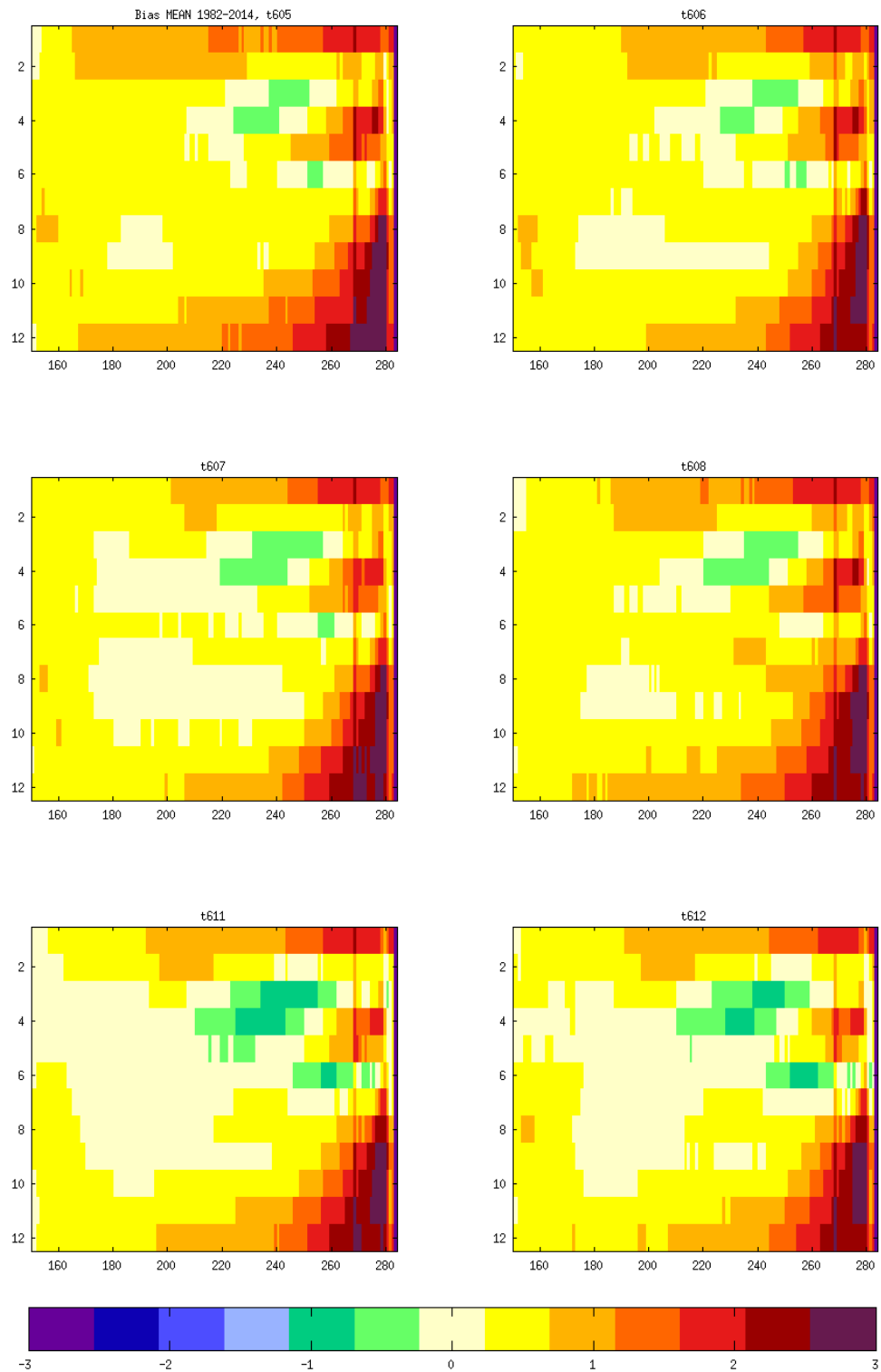


Figure 6-30. Zonal month-longitude cross sections between 150E and 285E for EC-Earth3-Veg SST mean biases compared to ESA CCI analysis v2.2, averaged for 5S to 5N for the period 1982 to 2014 for 6 historical CMIP6 simulations.

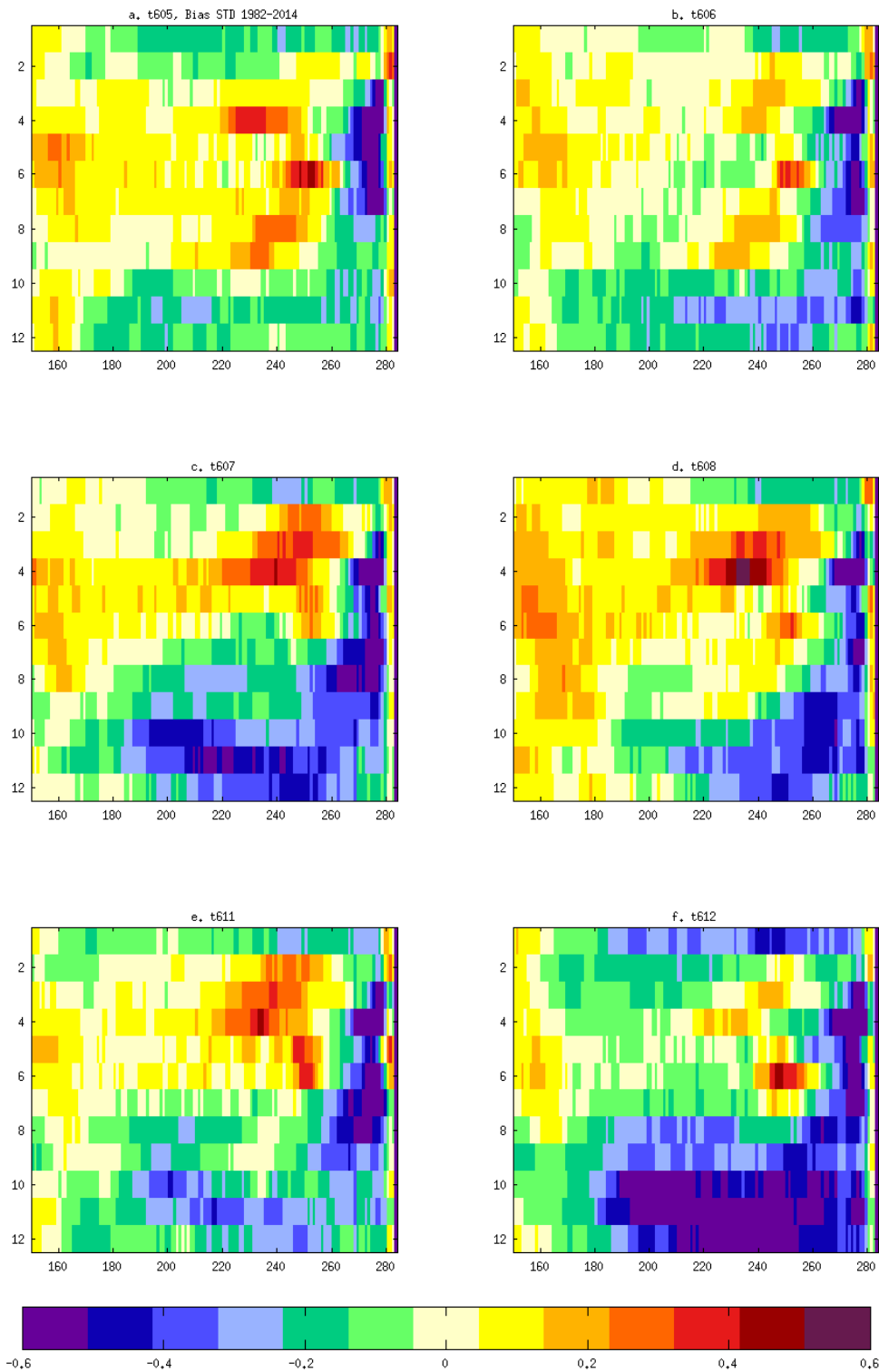


Figure 6-31. Zonal month-longitude cross sections between 150E and 285E for EC-Earth3-Veg SST Standard Deviation biases compared to ESA CCI analysis v2.2, averaged for 5S to 5N for the period 1982 to 2014 for 6 historical CMIP6 simulations.

7. FURTHER ISSUES AND RECOMMENDATIONS REPORTED BY REGISTERED USERS

7.1 Feedback on ease of use of the products and documentation

- The SST CCI analysis v2.0 data files are well organised and contain essential information, and are thus very easy to use.
- It would have been useful to have a climatology (or sets of climatologies with different base periods) provided.
- The use of NetCDF format makes the data technically straightforward to use in our reanalysis.
- Daily global datasets are readily accessible and easy to work with. The processing and analysis of the data during this work was performed using SNAP and Python 2.7 and no relevant problems were encountered.
- The documentation (SST_CCI-PUG-UKMO-001) was clear and sufficient to understand the data and use it.
- It would be good if that information and information about the different datasets (L3, L4...) also was available in a README file in the top folder.
- I went to the ESA-CCI SST website (a bit late) and found valuable information on how to process the data (making monthly means) and on using a “simulator”. A link to that web page could also be included in the README file at http://gws-access.ceda.ac.uk/public/esacci-sst/CDR2.0_release/.

7.2 Recommendations

- Monthly files are suggested together with the daily files.
- Further validation with in-situ data should be undertaken in order to improve the product by minimizing the bias and error from interpolations.
- It would be good if the data will be available through Obs4MIP, including a link to the “simulator” so modellers compare the “same thing”.